Haris Stamatopoulos

Withdrawal Properties of Threaded Rods Embedded in Glued-Laminated Timber Elements

Haris Stamatopoulos

Doctoral thesis

☐ **NTNU**
Norwegian University of
Science and Technology

☐ **NTNU**
Norwegian University of
Science and Technology

☐ NTNU

Haris Stamatopoulos

Withdrawal Properties of Threaded Rods Embedded in Glued-Laminated Timber Elements

Thesis for the Degree of Philosophiae Doctor

Trondheim, March 2016

Norwegian University of Science and Technology
Faculty of Engineering Science and Technology
Department of Structural Engineering

◨ NTNU
Norwegian University of
Science and Technology

Preface

The present doctoral thesis has been submitted to the Norwegian University of Science and Technology (NTNU) in partial fulfilment of the requirements for the degree of Philosophiae Doctor (Ph.D.). It is a paper-based type of thesis containing 4 appended papers, an introductory part and 3 appendices. This work has been carried out at the Department of Structural Engineering, NTNU, Trondheim and supervised by Professor Kjell Arne Malo.

The author hereby declares that this thesis and the appended papers have been written by him and that the presented work is a result of original research which has not been submitted for a degree at this university or any other institution. All experiments have been executed by the author.

Haris Stamatopoulos
Trondheim, January 2016

Acknowledgements

I would like to thank my supervisor, Professor Kjell Arne Malo, for giving me the opportunity to work on this Ph.D. project, for his guidance and for taking care of administrative issues. His door has always been open for our fruitful and often lengthy discussions. The critical feedback on the research methods and results and the critical reading of my manuscripts have been invaluable. I would also like to thank him for transferring me his great enthusiasm for timber engineering.

I am also thankful to my colleagues at NTNU and especially to all current and former members of the Timber Structures Research Group for the creative and very pleasant working environment. Special thanks to Professor Emeritus Kolbein Bell for critical reading of some of my manuscripts and to Anna Ostrycharczyk who has been a very good company inside but also outside the campus.

Since experimental testing has been a major part of this project, I am thankful to the stuff of the laboratory of the Department of Structural Engineering. The technicians Pål Brokka Rike, Ragnar Moen, Terje Petersen, Christian Frugone, Gøran Loraas, Per Nordtug and the laboratory manager Odd Kristian Nerdahl made it all possible and their help in the preparation of experiments is kindly acknowledged. The contribution of students Joakim Troller and Roland Falk in the preparation of some of the experiments is also appreciated. I would also like to thank Moelven Limtre AS for providing all glulam beams which were required for the experimental program.

I am also very grateful to all my friends. I met many of them in Trondheim during my Ph.D. study. These years have been truly exciting with them!

Last but not least, I would like to express my deepest gratitude to my brother, my mother and my girlfriend for their patience, their understanding and above all their support and encouragement. Νίκο, Ρούλα και Ειρήνη σας ευχαριστώ πολύ!

This work is dedicated to my father. I miss him every single day...

Abstract

The competitiveness of timber structures is largely governed by the design and effectiveness of the connections. Connections with long axially loaded self-tapping screws or threaded rods embedded with an inclination to the grain direction can be an alternative to connections with dowel-type fasteners or glued-in rods. Self-tapping screws and especially threaded rods with large diameters feature high withdrawal capacity and stiffness. This ability makes them suitable as fasteners in connections in order to realize stiff and strong joints.

Eurocode 5 does not provide rules for the estimation of the withdrawal stiffness of axially loaded fasteners, which is necessary for the determination of the stiffness of connections. Some rules can be found in technical approvals; however they are only valid for the instantaneous withdrawal stiffness under service load of self-tapping screws with small diameters. Consequently, there is a complete lack of guidelines for the estimation of the withdrawal stiffness of threaded rods with larger diameters. Moreover, Eurocode 5 imposes a limitation to the angle between the rod-axis and the grain direction ($\alpha \geq 30°$) without taking into account that splitting may be prevented by reinforcement. The lack of knowledge of proper design, documentation of mechanical behaviour, design guidelines and design codes for threaded rods are barriers for the development of timber connections with these fasteners.

The withdrawal properties (capacity and stiffness) of axially loaded threaded rods were investigated in the present thesis by use of experimental, analytical and numerical methods. An overview of the background information and research on withdrawal of screws and threaded rods is presented in Part I of the present thesis. Part II consists of 4 appended papers where the findings of this Ph.D. project are presented. Part III consists of 3 appendices where some analytical remarks together with the detailed experimental and numerical results are presented.

The review on the existing approaches and experimental results have shown that, up-to-date, most research effort has been devoted on the determination of the withdrawal strength of self-tapping screws with diameters up to 12-14 mm. On the contrary, available research results for threaded rods with larger diameters are sparse and the vast majority of these results are limited to relatively stocky rods embedded either parallel or perpendicular to the grain. Therefore, the effect of the rod-to-grain angle and the embedment length on the withdrawal properties remains unknown.

The parameters of the experimental investigation were the rod-to-grain angle (α = 0-90°) and the embedment length (l = 100-600 mm). Specimens with single rods and with a pair of rods (arranged in a row perpendicular to the plane of the grain) embedded in glued-laminated timber (abbr. glulam) elements were tested. Moreover, an analytical approach based on Volkersen theory and a bi-linear constitutive relationship was used for the estimation of the elastic and post-elastic withdrawal properties. Finally, Finite Element (abbr. FE) simulations were performed to estimate the instantaneous withdrawal stiffness (under service load) and the elastic distributions of stresses and displacements.

According to experimental observation, the specimens exhibited high withdrawal capacity and stiffness (without initial soft response). Based on the experimental results, the necessary input parameters for the analytical method were quantified. In particular, simple expressions for the mean and 5%-percentile withdrawal strength, the shear stiffness and the brittleness were developed. In general, the analytical estimations and the experimental results were in good agreement. Numerical estimations overestimated stiffness especially for small angles and short embedment lengths; however this overestimation was smaller in the case of longer rods. Finally, the experimental results from tests with pairs of rods showed that the effectiveness per each rod was quite high, despite the fact that rods were placed with small edge distances and spacings.

Table of contents

Part II: Appended Papers

   i.   **Withdrawal stiffness of threaded rods embedded in timber elements**
       Haris Stamatopoulos and Kjell Arne Malo
       Under revision in Construction and Building Materials (2015)

   ii.   **Withdrawal capacity of threaded rods embedded in timber elements**
       Haris Stamatopoulos and Kjell Arne Malo
       Construction and Building Materials, 94:387-97 (2015)

  iii.   **Withdrawal of pairs of threaded rods with small edge distances and spacings**
       Haris Stamatopoulos and Kjell Arne Malo
       Submitted to European Journal of Wood and Wood Products (2016)

Nomenclature

Abbreviations

CoV	coefficient of variation
EC5	Eurocode 5
ETA	European Technical Approval
FE	Finite Element
Glulam	glued-laminated timber
MC	moisture content
RH	relative humidity
SLS	serviceability limit state
STS	self-tapping screws
ULS	ultimate limit state

Upper-case Latin letters

A, B, C, D	regression parameters (-)
A_s	core cross-sectional area of screw or threaded rod (mm^2)
A_w	cross-sectional area of wood subjected to axial stress (mm^2)
$A_{w.eff}$	effective cross-sectional area of wood subjected to axial stress (mm^2)
D_1, D_2	constants determined by the boundary conditions of the differential equation (mm)
E_L	Young's modulus in the longitudinal direction (MPa)
E_R	Young's modulus in the radial direction (MPa)
E_s	Young's modulus of steel (MPa)
E_T	Young's modulus in the tangential direction (MPa)
$E_{w.\alpha}$	Young's modulus of wood as function of angle to the grain (MPa)
E_{w^*}	Young's modulus for estimation of mean stress length (MPa)
F_{ax}	withdrawal capacity (N)
$F_{ax.\alpha.Rk}$	characteristic withdrawal capacity (N)

F_{max}	maximum withdrawal force (N)	
G	shear modulus (MPa), relative density (-)	
G_f	fracture energy (N/mm)	
G_{LR}	shear modulus for L-R plane (MPa)	
G_{LT}	shear modulus for L-T plane (MPa)	
G_{RT}	shear modulus for R-T plane - rolling shear modulus (MPa)	
K_0	axial stiffness of non-embedded part of the screw or threaded rod (N/mm)	
$K_{ax.ser}$	withdrawal stiffness (instantaneous, under service load) (N/mm)	
K_{ser}	slip modulus (instantaneous, under service load) per shear plane per fastener - laterally loaded fasteners (N/mm)	
K_{tot}	total axial stiffness (instantaneous, under service load) (N/mm)	
K_u	instantaneous slip modulus per shear plane per fastener for the ULS - laterally loaded fasteners (N/mm)	
K_w	withdrawal stiffness (instantaneous, under service load) (N/mm)	
$K_{w.06}$	instantaneous secant withdrawal stiffness corresponding to 60% of P_u (N/mm)	
$K_{w.08}$	instantaneous secant withdrawal stiffness corresponding to 80% of P_u (N/mm)	
$K_{w.u}$	instantaneous secant withdrawal stiffness corresponding to P_u (N/mm)	
L	specimen dimension along the rod axis (mm)	
N	number of penetrated layers, population, normal distribution	
P	withdrawal force (N)	
P_e	elastic withdrawal capacity (N)	
P_{est}	estimated withdrawal capacity (N)	
P_f	withdrawal force level after failure (N)	
$P_{u.w}$	withdrawal capacity (N)	
$P_{u.w.k}$	characteristic withdrawal capacity (N)	
$P_{u.w.mean}$	mean withdrawal capacity (N)	
$P_{u.k.rod}$	characteristic tensile capacity of rod (N)	

T	temperature (°C)
X	withdrawal strength (MPa) or normalized withdrawal stiffness (N/mm^3)
X_{ref}	Reference value of X (MPa or N/mm^3)

Lower-case Latin letters

a	edge distance or spacing (mm)
a_1	spacing of screws along the same plane parallel to the grain (mm)
$a_{1.CG}$	end distance of screw (mm)
a_2	spacing of screws in rows perpendicular to the plane of the grain (mm)
$a_{2.CG}$	edge distance of screw (mm)
b	beam width (mm)
c	thread pitch (mm), parameter (-)
d	outer-thread diameter (mm)
d_1	core diameter or outer-thread diameter (mm)
d_c	core diameter (mm)
d_{ef}	effective diameter (mm)
d_h	head diameter (mm)
e	standard error (-), support edge distance (mm)
f_{ax}	withdrawal strength, withdrawal strength parameter (MPa)
$f_{ax.\alpha.k}$	characteristic withdrawal strength parameter for angle α (MPa)
$f_{ax.\alpha.mean}$	mean withdrawal strength parameter for angle α (MPa)
$f_{ax.ref}$	reference withdrawal strength (MPa)
$f_{head.k}$	characteristic pull through parameter (MPa)
f_v	shear strength (MPa)
f_w	mean withdrawal strength (MPa)
$f_{w.\alpha}$	mean withdrawal strength for angle α (MPa)
h	beam height (mm)
k_{ax}	angle factor (-)

$k_{ax.ser}$	withdrawal stiffness normalized per unit area (N/mm^3)
$k_{ax.ser.ref}$	reference withdrawal stiffness normalized per unit area (N/mm^3)
k_d	factor for capacity of screws with d = 6-8 mm (-)
k_{diam}	diameter factor (-)
k_{emb}	embedment factor (-)
$k_{Hankinson.mod}$	angle factor (-)
k_{length}	factor taking into account the effect of the tip (-)
k_{MC}	moisture content factor (-)
k_{red}	factor taking into account spacings (-)
k_{sys}	system strength factor (-)
k_{temp}	temperature factor (-)
k_{ρ}	density factor (-)
k_{90}	ratio of withdrawal properties parallel and perpendicular to the grain (-)
l	embedment length (mm)
l_e	length of the shear zone in the elastic domain (mm)
l_{ef}	effective length of a screw or threaded rod (mm)
l_{emb}	embedment depth of threaded part (mm)
l_f	length of the shear zone in the fracture domain (mm)
l_g	length of threaded part of a screw (mm)
l_0	mean stress length (mm), non-embedded length of screw or threaded rod (mm)
m	brittleness parameter (-)
n	number of fasteners (-)
n_{ef}	effective number of fasteners (-)
$n_{ef.ser}$	effective number of fasteners under service load (-)
r^2	coefficient of determination (-)
s	distance between supports (mm)
s_s	width of the support (mm)
t	thickness of the shear layer (mm)

u_s	displacement of the screw or threaded rod (mm)
u_w	displacement of wooden element (mm)
x	coordinate (mm)
x_e	coordinate - elastic domain (mm)
x_f	coordinate - fracture domain (mm)

Upper-case Greek letters

Γ	shear stiffness parameter of the bond line (MPa/mm)
Γ_e	equivalent shear stiffness parameter of the shear zone - elastic domain (MPa/mm)
Γ_f	equivalent shear stiffness parameter of the shear zone - fracture domain (MPa/mm)

Lower-case Greek letters

α	angle between the screw/threaded rod axis and the grain direction (°), wooden element-screw stiffness ratio (-)
β	parameter (N^{-1})
δ	relative displacement of the shear zone (mm)
$\delta_{ax.\alpha}$	withdrawal displacement corresponding to the withdrawal capacity (mm)
δ_e	maximum elastic displacement of the shear zone (mm)
δ_f	displacement of the shear zone after failure (mm)
δ_{tot}	total displacement (mm)
$\delta_{tot.u}$	total displacement corresponding to 100% of P_u (mm)
δ_w	withdrawal displacement (mm)
$\delta_{w.01}$	withdrawal displacement corresponding to 10% of P_{est} (mm)
$\delta_{w.04}$	withdrawal displacement corresponding to 40% of P_{est} (mm)
$\delta_{w.06}$	withdrawal displacement corresponding to 60% of P_u (mm)
$\delta_{w.08}$	withdrawal displacement corresponding to 80% of P_u (mm)
$\delta_{w.u}$	withdrawal displacement corresponding to 100% of P_u (mm)

ε_s	axial strain in the screw or threaded rod (-)
ε_w	axial strain in the wood (-)
λ	dimensionless fracture length (-)
λ_u	dimensionless fracture length at failure (-)
μ	friction coefficient (-)
ν	Poisson's ratio (-)
ν_{LR}	Poisson's ratio for *L-R* plane (-)
ν_{LT}	Poisson's ratio for *L-T* plane (-)
ν_{TR}	Poisson's ratio for *T-R* plane (-)
ν_{RT}	Poisson's ratio for *R-T* plane (-)
ρ	wood density (kg/m^3)
ρ_a	associated wood density (kg/m^3)
ρ_k	characteristic wood density (kg/m^3)
ρ_m	mean wood density (kg/m^3)
ρ_{ref}	reference wood density (kg/m^3)
ρ_{test}	wood density in tested specimens (kg/m^3)
σ_s	axial stress in the screw or threaded rod (MPa)
σ_w	axial stress in the wood (MPa)
τ	shear stress (MPa)
τ_{ini}	initial shear stress (MPa)
τ_{max}	maximum shear stress (MPa)
τ_f	shear stress after failure (MPa)
ω	parameter (-)

Part I:

Introduction, background and overview of

present work

1. Introduction

1.1 Starting point and problem statement

The competitiveness of timber structures is largely governed by the design and effectiveness of the connections. The manufacturing costs and the extent of labour can make timber structures rather expensive and thus exclude them from further consideration in comparison to other building materials. In addition, some types of connections in modern timber structures are characterized by low stiffness. This is especially true for beam-to-column connections where usual connections have only minor rotational stiffness and therefore they are considered as pinned. Too low stiffness in the connections results in ineffective moment transfer or excessive deformations. Too low overall stiffness results in flexible structures, unacceptable deformations and can possibly lead to instability or uncomfortable movements due to wind loading or vibrations.

Without some form of bracing or moment-stiff connections, the overall structural stiffness can be severely reduced. To overcome this limitation separate stiffening structural components are usually added, like X-bracing or some type of sheeting. However, bracing or sheeting put strong architectural restrictions on the appearance as well as on the use of structures. Consequently, the use of structural timber is, in many situations, hampered due to lack of connections with high stiffness.

For the analysis and the design of a timber structure (both for the serviceability limit state (abbr. SLS) and the ultimate limit state (abbr. ULS)), the following properties of its connections are required:

- the stiffness of the connections under service load (SLS)
- the stiffness of the connections for the ULS;
- the load-carrying capacity of the connections.

Connections with high stiffness for the SLS and ULS can enhance the performance of timber structures. Some examples are the following:

- enhanced performance in the SLS;
- enhanced vibrational performance [1];
- achievement of optimized moment distribution [2, 3], leading to a more economical design;
- enhanced sideway stability of timber arches [4].

The post-elastic behaviour of a connection and its ability to dissipate energy may, as well, be important with respect to robustness [5, 6] or seismic design [7].

The load-carrying capacity and the stiffness of traditional connections with fasteners loaded perpendicular to their axis (e.g. dowels, bolts or screws) are limited by the embedding strength and stiffness of wood as well as the bending capacity and stiffness of the fasteners. A typical drawback of these connections is the low initial stiffness as a result of the gap between the fasteners and the surrounding wood. Moreover, connections with dowel-type fasteners require a significant amount of time for assembly on site. When subjected to cyclic loading they are prone to the 'pinching effect', i.e. the stiffness degradation and thinning of hysteresis loops during subsequent cycles [8]. Finally, these fasteners induce tensile stresses perpendicular to the grain. As a result, reinforcement in the form of self-tapping screws (abbr. STS) or glued plates is often used to enhance their mechanical behaviour.

Connections with fasteners loaded mainly along their axis (either screwed-in or glued-in) can be an alternative to connections with dowel-type fasteners. These fasteners may, to some extent, play the same role in timber structures as reinforcement bars do in concrete structures. They feature high withdrawal capacity and stiffness due to their ability to distribute stresses over their length and thus they can contribute to the development of strong and stiff connections. In comparison to the connections with dowels the pinching effect is significantly smaller [8]. Pre-installation in components can make them suitable for industrialized building concepts and reduce the erection time and labour costs on site.

Connections with axially loaded glued-in-rods (e.g. [8, 9]) are prone to uncertainties in the constructional quality during the gluing-in process and the sensitivity of glue to high temperatures with respect to their capacity [10] and stiffness [11]. They are also characterized by a very brittle behaviour which combined with the uncertainties in constructional quality may put a structure at risk.

Connections with axially loaded STS or threaded rods embedded with an inclination to the grain direction can be an alternative to connections with dowel-type fasteners or glued-in rods. Today, STS with lengths up to 1000 mm and diameters up to 12-14 mm are available on the market. Threaded rods with diameters up to 25-30 mm can be purchased with almost any length. Inclined arrangements of axially loaded screws allow transfer of shear, tensile and

compressive forces parallel to their axis and moment-resisting connections are possible, see for example [12].

Connections with axially loaded fasteners embedded with small inclinations to the grain direction are prone to splitting cracks. Furthermore, cracking perpendicular to the grain can also occur due to moisture induced stresses [13]. Moisture induced stresses are generally highest at member ends where connections are usually located. However, the inclined STS or threaded rods of the connection can arrest cracks which may form along the grain, and thus transfer stresses across cracks. Moreover, cracking may be reduced by the introduction of reinforcement in the form of long self-tapping screws, see for example [14, 15]. Reinforcements can also reduce the brittleness of connections.

For axially load loaded screws, the risk of cracks and consequently brittle failure modes is probably the major reason for the lack of design rules. Eurocode 5 (abbr. EC5) [16] imposes a limitation to the angle between the screw-axis and the grain direction ($\alpha \geq 30°$) without taking into account that splitting may be prevented by reinforcement. This limitation leads to a lack of guidelines for the strength verification of STS and threaded rods embedded with small inclinations to the grain direction. Ductile connections can be achieved by use of capacity design [17]. In this case, the embedment length which is required to achieve ductile steel failure is required.

EC5 [16] contains no rules for the withdrawal stiffness of axially loaded screws which is necessary for the determination of the stiffness of connections, see for example [18, 19]. Some rules for the determination of the withdrawal stiffness of STS with diameters up to 12-14 mm can be found in some technical approvals. However, for threaded rods with greater diameters there is lack of guidelines concerning their stiffness properties. The respective available research results are generally limited to relatively short threaded rods embedded either parallel or perpendicular to the grain, see for example [20, 21]; exception is the experimental investigation carried out by Blaβ and Krüger [22] for threaded rods with embedment lengths 200 and 400 mm and α= 45°, 90°. Moreover, EC5 [16] provides no means for the estimation of the distributions of stresses and displacements.

Finally, a pair of axially loaded threaded rods in a connection can be sufficient to achieve high capacity and stiffness. In order to avoid block failures, it is favourable to insert rods in a 'parallel' configuration, i.e. in a row perpendicular to the plane of the grain. The minimum required width of a timber element is governed by the minimum edge distances and spacings according to EC5 [16]. For threaded rods

with large diameters the minimum required width is also large and it may be necessary to insert the rods with smaller edge distances and spacings due to lack of available width. Therefore, the effect of small edge distances and spacings on the withdrawal properties is worth investigating.

In short, the lack of knowledge of proper design, documentation of mechanical behaviour, design guidelines and design codes for STS and threaded rods are obstacles for the development of timber connections with these fasteners.

1.2 Objectives

With respect to the problem statement in Section 1.1, the aim of the research presented in this thesis is to provide more comprehensive knowledge about the behaviour of long axially loaded threaded rods with respect to their capacity and their elastic and post-elastic deformation. The following objectives are pursued:

- Review of existing approaches and experimental results.
- Investigation of the withdrawal capacity of single axially loaded threaded rods with varying embedment length and rod-to-grain angle, with emphasis given for angles in the range 0-30° where there is a lack of design rules and experimental results. The determination of the embedment length which is required to achieve ductile steel failure is also an objective with respect to capacity.
- Investigation of the elastic and post-elastic deformation of single axially loaded threaded rods and determination of the withdrawal stiffness.
- Investigation of the withdrawal properties of pairs of threaded rods with small edge distances and spacings embedded in 'parallel', i.e. in a row perpendicular to the plane of the grain.
- Development of methods for the estimation of stress distributions and displacement of threaded rods.

1.3 Limitations

The scope of the present thesis is subjected to the following limitations:

- The withdrawal behaviour of rods subjected to static short-term monotonic loading is investigated. The withdrawal of rods subjected to cyclic, dynamic or long-term loading is not covered and therefore the effects of rate of loading and duration of load are not studied.

4

- Only rods subjected to axial forces are considered. The interaction between axial and lateral forces is not studied.
- The withdrawal behaviour of STS with diameters up to 12-14 mm has been studied by many researchers. In this project, only one type of rods is used, in particular SFS WB-T-20 rods [23] with a diameter of 20 mm.
- Only one strength class of glulam (combined glulam of Scandinavian class L40c) was used in the experimental investigation.
- All specimens were conditioned to standard temperature and relative humidity conditions (20°C/65%RH) leading to approximately 12% moisture content (abbr. MC) in the wood. Therefore the investigation of climate effects is not part of this study. Besides, the influence of MC on the withdrawal properties has already been investigated for STS, see for example [24, 25].

1.4 Structure of the present thesis

The present thesis is divided in three parts:

- **Part I** consists of 5 chapters, including this one. A description of the objectives and limitations of the present work is given. Moreover, an overview of the background research and the present work is provided.
- **Part II** consists of 4 appended papers. In Papers i and ii the elastic and post-elastic behaviour of axially loaded rods is studied. In Paper iii, the behaviour of pairs of threaded rods embedded with small edge distances and spacings is investigated. In Paper iv, the characteristic withdrawal capacity of single rods is studied.
- **Part III** consists of 3 appendices. In Appendix A, some analytical remarks are provided. In Appendix B, the experimental results for single rods are presented in detail. In Appendix C, the numerical results for single rods are presented in detail.

2. Self-tapping screws and threaded rods

2.1 General remarks

Screws for structural timber applications are produced with a variety of sizes and shapes, as shown in Figures 2.1 and 2.2. The European basis for the design of screws is provided by Section 8.7 of Eurocode 5 [16] and by European Technical Approvals (abbr. ETAs). Some ETAs provide also design rules for applications which are not covered by the present version of EC5 [16].

As shown in Figure 2.1 [26], a screw has some or all of the following features:

- head with drive;
- shank;
- shank cutter;
- threaded part;
- tip.

The head diameter, the outer-thread diameter and the core diameter are denoted d_h, d and d_c respectively (note that the symbol d_1 is used for the core diameter in EC5 [16] or for the outer-thread diameter elsewhere, see for example [27]). The outer-thread diameter is also referred to as nominal diameter or just diameter. The length of the threaded part is denoted l_g. The length of the threaded part which is embedded in the timber, is commonly referred to as the embedment/penetration/anchorage length l or as the effective length l_{ef} in EC5 [16]. Some researchers (e.g. [24, 28]) consider a value of l_{ef} smaller than l to take into account the effect of the tip.

According to EC5 [16], metal fasteners should comply with EN 14592 [29]. In this standard, the following requirements for screws are specified:

- Screws should be produced from mild steel or carbon steel wires or austenitic stainless steel wire.
- The diameter of screws should not be less than 2.4 mm and not greater than 24 mm, i.e. 2.4 mm $\leq d \leq$ 24 mm.
- The core diameter should not be less than 60% and not more than 90% of the diameter, i.e. $0.6d \leq d_c \leq 0.9d$.
- Screws should be threaded over a length at least equal to four times the nominal diameter, i.e. $l_g \geq 4d$.

- Characteristic values of (a) yield moment, (b) withdrawal strength parameter, (c) head pull-through parameter, (d) tensile capacity and (e) torsional ratio should be specified according to relevant standards [30-33].
- The grade of the parent material or the thickness of coating should be declared in accordance to annex A of EN 14592 [29], where corrosion protection is required.

Screws not complying with the requirements of EN 14592 [29] can be used, given that their applicability is proven by a technical approval. According to EC5 [16], l_{ef} should be at least $6d$ for axially loaded screws and $4d$ for laterally loaded screws.

Figure 2.1: Features of self-tapping screws [26]

Figure 2.2: Threaded rods

Depending on the manufacturing techniques, screws can be divided in two categories [29, 34]:

- **Traditional screws:** Traditional screws are typically threaded over a part of their length. Their threaded part is turned down from the original rod diameter and therefore their shank diameter is equal to the outer-thread diameter. The mechanical properties of steel are not influenced by the manufacturing technique. Due to the time-consuming and costly manufacturing process and the low strength, traditional screws are not used to a large extent in timber structures [34]. Traditional screws with a shank diameter greater than 6 mm should be driven in pre-drilled holes, given that the timber density is not exceeding 500 kg/m^3 [16]. For higher timber densities the pre-drilling diameter should be determined by tests.

- **Self-tapping screws and threaded rods:** Their threaded part is produced by rolling or forging the wire rod and therefore their shank diameter is thinner compared to the maximum outer-thread diameter. This process results in steel hardening which leads to increased bending, torsional and tensile strength but also to a decrease in ductility. STS with outer-thread diameters up to 12-14 mm and length up to 1000 mm are available today on the market. STS may be threaded over a part of their length or over their entire length, see Figure 2.1. On the other hand, threaded rods feature diameters greater than 15 mm and lengths up to 3000 mm. Threaded rods are typically threaded over their entire length. They are always driven in pre-drilled holes. The diameter and the depth of the lead hole should be equal to the core diameter and the embedment length of the rod, respectively. Threaded rods are also referred to as lagscrews.

Screws and threaded rods are useful in a wide range of applications in timber engineering. Axially loaded screws embedded with an inclination to the grain, have the ability to carry stresses through shear in areas subjected to stresses perpendicular to the grain. Therefore they can prevent or bridge cracks and increase the capacity and stiffness in several applications. This ability makes them suitable in the following applications:

- reinforcement of notched members [14, 35-38] ;
- reinforcement of members with holes [14, 35, 39, 40];
- perpendicular to the grain reinforcements in connections [14, 35, 41-45];
- reinforcement against moisture induced stresses [46];
- reinforcement in the apex zones of double tapered, curved and pitched cambered beams [35, 47];

- reinforcement in members subjected to compressive stresses perpendicular to the grain [14, 48];
- shear reinforcement of members [15, 49];
- connection of composite floors or elements [50-52].

A comprehensive state-of-the-art report of self-tapping screws as reinforcements can be found here [26].

Long screws and threaded rods feature high withdrawal capacity and stiffness due to their ability to distribute shear stresses over their length. This ability makes them suitable as fasteners in connections in order to realize stiff and strong axially loaded or moment-resisting joints. An overview is given in Section 2.3.

2.2 European design regulations

According to EC5 [16], for the verification of resistance of axially loaded screws the following failure modes should be taken into account:

- the withdrawal failure of the threaded part of the screw;
- the tear-off failure of the screw head;
- the pull-through failure of the screw head;
- the tensile failure of the screw;
- the buckling failure of the screw when loaded in compression;
- block shear or plug shear for axially loaded group of screws.

The effectiveness of connections with axially loaded screws may be influenced by insufficient edge and end distances and spacings, as failure modes (splitting or block shear) other than withdrawal may occur. In order to take this into account, modern design codes and technical approvals set restrictions on the minimum edge and end distances and spacings. The minimum edge and end distances and spacings are typically provided as multiple of the diameter. The minimum edge and end distances and spacings according to Eurocode 5, EC5 [16] are provided in Table 2.1. The associated definitions are specified in Figure 2.3. Recent research [53] has shown that block shear failure can occur, even if the minimum spacings are maintained.

The insertion of screws in pre-drilled holes has a positive effect with respect to splitting prevention. DIN 1052 [35] and some technical approvals take into account this positive effect of pre-drilling and allow for reduced edge and end distances and spacings where screws are embedded in pre-drilled holes. However, this positive effect of pre-drilling is not taken into account by EC5 [16].
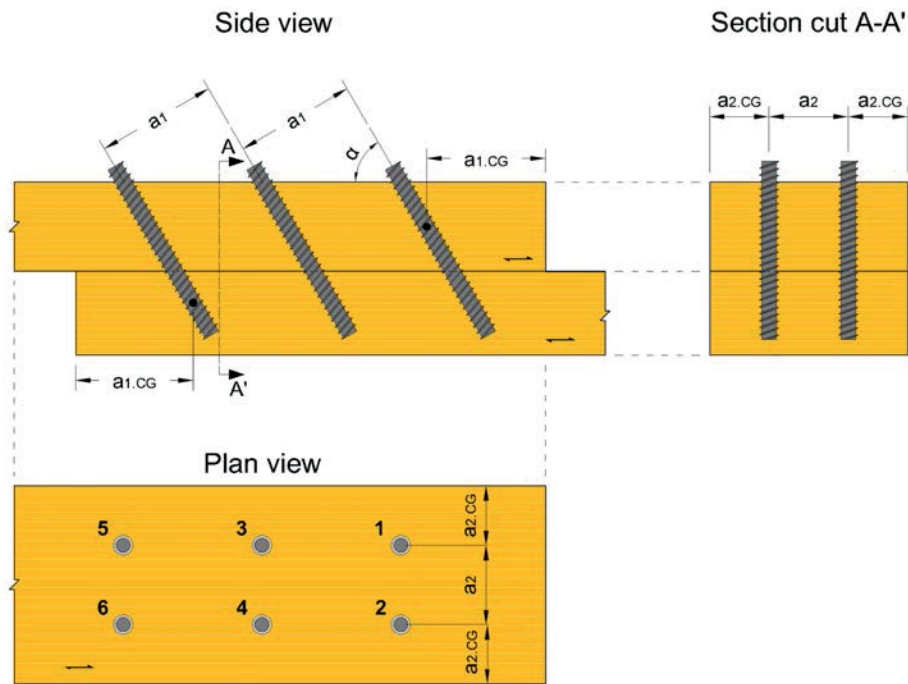
Figure 2.3: Definitions of edge and end distances and spacings according to EC5
[16]

Table 2.1: Minimum edge and end distances and spacings according to EC5 [16]

a_1	$7d$
$a_{1.CG}$	$10d$
a_2	$5d$
$a_{2.CG}$	$4d$

According to EC5 [16], for connections with axially loaded screws the characteristic withdrawal capacity is given as the product of the effective number of screws n_{ef}, the withdrawal strength parameter $f_{ax.\alpha.k}$, the diameter and the embedment length, see Equation (2.1). The withdrawal strength parameter expresses the capacity of a single screw normalized to the product of the diameter and the embedment length (i.e. it equals the withdrawal strength times π). The effective number of screws is taken as the actual number in the power of 0.9, i.e. $n_{ef} = n^{0.9}$ and it also applies to the calculation of the tensile and pull-through capacities of connections with multiple screws.

$$F_{ax.\alpha.Rk} = n_{ef} \cdot f_{ax.\alpha.k} \cdot d \cdot l_{ef} \qquad (2.1)$$

Equation (2.1) provides the characteristic withdrawal capacity both for tensile and compressive loading of the screw.

According to studies [54, 55], the shape of the thread has not a very significant influence on the withdrawal strength. On the other hand, it is mainly depended on the strength class (typically expressed in terms of timber density), the diameter and the angle, α, between the screw axis and the grain direction. It is generally higher for decreasing diameter due to size effect. With regard to the angle, the characteristic withdrawal strength is highest for $\alpha \to 90°$. This is generally not true in terms of mean values but results from the lower variability of the withdrawal strength for increasing angles. This difference in the variability can be attributed to the difference in the failure mode.

For screws embedded parallel to the grain, the surrounding wood is subjected to a combination of longitudinal shear, radial compression, tangential tension and axial stress parallel to the grain. Brittle failure takes place at the interface due to longitudinal shear. The behaviour is stiff and the deformation capacity is small. For screws embedded perpendicular to the grain, the surrounding wood is subjected to cross-grain shear, rolling shear and axial stresses both parallel and perpendicular to the grain depending on the circumferential point. The failure takes place due to cracks which form along the fibres which are bended and subjected to extensive normal deformation. The behaviour is softer, less brittle and characterized by higher deformation capacity. The stress-state is more complex for screws embedded with an angle to the grain.

For screws complying with the requirements of EN 14592 [29] with 6 mm $\leq d \leq$ 12 mm and $0.60 \leq d_c/d \leq 0.75$, the characteristic withdrawal strength parameter is given by Equation (2.2) [16] ($f_{ax.\alpha.k}$ in MPa, d and l_{ef} in mm and ρ_k in kg/m^3).

$$f_{ax.\alpha.k} = \frac{0.52 \cdot d^{-0.5} \cdot l_{ef}^{-0.1} \cdot \rho_k^{0.8}}{1.2 \cdot \cos^2\alpha + \sin^2\alpha} \cdot k_d \quad (\alpha \geq 30°) \qquad (2.2)$$

where $k_d = \min(d/8, 1)$. For all other screws the withdrawal strength parameter is given by Equation (2.3):

$$f_{ax.\alpha.k} = \frac{f_{ax.90.k}}{1.2 \cdot \cos^2\alpha + \sin^2\alpha} \cdot \left(\frac{\rho_k}{\rho_a}\right)^{0.8} \quad (\alpha \geq 30°) \qquad (2.3)$$

where $f_{ax.90.k}$ is the characteristic withdrawal strength parameter perpendicular to the grain, determined in accordance with EN 14592 [29] for the associated density ρ_a.

As indicated by Equations (2.2)-(2.3), EC5 [16] does not allow the installation of rods in an angle to the grain less than 30° in order to eliminate the risk of splitting failure. In practice however, it may be desired to install STS or threaded rods in an angle to the grain smaller than 30°, in combination with some sort of reinforcement to prevent splitting failure.

The characteristic pull-through capacity of connections with axially loaded screws is given by Equation (2.4):

$$F_{ax.\alpha.Rk} = n_{ef} \cdot f_{head.k} \cdot d_h{}^2 \cdot \left(\frac{\rho_k}{\rho_a}\right)^{0.8} \tag{2.4}$$

where $f_{head.k}$ is the characteristic pull-through parameter of the screw determined in accordance with EN 14592 [29] for the associated density ρ_a.

In EC5 [16], the load-carrying capacity of fasteners loaded perpendicular to their axis is calculated by the modified Johansen's equations. These equations are also applicable for screws by use of an effective diameter d_{ef}. For smooth shank screws where the smooth shank penetrates into the member (containing the tip of the screw) by not less than $4d$, d_{ef} should be taken as the smooth shank diameter. In all other cases d_{ef} should be taken as 1.1 times the thread root diameter. Moreover, in connections with laterally-loaded screws the contribution from the rope effect ($F_{ax.\alpha.Rk}/4$) is 100% of the Johansen's part. For screws subjected to combined axial and lateral loading a quadratic failure criterion is proposed by EC5 [16].

Apart from the strength properties, the accurate estimation of deformations is also important for the design both in the SLS and the ULS. In the SLS, the instantaneous stiffness (commonly referred as slip modulus) is necessary input to verify the deformation according to the respective design checks. In the ULS, the corresponding stiffness of connections may have an influence on the distribution of forces and moments in the members and thus it should be accurately estimated and taken into account in the analysis.

In accordance with EC5 [16], for laterally loaded screws the instantaneous slip modulus (under service load) per shear plane per screw is given by Equation (2.5) (K_{ser} in N/mm, ρ_m in kg/m^3 and d in mm). The instantaneous slip modulus for the ULS, K_u, is calculated as 2/3 of K_{ser}, see Equation (2.6).

$$K_{ser} = \frac{\rho_m^{1.5} \cdot d}{23} \tag{2.5}$$

$$K_u = \frac{2}{3} \cdot K_{ser} \tag{2.6}$$

On the other hand, EC5 [16] does not provide any guidelines for the determination of the withdrawal stiffness of axially loaded screws. The instantaneous withdrawal stiffness under service load (in short, withdrawal stiffness) is denoted K_w. It is also referred to as the axial slip modulus and denoted $K_{ax.ser}$ in technical approvals. Some expressions for the determination of the withdrawal stiffness can be found in some technical approvals as functions of the diameter and the embedment length. Equations (2.7)-(2.8) are two examples of such expressions (K_w in N/mm, d and l_{ef} in mm):

- ETA-11/0190[56], ETA-13/0090 [57]:

$$K_w = 780 \cdot d^{0.2} \cdot l_{ef}^{0.4} \tag{2.7}$$

- Z-9.1-472 [27]:

$$K_w = 25 \cdot d \cdot l_{ef} \tag{2.8}$$

With respect to the withdrawal stiffness of STS and threaded rods for the ULS, no guidelines can be found, up-to-date, in technical approvals. According to some researchers, e.g. [58, 59], the stiffness for the ULS may be assumed as the experimentally determined secant stiffness for a load level equal to 60% of the ultimate load.

Concerning Equations (2.7)-(2.8), the following points should be emphasized:

- Equations (2.7)-(2.8) are based on curve-fitting to experimental results and thus they are applicable only for the certain range of diameters and embedment lengths from which they have been derived. Extrapolation outside this range would lead to inaccurate results. Typically, such expressions are derived for screws with diameters up to 12-14 mm and therefore they are not applicable for threaded rods. This is illustrated in Table 2.2 where K_w is determined for various diameters and embedment

lengths according to Equations (2.7)-(2.8) and the method used by the present author [60].

- The influence of the angle between the screw axis and grain direction is not taken into account. Several studies (e.g. [20, 60]) have however shown that the angle has a very significant influence on K_w which increases for decreasing angles. The results in Table 2.2 are illustrative.

- The influence of the diameter and the embedment length is highly non-linear in Equation (2.7) and linear in Equation (2.8). In the investigation carried by the present author [60], it has been shown that the withdrawal stiffness is almost linearly dependent on l_{ef} for small values of l_{ef} and almost independent for large values of l_{ef}.

- As a consequence of the previous point, Equations (2.7)-(2.8) may lead to different results even when they are applied within their valid range. This variation can be explained by the variability of the experimental results. The variability in the experimental results may be attributed to the inherent variability of K_w but also to the lack of a standardized method to measure it.

- The loading conditions are not taken into account in Equations (2.7)-(2.8)

In general, the withdrawal stiffness of screws is much higher than their lateral stiffness, as indicated by the values in Table 2.2. Thus axially loaded screws and threaded rods can contribute to the development of joints with high stiffness. However, the lack of reliable models for the prediction of the withdrawal stiffness is a significant drawback.

Table 2.2: Comparison of estimated withdrawal stiffness values for screws with varying diameter and embedment length

Screw features			K_w (kN/mm)				K_{ser} [b] (kN/mm)
d (mm)	l_{ef} (mm)	l_{ef}/d (-)	Eq.(2.7)	Eq.(2.8)	[60] [a] $\alpha = 0°$	[60] [a] $\alpha = 90°$	Eq.(2.5)
8	40	5	5.2	8.0	9.2	6.1	3.5
	120	15	8.0	24.0	23.8	16.1	
	180	22.5	9.4	36.0	30.2	20.8	
12	60	5	6.6	18.0	20.5	13.4	5.3
	180	15	10.2	54.0	49.6	31.7	
	270	22.5	12.0	81.0	59.9	38.4	
16	80	5	7.8	32.0	35.9	22.7	7.1
	240	15	12.2	96.0	81.9	47.6	
	360	22.5	14.3	144.0	95.5	54.6	
20	100	5	9.0	50.0	55.4 (54.6[c])	33.1 (29.1[c])	8.9
	300	15	13.9	150.0	119.2 (121.0[c])	61.6 (61.4[c])	
	450	22.5	16.4	225.0	135.0 (121.8[c])	68.2 (66.6[c])	

[a] assuming $d_c/d = 0.75$ and the same geometry features as in the experimental specimens [60]

[b] assuming $\rho_m = 470 \, kg/m^3$

[c] experimental results (mean values)

2.3 Joints with axially loaded STS and threaded rods as main fasteners

2.3.1 Axially loaded joints

The load-carrying capacity and stiffness of fasteners loaded perpendicular to their axis (e.g. dowels, screws or bolts) are limited by the wood embedding strength and stiffness, and the bending capacity and stiffness of the fasteners. The introduction of long STS led to an alternative structural concept for axially loaded joints. In this concept, screws are not embedded perpendicular to the member axes but with an inclination, as shown in Figure 2.4.
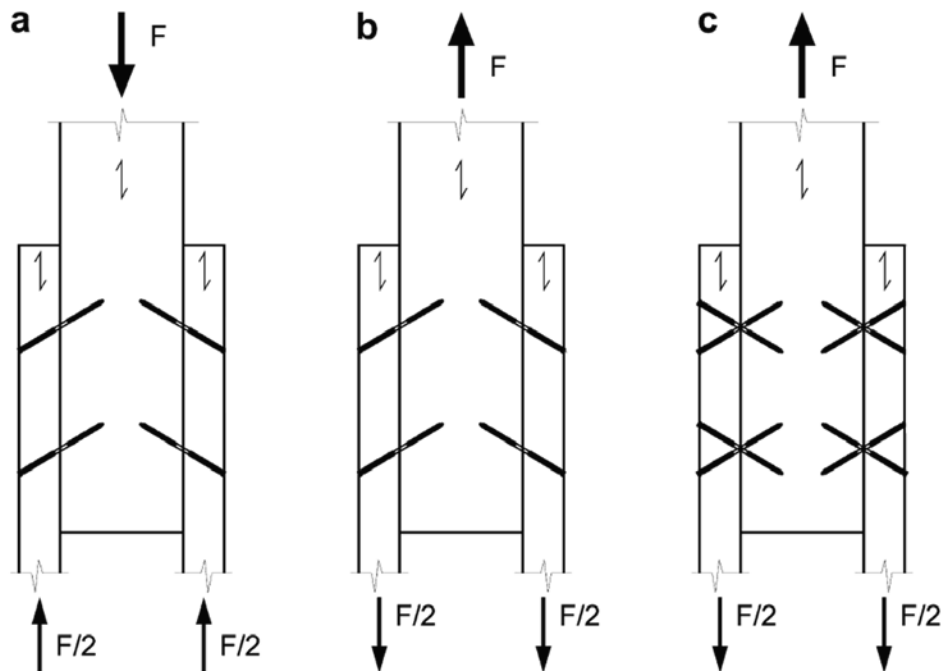
Figure 2.4: Axially loaded joints with inclined screws [18]

Many researchers have investigated the behaviour of axially loaded joints with inclined screws [18, 61-63]. It has been shown that increasing inclination of the screws leads to an increase of the load-carrying capacity and stiffness of the joints. The experimental results obtained by Blass and Bejtka [63] are illustrative for the improved behaviour of joints with inclined screws. In these experiments, the maximum load-carrying capacity was obtained for joints where the screws were embedded with an inclination to the grain, α, equal to 60° and it was 53% higher than the capacity of the reference joint (for α= 90°). The maximum stiffness was obtained for α= 45° and it was 12 times higher than the stiffness of the reference joint. Models for calculation of the load-bearing capacity and stiffness of timber-to-timber joints with inclined screws can be found here [18, 61, 62]. Inclined screws can also be very efficient in steel-to-timber joints where steel plates are used as outer members. An experimental investigation as well as a design proposal can be found here [64].

Another potential application of axially loaded STS or threaded rods could be the fastening of hangers in arch bridges. An example can be found in the conceptual study of the timber network arch bridge [65]. A layout is shown in Figure 2.5. In

such applications fatigue might be of major importance for the withdrawal strength.
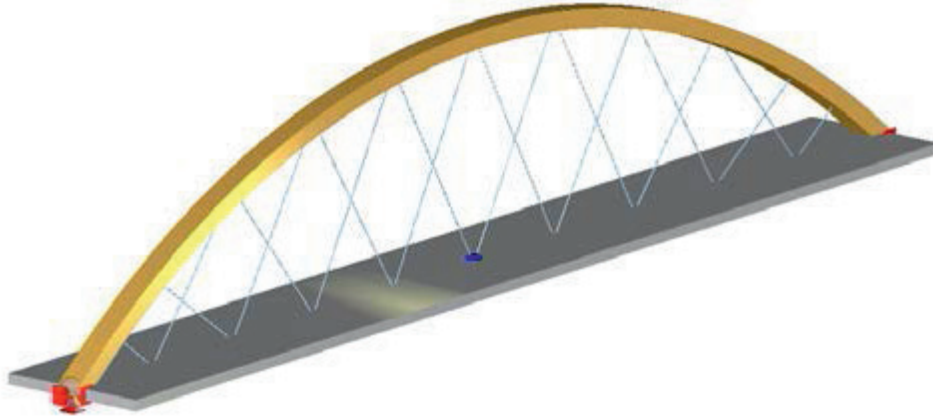

Figure 2.5: Network arch [65]

2.3.2 Moment-resisting joints

Threaded rods and STS have also been used as the main fasteners in moment-resisting joints. In some cases they are embedded parallel to the grain in the beam (and thus perpendicular to the grain in the column), as shown in Figure 2.6a. Examples of such joints can be found in [17, 66]. However, timber members with rods or screws embedded parallel to the grain are prone to splitting due to tensile stresses in the vicinity of the rods. Moreover, additional reinforcement is required to resist shear stresses in the beam. Another drawback may be their poor long-term behaviour [67]. To overcome these drawbacks, threaded rods may be embedded with an inclination to the grain, as shown on principle in Figure 2.6b. Examples of moment-resisting joints with inclined fasteners can be found here [12, 19, 68-70]. The low stiffness of the column, which is subjected to compression perpendicular to the grain, is a drawback. However, its stiffness can be enhanced by reinforcing with STS [48].
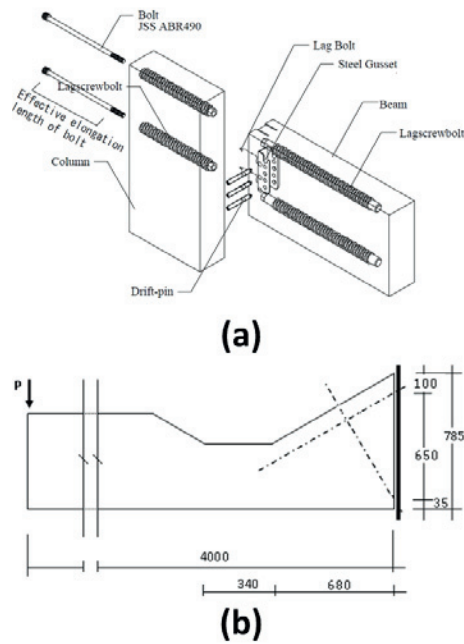
Figure 2.6: Moment-resisting joints with (a) straight rods [17] and (b) inclined rods [19]

An illustrative example of moment-resisting connection with threaded rods is the connection of propeller blades in massive glulam for use in a submerged floating power station [19]. The submerged floating power station (Figure 2.7a) is used for energy production based on ocean currents. The concept for the attachment of the propeller blades to the steel spindle head on the turbine rotor is shown in Figure 2.7b. It consists of long threaded steel rods installed through holes in an adapter steel-plate. The propeller blades carry huge moments. The design moment in this case was about 2500 kNm.

Figure 2.7: (a) Submerged floating power station and (b) concept for fastening of propeller blades [19]

3. Background

The background for the most important research and methods with respect to withdrawal of STS and threaded rods is given in the present Chapter. This background is limited to recent research on screws embedded in solid timber and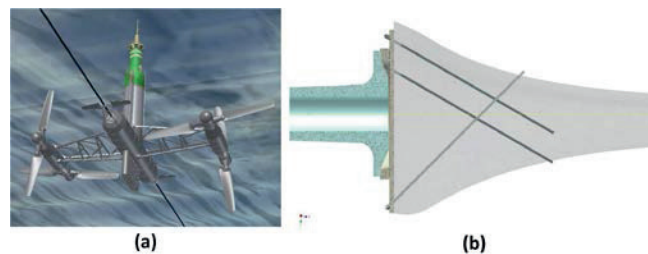 glulam made of softwood. Examples of research on screws embedded in hardwood or other timber products such as LVL and CLT as well as on glued-in rods can be found in [71, 72], [73-75] and [76, 77], respectively. In general, two different approaches can be found in the literature. The first approach is based on regression analysis to experimental results. The second approach is analytical and based on Volkersen theory [78].

3.1 Models based on experimental results

3.1.1 Blaβ et al 2006, 2010

Blaβ et al [79] performed about 800 withdrawal tests of STS produced by various manufacturers. The parameters of this investigation were the diameter (6 mm $\leq d$ $\leq$ 12 mm), the embedment length ($l_{ef} \leq$ 120 mm), the angle between the screw and the grain direction (α= 0, 15, 30, 45, 60, 75, 90°) and the timber density. By regression analysis on the experimental results, they proposed the Equations (3.1)-(3.3) for the characteristic withdrawal capacity, the withdrawal stiffness and the withdrawal displacement which corresponds to the withdrawal capacity, $\delta_{ax.\alpha}$ ($F_{ax.a.Rk}$ in N, $K_{ax.ser}$ in N/mm, $\delta_{ax.\alpha}$, d and l_{ef} in mm).

$$F_{ax.\alpha.Rk} = \frac{0.52 \cdot \sqrt{d} \cdot l_{ef}^{0.9} \cdot \rho_k^{0.8}}{1.2 \cdot \cos^2\alpha + \sin^2\alpha} \tag{3.1}$$

$$K_{ax.ser} = 234 \cdot (\rho_m \cdot d)^{0.2} \cdot l_{ef}^{0.4} \tag{3.2}$$

$$\delta_{ax.\alpha} = \frac{0.0016 \cdot d \cdot \sqrt{\rho_m \cdot l_{ef}}}{1.54 \cdot \cos^2\alpha + \sin^2\alpha} \tag{3.3}$$

Equation (3.1) was the basis for the equation provided in the present version of EC5 [16], while Equation (3.2) is the basis for Equation (2.7) which can be found in several technical approvals.

Blaβ and Krüger [22] performed withdrawal tests of threaded rods embedded in glulam elements. The parameters of this investigation were the diameter (d = 16,

20 mm), the embedment length (l_{ef} = 200, 400 mm) and the rod-to-grain angle (α= 45, 90°). 10 tests were performed for each combination of parameters, giving a total number of 80 tests. Both the withdrawal capacity and stiffness were determined. The withdrawal stiffness was determined for a load level equal to 80% of the maximum load. Two stiffness values corresponding to the displacements on the loading point and the tip of the rod were determined (denoted $K_{ax.o}$ and $K_{ax.u}$ respectively). The results are summarised in Table 3.1.

Table 3.1: Test results by Blaβ and Krüger [22] (Mean values, CoV in parentheses)

d (mm)	α (deg)	l (mm)	F_{ax} (kN)	$K_{ax.o}$ (kN/mm)	$K_{ax.u}$ (kN/mm)
	45	200	45.6 (11%)	32.4 (21.5%)	43.7 (11%)
16	45	400	92.4 (6.4%)	44.3 (8.5%)	102.0 (19%)
	90	200	37.4 (8.5%)	18.2 (11.6%)	22.4 (15%)
	90	400	94.1 (7.1%)	29.7 (11.7%)	79.0 (27%)
	45	200	56.6 (11%)	37.7 (16.3%)	44.8 (22%)
20	45	400	117 (7.1%)	57.7 (11.7%)	120.0 (13%)
	90	200	47.9 (7.5%)	22.6 (11.6%)	25.5 (13%)
	90	400	115 (3.8%)	37.8 (5.6%)	76.3 (15%)

3.1.2 Pirnbacher et al 2009

Pirnbacher et al. [24, 28] analysed a sample of 5524 withdrawal tests of STS embedded in solid timber and glulam elements. Screws produced by two different manufacturers were used in the tests. The effect of the following parameters on the withdrawal strength was investigated:

- moisture content (MC= 0, 6, 12, 20 %);
- temperature (T= -20, 0, 20, 50 °C);
- diameter (d= 8, 10, 12 mm);
- effective length (l_{ef} = 4d, 8d, 12d, 15d);
- embedment of the threaded part (0 ≤ l_{emb} ≤ 240 mm);
- angle to the grain direction (α= 0, 12.5, …, 90°);
- pre-drilling (with and without pre-drilling).

The effect of each parameter on the withdrawal strength was taken into account by a corresponding k-factor derived by the experimental results. These factors express the ratio of the withdrawal strength of specimens with a certain parameter to a reference value.

The proposed k-factor for effect of the MC is given by Equation (3.4). The withdrawal strength of specimens with MC=12% was used as the reference value. In accordance with Equation (3.4), k_{MC} = 0.95 for screws in connections exposed to service class 2 conditions.

$$k_{MC} = \frac{f_{ax.MC}}{f_{ax.MC=12\%}} = \begin{cases} 1.0 & 8\% \leq MC \leq 12\% \\ 1.0 - 0.0065 \cdot (MC - 12\%) & 12\% \leq MC \leq 20\% \end{cases} \quad (3.4)$$

The effect of temperature was not very significant in the tested range and therefore the corresponding factor was taken equal to unity:

$$k_{temp} = 1.0, \quad -20°C \leq T \leq 50°C \quad (3.5)$$

Similarly, the effect of pre-drilling was not very significant and therefore the authors suggested that there should be no differentiation between the two cases.

Concerning the effect of the diameter, the experimental results verified the size-effect (i.e. decreasing strength for increasing diameter). The factor k_{diam} was derived both as a linear function (Equation (3.6)) and as a power function (Equation (3.7)) of the diameter. The withdrawal strength of specimens with d= 8 mm was used as the reference value.

$$k_{diam} = \frac{f_{ax.d}}{f_{ax.d=8}} = 1.322 - 0.0402 \cdot d \quad (d \text{ in mm}) \quad (3.6)$$

$$k_{diam} = \frac{f_{ax.d}}{f_{ax.d=8}} = 2.44 \cdot d^{-0.428} \quad (d \text{ in mm}) \quad (3.7)$$

To take into account the effect of the screw tip the authors proposed the use of a reduced effective length obtained by subtracting $1.17d$ from the embedment length, as indicated by Equation (3.8). The corrected effective length was obtained on the assumption that the withdrawal strength should be independent of the effective length.

$$l_{ef} = l - k_{length} \cdot d = l_{thread} - 1.17 \cdot d \quad (3.8)$$

The effect of the angle α on the characteristic value of the withdrawal strength was taken into account by Equation (3.9) which is a slight modification of the Hankinson formula. The withdrawal strength of specimens with screws embedded perpendicular to the grain was used as the reference value.

$$k_{Hankinson.mod} = \frac{f_{ax.\alpha}}{f_{ax.90}} = \frac{1}{sin^{2.2}(\alpha) + 1.30 \cdot cos^{2.2}(\alpha)} \qquad (3.9)$$

The embedment depth of the threaded part (i.e. the minimum distance of the threaded part of the screw to the surface of the timber element) was also investigated. The mean withdrawal strength of screws whose threaded part was embedded by 15 mm was 1.13 times greater than the strength of screws whose threaded part was not embedded. A slightly increasing mean strength was observed for increasing embedment depths. The effect of embedment depth of the threaded part was taken into account by Equation (3.10). The same effect has been shown also by Baek et al [54].

$$k_{emb} = \frac{f_{ax.emb>15}}{f_{ax.emb=0}} = 1.15 \,, \qquad l_{emb} \geq 2 \cdot d \qquad (3.10)$$

Further investigation carried out by Burgschwaiger [80] showed that the positive effect of the embedment depth of the threaded part is smaller for decreasing angle. The following expression was proposed:

$$k_{emb} = \frac{f_{ax.emb}}{f_{ax.emb=0}} = \begin{cases} 1.0 & l_{emb} = 0 \\ 1.05 + 1.11 \cdot 10^{-3} \cdot \alpha & l_{emb} \geq 2d \end{cases} \qquad (3.11)$$

Equation (3.12) provides the mean or the characteristic withdrawal strength (in MPa) derived from experimental tests under constant climate, as function of the density (in kg/m^3) and the diameter (in mm). The size-effect of the diameter was incorporated in Equation (3.12). These tests were performed without embedment of the threaded part and the withdrawal strength given by Equation (3.10) should be multiplied by k_{emb}= 1.15 if $l_{emb} \geq 2d$. The regression parameters A, B and C are given in Table 3.1 both for α= 90° and α= 0°

$$f_{ax} = A \cdot \rho_{test} + B \cdot (2.44 \cdot d^{0.572}) + C \qquad (3.12)$$

Table 3.2: Regression parameters for Equation (3.12)

	Mean f_{ax}		5%-percentile f_{ax}	
	$\alpha = 90°$	$\alpha = 0°$	$\alpha = 90°$	$\alpha = 0°$
Parameter A	0.01353	0.00538	0.0116	0.0042
Parameter B	-0.28147	-0.45875	-0.272	-0.455
Parameter C	2.18888	5.92460	1.97	5.34

3.1.3 Ringhofer et al 2015

Ringhofer et al [81] presented a universal approach for the determination of withdrawal properties of STS embedded in solid timber, unidirectional (e.g. glulam) and orthogonal (e.g. CLT) timber products. This approach was based in the analysis of 8000 withdrawal tests for the withdrawal strength (with d= 4-12 mm, l_{ef}= 2.5d-15d and 0° $\leq \alpha \leq$ 90°) and 5500 tests for the withdrawal stiffness (with d= 6-12 mm, l_{ef} = 2.5d-39d and 0° $\leq \alpha \leq$ 90°). The timber density, the angle, the system effect for screws penetrating multiple layers in laminated timber products and the MC were taken into account. The authors proposed Equation (3.13) for the determination of withdrawal properties:

$$X = k_{ax} \cdot k_{sys}(N) \cdot X_{ref} \cdot (\frac{\rho}{\rho_{ref}})^{k_\rho} \qquad (3.13)$$

where X = {f_{ax} , $k_{ax.ser}$} represents either the withdrawal strength f_{ax} = F_{ax}/($\pi \cdot d \cdot l_{ef}$) or the withdrawal stiffness normalized per unit area i.e. $k_{ax.ser}$ = $K_{ax.ser}$/($\pi \cdot d \cdot l_{ef}$). The factor k_{ax} takes into account the effect of α, $k_{sys}(N)$ is the system strength factor for screws penetrated in N layers of laminated timber elements and k_ρ is a factor which adjusts a property derived for the reference density to the actual (mean or characteristic) density. For solid timber and glulam, these factors are given by Equations (3.14)-(3.16).

$$k_{ax} = \begin{cases} 1.0 & 45° \leq \alpha \leq 90° \\ c + (1-c) \cdot \dfrac{\alpha}{45°} & 0° \leq \alpha \leq 45° \end{cases} \qquad (3.14)$$

$$k_{sys} = \begin{cases} 1.0 & \text{Solid Timber} \\ 1.13 & \text{Glulam } (N \geq 3) \end{cases} \qquad (3.15)$$

$$f_{ax}: k_\rho = \begin{cases} 1.10 & \alpha = 0° \\ 1.25 - 0.05d & \alpha \neq 0° \end{cases} ; \quad k_{ax.ser}: k_\rho = 0.75 \qquad (3.16)$$

where $c = k_{90}^{-1}$= X_0 / X_{90} and k_{90}= {1.35; 1.56; 0.75} for {$f_{ax.mean}$; $f_{ax.k}$; k_{ser}}.

The reference characteristic withdrawal strength and the stiffness are determined by Equations (3.17)-(3.18).

$$f_{ax.ref.k} = 0.013 \cdot \rho_{ref.k}^{1.11} \cdot d^{-0.33} \qquad (3.17)$$

$$k_{ax.ser.ref} = 24.7 \cdot \rho_{ref}^{0.75} \cdot d^{-1.70} \cdot l_{ef}^{-0.60} \qquad (3.18)$$

The effect of the MC on the withdrawal properties is given by Equation (3.19) [25], where k_{MC} = {0.034; 0.016} for {f_{ax}; $k_{ax.ser}$}.

$$\frac{X_{MC}}{X_{ref}} = \begin{cases} 1.0 & 8\% \leq MC \leq 12\% \\ 1.0 - k_{MC} \cdot (MC - 12\%) & MC \geq 12\% \end{cases} \qquad (3.19)$$

3.1.4 Ringhofer and Schickhofer 2014

In accordance with EN 14592 [29], the experimental determination of the withdrawal strength parameter should comply with the standard test configuration (pull-push) and the loading rate (90±30 sec to reach failure) given by EN 1382 [30]. The load transfer mechanism from the screw to the supports depends on the test configuration, as shown in Figure 3.1. Ringhofer and Schickhofer [67] investigated the effect of several test configurations and loading rates on the withdrawal strength parameter of STS.
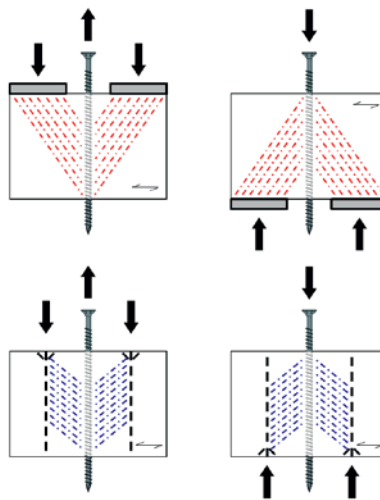
Figure 3.1: Different loading and load path situations [67]

Four different test configurations were investigated as shown schematically in Figure 3.2a; (i) push-pull (ii) push-pile (iii) pull-pull and (iv) pull-pile configurations. STS with d= 8 mm were embedded parallel and perpendicular to the grain both with and without pre-drilling. The experimental results indicated that the mean values of the withdrawal strength and the standard deviation are not significantly affected by different test configurations. Pre-drilling resulted in higher withdrawal

strength for screws embedded parallel to the grain. For screws embedded perpendicular to the grain the effect of pre-drilling was negligible.
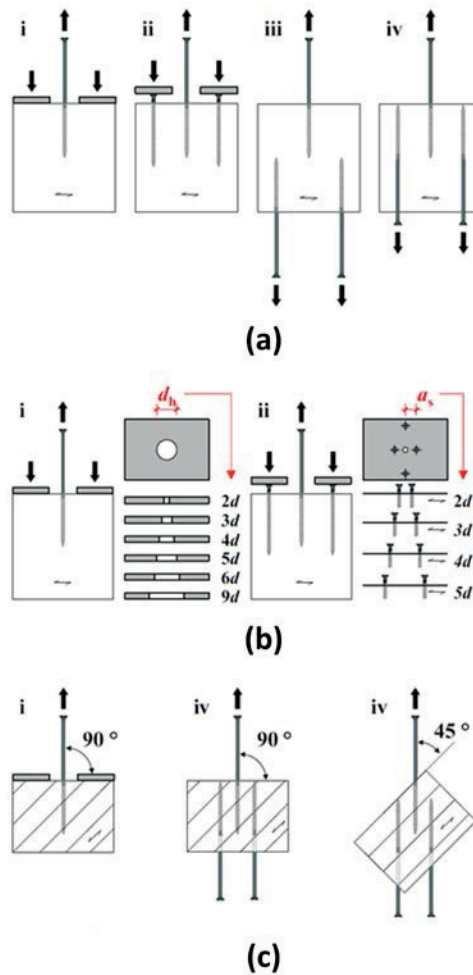
Figure 3.2: Tested configurations [67]

Additional tests were performed in the push-pull and push-pile configurations where the supporting distance was varied, as shown in Figure 3.2b. In general, the varying supporting distance had a small or negligible effect on the withdrawal strength. Significantly lower withdrawal strength was observed for the push-pile configuration with the minimum supporting distance of $2d$, where the volume of the shear field is minimal.

Another test series was executed where the angle between the screw and the surface of the specimen was varied, as shown in Figure 3.2c. Screws with d= 6 mm

were used in this series. The experimental results indicated that the withdrawal strength was not influenced by the angle between the screw and the surface.

Finally, a test series was performed with varying rate of deformation (0.6, 1.50, 2.20, 4.0 and 500 mm/min) so that the targeted time to failure was in the range of 0-300 sec. Screws with d= 8 mm embedded perpendicular to the grain were used in this series. Specimens tested with the 500 mm/min rate of deformation showed higher withdrawal strengths. In the rest specimens, the withdrawal strength was not affected by the rate.

3.1.5 Frese and Blaβ 2009

Frese and Blaβ [55] proposed an optimized regression method for the determination of the characteristic withdrawal strength of STS. The aim was to improve the accuracy and reduce the number of the tests required. The method was based on the analysis of more than 2400 withdrawal tests of STS. The parameters of this investigation were the diameter (d= 4-14 mm), the angle to the grain (α= 45-90°), the effective length (l_{ef} = 18.8-140 mm), the timber density (ρ= 325-602 kg/m^3), the thread pitch (c= 2-8 mm) and the core diameter (d_c/d= 0.559-0.70). A preliminary analysis showed that the thread pitch had negligible influence on the withdrawal capacity and it was excluded from the input parameters. In order to obtain a dataset with the same number of observations per parameter, the dataset size was reduced to 1847 tests. The mean value and the standard deviation was determined for all input and output parameters.

The final dataset was used for regression analysis. The input parameters, their squared values and their products, excluding the term $d \cdot d_c/d$, were used as the independent variables (25 terms in total). The natural logarithms of the withdrawal capacity and the withdrawal strength parameter were the output variables. Regression from the output variables, where the number of terms was increased from 1 to 25, resulted in the combinations with the highest coefficients of determination. As expected, the influence of d and d_c was similar. Moreover, there was no indication that α was relevant in its range (45-90°). Equations (3.20)-(3.21) were derived by following this procedure and by selecting models with a limited number of input variables so that they are mechanically logical and easy to apply. The errors of Equations (3.20)-(3.21) were taken into account by adding an error term e, which follows a normal distribution. A few observations with standard errors out of (-3; 3) were excluded as outliers. The size of the dataset without the outliers, the coefficient of determination and the distribution parameters of the standard errors are also provided in Equations (3.20)-(3.21).

$$\ln(F_{ax}) = 6.739 + 0.03257 \cdot l_{ef} + 2.148 \cdot 10^{-4} \cdot d \cdot \rho - 1.171 \cdot 10^{-4} \cdot l_{ef}{}^2 + e \qquad (3.20)$$
$$N = 1838, \quad r^2 = 0.945, \quad e: N(0; 0.1365)$$

$$\ln(f_{ax}) = 2.359 - 0.04172 \cdot d + 2.039 \cdot 10^{-3} \cdot \rho + e \qquad (3.21)$$
$$N = 1839, \quad r^2 = 0.466, \quad e: N(0; 0.1331)$$

Equations (3.20)-(3.21) provide the withdrawal capacity and the withdrawal strength parameter as function of the individual density. In design however, characteristic values are involved. In order to obtain expressions which incorporate characteristic values, Equations (3.20)-(3.21) were used to create datasets with simulated values. STS with d= (4, 6, 8, 10, 12, 14 mm) and l_{ef} = (20, 40, 60, 80, 100, 120, 140 mm) and six strength classes (C14, C18, C24, C30, C40 and C50) were considered. The density for each strength class follows a normal distribution with known mean value and standard deviation. The total number of possible combinations of d, l_{ef} and strength class is 252. For each one of these combinations, 1000 values were simulated both for the withdrawal capacity and the withdrawal strength parameter. Based on the simulated values, the characteristic output values for each combination were determined. A new regression from the simulated characteristic values lead to Equations (3.22)-(3.23) which provide the characteristic values of the withdrawal capacity and the withdrawal strength parameter.

$$\ln(F_{ax.Rk}) = 6.54 + l_{ef} \cdot \left(0.03265 - 1.173 \cdot 10^{-4} \cdot l_{ef}\right) + 2.35 \cdot 10^{-4} \cdot d \cdot \rho_k \qquad (3.22)$$

$$\ln(f_{ax.k}) = 2.182 - 0.04175 \cdot d + 2.21 \cdot 10^{-3} \cdot \rho_k \qquad (3.23)$$

An alternative expression, simpler than Equation (3.23), for the withdrawal strength parameter was also derived by use of the same procedure. This expression is given by Equation (3.24).

$$f_{ax.k} = 0.0872 \cdot \rho_k \cdot d^{-0.4119} \qquad (3.24)$$

3.1.6 Kennedy et al 2014

Kennedy et al [82] evaluated five different equations for the withdrawal capacity. The following equations were evaluated:

- the equation given by the Canadian standard CSA O86-09 [83] for wood screws;

- the equations given by the American standard NDS-2012 [84] for wood screws and lagscrews;
- McLain [85] equation for lagscrews;
- MHBH [82, 86] equation for lagscrews.

All equations relate the characteristic withdrawal capacity with the diameter d, the relative density G and the effective length l_{ef} and they have the following format (units N and mm):

$$P_{u.w.k} = A \cdot d^B \cdot G^C \cdot l_{ef}{}^D \qquad (3.25)$$

The parameters A, B, C and D are given in Table 3.3.

Table 3.3 Parameters A, B, C and D for Equation (3.25) [82]

Equation	A [a]	B	C [a]	D
CSA O98-09 [83]	59 (112)	0.82	1.77	1.0
NDS-2012-Lagscrews [84]	57 (116)	0.75	1.50	1.0
NDS-2012-Wood screws [84]	40 (98)	1.00	2.00	1.0
McLain [85]	74 (165)	0.61	1.35	1.0
MHBH [b] [86]	82 (110)	0.75	1.50	1.0

[a] The values in parentheses are used for the calculation of mean values. The measured relative density G_0 should be used instead of G in this case.

[b] The equation for the characteristic density has different format than Equation (3.25): $P_{u.w.k} = \left(82 \cdot d^{0.75} \cdot G_0{}^{1.5} - 56\right) \cdot l_{ef}$, $P_{u.w.mean} = 110 \cdot d^{0.75} \cdot G^{1.5} \cdot l_{ef}$

In order to evaluate the validity of all equations, experimental results from several studies were collected to build a database. The database consisted of experimental results from tests of wood screws (STS) and lagscrews with various diameters and effective lengths, embedded in both solid timber (563 tests) and in glulam (2580 tests). The database for solid timber was composed of the results from Kennedy [87], Newlin and Gahagan [88] and Baek et al [54]. The database for glulam was composed of the results from Kennedy [87], Abukari et al [89], Abukari [90], Gehloff [91] and Simpson Strong Tie [92].

Non-linear regression analysis was performed for the mean values and several statistical parameters which estimate the error were determined. After evaluating these parameters, the authors concluded that all equations were capable of predicting the mean withdrawal capacity reasonably well. Among them, the

equation of NDS-2012 for lagscrews [84] showed the best fit to the experimental results. However, they proposed the equation of CSA O86 [83] for the next edition of the Canadian standard, because it is reasonably conservative and it allows harmonization of design for all types of screws.

3.1.7 Mahlknecht et al 2014

Mahlknecht et al 2014 [53] investigated experimentally the behaviour of axially loaded groups of STS with d= 6 mm, embedded perpendicular to the grain. Three experimental series were executed. In the first series, 5×5 screws with l_{ef}= 11.2d, a_2 = 3.5d and a_1= (5d, 7.5d, 10d, 12.5d) were embedded in solid timber elements (C24). In the second one, 3×4 screws with l_{ef}= 28.3d, a_2= (2.5d, 3.5d, 5d) and a_1= (5d, 7.5d, 10d) were embedded in glulam elements (GL24h). In the third one, 3×5 screws with l_{ef} = 17.8d, a_2= (3.5d, 5d, 7d) and a_1= (5d, 7.5d, 10d) were embedded in glulam elements (GL24h). The effective length was determined according to Pirnbacher et al [24].

The observed failure modes are shown in Figure 3.3. In general, specimens with greater effective length and spacings failed due to steel fracture, specimens with intermediate effective length and large spacings failed due to withdrawal of the screws and specimens with small spacings failed due to block shear. Mixed failure modes were also observed. Block shear has also been observed in the experiments performed by Plieschounig [93] in specimens with 9, 16 and 25 screws, l_{ef}= 11.3d and a_1= a_2= 5d. It is worth mentioning that block shear occurred even at specimens with spacings allowed by EC5 [16] or technical approvals. In cases where block shear did not occur, the capacity of the group of screws was equal to the capacity of single screws times the number of screws, i.e. n_{ef}= n.

The principle of the model presented by Zarmani and Queneville [94] for rivet connections was used in order to develop a first analytical approach for the determination of the block shear capacity. The predictions of this approach were conservative but able to follow the trends observed in the experimental results.

Figure 3.3: Failure modes of specimens (a) steel fracture, (b) withdrawal and (c) block shear [53]

3.1.8 Gehri 2009

Gehri [95] investigated experimentally the effect of spacings on the withdrawal strength of screws embedded parallel to the grain in solid timber and glulam elements. STS with d= 10 mm and l_{ef} = 130 mm were used. Specimens with a variation of the number fasteners (n= 1, 4, 9, 16) and spacings (a/d= 3, 4, 6) were tested.

Based on the experimental results, the author concluded that the withdrawal strength is not influenced for spacings greater than a threshold value of 5d. It follows that n_{ef} = n in this case. Smaller spacings resulted in lower withdrawal strength. The test results were similar to respective results for glued-in-rods [96, 97]. The author proposed Equation (3.26), based on an equation initially developed for glued-in-rods [97], to determine the factor k_{red} which takes into account the effect of spacings.

$$k_{red} = (a/5d)^{0.35} \leq 1.0 \qquad (3.26)$$

3.1.9 Krenn and Schickhofer 2009

As discussed in Section 2.3.1, Krenn and Schickhofer [64] investigated the behaviour of axially loaded joints with multiple inclined screws and steel plates as outer members. STS with d= 8 mm were embedded in glulam elements with an inclination of 45° and 30° to the grain direction. The spacings and edge and end distances were complying with the requirements of the technical approvals.

Several failure modes were observed (withdrawal, head tear off, splitting and tension failure of the timber member). The values of n_{ef} for the capacity (5%-level) are shown in Figure 3.4 for all failure modes. According to Figure 3.4, the effect of the number of fasteners on the capacity is rather small. The prediction of EC5 [16] is very conservative for increasing number of fasteners. The authors proposed n_{ef} = 0.9n (solid green line) instead of n_{ef} = $n^{0.9}$ which provides a less conservative but still safe-side estimation. This proposal is very similar to Equation (3.27) which is provided by some technical approvals for inclined screws with 30° ≤ α ≤ 60° (e.g. [56, 98, 99]) and results in a different value only for n= 2.

$$n_{ef} = max(n^{0.9}, 0.9n) \qquad (3.27)$$

The obtained effective numbers of screws under service load $n_{ef.ser}$ are plotted in Figure 3.5. The authors proposed $n_{ef.ser}$ = $n^{0.8}$ to take into account the effect of the number of screws on the stiffness.
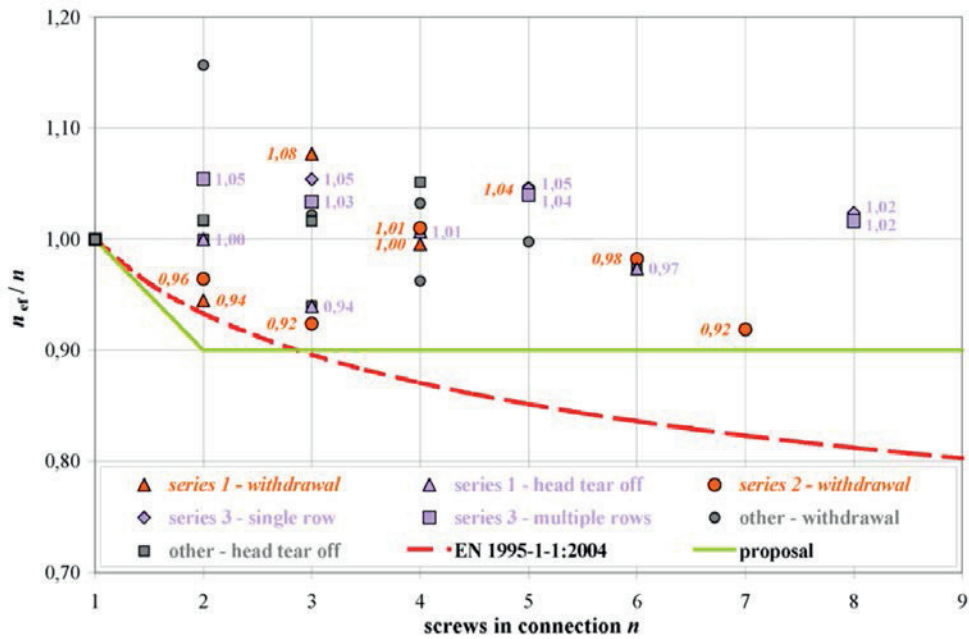
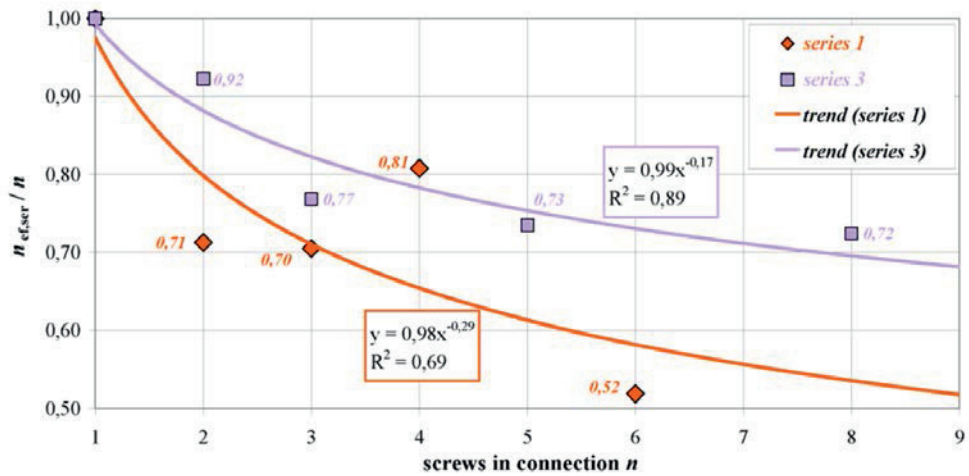**Figure 3.4:** Effective number of screws for capacity [64]

Figure 3.5: Effective number of screws for stiffness [64]

3.1.10 Uibel and Blaß 2010

According to results from conventional tests [100] minimum spacings and end distances vary for screws with the same diameter but different geometry. They also vary for screws with the same geometry but different diameter.

31

Consequently, tests results for a specific screw are not transferable to other screws of the same type or screws with the same diameter. Uibel and Blass [100] developed a method for the determination of suitable end distances and spacings for axially loaded screws. This method was based on the measurement of lateral forces during process of screwing-in and therefore it could be an alternative to extensive conventional pull-out testing.

Two-part specimens made of solid timber or glulam were used. The specimens were connected with 6 bolts which were also used to measure the lateral forces during the process of screwing-in. The forces were measured indirectly by strain gauges attached in a hole at the centre of each bolt. The specimen is shown in Figure 3.6a. Three types of screws with d= 8 mm were embedded in the specimens. High correlation was observed between the total measured lateral force in the bolts and the minimum end distances determined by conventional tests. Therefore the method was able to predict the effect of screw shape and geometry on splitting behaviour.

The effect of end and edge distances and material properties on the splitting behaviour was taken into account by a developed FE model. The model was used to predict the resulting split area. The screw insertion was approximated by an equivalent moving load which is iteratively determined so that the best fit with the experimental results is obtained. The split area was also experimentally observed using a dyeing technique. The experimentally observed and the simulated split areas were in good agreement as shown for example in Figure 3.6b.
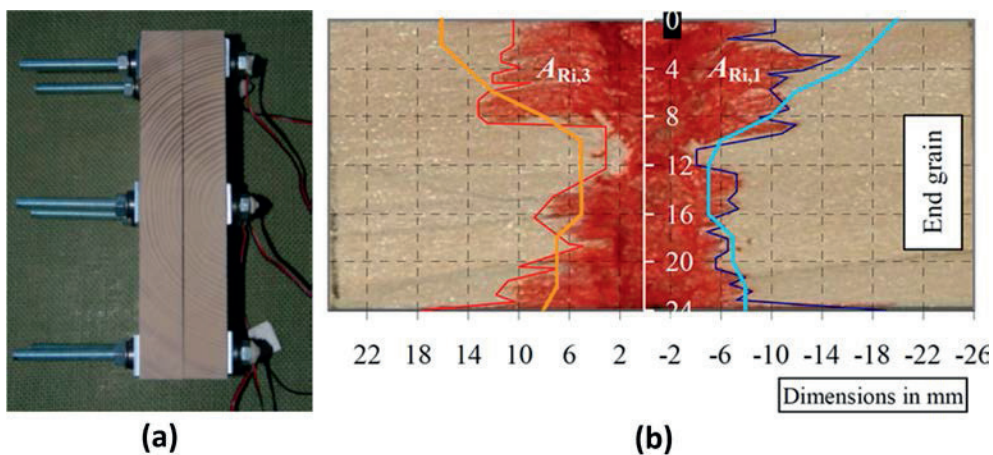

Figure 3.6: (a) two-part specimen and (b) split area [100]

3.2 Analytical models

The approaches presented in Section 3.1 are based on regression analysis on experimental results. These approaches lead to relatively simple expressions which provide the withdrawal capacity and/or stiffness and they are suitable for practical design. The effect of various parameters, such as the MC, the size and the number of screws on the withdrawal properties has also been quantified.

On the other hand, the applicability of such expressions is limited to screws with parameters within the range of the tested specimens and, in general, they cannot be extrapolated outside this range. Moreover, these approaches do not provide explicit information about important aspects of the mechanical behaviour as for example the stress and displacement distributions along the screws, the force-displacement curves and the brittleness.

In the following Sections, the existing analytical models are briefly presented. All these models are based on the theory of Volkersen [78] which was initially developed for rivet connections. Essentially the same theory has been successfully used for the analysis of lap joints [101], axially loaded glued-in rods [102] and axially loaded glued-in hardwood dowels [103].

3.2.1 Volkersen model for axially loaded screws

Volkersen theory [78] has successfully been applied for axially loaded screws. The theory and the assumptions are very similar to the model presented by Jensen et al [103] for axially loaded glued-in hardwood dowels. A brief description of this model is given in this Section.

An axially loaded threaded fastener embedded parallel to the grain in a wooden element and the stress state of an infinitesimal thin slice dx are shown schematically in Figures 3.7a and 3.7b, respectively. Two different loading conditions are considered; pull-pull and pull-push as shown in Figure 3.7c. The fastener and the element are assumed to be in a state of pure axial stress and linear-elastic behaviour is assumed:

$$\sigma_s(x) = E_s \cdot \varepsilon_s(x) \tag{3.28}$$

$$\sigma_w(x) = E_w \cdot \varepsilon_w(x) \tag{3.29}$$

where σ, ε, E symbolize the axial stress, the axial strain and the Young's modulus respectively. The subscripts s and w denote the fastener and the wooden element respectively. Here E_w is equal to the Young's modulus parallel to the grain.
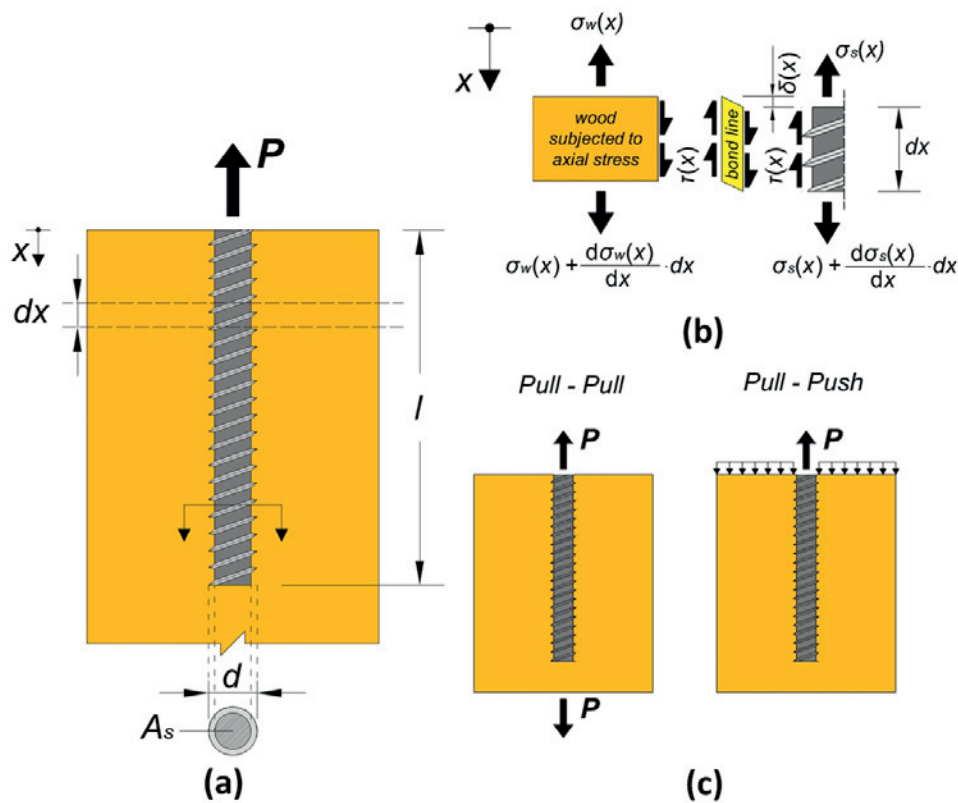
Figure 3.7: Axially loaded fastener: (a) geometric features, (b) stress state of infinitesimal slice dx and (c) loading conditions

All shear deformation is assumed to occur in an infinitely thin layer (bond line) which is in a state of pure shear. The shear stress is denoted $\tau(x)$. The shear displacement of the bond line $\delta(x)$ is equal to the relative displacement between the fastener and the wooden element:

$$\delta(x) = u_s(x) - u_w(x) \tag{3.30}$$

A linear constitutive law is assumed for the relationship between $\tau(x)$ and $\delta(x)$:

$$\tau(x) = \Gamma \cdot \delta(x) \tag{3.31}$$

Γ is a shear stiffness parameter of the bond line. The parameters α and ω are defined as follows:

$$\alpha = \frac{E_w A_w}{E_s A_s} \tag{3.32}$$

$$\omega = \sqrt{\pi d \Gamma l^2 \cdot \left(\frac{1}{E_s A_s} + \frac{1}{E_w A_w}\right)} \tag{3.33}$$

where A_s and A_w are the cross-section areas of the fastener and the wooden element respectively. Static equilibrium of the infinitesimal slice dx and use of Equations (3.28)-(3.33) lead to the following governing differential equation:

$$\frac{d^2 \delta(x)}{dx^2} - \left(\frac{\omega}{l}\right)^2 \cdot \delta(x) = 0 \tag{3.34}$$

The solution of Equation (3.34) and therefore the stress and displacement distributions depend on the loading conditions.

- **Pull-pull**

For the pull-pull loading condition, the distribution of the shear stress is given by Equation (3.35).

$$\tau(x) = -\frac{P\omega}{\pi dl(1+\alpha)\sinh\omega} \cdot \left(\cosh\left(\frac{\omega x}{l}\right) + \alpha\cosh\left(\omega\left(1-\frac{x}{l}\right)\right)\right) \tag{3.35}$$

Equation (3.35) is a hyperbolic function, whose absolute maximum is either at $x=0$ or $x=l$, depending on the value of α. The withdrawal capacity $P_{u.w}$ is given by Equation (3.36) and it is obtained by setting the maximum shear stress, $\tau_{max}=\max(\tau(0), \tau(l))$ according to Equation (3.35) equal to the shear strength f_v, i.e. a maximum stress criterion is used.

$$\frac{P_{u.w}}{\pi dl f_v} = \frac{(1+\alpha)\sinh\omega}{\omega} \begin{cases} \dfrac{1}{\alpha + \cosh\omega}, & \alpha \leq 1 \\[2mm] \dfrac{1}{1+\alpha \cdot \cosh\omega}, & \alpha \geq 1 \end{cases} \tag{3.36}$$

The withdrawal stiffness is given by Equation (3.37).

$$K_w = \pi dl\Gamma \frac{(1 + \alpha)\sinh\omega}{\omega \cdot (1 + \alpha\cosh\omega)} \qquad (3.37)$$

- **Pull-push**

For the pull-push loading condition, the distribution of the shear stress is given by Equation (3.38).

$$\tau(x) = -\frac{P\omega}{\pi dl} \cdot \frac{\cosh\big(\omega(1 - x/l)\big)}{\sinh\omega} \qquad (3.38)$$

Equation (3.38) is a monotonic hyperbolic function, whose absolute maximum is always at x= 0. The withdrawal capacity $P_{u.w}$ is given by Equation (3.39) and it is obtained by setting the maximum shear stress according to Equation (3.38) , τ_{max} = $\tau(0)$, equal to the shear strength f_v. The withdrawal stiffness is given by Equation (3.40).

$$\frac{P_{u.w}}{\pi dl f_v} = \frac{\tanh\omega}{\omega} \qquad (3.39)$$

$$K_w = \pi dl\Gamma \frac{\tanh\omega}{\omega} \qquad (3.40)$$

3.2.2 Nakatani et al 2004-2010

Essentially the same expressions as the ones presented in Section 3.2.1 have been derived by Nakatani et al [21, 104] for axially loaded screws embedded either parallel or perpendicular to the grain. In these expressions, f_v is replaced by the withdrawal strength ($f_{w.0}$ or $f_{w.90}$) which can be determined by pull-out tests of specimens with small embedment length. The shear stiffness parameter Γ can also be determined by these tests. Depending on α, the respective Young's modulus ($E_{w.0}$ or $E_{w.90}$) should be used.

A lagscrew-bolt is a special type of screw which features an internal hole with female thread so as to allow bolts to be screwed into this hole. Lagscrew-bolts feature outer-thread diameters 25-35 mm. An example of a lagscrew-bolt is shown in Figure 3.8.

Nakatani and Komatsu [21] performed withdrawal tests of *Douglas-fir* glulam specimens with lagscrew-bolts embedded parallel to the grain direction. The outer-thread diameter of the lagscrew-bolts was $d=$ 30 mm. The loading condition in these tests was pull-push. The embedment length varied from 50 mm to 280 mm. The experimentally recorded withdrawal capacity and stiffness and the predictions by Equations (3.39)-(3.40) are shown as functions of l in Figure 3.9. The predictions and the experimental results were generally in good agreement. However, the withdrawal capacity is underestimated by Equation (3.39) for the maximum embedment length.
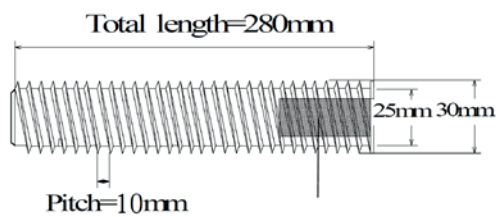
Figure 3.8: Example of a lagscrew-bolt [21]
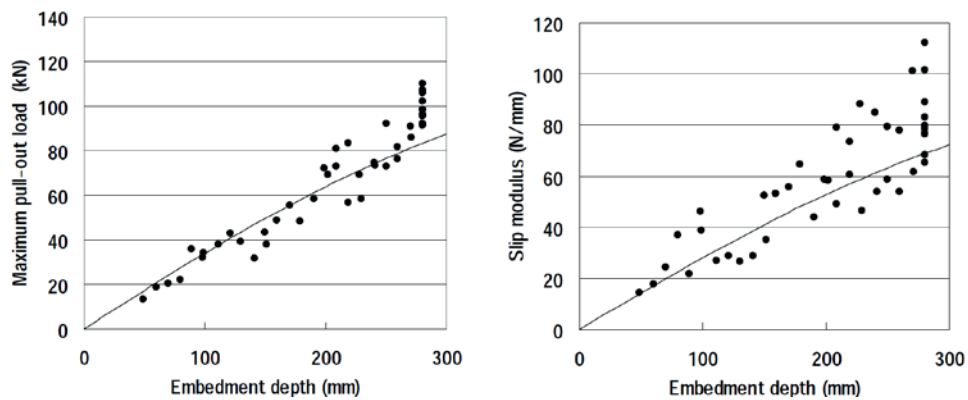
Figure 3.9: Withdrawal capacity and stiffness as function of the embedment length l [21]

Mori et al [20] performed withdrawal experiments of multiple lagscrew-bolts with $d=$ 25 mm and $l=$ 200 mm, embedded parallel and perpendicular to the grain in glulam elements made of European red pine (*Pinus Sylvestris*). Pull-pull loading was applied. The authors proposed methods for calculation of an effective value of A_w. The agreement between the theoretical predictions for withdrawal capacity

37

and the corresponding experimental results was relatively good. On the other hand, a disagreement between the prediction for stiffness and the experimental results was observed. The authors concluded that the withdrawal capacity per fastener is equal to the capacity of a single fastener, if the spacings were greater than $4d$. For smaller spacings, the capacity per fastener was found to be 80-90% of the capacity of a single fastener.

Nakatani and Walford [105] investigated the effect of edge distances on the withdrawal properties of lagscrew-bolts embedded parallel to the grain and loaded in the pull-pull loading condition. Lagscrew-bolts with $d=$ 25 mm and $l=$ (120, 170, 220, 270 mm) were used. Specimens were made of *Pinus Radiata* glulam and they had a square cross section with varied dimensions (75×75, 100×100 and 140×140 mm^2). According to experimental observation, almost all specimens with the smallest cross-section failed due to splitting failure while the vast majority of specimens with larger cross-section failed due to withdrawal. There was no effect of the cross-section on the withdrawal capacity. The authors used Equation (3.36) to predict the withdrawal capacity and a simple method that takes into account the thread geometry to estimate the splitting capacity. The prediction by Equation (3.36) generally overestimated the withdrawal capacity. The prediction for the splitting capacity was conservative for specimens with $l \geq$ 170 mm. According to the theoretical results the failure mode would change for a square cross section with dimensions 85×85 mm^2.

3.2.3 Jensen et al 2010-2012

Jensen et al [106-108] developed a modified version of the model presented in Section 3.2.1. The model is applicable for axially loaded screws embedded parallel to the grain direction.

One of the modifications was the adaptation of a failure criterion which takes into account the damage caused by the process of screwing-in. The damage is expressed in terms of an initial shear stress, τ_{ini}, and therefore a reduced shear strength value $(f_v - \tau_{ini})$ should be used instead of f_v in Equations (3.36) and (3.39).

An effective value for the shear stiffness parameter Γ was obtained using the fracture energy approach proposed by Jensen et al 2001 [103]. This approach is shown schematically in Figure 3.10. The real non-linear τ-δ relationship is idealized by a linearized constitutive relation with equal shear strength and mode II fracture energy dissipation, G_f. From Figure 3.10 it follows that:

$$\Gamma = \frac{f_v{}^2}{2 \cdot G_f} \tag{3.41}$$

The use of this effective value of Γ however would lead to unreasonable predictions for the stiffness according to Equations (3.37) and (3.40).
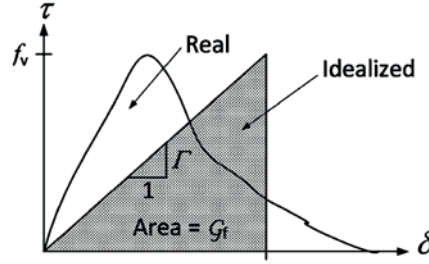
Figure 3.10: Linearized constitutive τ-δ relationship based on fracture energy [103]

Another modification [107] was the introduction of a mean-stress failure criterion instead of the maximum stress criterion used in Equations (3.36) and (3.39), to take into account that a high shear stress over a very limited length may not lead to failure. According to the mean-stress criterion failure takes place when the mean stress over a certain length l_0 reaches the shear strength, as shown in the shear stress distribution in Figure 3.11. The mean stress length for pure II failure mode as given by Gustafsson [109] was used:

$$l_0 = \frac{2}{\pi} \cdot \frac{E_{w*} \cdot G_f}{f_v{}^2} \tag{3.42}$$

$$\frac{1}{E_{w*}} = \frac{1}{E_{w.0}} \cdot \sqrt{\frac{1}{2} \cdot \sqrt{\sqrt{\frac{E_{w.0}}{E_{w.90}}} + \frac{E_{w.0}}{2G} + \nu_{90.0} \cdot \frac{E_{w.0}}{E_{w.90}}}} \tag{3.43}$$

where G is the shear modulus and $\nu_{90.0}$ is the Poisson ratio for strain applied in the perpendicular to the grain direction.
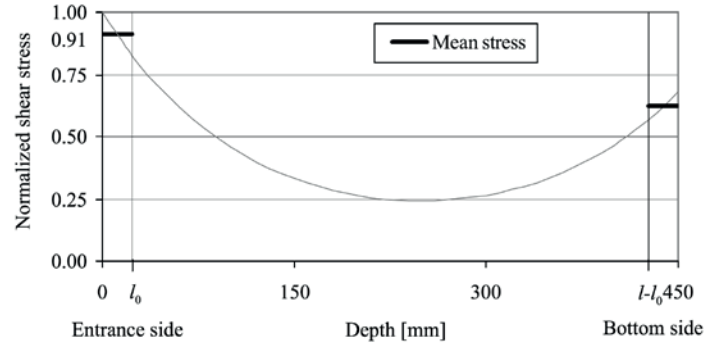
Figure 3.11: Normalized shear stress distribution along screw (pull-pull) [107]

Incorporating these modifications, Equations (3.36) and (3.39) can be re-formulated as follows:

- Pull-pull:

$$\frac{P_{u.w}}{\pi dl(f_v - \tau_{ini})} = \frac{l_0}{l}(1 + \alpha) \cdot min \begin{cases} \dfrac{1}{\dfrac{\sinh(\omega\, l_0/l)}{\sinh\omega} + \alpha\left(1 - \dfrac{\sinh\big(\omega(1 - l_0/l)\big)}{\sinh\omega}\right)} \\[4mm] \dfrac{1}{1 - \dfrac{\sinh\big(\omega(1 - l_0/l)\big)}{\sinh\omega} + \alpha\dfrac{\sinh(\omega\, l_0/l)}{\sinh\omega}} \end{cases} \quad (3.44)$$

- Pull-push:

$$\frac{P_{u.w}}{\pi dl(f_v - \tau_{ini})} = \frac{l_0}{l} \cdot \frac{1}{1 - \dfrac{\sinh\big(\omega(1 - l_0/l)\big)}{\sinh\omega}} \quad (3.45)$$

In a subsequent work [108], the same authors modified further the model so that the thread geometry is taken into account. The principle was to apply a global-stress analysis to quantify the distribution of the axial force on the screw and a local-stress analysis in every pitch length in order to quantify the maximum shear stress. They concluded that the effect of taking into account the thread geometry is not significant for usual pitch lengths.

The predictions of Equations (3.44)-(3.45) were compared with experimental results from withdrawal tests of lagscrew-bolts embedded parallel to the grain in *Douglas-fir* glulam elements. Lagscrew-bolts with diameter $d=$ (25, 30, 35 mm) and varying embedment length (up to 10-13d) were used. The loading condition

40

was pull-pull. An additional series (SL2-series) was conducted for specimens with d= 30 mm in the pull-push loading condition. The experimentally recorded withdrawal capacities and the predictions by Equations (3.44)-(3.45) are shown as function of l in Figure 3.12. Series PL1, PL2 and PL3 correspond to pull-pull loading and specimens with diameters 25, 30 and 35 mm, respectively. The theoretical values were obtained assuming G_f = 0.7 N/mm, f_v= 9 MPa and $v_{90.0}$= 0.015. The initial stress was taken equal to τ_{ini} = 2 MPa, as this value provided a good fit to the experimental results. The authors stated that the mean stress criterion would lead to insignificant differences as compared to the maximum stress failure criterion for lagscrews and threaded rods with considerable embedment length compared to mean stress length l_0. As seen in Figure 3.12, Equations (3.44)-(3.45) generally overestimate the withdrawal capacity for small values of l and they underestimate it for the maximum values of l. Ellingsbø and Malo [110] applied the same model for STS with d= 8 mm and l_{ef} = 150 mm. They concluded that G_f= 0.7 N/mm and τ_{ini}= 1.2 MPa provided the best fit to their experimental data.
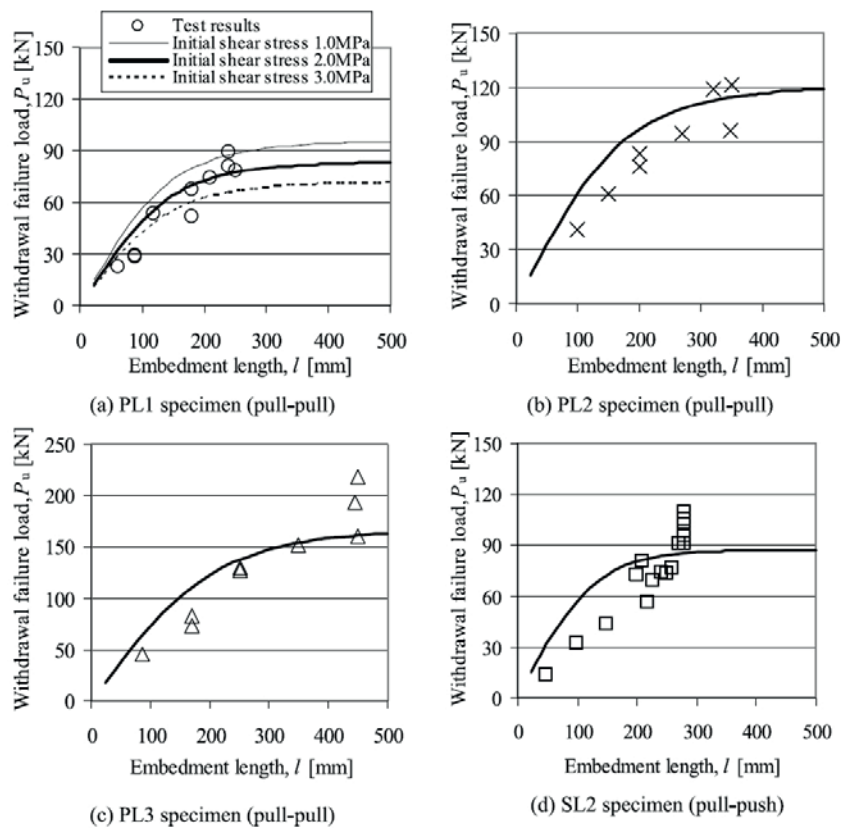

Figure 3.12: Withdrawal capacity as function of l for all experimental series [107]

41

3.2.4 Ringhofer and Schickhofer 2014

According to Volkersen theory applied for axially loaded screws, the axial force distribution in a screw loaded in the pull-push loading condition is given by Equation (3.46).

$$P(x) = P \cdot \frac{\sinh\big(\omega(1 - x/l)\big)}{\sinh\omega} \tag{3.46}$$

Ringhofer and Schickhofer [111] performed a series of experiments in order to validate the applicability of Volkersen theory for axially loaded screws. In particular, they measured indirectly the axial force distribution in the screws by use of strain gauges attached on the screws and compared it with Equation (3.46).

STS with d=12 mm were used in the tests. The screws were embedded in solid timber elements. In the first test series, screws were embedded perpendicular to the grain and the embedment length was varied from 60-240 mm. A second series of tests was conducted with screws embedded parallel and with an angle of 45° to the grain. In this series the embedment length was only varied from 180 mm to 240 mm. In the sections where strain gauges were attached, the axial forces were quantified for two load levels; 30% and 90% of the maximum force. The axial force distribution was quantified by use of polynomial trend lines fitted to the experimentally measured values.

The authors highlighted the significant influence of A_w on the accuracy of the analytical prediction for the axial force distribution. Compared to A_w calculated as a small area around the interface, assuming A_w equal to the total cross-sectional area of the specimen led in general to better agreement with the experimental results. The shear stiffness parameter was taken equal to $\Gamma = G/t$, where t is the thickness of the shear layer which was approximated by experimental observation at failure. It was assumed equal to 14.5 mm for specimens with α= 0° and 22.5 mm for specimens with α= 45°, 90°. The analytical and the experimental results were in good agreement for α= 0°, 90°. It was therefore concluded that Volkersen model can be used for axially loaded screws.

4. Overview of present work

4.1 Research methods

4.1.1 Experimental

As discussed in Chapter 3, the effect of the angle α and the embedment length l on the withdrawal properties of STS with diameters up to d= 14 mm has been thoroughly investigated. However, the available experimental results in the case of threaded rods are, in general, limited to relatively stocky threaded rods (with small l/d values) embedded parallel or perpendicular to the grain. Moreover, the effect of edge distances and spacings which are smaller than the minimum requirements of EC5 [16] and some ETAs has not been fully investigated especially in the case of threaded rods with varying angle to the grain α.

Within this thesis, the effect of α and l on the withdrawal properties has been experimentally investigated. Specimens with values of l/d up to 30 were tested. Moreover, the influence of small edge distances and spacings on the withdrawal properties was experimentally investigated for pairs of rods embedded in 'parallel', i.e. in a row perpendicular to the plane of the grain.

SFS WB-T-20 [23] steel threaded rods were used in all specimens. These rods are made according to DIN7998 [112] and a lay-out is shown in Figure 4.1. The outer-thread diameter and the core diameter of these rods are d= 20 mm and d_c = 15 mm, respectively. The pitch distance is c = 7 mm. According to the manufacturer, the steel grade of the rods is 8.8. The strength class of glulam was Scandinavian class L40c which corresponds to European strength class GL30c [113]. This type of glulam is fabricated with 45 mm thick laminations made of Norwegian spruce (*Picea Abies*).

All specimens were conditioned to standard temperature and relative humidity conditions (20°C / 65% R.H.), leading to approximately 12% MC in the wood. Two displacement transducers were placed next to the supports of the specimen, measuring the relative displacement between the rod and each support. The distance between the rod and each displacement transducer was equal to $4d$ in order to take into account the deformation due to concentrated stresses in the vicinity of the interface. The average of these two measurements was used for the displacement. The loading protocol and the stiffness determination were in accordance with EN 26891:1991 (ISO6891:1983) [114].
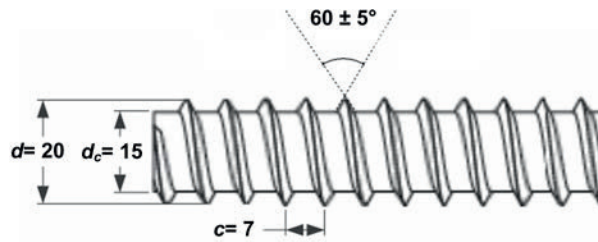
Figure 4.1: Geometry of SFS WB-T-20 threaded rod (DIN 7998 [112])

In the case of single rods, specimens with 6 different rod-to-grain angles ($\alpha = 0$, 10, 20, 30, 60 and 90°) and 4 different embedment lengths ($l = 100$, 300, 450, 600 mm) were tested. Five tests were performed for each sub-group of parameters but no tests were performed for the combinations $\alpha = 60°$, 90° and $l = 600$ mm, giving 110 tests in total. The experimental setup, the dimensions of the specimens and the experimental results for single rods are presented in Papers i, ii and iv [60, 115, 116]. The experimental results for single rods are presented in detail in Appendix B.

In the case of pairs of rods, specimens with 4 different rod-to-grain angles ($\alpha = 15$, 30, 60 and 90°) and 2 different configurations with respect to edge distances and spacings were tested. Two tests were performed for each combination of angle and configuration, 16 in total. The embedment length was equal to $l = 450$ mm for all specimens. The experimental setup, the dimensions of the specimens and the experimental results for pairs of rods are presented in Paper iii [117].

4.1.2 Analytical

As discussed in Section 3.2, Volkersen theory has been applied on axially loaded STS and threaded rods assuming that the constitutive relationship between the shear stress, $\tau(x)$ and the displacement of the shear layer, $\delta(x)$, is linear, confer Equation (3.31). The stiffness of the shear layer is taken into account by the shear stiffness parameter Γ. In many of the presented models, the shear layer is assumed to be infinitely thin.

According to this approach the withdrawal capacity is reached when the maximum shear stress is equal to the corresponding withdrawal strength (maximum stress criterion). This assumption implies that the behaviour of the shear layer is elastic-perfectly brittle and therefore there is no residual strength after the maximum shear stress has reached the withdrawal strength. The

predicted withdrawal capacity is given as a highly non-linear function of the embedment length. For large embedment lengths the predicted capacity converges to a limit value. However, experimental results for axially loaded screws show that the relationship between the withdrawal capacity and the embedment length is nearly linear. As a result, the theoretical predictions underestimate the withdrawal capacity in the case of long threaded rods and STS.

The reason for this underestimation for axially loaded screws is the fact that the real $\tau(x)$-$\delta(x)$ relationship is highly non-linear, as shown in Figure 4.2. Therefore it cannot be sufficiently approximated by a linear constitutive relationship. It follows that the withdrawal capacity, the deformation and the distributions of stress and displacements can be estimated more accurately if a more appropriate constitutive relationship is used instead of the linear one.
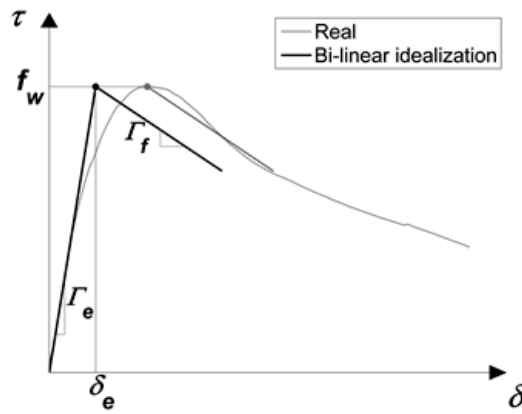
Figure 4.2: Real and idealized bi-linear τ-δ curve

In the present approach, it is assumed that the shear deformation occurs in a shear zone of finite dimensions so that the relative displacement between the threaded rod and the supports is taken into account. The real $\tau(x)$-$\delta(x)$ relationship is approximated by a bi-linear constitutive relationship:

$$\tau(x) = \begin{cases} \Gamma_e \cdot \delta(x) & \delta(x) \leq \delta_e \\ f_w - \Gamma_f \cdot (\delta(x) - \delta_e) & \delta(x) > \delta_e \end{cases} \tag{4.1}$$

where f_w and δ_e are the withdrawal strength and the maximum elastic displacement of the shear zone respectively. The bi-linear idealization separates the curve in two distinct domains; the linear elastic domain and the fracture

domain. These domains are characterized by the equivalent shear stiffness parameters Γ_e and Γ_f which are the slopes of the two branches of the bi-linear constitutive relationship. The term equivalent is used because $\delta(x)$ does not solely depend on shear deformation of wood, but also on the relative slip between the threaded rod and the surrounding wood at the interface. The use of a bi-linear constitutive relationship instead of a linear one allows for better approximation of the real behaviour, as visualized in Figure 4.2. Analytical expressions based on a bi-linear constitutive relationship have been previously derived for lap joints [101] and for axially loaded rods [118].

For pull-push or pull-shear loading conditions, the withdrawal stiffness and capacity are given by the following expressions:

$$K_w = \pi \cdot d \cdot l \cdot \Gamma_e \cdot \frac{\tanh\omega}{\omega} \tag{4.2}$$

$$\frac{P_{u.w}}{\pi \cdot d \cdot l \cdot f_w} = \frac{\sin(m \cdot \omega \cdot \lambda_u)}{\omega \cdot m} + \frac{\tanh\{(1 - \lambda_u) \cdot \omega\} \cdot \cos(m \cdot \omega \cdot \lambda_u)}{\omega} \tag{4.3}$$

The parameters ω, β and m have been defined as follows:

$$\omega = \sqrt{\pi \cdot d \cdot \Gamma_e \cdot \beta \cdot l^2} \tag{4.4}$$

$$\beta = \frac{1}{A_s \cdot E_s} + \frac{1}{A_w \cdot E_{w.\alpha}} \tag{4.5}$$

$$m = \sqrt{\Gamma_f / \Gamma_e} \tag{4.6}$$

Threaded rods feature a continuous thread without a tip and therefore their effective length is assumed equal to their embedment length. Thus $l_{ef} = l$ is used in Equations (4.2)-(4.6). A modified approach where a reduced effective length is assumed is presented in Appendix A. The dimensionless fracture length parameter, $\lambda = l_f / l$, expresses the length of the shear zone which exhibits non-elastic behaviour, as shown in Figure 4.3. The ultimate value λ_u, which corresponds to the ultimate withdrawal force, can be obtained as function of m and ω by use of a diagram.

An important input parameter for the analytical approach is the cross sectional area of wood, A_w, which is subjected to axial stress. In reality, the distribution of the axial stress in wood along the length of the threaded rod is non-uniform. A constant effective area of wood subjected to axial stress, $A_{w.eff}$, is assumed in this

approach. $A_{w.eff}$ is assumed equal to the width s_s of the provided supports extended by $l/6$ on both sides of each support and limited by the available edge distances and the distance between the supports and the rod, as shown in Figure 4.4. The modulus of elasticity of wood in an angle to the grain, $E_{w.\alpha}$, is estimated by Hankinson formula:

$$E_{w.\alpha} = \frac{E_{w.0} \cdot E_{w.90}}{E_{w.0} \cdot sin^2\alpha + E_{w.90} \cdot cos^2\alpha}$$
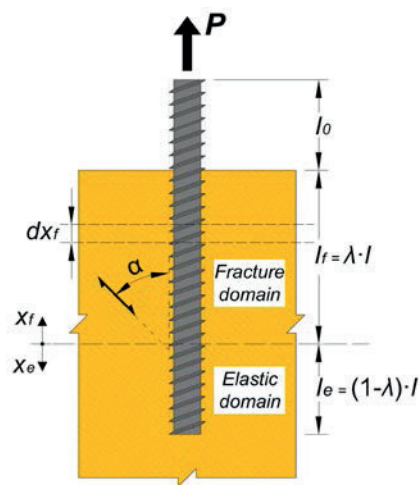(4.7)

Figure 4.3: Post-elastic behaviour of axially loaded threaded rod
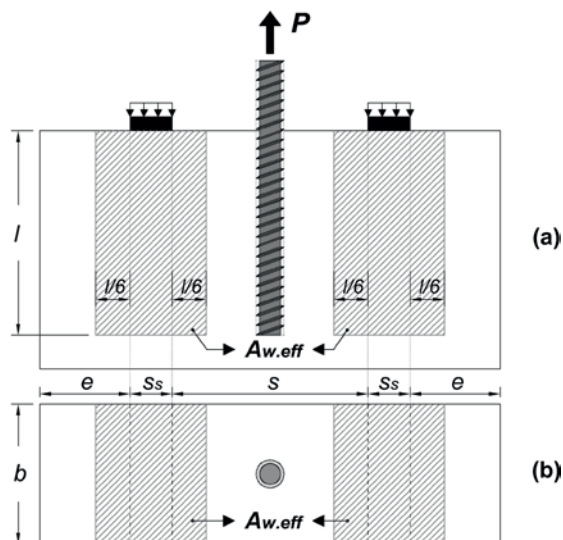
Figure 4.4: Determination of $A_{w.eff}$: (a) side view and (b) plan view

This analytical model allows the estimation of the full force-displacement curve and the elastic and post-elastic stress and displacement distributions. A full description of the model is given in Papers i [60] and ii [115]. The model has been also applied to withdrawal of pairs of rods in Paper iii [117].

4.1.3 Numerical

The elastic behaviour of all specimens was studied by finite element (abbr. FE) simulations. The withdrawal stiffness as well as the stresses and displacement distributions were numerically quantified and compared to the analytical estimations and the experimental results. The FE simulations were performed using Abaqus software [119]. The model assembly consisted of a rectangular box-type timber part and the threaded rod in surface contact with each other. These two parts were meshed with three dimensional, 8-node, linear brick elements. Damage and constructional imperfections, such as cavities, were not taken into account in the FE model.

Wood was modelled as transversely isotropic. Due to an incomplete set of material properties provided by the manufacturer, the lacking properties were taken from a study on mechanical properties of Norwegian spruce [120]. The contact interaction between the wood and the rod was modelled with hard contact normally to the surface and frictional behaviour tangentially. The friction coefficient for the wood-steel surface was set equal to $\mu = 0.20$.

The threaded rod was loaded by a unit vertical pull-out force, $P = 1$ kN, which resulted in an elastic state of stress in the rod and the timber part. Lateral displacements of the rod at the loading point were restrained. FE simulation showed that the non-linearity due to contact interaction was not significant and therefore the behaviour with respect to deformation was nearly linear-elastic.

A full description of the FE model is given in Paper i [60]. FE results for single rods are also given in Paper i [60] and, in detail, in Appendix C. The estimated values for the withdrawal stiffness of pairs of threaded rods are provided in Paper iii [117].

4.2 Main results and conclusions

4.2.1 Paper i

In Paper i [60] the elastic behaviour of single rods was studied. The numerical and analytical estimations for the withdrawal stiffness were compared to the experimental results. Moreover, the numerically estimated lengthwise distributions of stresses and displacements were compared to the respective analytical estimations.

The equivalent shear stiffness parameter Γ_e which is a necessary input parameter for the analytical model was derived by applying regression analysis on the experimental results. This analysis showed that Γ_e is highly correlated with α. On the other hand, the correlation between Γ_e and l was negligible. Application of regression on a generalized Hankinson formula led to the following expression for Γ_e (units MPa/mm):

$$\Gamma_{e.\alpha} = \frac{9.35}{1.5 \cdot \sin^{2.2}\alpha + \cos^{2.2}\alpha} \tag{4.8}$$

Experimental results showed that threaded rods exhibit high withdrawal stiffness especially for small rod-to-grain angles and long embedment lengths. The analytical estimations were in good agreement with the experimental results. The analytical model and the FE simulations estimated that the increase of K_w due to increasing l becomes gradually smaller for long embedment lengths. This estimation was validated by experimental results. No initial slip was observed when the threaded coupling parts of the set-up were tightly fastened. Thus, it was concluded that initial slip is not a characteristic property of withdrawal of threaded rods.

In general, the numerical estimations for K_w overestimated the experimental results, especially in the case of specimens with short embedment lengths (l= 100 mm). In the case of specimens with $l \geq 300$ mm, the overestimation of K_w was significantly smaller. This overestimation was attributed to damage and constructional imperfections which were not taken into account in the numerical simulations. For increasing values of α, this overestimation was smaller because the elastic deformation of wood, which can reliably be predicted by FE simulation, is more significant. The numerically estimated lengthwise distributions of stresses and displacements were in good agreement with the analytical ones. Numerical results showed that a relative slip between the rod and the surrounding wood

occurs at the interface. The relative slip is highest for rods embedded parallel to the grain and lowest for rods embedded perpendicular to the grain.

4.2.2 Paper ii

In Paper ii [115] the post-elastic behaviour of single rods was studied. The mean withdrawal strength f_w and the parameter m were derived from the experimental results for all specimens with the shortest embedment length, i.e. l = 100 mm. Results from these specimens were used because the shear stress and the displacement of the shear zone at and after failure, can be approximated as uniformly distributed along the rod. A generalized Hankinson formula was used to fit the experimentally obtained results and regression led to the following expressions for f_w (units MPa) and m as functions of α:

$$f_{w.a} = \frac{4.35}{0.91 \cdot \sin^2\alpha + \cos^2\alpha} \tag{4.9}$$

$$m_\alpha = \frac{m_0}{(m_0/m_{90}) \cdot \sin\alpha + \cos\alpha} = \frac{0.332}{1.73 \cdot \sin\alpha + \cos\alpha} \tag{4.10}$$

The specimens exhibited high withdrawal capacity. A nearly linear relationship between $P_{u.w}$ and l was estimated by the analytical model, which was validated by experimental results. The estimations were slightly conservative (less conservative estimations were obtained by assuming a reduced effective length, confer Appendix A). The dimensionless fracture length parameter at failure was λ_u = 0.88-0.97 for all specimens; i.e. 88-97% of the length of the shear zone was in the fracture domain at failure.

Steel yielding was observed in almost all specimens with l = 600 mm, and most of them failed due to steel fracture. It was concluded that embedment lengths in the range of 30d or more would lead to ductile steel failure instead of withdrawal failure. Yielding and steel fracture of the rods occurred at load levels which were significantly higher than those predicted by the specified yield and ultimate strength properties of steel. The elevated strength of steel was attributed to steel hardening due to rolling of the thread.

The analytically estimated force-displacement curves were in general in good agreement with the experimental ones. However, the inelastic displacements were underestimated by the analytical model because the bi-linear $\tau(x)$-$\delta(x)$ constitutive relationship does not account for the effect of softening prior to

failure as shown in Figure 4.2. Specimens with small rod-to-grain angles exhibited more brittle behaviour than the ones with larger angles.

4.2.3 Paper iii

In Paper iii [117] the withdrawal of rods embedded in 'parallel', i.e. in a row perpendicular to the plane of the grain, was investigated. Rods were embedded in two different configurations with $(a_{2.CG}, a_2) = (2.5d, 2d)$ or $(a_{2.CG}, a_2) = (1.5d, 4d)$. The angle was varied ($\alpha$ = 15, 30, 60, 90°). The embedment length was l= 450 mm for all specimens.

According to experimental observation, there was no significant difference between the results for the two configurations. The withdrawal capacities were compared to the results for single rods and the effective number of rods n_{ef}, was determined. The effectiveness per each rod was quite high, despite the fact that rods were placed with small edge distances and spacings. The following expression was proposed for n_{ef}:

$$
n_{ef} = \begin{cases} 1.75 + 0.116 \cdot \left(\dfrac{\alpha}{60} ° \right) & \alpha < 60° \\ n^{0.9} = 1.866 & \alpha \geq 60° \end{cases} \tag{4.11}
$$

The analytical model was used to predict the withdrawal stiffness and capacity (using the reduced effective length, confer Appendix A). FE simulations were also performed to estimate the withdrawal stiffness. The analytical and numerical estimations were in good agreement with the experimental results.

4.2.4 Paper iv

The 5-% characteristic values of the withdrawal strength parameter ($f_{ax}= F_{max}/l \cdot d$) were calculated in paper iv [116], based on the experimental results of Paper ii [115] and some additional experimental results. It is emphasized that in this investigation the strength was expressed in terms of the withdrawal strength parameter (i.e. the withdrawal strength f_w times π). The characteristic values were calculated in accordance with EN14358 [121] for each rod-to-grain angle. It should be noted that the requirements of EN1382 [30] with respect to the embedment length and the edge distances were not always met.

The characteristic withdrawal strengths for α= 0°, 10° were significantly smaller than the strengths for greater angles. For rods embedded perpendicular to the

51

grain, the characteristic withdrawal strength parameter was equal to $f_{ax.90.k}$= 11.92 MPa. Therefore in accordance with Equation (2.3), $f_{ax.\alpha.k}$ is given by Equation (4.12). The ratio $f_{ax.90.k}/f_{ax.0.k}$ was equal to 1.17 which was very close to the ratio 1.20 according to Equation (2.3).

$$f_{ax.\alpha.k} = \frac{11.92 \ (MPa)}{1.2 \cdot \cos^2\alpha + \sin^2\alpha} \tag{4.12}$$

Equation (4.12) was extrapolated outside its range ($\alpha < 30°$) and provided estimations on the safe side for all α, especially for α= 20°, 30°.

Finally, the characteristic withdrawal capacity according to EC5 [16] (Equation (2.1)) and the analytical model (Equation (4.3)) were compared to the experimental results. The difference between the predictions of the two Equations was very small. The capacity of specimens with α= 20° was, in general, equally reliable as the capacity of specimens with larger angles.

4.3 Proposals for future work

Based on the state of the art knowledge as well as the findings and the limitations of the present thesis, the following recommendations for future research are proposed:

- **Effect of lateral stresses on withdrawal properties:** In the vast majority of practical applications screws and threaded rods are loaded with a combination of axial and lateral loading. This load combination results in bending moment and shear forces in the screw. In fact, some bending moment and shear forces in the screw would develop as a result of non-symmetric conditions, for example insertion of screws with an angle to the grain. Compared to pure withdrawal conditions, the existence of lateral stresses will affect the shear stress distribution on the circumference of the interface and therefore the withdrawal properties.
- **Duration of Loading:** It has been shown that the long-term behaviour of axially loaded screws embedded parallel to the grain is poor compared to short time loading. The duration-of-load effect on the withdrawal properties of axially loaded screws and threaded rods with varying angles to the grain and embedment lengths needs further investigation.
- **Fatigue:** Axially loaded threaded rods may be used as fasteners in cyclically loaded timber structures like bridges and towers. Their fatigue

withdrawal strength is hence of major importance. However, available results on this topic are very sparse.

- **Improved numerical modelling:** FE modelling capable of estimating the inelastic behaviour of axially loaded screws would provide a better insight and estimations. The extended FE method (XFEM) or cohesive zone modelling may be appropriate techniques to model post-elastic behaviour. Moreover, the modelling of damage and constructional imperfections would result in improved estimations of the elastic behaviour of axially loaded screws.

5. References

[1] Malo KA, Köhler J. Vibrations of timber floor beams with end restraints. Structures and Architecture: Concepts, Applications and Challenges - Proceedings of the 2nd International Conference on Structures and Architecture (ICSA)2013. p. 181-9.

[2] Leijten AJM. Requirements for moment connections in statically indeterminate timber structures. Engineering Structures. 2011;33:3027-32.

[3] Malo KA, Ellingsbø P, Stamatopoulos H. Notes on deformation and ductility requirements in timber structures. Proceedings of the 44th CIB-W18 meeting Alghero, Italy2011.

[4] Wollebæk L. Analyses of geometrical nonlinearities with applications to timber bridges [Ph.D. Thesis]. Trondheim, Norway: Norwegian University of Science and Technology; 2005.

[5] Malo KA, Stamatopoulos HC. Impact loading and robustness of wooden beam structures. Proceedings of WCTE 2012 - World Conference on Timber Engineering. Auckland, New Zealand2012. p. 362-8.

[6] Malo KA, Siem J, Ellingsbø P. Quantifying ductility in timber structures. Engineering Structures. 2011;33:2998-3006.

[7] Stamatopoulos H, Malo KA. A review on seismic response of timber frames. Structures and Architecture: Concepts, Applications and Challenges - Proceedings of the 2nd International Conference on Structures and Architecture (ICSA)2013. p. 74-81.

[8] Buchanan AH, Fairweather RH. Seismic design of glulam structures. Bulletin of the New Zealand National Society for Earthquake Engineering. 1993;26:415-36.

[9] Andreolli M, Piazza M, Tomasi R, Zandonini R. Ductile moment-resistant steel-timber connections. Proceedings of the Institution of Civil Engineers: Structures and Buildings. 2011;164:65-78.

[10] Mischler A, Frangi A. Pull-out tests on glued-in-rods at high temperatures. Proceedings of the 34th CIB-W18 meeting Venice, Italy2001.

[11] Lartigau J, Coureau JL, Morel S, Galimard P, Maurin E. Effect of temperature on the mechanical performance of glued-in rods in timber structures. International Journal of Adhesion and Adhesives. 2015;57.

[12] Ellingsbø P, Malo KA. Cantilever glulam beam fastened with long threaded steel rods. Proceedings of WCTE 2010 - World Conference on Timber Engineering. Trentino, Italy2010. p. 468-75.

[13] Angst V, Malo KA. The effect of climate variations on glulam-An experimental study. European Journal of Wood and Wood Products. 2012;70:603-13.

[14] Blaß HJ, Bejtka I. Reinforcements perpendicular to grain using self-tapping screws. Proceedings of the 8th World Conference on Timber Engineering. Lahti, Finland2004. p. 233-8.

[15] Dietsch P, Kreuzinger H, Winter S. Design of shear reinforcement for timber beams. Proceedings of the 46th CIB-W18 meeting Vancouver, Canada2013. p. 193-209.

[16] CEN, European committee for standardization. EN 1995-1-1:2004: Design of timber structures. Part 1-1: General-Common rules and rules for buildings. Brussels, Belgium2004.

[17] Wakashima Y, Okura K, Kyotani K. Development of ductile semi-rigid joints with lagscrewbolts and glued-in rods. Proceedings of WCTE 2010 - World Conference on Timber Engineering. Trentino, Italy2010. p. 3221-8.

[18] Tomasi R, Crosatti A, Piazza M. Theoretical and experimental analysis of timber-to-timber joints connected with inclined screws. Construction and Building Materials. 2010;24:1560-71.

[19] Malo KA, Ellingsbø P. On connections for timber bridges. Proceedings of the International Conference Timber Bridges (ICTB). Lillehammer, Norway2010. p. 297-312.

[20] Mori T, Nakatani M, Kawahara S, Shimizu T, Komatsu K. Influence of the number of fastener on tensile strength of lagscrewbolted glulam joint. Proceedings of the 10th World Conference on Timber Engineering. Miyazaki, Japan2008. p. 1100-7.

[21] Nakatani M, Komatsu K. Development and verification of theory on pull-out properties of Lagscrewbolted timber joints. Proceedings of the 8th World Conference on Timber Engineering. Lahti, Finland2004. p. 95-9.

[22] Blaß HJ, Krüger O. Schubverstärkung von Holz mit Holzschrauben und Gewindestangen. Karlsruhe: KIT Scientific Publishing; 2010.

[23] DIBt, Deutsches Institut für Bautechnik. SFS intec, GmbH., Gewindestangen mit Holzgewinde als Holzverbindungsmittel, Allgemeine bauaufsichtliche Zulassung Z-9.1-777. 2010.

[24] Pirnbacher G, Brandner R, Schickhofer G. Base parameters of self-tapping screws. Proceedings of the 42nd CIB-W18 meeting Dübendorf, Switzerland2009.

[25] Ringhofer A, Grabner M, Silva C, Branco M, Schickhofer G. The influence of moisture content variation on the withdrawal capacity of self-tapping screws. Holztechnologie 2014;55:33-40.

[26] Dietsch P, Brandner R. Self-tapping screws and threaded rods as reinforcement for structural timber elements-A state-of-the-art report. Construction and Building Materials. 2015;97:78-89.

[27] DIBt, Deutsches Institut für Bautechnik. SFS intec, GmbH., SFS Befestiger WT-S-6,5; WT-T-6,5; WT-T-8,2; WR-T-9,0 und WR-T-13 als Holzverbindungsmittel, Zulassungnummer Z-9.1-472. 2011.

[28] Pirnbacher G, Schickhofer G. Load bearing- and optimization potential of self-tapping wood screws. Proceedings of WCTE 2010 - World Conference on Timber Engineering2010. p. 1228-38.

[29] CEN, European committee for standardization. EN 14592:2008+A1:2012: Timber structures- Dowel type fasteners- Requirements. Brussels, Belgium2012.

[30] CEN, European committee for standardization. EN 1382-1999: Timber structures - Tests methods - Withdrawal capacity of timber fasteners. Brussels, Belgium1999.

[31] CEN, European committee for standardization. EN 1383-1999: Timber structures- Tests methods - Pull through resistance of timber fasteners. Brussels, Belgium1999.

[32] CEN, European committee for standardization. EN 409:2009 Timber structures- Tests methods - Determination of the yield moment of dowel type fasteners. Brussels, Belgium2009.

[33] CEN, European committee for standardization. EN ISO 10666:1999 Drilling screws with tapping screw thread - Mechanical and functional properties. Brussels, Belgium1999.

[34] Thelandersson S, Larsen HJ. Timber Engineering. Chichester, West Sussex, England: John Wiley and Sons; 2003.

[35] DIN, Deutsches Institut für Normung. DIN 1052:2008-12: Design of timber structures-General rules and rules for buildings. Berlin, Germany2008.

[36] Jockwer R, Frangi A, Serrano E, Steiger R. Enhanced design approach for reinforced notched beams. Proceedings of the 46th CIB-W18 meeting Vancouver, Canada2013.

[37] Jockwer R. Structural behaviour of glued laminated timber beams with unreinforced and reinforced notches [Ph.D. Thesis]. Zurich, Switzerland: ETH; 2014.

[38] Jockwer R, Steiger R, Frangi A, Serrano E. Load-carrying capacity and failure modes of glulam beams with reinforced notches. European Journal of Wood and Wood Products. 2015.

[39] Aicher S, Höfflin L. Glulam beams with holes reinforced by steel bars. Proceedings of the 42nd CIB-W18 meeting Dübendorf, Switzerland2009.

[40] Aicher S. Glulam beams with internally and externally reinforced holes –tests, detailing and design. Proceedings of the 44th CIB-W18 meeting Alghero, Italy2011.

[41] Lathuillière D, Bléron L, Descamps T, Bocquet JF. Reinforcement of dowel type connections. Construction and Building Materials. 2015;97:48-54.

[42] Bejtka I, Blaß HJ. Self-tapping screws as reinforcements in connections with dowel-type fasteners. Proceedings of the 38th CIB-W18 meeting Karlsruhe, Germany2005.

[43] Lam F, Schulte-Wrede M, Yao CC, Gu JJ. Moment resistance of bolted timber connections with perpendicular to grain reinforcements. Proceedings of the 10th World Conference on Timber Engineering. Miyazaki, Japan2008. p. 978-85.

[44] Lam F, Gehloff M, Closen M. Moment-resisting bolted timber connections. Proceedings of the Institution of Civil Engineers: Structures and Buildings. 2010;163:267-74.

[45] Blaß HJ, Schmid M. Self-tapping screws as reinforcement perpendicular to the grain in timber connections. Proceedings of RILEM Symposium: Joints in Timber Structures. Stuttgart, Germany2001. p. 163-72.

[46] Angst V, Malo KA. Effect of self-tapping screws on moisture induced stresses in glulam. Engineering Structures. 2012;45:299-306.

[47] Jönsson J. Load carrying capacity of curved glulam beams reinforced with self-tapping screws. Holz als Roh - und Werkstoff. 2005;63:342-6.

[48] Bejtka I, Blaß HJ. Self-tapping screws as reinforcements in beam supports. Proceedings of the 39th CIB-W18 meeting Florence, Italy2006.

[49] Nakatani M, Morita H, Mori T. Reinforcement of shear failure with long screw in moment-resisting joint. Proceedings of WCTE 2014 - World Conference on Timber Engineering. Quebec City, Canada2014.

[50] Symons D, Persaud R, Stanislaus H. Slip modulus of inclined screws in timber-concrete floors. Proceedings of the Institution of Civil Engineers: Structures and Buildings. 2010;163:245-55.

[51] Symons D, Persaud R, Stanislaus H. Strength of inclined screw shear connections for timber and concrete composite construction. Structural Engineer. 2010;88:25-32.

[52] Giongo I, Piazza M, Tomasi R. Investigation on the self tapping screws capability to induce internal stress in timber elements. Advanced Materials Research2013. p. 604-11.

[53] Mahlknecht U, Brandner R, Ringhofer A, Schickhofer G. Resistance and Failure Modes of Axially Loaded Groups of Screws. In: Aicher S, Reinhardt HW, Garrecht H, editors. Materials and Joints in Timber Structures -Recent Developments of Technology: Springer: RILEM Bookseries; 2014. p. 289-300.

[54] Baek HS, Morita H, Shiiba A, Limura Y, Imai F. Influence of shape factors of wood screw on withdrawal performance: Development of wood screw used for soft and light wood. Proceedings of WCTE 2012 - World Conference on Timber Engineering. Auckland, New Zealand2012. p. 573-8.

[55] Frese M, Blaß HJ. Models for the calculation of the withdrawal capacity of self-tapping screws. Proceedings of the 42nd CIB-W18 meeting Dübendorf, Switzerland2009.

[56] DIBt, Deutsches Institut für Bautechnik. European Technical Approval ETA-11/0190. 2013.

[57] ETA Danmark A/S. European Technical Approval ETA-13/0090. 2013.

[58] Yeoh D, Fragiacomo M, De Franceschi M, Buchanan AH. Experimental tests of notched and plate connectors for LVL-concrete composite beams. Journal of Structural Engineering. 2011;137:261-9.

[59] Gerber C, Crews K. Development of a design procedure for timber concrete composite floors in Australia and New Zealand. New Zealand Timber Design Journal. 2011;19:6-15.

[60] Stamatopoulos H, Malo KA. Withdrawal stiffness of threaded rods embedded in timber elements. Submitted to Construction and Building Materials. 2015.

[61] Bejtka I, Blaß HJ. Joints with inclined screws. Proceedings of the 35th CIB-W18 meeting Kyoto, Japan2002.

[62] Kevarinmäki A. Joints with inclined screws. Proceedings of the 35th CIB-W18 meeting Kyoto, Japan2002.

[63] Blaß HJ, Bejtka I. Screws with continuous threads in timber connections. RILEM Symposium. Stuttgart2001.

[64] Krenn H, Schickhofer G. Joints with inclined screws and steel plates as outer members. Proceedings of the 42nd CIB-W18 meeting Dübendorf, Switzerland2009.

[65] Malo KA, Ostrycharczyk A, Barli R, Hakvåg I. On development of network arch bridges in timber. Proceedings of the 2nd International Conference Timber Bridges (ICTB). Las Vegas, USA2013.

[66] Nakatani M, Mori T, Komatsu K. Development of moment-resisting joint systems using lagscrewbolts. Proceedings of the 9th World Conference on Timber Engineering2006. p. 845-51.

[67] Ringhofer A, Schickhofer G. Influencing parameters on the experimental determination of the withdrawal capacity of self-tapping screws. Proceedings of WCTE 2014 - World Conference on Timber Engineering. Quebec City, Canada2014.

[68] Kasal B, Guindos P, Polocoser T, Heiduschke A, Urushadze S, Pospisil S. Heavy laminated timber frames with rigid three-dimensional beam-to-column connections. Journal of Performance of Constructed Facilities. 2014;28.

[69] Westerheim N. Conceptual study of connections using glulam and long threaded bars exposed to fire loading [Master's Thesis]. Trondheim, Norway: Norwegian University of Science and Technology (NTNU); 2013.

[70] Closen M, Lam F. Performance of moment resisting self-tapping screw assembly under reverse cyclic load. Proceedings of WCTE 2012 - World Conference on Timber Engineering. Auckland, New Zealand2012. p. 433-40.

[71] Hübner U, Rasser M, Schickhofer G. Withdrawal capacity of screws in European ash (Fraxinus excelsior L.). Proceedings of WCTE 2010 - World Conference on Timber Engineering. Trentino, Italy2010. p. 241-9.

[72] Hübner U. Withdrawal strength of self-tapping screws in hardwoods. Proceedings of the 46th CIB-W18 meeting Vancouver, Canada2013.

[73] Mori T, Nakatani M, Chui YH, Gong M, Isoda H, Komatsu K. Pull-out strength properties of lagscrewbolt connection in cross laminated timber. Proceedings of WCTE 2014 - World Conference on Timber Engineering. Quebec City, Canada2014.

[74] Ringhofer A, Brandner R, Schickhofer G. Withdrawal resistance of self-tapping screws in unidirectional and orthogonal layered timber products. Mater Struct. 2013:1-13.

[75] Carradine D, Newcombe P, Buchanan A. Using screws for structural applications in laminated veneer lumber. Proceedings of the 42nd CIB-W18 meeting Dübendorf, Switzerland2009.

[76] Stepinac M, Hunger F, Tomasi R, Serrano E, Rajcic V, Van De Kuilen JWG. Comparison of design rules for glued-in-rods and design rule proposal for implementation in European standards. Proceedings of the 46th CIB-W18 meeting Vancouver, Canada2013.

[77] Tlustochowicz G, Serrano E, Steiger R. State-of-the-art review on timber connections with glued-in steel rods. Materials and Structures/Materiaux et Constructions. 2011;44:997-1020.

[78] Volkersen O. Die nietkraftverteilung in zugbeanspruchten nietverbindungen mit konstanten laschenquerschnitten. Luftfahrtforschung. 1938;15:41-7.

[79] Blaß HJ, Bejtka I, Uibel T. Tragfähigkeit von verbindungen mit selbstbohrenden holzschrauben mit vollgewinde. Karlsruhe: Universitätsverlag Karlsruhe 2006.

[80] Burgschwaiger M. Einfluss der einbindelänge auf die ausziehfestigkeit von teilgewindeschrauben. [Bachelor Thesis]. Graz: Graz University of Technology; 2010.

[81] Ringhofer A, Brandner R, Schickhofer G. A universal approach for withdrawal properties of self-tapping-screws in solid timber and laminated timber products. Proceedings of the 2nd INTER meeting Šibenik, Croatia2015.

[82] Kennedy S, Salenikovich A, Munoz W, Mohammad M. Design equation for withdrawal resistance of threaded fasteners in the Canadian timber design code. Proceedings of WCTE 2014 - World Conference on Timber Engineering. Quebec City, Canada2014.

[83] CSA Standards. CSA O86-09 Engineering Design in Wood, Canadian Standards Association. 2009.

[84] ANSI/AWC. National Design Specification for Wood Construction NDS-2012. Washington, D.C, USA.2012.

[85] McLain TE. Design axial withdrawal strength from wood: I. Wood screws and lag screws. Forest Products Journal. 1997;47:77-84.

[86] Morrison H, Burgess, Huggins (MHBH). Improved design of fastenings based on limit states design (Unpublished report). 1982.

[87] Kennedy S. Withdrawal and embedding resistance of fasteners in timber and CLT panels [Master's Thesis]. Quebec, Canada: Université Laval; 2014.

[88] Newlin JA, Gahagan JM. Lag-screw joints: Their behaviour and design. Techn Bulletin No 597 USDA Forest Serv, Forest Prod Lab. 1938.

[89] Abukari MH, Côté M, Rogers C, Salenikovich A. Withdrawal resistance of structural screws in Canadian glued laminated lumber. Proceedings of WCTE 2012 - World Conference on Timber Engineering. Auckland, New Zealand2012.

[90] Abukari MH. Project Report on Lag Screws. 2012.

[91] Gehloff M. Pull-out resistance of self-tapping wood screws with continuous thread [Master's Thesis]. Vancouver, Canada: The University of British Columbia; 2011.

[92] Strong-Tie S. Test Data on Self-drilling Lag Screws. 2006.

[93] Plieschounig S. Ausziehverhalten axial beanspruchter Schraubengruppen [Master's Thesis]. Graz, Austria: Graz University of Technology; 2010.

[94] Zarnani P, Quenneville P. Predictve analytical model for wood capacity of rivet connections in glulam and LVL. Proceedings of WCTE 2012 - World Conference on Timber Engineering. Auckland, New Zealand2012. p. 144-53.

[95] Gehri E. Influence of fasteners spacings on joint performance - Experimental results and codification. Proceedings of the 42nd CIB-W18 meeting Dübendorf, Switzerland2009.

[96] Blaß HJ, Laskewitz B. Effect of spacing and edge distance on the axial strength of glued-in rods. Proceedings of the 32nd CIB-W18 meeting Graz, Austria1999.

[97] Gehri E. Ductile behaviour and group effect of glued-in steel rods. Joints in timber structures RILEM-PRO 22. Stuttgard, Germany2001.

[98] ETA Danmark A/S. European Technical Approval ETA-13/0899. 2013.

[99] ETA Danmark A/S. European Technical Approval ETA-12/0114. 2013.

[100] Uibel T, Blaß HJ. Determining suitable spacings and distances for self-tapping screws by experimental and numerical studies. Proceedings of WCTE 2010 - World Conference on Timber Engineering. Trentino, Italy2010. p. 3204-12.

[101] Gustafsson PJ. Analysis of generalized Volkersen-joints in terms of non-linear fracture mechanics. Proceedings of the 20th CIB-W18 meeting Dublin, Ireland1987.

[102] Johansson CJ, Serrano E, Gustafsson PJ, Enquist B. Axial Strength of Glued in Bolts: Calculation Based on Non-linear Fracture Mechanics - A Preliminary Study. Proceedings of the 29th CIB-W18 meeting Copenhagen, Denmark1995.

[103] Jensen JL, Koizumi A, Sasaki T, Tamura Y, Iijima Y. Axially loaded glued-in hardwood dowels. Wood Science and Technology. 2001;35:73-83.

[104] Nakatani M, Komatsu K. Expression mechanism of pull-out performance in lagscrewbolted timber joints II. Development of theory on pull-out properties parallel to the grain. Mokuzai Gakkaishi. 2005;51:311-7.

[105] Nakatani M, Walford B. Influence of timber dimension on withdrawal behaviour of lagscrewbolt. Proceedings of WCTE 2010 - World Conference on Timber Engineering. Trentino, Italy2010. p. 1926-30.

[106] Jensen JL, Quenneville P, Nakatani M. Withdrawal of lag screws in end-grain. Proceedings of WCTE 2010 - World Conference on Timber Engineering. Trentino, Italy2010. p. 1921-5.

[107] Jensen JL, Nakatani M, Quenneville P, Walford B. A simple unified model for withdrawal of lag screws and glued-in rods. European Journal of Wood and Wood Products. 2011;69:537-44.

[108] Jensen JL, Nakatani M, Quenneville P, Walford B. A simplified model for withdrawal of screws from end-grain of timber. Construction and Building Materials. 2012;29:557-63.

[109] Gustafsson PJ. Mean stress approach and initial crack approach. Fracture Mechanics Models for Analysis of Timber Beams with A Hole or A Notch-a Report of RILEM TC-133 Report TVSM-7134. 2002.

[110] Ellingsbø P, Malo KA. Withdrawal capacity of long self-tapping screws paralell to grain direction. Proceedings of WCTE 2012 - World Conference on Timber Engineering. Auckland, New Zealand2012. p. 228-37.

[111] Ringhofer A, Schickhofer G. Investigations concerning the force distribution along axially loaded self-tapping screws. In: Aicher S, Reinhardt HW, Garrecht H,

editors. Materials and Joints in Timber Structures, Recent Developments of Technology: Springer; 2014. p. 201-10.

[112] DIN, Deutsches Institut für Normung. DIN 7998:Gewinde und Schraubenenden für Holz-schrauben. Berlin, Germany1975.

[113] CEN, European committee for standardization. EN 14080-2013: Timber structures- Glued laminated timber and glued solid timber - Requirements. Brussels, Belgium2013.

[114] CEN, European committee for standardization. EN 26891:1991 (ISO 6891:1983): Timber structures- Joints made with mechanical fasteners-General principles for the determination of strength and deformation characteristics. Brussels, Belgium1991.

[115] Stamatopoulos H, Malo KA. Withdrawal capacity of threaded rods embedded in timber elements. Construction and Building Materials. 2015;94:387-97.

[116] Stamatopoulos H, Malo KA. Characteristic withdrawal capacity and stiffness of threaded rods. Proceedings of the 2nd INTER meeting Šibenik, Croatia2015.

[117] Stamatopoulos H, Malo KA. Withdrawal of pairs of threaded rods with small edge distances and spacings. Submitted to European Journal of Wood and Wood Products. 2016.

[118] Pörtner C. Untersuchungen zum Verbund zwischen eingeklebten stiftförmigen faserverstärkten Kunststoffen und Holz [Ph.D. Thesis]. Kassel, Germany: Kassel University; 2005.

[119] Abaqus analysis user's guide, Version 6.13. Dassault Systèmes Simulia corp.; 2013.

[120] Dahl K. Mechanical properties of clear wood from Norway spruce [Ph.D. Thesis]. Trondheim, Norway: Norwegian University of Science and Technology; 2009.

[121] CEN, European committee for standardization. EN 14358-2006: Timber structures- Calculation of characteristic 5-percentile values and acceptance criteria of a sample. Brussels, Belgium2006.

Part II:

Appended Papers

Paper I

Withdrawal stiffness of threaded rods embedded in timber elements

Haris Stamatopoulos and Kjell Arne Malo

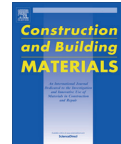*Under revision in Construction and Building Materials (2015)*

Is not included due to copyright

Paper II

Withdrawal capacity of threaded rods embedded in timber elements

Haris Stamatopoulos and Kjell Arne Malo

Withdrawal capacity of threaded rods embedded in timber elements

Haris Stamatopoulos *, Kjell Arne Malo

Department of Structural Engineering, Norwegian University of Science and Technology (NTNU), Rich. Birkelandsvei 1A, 7491 Trondheim, Norway

HIGHLIGHTS

- The withdrawal capacity of threaded rods embedded in timber elements was studied.
- Theoretical and experimental methods were used.
- In general, theoretical and experimental results are in good agreement.
- A nearly linear relation between withdrawal capacity and embedment length was observed.

ABSTRACT

In the present paper, the withdrawal capacity of threaded rods embedded in timber elements is investigated using both theoretical and experimental methods. A theoretical approach based on Volkersen theory, assuming a bi-linear constitutive law is developed. Moreover, an experimental investigation of withdrawal of threaded rods from glulam elements is presented. Results for specimens covering a wide range of varying embedment lengths and rod-to-grain angles are provided. The agreement between theoretical estimations and experimental results is good. A nearly linear relation between embedment length and withdrawal capacity, predicted by the theoretical approach, is validated by the experimental results.

© 2015 Elsevier Ltd. All rights reserved.

1. Introduction

1.1. Background

Threaded connectors, mostly self-tapping screws, have recently shown a great potential as reinforcements [1–4], in axially loaded timber-to-timber connections [5,6] and in moment resisting connections [7–10]. In general, connections with axially loaded threaded connectors show high withdrawal capacity and stiffness. Long threaded rods and self-tapping screws may, to some extent, play the same role in timber structures as reinforcement bars do in concrete structures. When placed with an inclination to the grain direction, they can arrest cracks which may form along the grain, and thus transfer stresses across cracks and retain the structural integrity of timber elements. Due to their length, their withdrawal capacity and stiffness are not significantly affected by local defects (knots, cracks etc.). Furthermore, connections with rods screwed into timber elements are less prone to construction

quality issues, less brittle and offer greater fire-protection than connections with glued-in-rods. They may also facilitate a high degree of pre-fabrication and hence contribute to easy and fast erection on construction sites. Finally, ductile connections can be achieved with these connectors, using the principle of capacity design [10].

During recent years, a significant amount of research has been performed on the withdrawal of self-tapping screws and threaded rods embedded in timber elements [9,11–23]. This research has focused almost exclusively on withdrawal capacity, neglecting withdrawal stiffness. Withdrawal stiffness is a part of the current investigation, and theoretical and numerical estimations along with experimental validation are presented in an accompanying paper, see [24]. The influence of important parameters, such as embedment length, diameter and angle between the rod axis and the grain direction, on withdrawal capacity, has been sufficiently investigated only for screws with relatively small diameters. Results available for withdrawal of large diameter threaded rods are limited to rods installed parallel or perpendicular to the grain and to rods with relatively short embedment lengths [9,12,14–16,19]. As for available theoretical models [15,16,19],

---

* Corresponding author.
E-mail address: haris.stamatopoulos@ntnu.no (H. Stamatopoulos).

they are based on the application of classical Volkersen [25] theory to axially loaded connectors [26], assuming a linear constitutive law between shear stress and withdrawal displacement. These models have been validated by experimental results only for rods with relatively short embedment lengths, and only for rods inserted parallel to the grain.

Some existing models for calculating the withdrawal capacity are based on application of regression models on experimental results [12,14,17,20,23]. This approach is also adopted by Eurocode 5, EC5 [27]. However, EC5 provides no means of determining the distribution of stresses and displacements, nor the withdrawal stiffness. Moreover, EC5 imposes a limitation to the angle between rod-axis and grain direction ($\geqslant 30°$), leading to a lack of guidelines for threaded rods embedded in small inclinations to the grain direction.

1.2. Outline

A theoretical approach for estimating the withdrawal capacity of axially loaded connectors embedded in timber elements is developed in the present paper. This approach is based on classical Volkersen theory [25] for axially loaded connectors [26], using a bi-linear constitutive law. In addition, an experimental investigation of withdrawal of threaded rods from glulam elements is presented. The parameters of this investigation are the embedment length and the rod-to-grain angle. The experimental withdrawal capacities of specimens with a wide range of these parameters are compared with the theoretical estimations.

2. Theoretical approach

2.1. Theoretical basis

An axially loaded connector embedded in a timber element is shown schematically in Fig. 1a. The embedment length is denoted

l and the length of the part of the connector that is not embedded in the timber element is denoted l_0. The angle between the connector axis and the grain direction is denoted α. The outer thread diameter and the core cross-sectional area of the connector, are denoted d and A_s respectively. The withdrawal force is denoted P. Axis x_e is defined with its origin at the entrance point of the connector, pointing downwards. Depending on the provided support, three main types of loading conditions may be considered as shown in Fig. 1b; pull-push, pull-pull and pull-shear loading conditions.

The theoretical approach is based on classical Volkersen theory [25] applied on axially loaded connectors [26]. According to [26], all shear deformation is assumed to occur in an infinitely thin shear layer while the connector and surrounding wood are assumed to be in states of pure axial stress. In the present approach, all shear deformation is assumed to occur in a shear zone of finite dimensions while, another zone of the wood with cross sectional area A_w is in a state of pure and uniform axial stress. In reality, parts of these two zones overlap.

The withdrawal force imposes a shear stress $\tau(x)$ in the interface between the timber element and the outer thread surface of the connector. The displacement of the shear zone is denoted $\delta(x)$ and is equal to the relative displacement between the displacements of the connector, $u_s(x)$, and the wood, $u_w(x)$:

$$\delta(x) = u_s(x) - u_w(x) \tag{1}$$

The relation between the interface shear stress, $\tau(x)$, and the displacement of the shear zone, $\delta(x)$, is approximated as bi-linear, instead of the real non-linear relation, as shown in Fig. 2. A similar approach can be found in [28]. The idealized, bi-linear constitutive law is described by the following expression:

$$\tau(x) = \Gamma_e \cdot \delta(x), \quad \delta(x) \leqslant \delta_e = f_w/\Gamma_e \tag{2a}$$

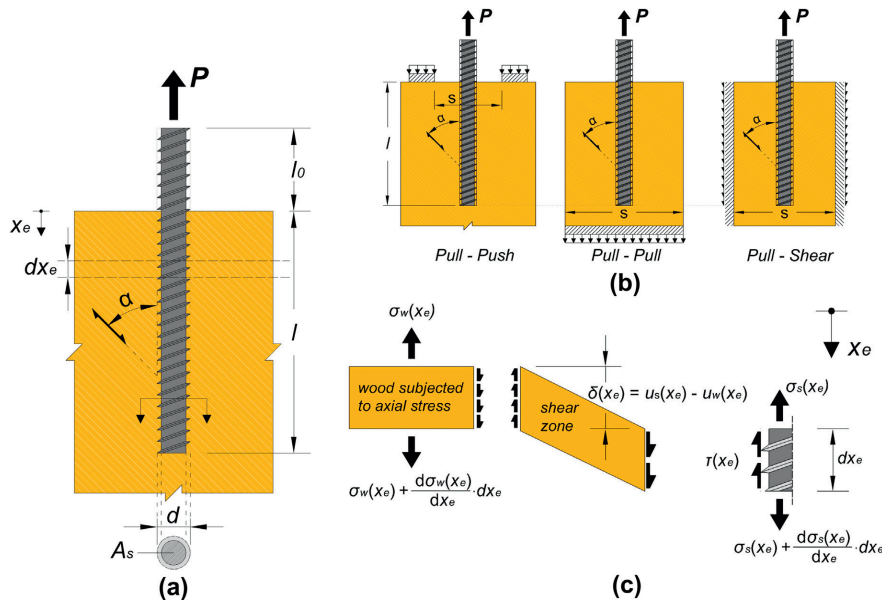$$\tau(x) = f_w - \Gamma_f \cdot (\delta(x) - \delta_e), \quad \delta(x) > \delta_e = f_w/\Gamma_e \tag{2b}$$

Fig. 1. Axially loaded connector: (a) geometric features, (b) loading conditions and (c) stress state of an infinitesimal small slice dx_e.
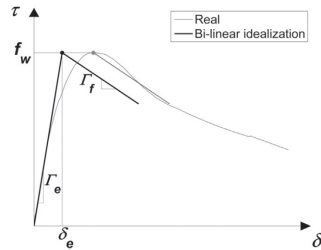
Fig. 2. Real and idealized bi-linear τ–δ curve.

where f_w and δ_e are the withdrawal strength and the maximum elastic displacement of the shear zone respectively. The bi-linear idealization separates the curve in two distinct domains; the linear elastic domain and the fracture domain. These domains are characterized by the equivalent shear stiffness parameters Γ_e and Γ_f, which are the slopes of the two branches of the bi-linear constitutive law. The term equivalent is used because these parameters account not only for shear deformation, but also for the relative slip between the connector and the surrounding wood at the interface. Note that a positive value of Γ_f indicates a negative slope of the curve. Wood is an anisotropic material and thus withdrawal leads to varying shear stress along the perimeter of the connector. Therefore, the shear stress should, in general, be considered as an average stress.

The axial stresses in the core of the connector and in the wood are assumed to be uniformly distributed and denoted $\sigma_s(x)$ and $\sigma_w(x)$ respectively. The mechanical behaviour of the connector and the wood is assumed to be linear-elastic at all times with moduli of elasticity denoted E_s and $E_{w\cdot\alpha}$ respectively (the modulus of elasticity of wood depends on α). Thus:

$$\varepsilon_s(x) = \frac{du_s(x)}{dx} = \frac{\sigma_s(x)}{E_s} \tag{3a}$$

$$\varepsilon_w(x) = \frac{du_w(x)}{dx} = \frac{\sigma_w(x)}{E_{w\cdot a}} \tag{3b}$$

where $\varepsilon_s(x)$ and $\varepsilon_w(x)$ are the axial strains in the connector and the wood respectively. It is assumed that the axial stress in wood distributes with a slope of stress dispersion equal to 1:3, as shown in Fig. 3. The area of wood subjected to axial stress is assumed to be constant and equal to an effective area $A_{w\cdot eff}$ [24]. $A_{w\cdot eff}$ is defined as the mean area in axial stress along the length of the connector, limited by the edge distances and the distance between the supports and the connector. For a rectangular box-type timber part symmetrically supported on both sides as depicted in Fig. 3 (which is the case for the present experimental investigation), $A_{w\cdot eff}$ is equal to:

$$A_{w\cdot eff} = 2 \cdot b \cdot \{s_s + \min(e, l/6) + \min(s/2, l/6)\} \tag{4}$$

where b is the width of the timber part, s_s the length of the provided support, e is the edge distance and s is the distance between supports.

The modulus of elasticity of wood in an angle to the grain can be estimated by Hankinson formula:

$$E_{w\cdot\alpha} = \frac{E_{w\cdot0} \cdot E_{w\cdot90}}{E_{w\cdot0} \cdot \sin^2\alpha + E_{w\cdot90} \cdot \cos^2\alpha} \tag{5}$$

where $E_{w\cdot0}$ and $E_{w\cdot90}$ are the moduli of elasticity of wood parallel and perpendicular to the grain direction respectively.
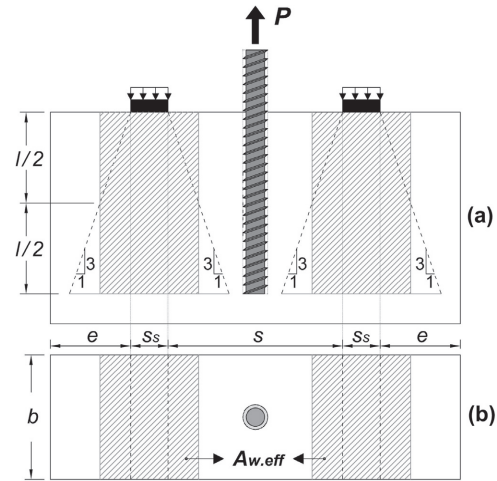
Fig. 3. Determination of $A_{w\cdot eff}$: (a) side view and (b) plan view.

2.2. Elastic analysis

Fig. 1c shows the stress state of an infinitesimal small slice dx_e of the embedded connector and the surrounding wood in the linear elastic domain. As long as $\delta(x)$ does not exceed δ_e, the behaviour is linear-elastic. For the pull-push loading condition the following analytical expressions can be derived for the distributions of the shear stress and the displacement of the shear zone [24]:

$$\tau(x_e) = -\frac{P}{\pi \cdot d \cdot l} \cdot \frac{\omega \cdot \cosh(\omega \cdot (1 - x_e/l))}{\sinh\omega} \tag{6}$$

$$\delta(x_e) = -\frac{P \cdot \beta \cdot l \cdot \cosh(\omega \cdot (1 - x_e/l))}{\omega \cdot \sinh\omega} \tag{7}$$

The parameters ω and β have been defined as follows:

$$\omega = \sqrt{\pi \cdot d \cdot \Gamma_e \cdot \beta \cdot l^2} \tag{8}$$

$$\beta = \frac{1}{A_s \cdot E_s} + \frac{1}{A_w \cdot E_{w\cdot\alpha}} \tag{9}$$

Eq. (6) is a hyperbolic monotonic function of x_e, whose maximum point is always at $x_e = 0$. Thus the absolute maximum shear stress, τ_{max} is equal to:

$$\tau_{max} = |\tau(x_e = 0)| = \frac{P}{\pi \cdot d \cdot l} \cdot \frac{\omega}{\tanh\omega} \tag{10}$$

By letting the maximum shear stress be equal to the withdrawal strength in Eq. (10), the elastic capacity P_e is obtained (in dimensionless form):

$$\frac{P_e}{\pi \cdot d \cdot l \cdot f_w} = \frac{\tanh\omega}{\omega} \tag{11}$$

The elastic capacity P_e, is the maximum withdrawal force that can be applied to the connector without initiation of in-elastic behaviour in the shear zone.

The withdrawal displacement is denoted δ_w and obtained by setting $x_e = 0$ in Eq. (7). The withdrawal stiffness, K_w, is provided by the following expression [24]:

$$K_w = \frac{P}{\delta_w} = \pi \cdot d \cdot l \cdot \Gamma_e \cdot \frac{\tanh\omega}{\omega}, \quad \delta_w \leqslant \delta_e = f_w/\Gamma_e \tag{12}$$

Fig. 4. Post-elastic behaviour of axially loaded connector: (a) Geometry and (b) stress state of an infinitesimal small slice dx_f in the fracture domain.

2.3. Post-elastic analysis

If the withdrawal force P exceeds the elastic capacity P_e as calculated by Eq. (11), a part of the length of the shear zone l_f will enter the fracture domain and exhibit non-elastic behaviour. In the remaining length, l_e the behaviour remains linear-elastic. The transition point that separates the elastic and the fracture domains is now taken as the new origin, as visualized in Fig. 4a.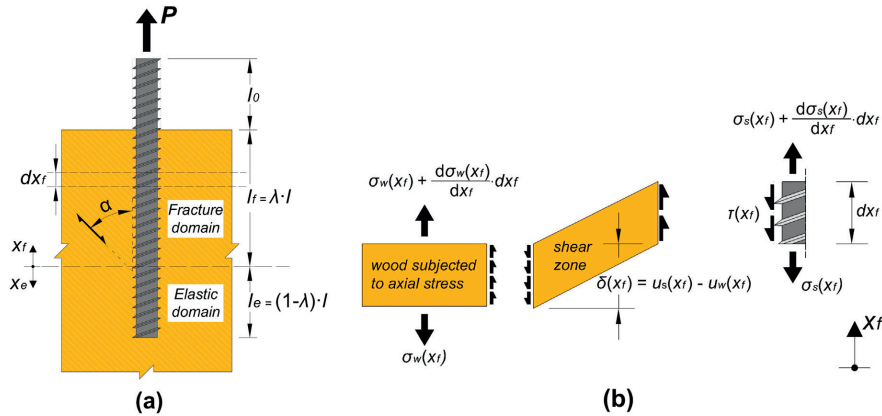 Positive x_e-axis is still pointing downwards while the positive x_f-axis is pointing upwards. The dimensionless fracture length parameter, $\lambda = l_f/l$, is defined, as explained in Fig. 4a. For the elastic domain, the expressions presented in the previous section apply, by setting $l_e = (1 - \lambda) \cdot l$ and $\omega_e = (1 - \lambda) \cdot \omega$ instead of l and ω and the corresponding elastic capacity $P_e(l_e)$ instead of P in Eqs. (6) and (7). $P_e(l_e)$ is obtained by setting $\omega_e = (1 - \lambda) \cdot \omega$ and $l_e = (1 - \lambda) \cdot l$ instead of ω and l in Eq. (11).

Fig. 4b shows the stress state of an infinitesimal small slice dx_f of the embedded connector and the surrounding wood in the fracture domain. Static equilibrium of this slice and use of Eqs. (1), (2b) and (3) lead to the following governing differential equation:

$$\frac{d^2\delta(x_f)}{dx_f^2} + \frac{m^2 \cdot \omega^2}{l^2} \cdot \delta(x_f) - \frac{(m^2 + 1) \cdot \omega^2}{l^2} \cdot \delta_e = 0 \qquad (13)$$

where the parameter m has been introduced as:

$$m = \sqrt{\Gamma_f / \Gamma_e} \qquad (14)$$

This parameter m is a measure of the brittleness of the shear zone. In the limits, $m \to 0$ indicates perfect plastic post-elastic behaviour, while $m \to \infty$ indicates totally brittle behaviour.

Eq. (13) is a linear, second-order, ordinary differential equation with the following solution:

$$\delta(x_f) = D_1 \cdot \sin\left(\frac{m \cdot \omega \cdot x_f}{l}\right) + D_2 \cdot \cos\left(\frac{m \cdot \omega \cdot x_f}{l}\right)$$
$$+ \left(1 + \frac{1}{m^2}\right) \cdot \delta_e \qquad (15)$$

D_1 and D_2 are constants to be determined by the following boundary conditions:

$$\delta(x_f = 0) = \delta_e \qquad (16a)$$

$$\left.\frac{d\delta(x_f)}{dx_f}\right|_{x_f=0} = \varepsilon_s(x_f = 0) - \varepsilon_w(x_f = 0) = P_e(l_e) \cdot \beta \qquad (16b)$$

Eqs. (15) and (16) provide the two equations from which D_1 and D_2 can be solved; the result is the displacement distribution of the shear zone:

$$\frac{\delta(x_f)}{\delta_e} = 1 + \frac{\tanh\left((1 - \lambda) \cdot \omega\right) \cdot \sin\left(\frac{m \cdot \omega \cdot x_f}{l}\right)}{m} + \frac{1 - \cos\left(\frac{m \cdot \omega \cdot x_f}{l}\right)}{m^2} \qquad (17)$$

It is noted that the displacement given by Eq. (17) may underestimate the real displacement, due to the bi-linear approximation of τ–δ curve, which neglects the effect of softening prior to fracture, confer Fig. 2. The withdrawal displacement δ_w is obtained by setting $x_f = \lambda \cdot l$ in Eq. (17).

Combining Eq. (2b) and (17) the shear stress distribution in the fracture domain is determined:

$$\frac{\tau(x_f)}{f_w} = \cos\left(\frac{m \cdot \omega \cdot x_f}{l}\right) - m \cdot \tanh\left((1 - \lambda) \cdot \omega\right)$$
$$\cdot \sin\left(\frac{m \cdot \omega \cdot x_f}{l}\right) \qquad (18)$$

It should be verified that the shear stress in the entrance is always positive, i.e. $\tau(x_f = \lambda \cdot l) > 0$.

For the pull-push loading condition the following boundary condition also applies:

$$\left.\frac{d\delta(x_f)}{dx_f}\right|_{x_f=\lambda \cdot l} = \varepsilon_s(x_f = \lambda \cdot l) - \varepsilon_w(x_f = \lambda \cdot l) = P \cdot \beta \qquad (19)$$

Combining Eqs. (17) and (19), an expression which relates the withdrawal force P with the dimensionless fracture length parameter λ is obtained:

$$\frac{P}{\pi \cdot d \cdot l \cdot f_w} = \frac{\sin(m \cdot \omega \cdot \lambda)}{\omega \cdot m} + \frac{\tanh((1 - \lambda) \cdot \omega) \cdot \cos(m \cdot \omega \cdot \lambda)}{\omega} \qquad (20)$$

The only variable in Eq. (20) is the dimensionless fracture length λ. Thus the withdrawal force takes its maximum value when the derivative of the force with respect to λ is equal to zero. Setting this derivative equal to zero, leads to the following equation:

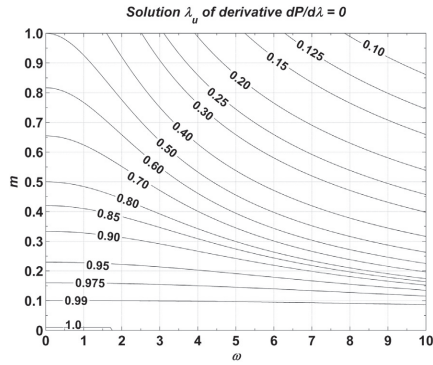$$\tanh((1 - \lambda) \cdot \omega) \cdot [m \cdot \tan(m \cdot \omega \cdot \lambda) - \tanh((1 - \lambda) \cdot \omega)] = 0 \qquad (21)$$

Fig. 5. Diagram for the determination of λ_u.

$$\frac{P_f}{\pi \cdot d \cdot l \cdot f_w} = \frac{\tan(m \cdot \omega)}{\omega \cdot m} \cdot \left(1 + m^2 - m^2 \cdot \frac{\delta_w}{\delta_e}\right),$$
$$\frac{\delta_w}{\delta_e} > 1 + \frac{1 - \cos(m \cdot \omega)}{m^2} \tag{23}$$

$$\tau_f(x_f) = \frac{P_f}{\pi \cdot d \cdot l} \cdot \frac{\omega \cdot m \cdot \cos\left(\frac{m \cdot \omega \cdot x_f}{l}\right)}{\sin(\omega \cdot m)} \tag{24}$$

The evolution of the shear stress distribution for increasing withdrawal displacement is plotted in Fig. 6. The entrance point of the connector is at $x = 0$ and the tip is at $x = l$.

The expressions derived in this section apply for the pull-push loading condition. However, they also apply for the pull-shear loading condition, assuming $A_w \to \infty$ and thus $\beta = 1/A_s \cdot E_s$. The respective expressions for the pull-pull loading condition are not presented herein.

3. Experimental tests

3.1. Experimental set-up

The experimental set-up for the withdrawal tests is presented in Fig. 7. As shown, the loading condition of the specimens was a 'remote' pull-push (i.e. the support was provided in the same plane surface as the entrance of the rod, but at a distance to the rod). A thin steel plate, as shown in Fig. 7d, was placed between the supports and the specimen. The plate was used to counteract tensile stresses due to bending, while allowing for local deformation on the surface of the specimen. Two displacement transducers were placed next to the supports of the specimen, measuring the relative displacement between the rod and support as shown in Fig. 7a, c and e. The average of these two measurements was used for the displacement. Testing was performed using the loading protocol given in EN 26891:1991 (ISO6891:1983) [29].

3.2. Materials

The specimens were cut from glulam beams of Scandinavian class L40c, which corresponds to European strength class GL30c [30]. This type of glulam is fabricated with 45 mm thick lamellas, made of Norwegian spruce (*picea abies*). For increased homogeneity, all specimens were manufactured such that the rods were inserted in the vicinity of the inner, weaker lamellas of the beams. SFS WB-T-20 [31] steel threaded rods were used. These rods are made according to DIN7998 [32] and a lay-out is shown in Fig. 8. The outer-thread diameter d of the rods is 20 mm and core diameter d_c is 15 mm. The pitch distance is $c = 7$ mm. According to the manufacturer, the steel grade of the rods is 8.8 and their characteristic tensile capacity $P_{u \cdot k \cdot rod}$ is 145 kN.

Eq. (21) is periodic and it may therefore have multiple roots in the physical domain of $\lambda = (0, 1)$. It has the obvious solution $\lambda = 1.0$ which accounts for the case in which the whole length of the shear zone has entered the fracture domain. However, there may be more solutions in the physical domain of λ, and since the shear stress distribution cannot be a periodic function, the only physically permissible solution is the minimum positive solution in the physical domain of λ, which is denoted λ_u. An analytical solution of Eq. (21) is not feasible; however λ_u can be obtained as a function of parameters m and ω by the diagram presented in Fig. 5. The withdrawal capacity of the connector, $P_{u \cdot w}$, is obtained by substituting λ_u into Eq. (20).

At some point, for increasing displacement and after the withdrawal capacity is reached, the shear zone will be entirely in the fracture domain, i.e. $\lambda = 1$. Beyond this displacement level, the displacement of the shear zone, the shear stress and the withdrawal force are denoted δ_f, τ_f and P_f respectively. The following boundary conditions apply in this case:

$$\left.\frac{d\delta_f(x_f)}{dx_f}\right|_{x_f=0} = \varepsilon_s(x_f = 0) - \varepsilon_w(x_f = 0) = 0 \tag{22a}$$

$$\left.\frac{d\delta_f(x_f)}{dx_f}\right|_{x_f=l} = \varepsilon_s(x_f = l) - \varepsilon_w(x_f = l) = P_f \cdot \beta \tag{22b}$$

By use of Eqs. (1), (2b), (3), (15) and (22), the following expressions are obtained for the relationship between the withdrawal force and the withdrawal displacement ($\delta_w = \delta_f (x_f = l)$), and for the shear stress distribution:
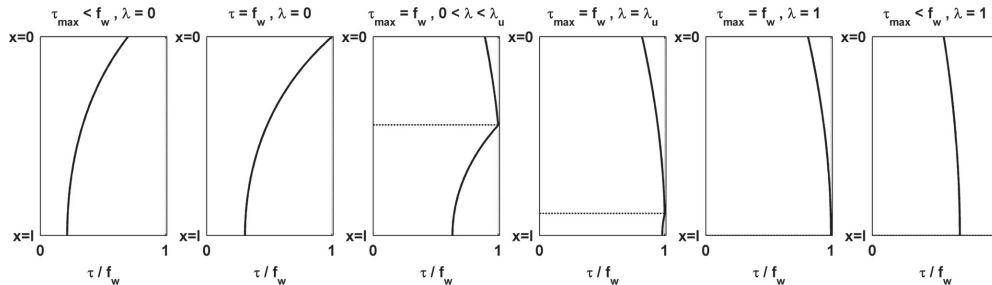

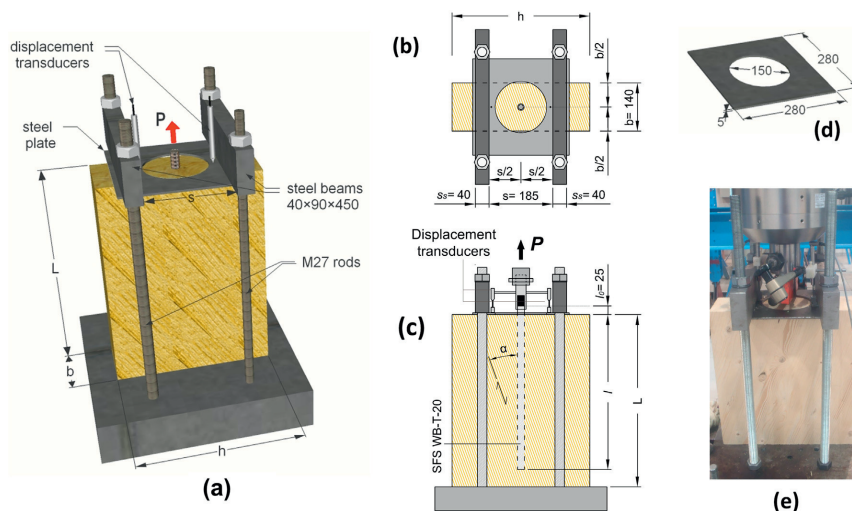**Fig. 6.** Evolution of shear stress distribution for increasing withdrawal displacement.

Fig. 7. Experimental set-up: (a) virtual 3D representation, (b) plan view, (c) side view, (d) geometry of steel plate and (e) photo.
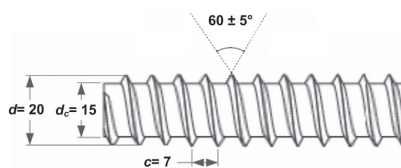

Fig. 8. Geometry of SFS WB-T-20 threaded rods (DIN 7998 [32]).

3.3. Specimens

Prior to rod installation, all specimens were pre-drilled with a diameter equal to the core diameter of the rods, i.e. 15 mm. All specimens were conditioned to standard temperature and relative humidity conditions (20 °C/65% R.H.), leading to approximately 12% moisture content in the wood. The parameters of the experimental investigation were the rod-to-grain angle and the embedment length of the rod. Specimens with 6 different rod-to-grain angles (α = 0°, 10°, 20°, 30°, 60° and 90°) and 4 different embedment lengths (l = 100, 300, 450, 600 mm) were tested. Five tests were performed for each sub-group of parameters. The width, b, of the glulam beams and consequently of all specimens was equal to 140 mm. The specimens are denoted Sα-l-no, based on their rod-to-grain angle α, the embedment length l and the serial number of the test within each set of parameters. The dimensions and parameters of the specimens are given in Table 1. The symbols are explained in Fig. 7. For all specimens, the distance between supports was s = 185 mm and the free length l_0 of the threaded rod (between the entrance point and the clamping point) was 25 mm.

4. Results and discussion

4.1. Experimental results and failure modes

The mean experimentally measured capacities, the standard deviation and the coefficient of variation for each sub-group of specimens are summarized in Table 1. Moreover, the failure modes

of specimens with different rod-to-grain angles are depicted in Fig. 9. All specimens with rods installed parallel to the grain direction failed due to withdrawal of the threaded rod along the interface plane between wood and the outer diameter, as shown in Fig. 9a–c. In some of these specimens a tensile crack developed on the surface as shown in Fig. 9a. As expected, the crack originated at the wood-rod interface and propagated in the radial direction. However, the steel plate might have prevented the propagation of this crack toward the edges of the specimen. Finally, the development of this crack did not seem to have any impact on the capacity of these specimens.

Yielding of the rod was observed in the majority of specimens with embedment length equal to 600 mm and also in some of the specimens with embedment length equal to 450 mm. Three specimens in series S10-600 and all 5 specimens in series S20-600 and S30-600 failed due to steel fracture as shown in Fig. 9g. In all these specimens the steel fracture was observed in the free part of the rod, between the entrance and the clamping point. In the other specimens where the rod yielded, the increasing force due to steel hardening, led to withdrawal failure prior to steel fracture. Yielding and steel fracture of the rods occurred at load levels which were significantly higher than those predicted by the specified yield and ultimate strength properties of steel. The observed increased strength of steel might be attributed to steel hardening due to thread rolling.

For specimens with rods installed at an angle to the grain direction, wood failure also occurred in the interface plane between wood and the outer-thread diameter; confer Fig. 9e, f, i, j and l. This failure mode was combined with a shear tear-off failure of a wooden piece at the entrance point, at an angle equal to the rod-to-grain angle; see Fig. 9d and h. Finally, specimens with rods installed perpendicular to the grain direction exhibited withdrawal failure combined with extensive normal deformation of the fibers, as shown in Fig. 9k and l.

4.2. Parameters of the bi-linear constitutive law

The necessary input parameters for the determination of the bi-linear constitutive law are the equivalent shear stiffness Γ_e,

Table 1
Specimens' parameters, dimensions and results.

Specimen	Dimensions	Density	Experimental results			Theoretical estimation[a]			
I.D. (Sα-l-no)	$b \times h \times L$ (mm)	ρ_m (kg/m³)	$P_{u \cdot mean}$ (kN)	St. Dev. (kN)	C.o.V. (–)	$A_{w \cdot eff}$ (mm²)	P_e (kN)	λ_u (–)	$P_{u \cdot w}$ (kN)
S0-100-(1-5)	$140 \times 270 \times 300$	447	27.3	3.9	0.14	16,567	25.8	0.90	27.2
S0-300-(1-5)	$140 \times 270 \times 350$	474	89.7	10.5	0.12	25,900	55.4	0.90	79.7
S0-450-(1-5)	$140 \times 270 \times 500$	458	130.2	31.1	0.24	32,900	62.8	0.89	115.4
S0-600-(1-5)	$140 \times 270 \times 650$	443	161.6	8.4	0.05	37,800	65.3	0.88	146.4
S10-100-(1-5)	$140 \times 300 \times 300$	457	26.3	4.9	0.19	20,533	25.7	0.94	27.3
S10-300-(1-5)	$140 \times 300 \times 350$	479	99.8	9.8	0.10	30,100	54.5	0.94	80.7
S10-450-(1-5)	$140 \times 300 \times 500$	446	127.5	17.6	0.14	37,100	61.5	0.93	118.4
S10-600-(1-5)	$140 \times 300 \times 650$	462	173.1[b]	5.2	0.03	42,000	63.9	0.93	152.9
S20-100-(1-5)	$140 \times 450 \times 300$	475	30.5	6.8	0.22	20,533	25.5	0.96	27.6
S20-300-(1-5)	$140 \times 450 \times 350$	478	98.7	10.6	0.11	39,200	53.2	0.95	81.7
S20-450-(1-5)	$140 \times 450 \times 500$	473	145.8	9.2	0.06	53,200	60.3	0.95	120.5
S20-600-(1-5)	$140 \times 450 \times 650$	481	175.7[c]	0.80	0.01	63,000	62.9	0.95	157.1
S30-100-(1-5)	$140 \times 500 \times 300$	479	27.0	4.0	0.15	20,533	25.2	0.96	27.9
S30-300-(1-5)	$140 \times 500 \times 350$	477	99.9	10.7	0.11	39,200	51.0	0.96	82.8
S30-450-(1-5)	$140 \times 500 \times 500$	475	144.6	13.3	0.09	53,200	57.9	0.96	122.4
S30-600-(1-5)	$140 \times 500 \times 650$	486	176.7[c]	0.9	0.01	65,100	60.9	0.96	160.2
S60-100-(1-5)	$140 \times 300 \times 500$	476	28.5	5.5	0.19	20,533	25.1	0.97	29.2
S60-300-(1-5)	$140 \times 350 \times 350$	488	93.6	11.6	0.12	37,100	47.1	0.97	86.7
S60-450-(1-5)	$140 \times 350 \times 500$	476	141.7	4.5	0.03	44,100	52.1	0.97	128.1
S90-100-(1-5)	$140 \times 350 \times 300$	475	29.9	2.9	0.10	20,533	25.4	0.96	29.9
S90-300-(1-5)	$140 \times 350 \times 350$	488	96.5	7.0	0.07	37,100	47.2	0.96	88.3
S90-450-(1-5)	$140 \times 350 \times 500$	486	139.2	7.4	0.05	44,100	52.3	0.96	129.8

[a] Input values: $A_s = \pi \cdot d_c^2/4 = 176.6$ mm² , $E_s = 210{,}000$ MPa, $E_{w \cdot 0} = 13{,}000$ MPa, $E_{w \cdot 90} = 410$ MPa.
[b] Steel fracture in 3/5 rods.
[c] Steel fracture in all 5 rods.
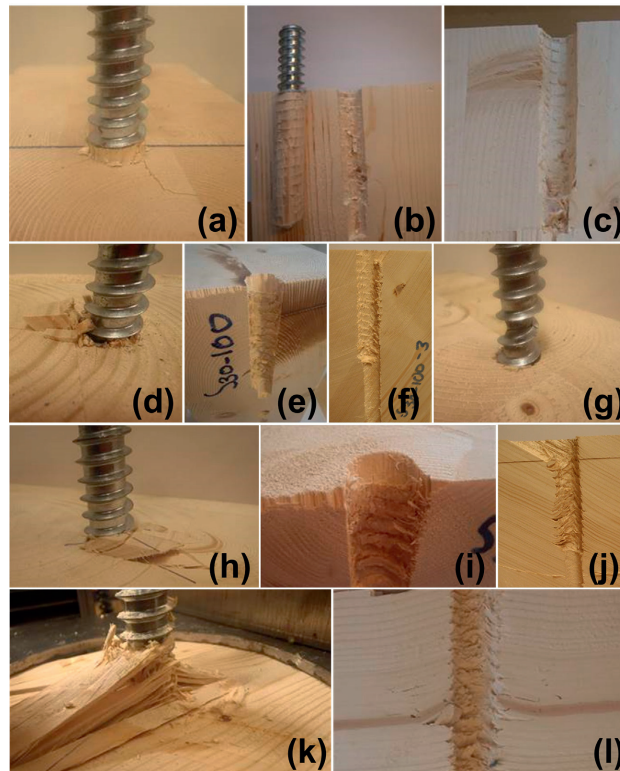
Fig. 9. Failure modes of specimens with α = 0° (a)–(c), α = 30° (d)–(g), α = 60° (h)–(j) and α = 90° (k)–(l).

(a)

(b)
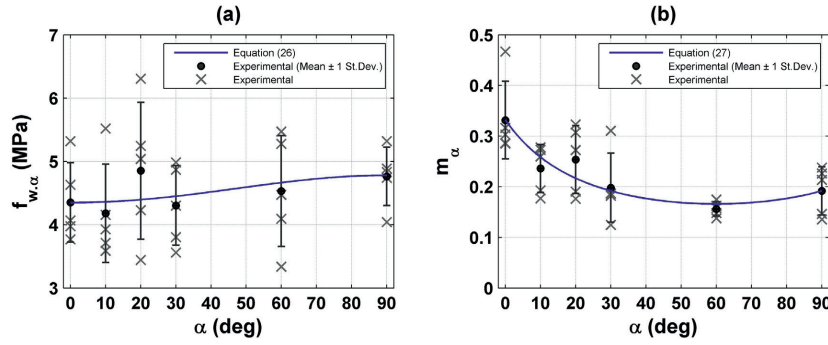
Fig. 10. (a) Withdrawal strength and (b) m-parameter as functions of α.

$\alpha = 0°$

$\alpha = 10°$

$\alpha = 20°$

$\alpha = 30°$

$\alpha = 60°$

$\alpha = 90°$
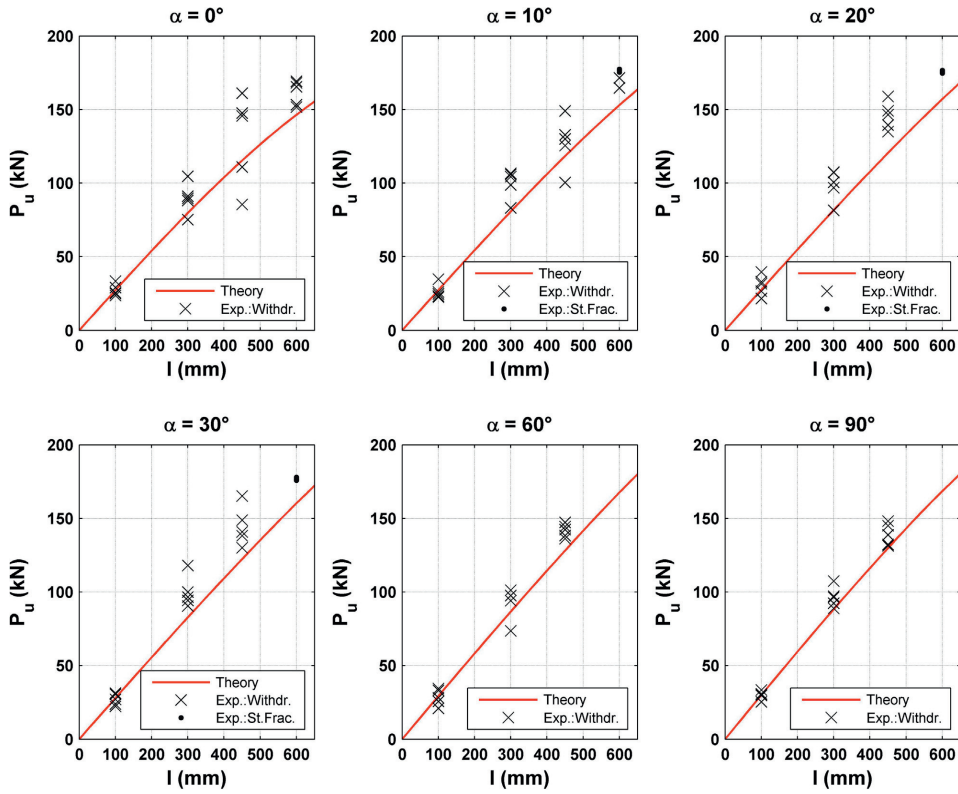
Fig. 11. Experimental and theoretical capacities as function of embedment length.

the withdrawal strength f_w and the brittleness parameter m. The elastic properties of wood depend on α and thus these parameters also depend on α. In an accompanying paper [24], the following expression has been derived for Γ_e as function of α for the same experimental specimens (in MPa/mm) [24]:

$$\Gamma_{e,\alpha} = \frac{9.35}{1.5 \cdot \sin^{2.2} \alpha + \cos^{2.2} \alpha} \qquad (25)$$

The withdrawal strength f_w and the parameter m can be derived from experimental results of specimens with a sufficiently short embedment length, so that the shear stress and displacement of
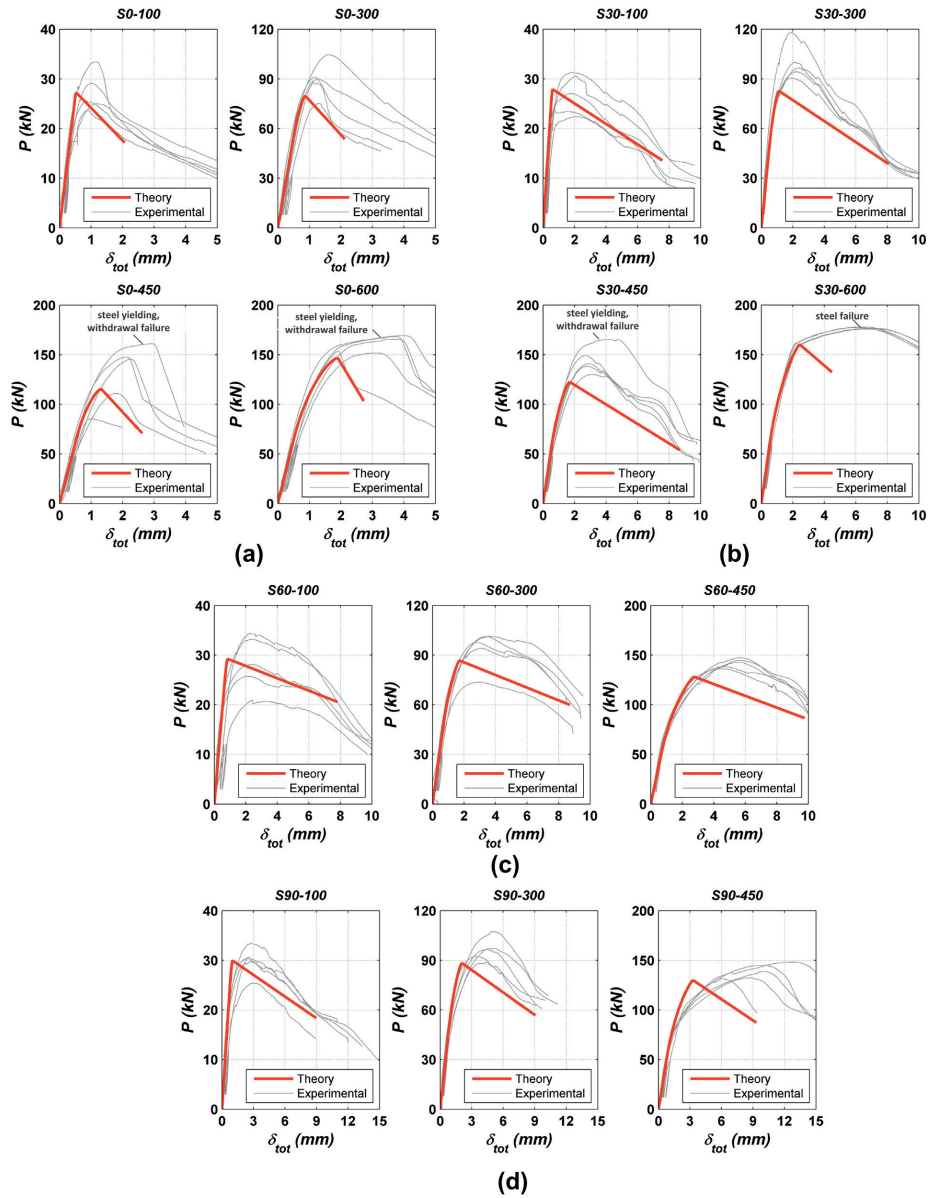
Fig. 12. P–δ_{tot} curves for specimens with (a) $\alpha = 0°$, (b) $\alpha = 30°$, (c) $\alpha = 60°$ and (d) $\alpha = 90°$.

the shear zone at and after failure, can be approximated as uniformly distributed. In such a case, the withdrawal strength can be calculated as the capacity of the specimen divided by the interface area. The slope of the descending part of τ–δ curve, Γ_f

and thus m can be found by fitting a line in this part, confer Fig. 2. The withdrawal strength f_w and parameter m were derived from the experimental results for all specimens with the smallest embedment length, i.e. $l = 100$ mm. Regression analysis showed

low correlation between f_w and α and high correlation between m and α. A generalized Hankinson formula was used to fit the experimentally obtained results and regression led to the following expressions for f_w (in MPa) and m as functions of α:

$$f_{w.\alpha} = \frac{f_{w.0}}{\frac{f_{w.0}}{f_{w.90}} \cdot \sin^2 \alpha + \cos^2 \alpha} = \frac{4.35}{0.91 \cdot \sin^2 \alpha + \cos^2 \alpha} \qquad (26)$$

$$m_\alpha = \frac{m_0}{\frac{m_0}{m_{90}} \cdot \sin \alpha + \cos \alpha} = \frac{0.332}{1.73 \cdot \sin \alpha + \cos \alpha} \qquad (27)$$

It is noted that Eq. (26) coincides with the classical Hankinson formula. In Eq. (27) the trigonometric functions are not squared. Fig. 10 shows the mean and the individual experimentally obtained values of f_w and m, as well as the estimated values determined by Eqs. (26) and (27), as function of rod-to-grain angle.

4.3. Theoretical versus experimental results

The withdrawal capacity was estimated for all specimens by use of Eq. (20), as discussed in Section 2.3. The theoretical estimations for the elastic capacity P_e, the withdrawal capacity $P_{u \cdot w}$ and the corresponding dimensionless fracture length, λ_u, can be found in Table 1, for each sub-group of specimens. The theoretical estimations for the withdrawal capacity and the experimentally measured capacities of the specimens, due to withdrawal or steel fracture, are plotted in Fig. 11 as functions of the embedment length for all rod-to-grain angles. The specimens which failed due to steel fracture had apparently greater withdrawal capacity. Fig. 11 shows that the agreement between the theoretical estimation and the experimental results is, in general, good. The theoretical approach predicts a nearly linear relation between the withdrawal capacity and the embedment length, until steel failure takes place. This prediction was validated by the experimental results. The theoretical values are slightly conservative; this can probably be explained by the fact that confining, due to the compressive stress from the specimen support, is not accounted for in the theoretical approach.

The theoretical and the experimental force-total displacement curves for all specimens with rod-to-grain angles equal to $0°$, $30°$, $60°$ and $90°$ are depicted in Fig. 12. The theoretical total displacement δ_{tot} was obtained by adding the elongation of the free length of the rod, $u_{s.0} = P \cdot l_0 / A_s \cdot E_s$, to the withdrawal displacement δ_w. The theoretically estimated curves are generally in good agreement with the experimental ones, especially for specimens with small rod-to-grain angles. However, they underestimate the withdrawal displacement because the bi-linear constitutive law does not account for the effect of softening prior to fracture. Moreover, in specimens S60-450 and S90-450 the compressive strength of the wood under the supports was exceeded for high withdrawal force levels, which resulted in a deviation between the theoretical and the experimental curves. Finally, Fig. 12 shows that increasing rod-to-grain angle led to a less brittle behaviour of the specimens.

5. Concluding remarks

The withdrawal capacity of axially loaded threaded rods screwed into timber elements was studied, using both theoretical and experimental methods. Specimens covering a wide range of rod-to-grain angles and embedment lengths were tested. The outer thread diameter of the threaded rods was constant and equal to 20 mm. The following main conclusions are drawn:

- The experimental specimens showed in general high withdrawal capacity.

- The withdrawal capacity can be predicted with good accuracy using a simple analytical procedure based on Volkersen theory. The theoretical estimations for withdrawal capacity are in general in good agreement with the experimental results, but might be slightly conservative.
- A nearly linear relation between the embedment length and the withdrawal capacity was predicted by the theoretical approach, which was validated by experimental results.
- The specimens with small rod-to-grain angles exhibited more brittle behaviour than the ones with larger angles.
- For several specimens with long embedment lengths (i.e. 450 mm and 600 mm), steel yielding was observed. Some of these specimens failed due to steel fracture. Embedment lengths in the range 600 mm and more will lead to ductile steel failure instead of withdrawal failure.

Appendix A. Supplementary material

Supplementary data associated with this article can be found, in the online version, at http://dx.doi.org/10.1016/j.conbuildmat. 2015.07.067.

References

[1] H.J. Blaß, I. Bejtka, Reinforcements perpendicular to grain using self-tapping screws, in: Proceedings of the 8th World Conference on Timber Engineering, Lahti, Finland, 2004, pp. 233–238.
[2] I. Bejtka, H.J. Blaß, Self-tapping screws as reinforcements in beam supports, in: Proceedings of the 39th CIB-W18 Meeting Florence, Italy, 2006.
[3] H.J. Blaß, M. Schmid, Self-tapping screws as reinforcement perpendicular to the grain in timber connections, in: Proceedings of RILEM Symposium: Joints in Timber Structures, Stuttgart, Germany, 2001, pp. 163–172.
[4] F. Lam, M. Schulte-Wrede, C.C. Yao, J.J. Gu, Moment resistance of bolted timber connections with perpendicular to grain reinforcements, in: Proceedings of the 10th World Conference on Timber Engineering, Miyazaki, Japan, 2008, pp. 978–985.
[5] I. Bejtka, H.J. Blaß, Joints with inclined screws, in: Proceedings of the 35th CIB-W18 Meeting Kyoto, Japan, 2002.
[6] R. Tomasi, A. Crosatti, M. Piazza, Theoretical and experimental analysis of timber-to-timber joints connected with inclined screws, Constr. Build. Mater. 24 (2010) 1560–1571.
[7] M. Closen, F. Lam, Performance of moment resisting self-tapping screw assembly under reverse cyclic load, in: Proceedings of the 12th World Conference on Timber Engineering, Auckland, New Zealand, 2012, pp. 433–440.
[8] P. Ellingsbø, K.A. Malo, Cantilever glulam beam fastened with long threaded steel rods, in: Proceedings of the 11th World Conference on Timber Engineering, Trentino, Italy, 2010, pp. 468–475.
[9] K.A. Malo, P. Ellingsbø, On connections for timber bridges, in: Proceedings of the International Conference Timber Bridges (ICTB), Lillehammer, Norway, 2010, pp. 297–312.
[10] Y. Wakashima, K. Okura, K. Kyotani, Development of ductile semi-rigid joints with lagscrewbolts and glued-in rods, in: Proceedings of the 11th World Conference on Timber Engineering, Trentino, Italy, 2010, pp. 3221–3228.
[11] P. Ellingsbø, K.A. Malo, Withdrawal capacity of long self-tapping screws paralell to grain direction, in: Proceedings of the 12th World Conference on Timber Engineering, 2012, pp. 228–237.
[12] D. Gaunt, The effect of thread geometry on screw withdrawal strength, NZ Timber Des. J. 6 (1997) 12–20.
[13] M. Gehloff, Pull-out Resistance of Self-Tapping Wood Screws with Continuous Thread [Master's Thesis], The University of British Columbia, Vancouver, Canada, 2011.
[14] U. Hübner, M. Rasser, G. Schickhofer, Withdrawal capacity of screws in European ash (*Fraxinus excelsior* L.), in: Proceedings of the 11th World Conference on Timber Engineering, Trentino, Italy, 2010, pp. 241–249.

[15] J.L. Jensen, M. Nakatani, P. Quenneville, B. Walford, A simple unified model for withdrawal of lag screws and glued-in rods, Eur. J. Wood Wood Prod. 69 (2011) 537–544.

[16] J.L. Jensen, M. Nakatani, P. Quenneville, B. Walford, A simplified model for withdrawal of screws from end-grain of timber, Constr. Build. Mater. 29 (2012) 557–563.

[17] S. Kennedy, A. Salenikovich, W. Munoz, M. Mohammad, Design equation for withdrawal resistance of threaded fasteners in the Canadian timber design code, in: Proceedings of the 13th World Conference on Timber Engineering, Quebec City, Canada, 2014.

[18] T. Mori, M. Nakatani, Y.H. Chui, M. Gong, H. Isoda, K. Komatsu, Pull-out strength properties of lagscrewbolt connection in cross laminated timber, in: Proceedings of the 13th World Conference on Timber Engineering, Quebec City, Canada, 2014.

[19] M. Nakatani, K. Komatsu, Development and verification of theory on pull-out properties of Lagscrewbolted timber joints, in: Proceedings of the 8th World Conference on Timber Engineering, Lahti, Finland, 2004, pp. 95–99.

[20] G. Pirnbacher, R. Brandner, G. Schickhofer, Base parameters of self-tapping screws, in: Proceedings of the 42nd CIB-W18 meeting Dübendorf, Switzerland, 2009.

[21] A. Ringhofer, G. Schickhofer, Investigations concerning the force distribution along axially loaded self-tapping screws, in: S. Aicher, H.W. Reinhardt, H. Garrecht (Eds.), Materials and Joints in Timber Structures, Recent Developments of Technology, Springer, 2014, pp. 201–210.

[22] A. Ringhofer, G. Schickhofer, Influencing parameters on the experimental determination of the withdrawal capacity of self-tapping screws, in: Proceedings of the 13th World Conference on Timber Engineering, Quebec City, Canada, 2014.

[23] A. Ringhofer, R. Brandner, G. Schickhofer, Withdrawal resistance of self-tapping screws in unidirectional and orthogonal layered timber products, Mater. Struct. (2013) 1–13.

[24] H. Stamatopoulos, K.A. Malo, Withdrawal stiffness of threaded rods embedded in timber elements, Constr. Build. Mater., 2015, submitted for publication.

[25] O. Volkersen, Die nietkraftverteilung in zugbeanspruchten nietverbindungen mit konstanten laschenquerschnitten, Luftfahrtforschung 15 (1938) 41–47.

[26] J.L. Jensen, A. Koizumi, T. Sasaki, Y. Tamura, Y. Iijima, Axially loaded glued-in hardwood dowels, Wood Sci. Technol. 35 (2001) 73–83.

[27] CEN, European Committee for Standardization, EN 1995-1-1:2004: Design of timber structures. Part 1-1: General-Common Rules and Rules for Buildings, Brussels, Belgium, 2004.

[28] C. Pörtner, Untersuchungen zum Verbund zwischen eingeklebten stiftförmigen faserverstärkten Kunststoffen und Holz [Ph.D. Thesis], Kassel University, Kassel, Germany, 2005.

[29] CEN, European Committee for Standardization, EN 26891:1991 (ISO 6891:1983): Timber Structures – Joints Made with Mechanical Fasteners-General Principles for the Determination of Strength and Deformation Characteristics, Brussels, Belgium, 1991.

[30] CEN, European Committee for Standardization, EN 14080-2013: Timber Structures – Glued Laminated Timber and Glued Solid Timber – Requirements, Brussels, Belgium, 2013.

[31] SFS intec, GmbH, Gewindestangen mit Holzgewinde als Holzverbindungsmittel, Allgemeine bauaufsichtliche Zulassung Z-9.1-777, Deutsches Institut für Bautechnik (DIBt), 2010.

[32] DIN, Deutsches Institut für Normung, DIN 7998: Gewinde und Schraubenenden für Holz-schrauben, Berlin, Germany, 1975.

Paper III

Withdrawal of pairs of threaded rods with small edge distances and spacings

Haris Stamatopoulos and Kjell Arne Malo

Submitted to European Journal of Wood and Wood Products (2016)

Is not included due to copyright

Paper IV

Characteristic withdrawal capacity and stiffness of threaded rods

Haris Stamatopoulos and Kjell Arne Malo

Proceedings of the 2nd meeting of the International Network on Timber Engineering Research (INTER). Paper 48-7-2. Šibenik, Croatia (2015).

Characteristic withdrawal capacity and stiffness of threaded rods

Haris Stamatopoulos and Kjell Arne Malo

Norwegian University of Science and Technology (NTNU), Trondheim, Norway

1 Introduction

Long threaded rods show high withdrawal capacity and stiffness and thus they may be used in order to realize strong and stiff connections for timber structures. In comparison to dowel-type connectors, they have no initial soft response and no initial slip. In comparison to glued-in-rods they are less prone to construction quality issues, less brittle and offer greater protection against high temperatures (Mischler and Frangi 2001). Due to their length, their withdrawal capacity and stiffness are not significantly affected by local defects. Furthermore, a high degree of pre-fabrication is possible and hence easy and fast erection on site may be achieved.

Over the last years, the vast majority of the research effort has been devoted to the withdrawal capacity of screws with diameters up to 12 mm. The influence of parameters such as the embedment length and the angle between the screw axis and the grain direction has been investigated; see for example (Pirnbacher, Brandner and Schickhofer 2009, Frese and Blaß 2009). On the other hand, the research effort on the withdrawal capacity and also stiffness of threaded rods with diameters up to 20-25mm has not been so intensive and mostly it is limited to rods installed parallel and perpendicular to the grain (Jensen et al. 2011, Jensen et al. 2012, Nakatani and Komatsu 2004, Mori et al. 2008).

Eurocode 5, EC5 (CEN 2004) do not provide guidelines for the estimation of the withdrawal stiffness which is required for the evaluation of the stiffness of connections with threaded connectors (Tomasi, Crosatti and Piazza 2010, Malo and Ellingsbø

2010). Some expressions may be found in technical approvals of screws, but mostly these expressions are valid for screws with relatively small diameters. Moreover, EC5 does not allow the installation of rods in an angle to the grain less than 30° in order to eliminate the risk of splitting failure. However, in practice, it may be desired to install threaded rods in an angle to the grain smaller than 30˚ (in combination with some sort of reinforcement to prevent splitting failure).

In the present paper, an experimental study on withdrawal of threaded rods embedded in glue-laminated timber (abbr. glulam) elements is presented. The parameters of this study were the embedment length and the angle between the rod axis and the grain direction (with emphasis on angles which are smaller than 30°). Moreover, analytical expressions for the estimation of withdrawal capacity and stiffness are provided. The characteristic withdrawal capacity and the mean withdrawal stiffness were obtained by the experimental results and compared to the analytical estimations.

2 Experimental methods

2.1 Experimental set-up

The experimental set-up for the withdrawal tests is presented in Figure 1. As shown, the loading condition of the specimens was a 'remote' pull-push (i.e. the support was provided in the same plane surface as the entrance of the rod, but at a distance to the rod). A thin steel plate, as shown in Fig. 1d, was placed between the supports and the specimen. The plate was used to counteract bending stresses and prevent tensile splitting failure, while allowing local deformation on the surface of the specimen in the vicinity of the rod. Two displacement transducers were placed next to the supports of the specimen, measuring the relative displacement between the rod and support as shown in Figures 1a, 1c and 1e. The average of these two measurements was used for the displacement. Testing was performed using the loading protocol given in EN 26891:1991 (ISO6891:1983) (CEN 1991).

2.2 Materials

The specimens were cut from glulam beams of Scandinavian class L40c which corresponds to European strength class GL30c (CEN 2013). This type of glulam is fabricated with 45 mm thick lamellas, made of Norwegian spruce (*Picea Abies*). The mean and characteristic density of L40c is ρ_{mean} = 470 kg/m^3 and ρ_k = 400 kg/m^3 respectively. The mean moduli of elasticity, parallel and perpendicular to the grain, are $E_{0.mean}$ = 13000 MPa and $E_{90.mean}$ =410 MPa respectively, and the shear modulus is G= 760 MPa.

For increased homogeneity, all specimens were manufactured such that the rods were inserted in the inner, weaker lamellas of the beams. SFS WB-T-20 (DIBt 2010) steel threaded rods were used. These rods are made according to DIN7998 (DIN 1975). The outer-thread diameter d of the rods is 20 mm and the core diameter, d_c, is 15 mm. According to the manufacturer, the steel grade of the rods is 8.8 and their characteristic tensile capacity is 145 kN.

2.3 Specimens

Prior to rod installation, all specimens were pre-drilled with a diameter equal to d_c. All specimens were conditioned to standard temperature and relative humidity conditions (20°C / 65% R.H.), leading to approximately 12% moisture content in the wood. The parameters of the experimental investigation were the rod-to-grain angle, α, and the embedment length of the rod, l_{ef}. Specimens with 6 different rod-to-grain angles (α = 0, 10, 20, 30, 60 and 90°) and 4 different embedment lengths (l_{ef} = 100, 300, 450, 600 mm) were tested. The series of specimens are denoted Sα-l_{ef}, based on their rod-to-grain angle and embedment length. The width, b, of the glulam beams and consequently of all specimens was equal to 140 mm. A full description of the specimens' dimensions can be found in (Stamatopoulos and Malo 2015b).
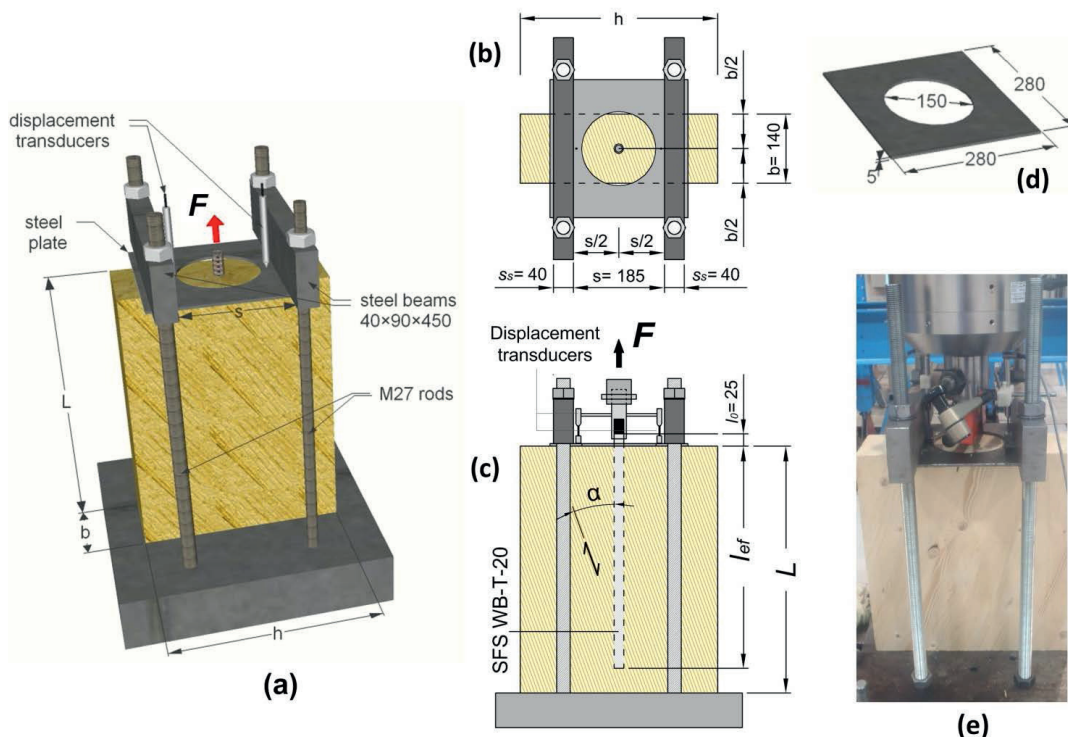
Figure 1. Experimental set-up: (a) 3D representation, (b) plan view, (c) side view, (d) steel plate and (e) photo

3 Eurocode 5

According to EC5 (for screws with $d > 12$ mm) the characteristic withdrawal capacity, $F_{ax.Rk}$, is given by (the expression is re-arranged):

$$F_{ax.Rk} = n_{ef} \cdot f_{ax.\alpha.k} \cdot d \cdot l_{ef} \tag{1}$$

The parameter n_{ef} is the effective number of screws and equal to $n_{ef} = n^{0.9}$, where n is the number of screws acting together in a connection. The withdrawal strength parameter, $f_{ax.\alpha.k}$, is given by:

$$f_{ax.\alpha.k} = \frac{f_{ax.90.k}}{1.2 \cdot \cos^2\alpha + \sin^2\alpha} \cdot \left(\frac{\rho_k}{\rho_a}\right)^{0.8} \quad (\alpha \geq 30°) \tag{2}$$

where $f_{ax.90.k}$ is the withdrawal strength parameter perpendicular to the grain which must be experimentally determined, for the associated density ρ_a. EC5 provides no guidelines for the estimation of withdrawal stiffness.

In the technical approval of WB-T-20 rods, Z-9.1-777 (DIBt 2010), the following expression is provided for the withdrawal strength parameter (unit MPa and kg/m^3):

$$f_{ax.k} = 70 \cdot 10^{-6} \cdot \rho_k{}^2 \quad (45° \leq \alpha \leq 90°) \tag{3}$$

4 Analytical model

Analytical estimations can be obtained by use of the concept of the classical Volkersen theory (Volkersen 1938), applied for axially loaded connectors (Jensen et al. 2001). This model has initially been developed assuming that all shear deformation occurs in an infinitely thin shear layer, while the connector and surrounding wood are assumed to be in states of pure axial stress. The shear stress-displacement behaviour (τ - δ) of the shear layer is approximated by a linear constitutive law, which is a reasonable approximation for glued-in-connectors.

In the case of screwed-in connectors, however, it is more convenient to assume a bi-linear constitutive law, because these connectors are by far less brittle than glued-in connectors and their post-elastic behaviour should not be omitted. The bi-linear constitutive law is presented in Figure 2. The bi-linear idealization separates the curve in two distinct domains; the linear elastic domain and the fracture domain. These domains are characterized by the equivalent shear stiffness parameters Γ_e and Γ_f, which are the slopes of the two branches of the bi-linear constitutive law. The advantage of this method is that, apart from the withdrawal capacity and stiffness, it also allows

the estimation stress and displacement distributions for any given withdrawal force level. Thus, an analytical estimation of the force-displacement curve can be obtained. Note that all shear deformation is assumed to occur in a shear zone of finite dimensions. A full description of this method is given in (Stamatopoulos and Malo 2015a).
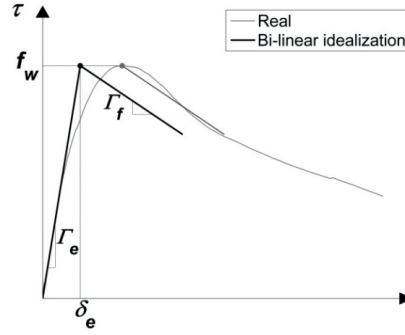
Figure 2. Bi-linear approximation of τ-δ curve

The withdrawal stiffness, K_w, and the characteristic withdrawal capacity, $F_{ax.Rk}$, are provided by the following expressions (Stamatopoulos and Malo 2015a, Jensen et al. 2001):

$$K_w = \pi \cdot d \cdot l_{ef} \cdot \Gamma_e \cdot \frac{\tanh\omega}{\omega} \tag{4}$$

$$\frac{F_{ax.\alpha.Rk}}{d \cdot l_{ef} \cdot f_{ax.\alpha.k}} = \frac{\sin(m \cdot \omega \cdot \lambda_u)}{\omega \cdot m} + \frac{\tanh\{(1 - \lambda_u) \cdot \omega\} \cdot \cos(m \cdot \omega \cdot \lambda_u)}{\omega} \tag{5}$$

Note that these expressions are valid for pull-push or pull-shear loading conditions, but not for the pull-pull loading condition. The parameter m has been introduced as:

$$m = \sqrt{\Gamma_f/\Gamma_e} \tag{6}$$

This parameter is a measure of the brittleness of the shear zone. In the limits, $m \rightarrow 0$ indicates perfect plastic post-elastic behaviour, while $m \rightarrow \infty$ indicates totally brittle behaviour. The parameters ω and β have been defined as follows:

$$\omega = \sqrt{\pi \cdot d \cdot \Gamma_e \cdot \beta \cdot l_{ef}^2} \tag{7}$$

$$\beta = \frac{1}{A_s \cdot E_s} + \frac{1}{A_w \cdot E_{w.\alpha}} \tag{8}$$

5

where E_s and $E_{w.\alpha}$ are the moduli of elasticity of steel and wood (as function of α), respectively. The core cross-sectional area of the rod is $A_s = \pi \cdot d_c^2/4$ and A_w is the area of wood subjected to axial stress. $E_{w.\alpha}$ may be estimated by the Hankinson formula and A_w by an effective area, confer (Stamatopoulos and Malo 2015b). The parameter λ_u is a dimensionless length parameter which expresses the percentage of the embedment length (at failure), in which post-elastic behaviour takes place and it can be determined by the diagram in Figure 3.
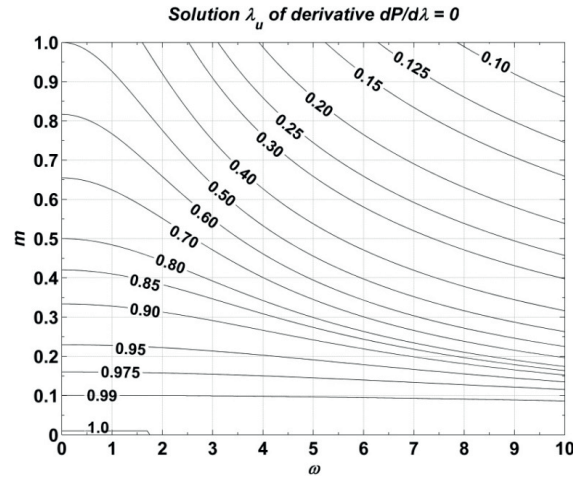
Figure 3. Diagram for the determination of parameter λ_u

The parameters Γ_e (in MPa/mm) and m are provided as functions of α, by the following expressions(Stamatopoulos and Malo 2015a):

$$\Gamma_{e.\alpha} = \frac{9.35}{1.5 \cdot \sin^{2.2}\alpha + \cos^{2.2}\alpha} \tag{9}$$

$$m_\alpha = \frac{m_0}{(m_0/m_{90}) \cdot \sin\alpha + \cos\alpha} = \frac{0.332}{1.73 \cdot \sin\alpha + \cos\alpha} \tag{10}$$

Finally, $f_{ax.\alpha.k}$ can be calculated by Equation (2).

5 Results and discussion

5.1 Withdrawal stiffness

The experimentally derived mean values of K_w and the coefficient of variation (abbr. C.o.V.) for all embedment lengths and rod-to-grain angles are summarized in Table 1. The sample size for each sub-set of parameters (l_{ef} and α) was 5 tests. The analytical

estimations are compared to the experimental results in Figure 4, where K_w is plotted as function of l_{ef} for all rod-to-grain angles. Results from finite element simulations are also provided in Figure 4. The finite element model has been presented in detail in (Stamatopoulos and Malo 2015b).

Table 1. Experimentally recorded mean withdrawal stiffness (units kN/mm) and C.o.V.

	l_{ef} =100 mm	l_{ef} =300 mm	l_{ef} = 450 mm	l_{ef} = 600 mm
	$K_{w.mean}$ /C.o.V.	$K_{w.mean}$ /C.o.V.	$K_{w.mean}$ /C.o.V.	$K_{w.mean}$ /C.o.V.
α = 0°	54.6 / 0.16	121.0 / 0.30	121.8 / 0.13	128.6 / 0.17
α = 10°	56.0 / 0.27	137.3 / 0.19	132.8 / 0.22	131.1 / 0.05
α = 20°	53.8 / 0.23	125.9 / 0.20	121.7 / 0.16	128.0 / 0.14
α = 30°	42.6 / 0.27	111.2 / 0.11	100.3 / 0.10	114.8 / 0.11
α = 60°	36.6 / 0.33	73.5 / 0.17	90.1 / 0.09	(-)[1]
α = 90°	29.0 / 0.31	61.4 / 0.11	66.6 / 0.16	(-)[1]

[1] Experiments were not performed for l_{ef} = 600mm and α = 60°, 90°
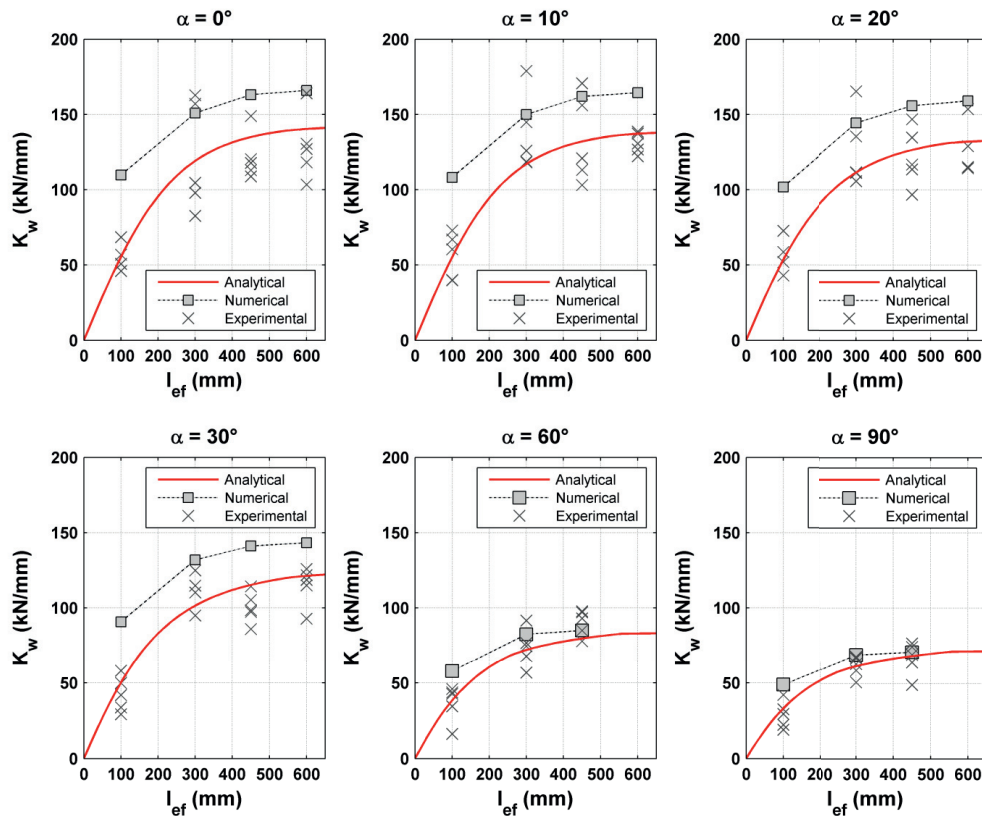
Figure 4. Withdrawal stiffness as function of l_{ef}

It is clear from the experimental results that the specimens exhibited high stiffness, especially for small rod-to-grain angles. As shown in Figure 4, the increase of withdrawal stiffness due to increasing embedment length becomes gradually smaller as the embedment length increases. This is estimated both analytically and by numerical results and validated experimentally. In fact, the experimental results for these threaded rods suggest that K_w has no correlation with the embedment length if $l_{ef} \geq$ 300 mm. This is especially true for small rod-to-grain angles. Finally, according to experimental observations, no initial slip occurred if the threaded steel coupling parts of the set-up were tightly fastened.

5.2   Withdrawal strength parameter

The withdrawal strength parameter was calculated for all angles from the experimental results for all specimens. The mean values, the C.o.V., the median and the 5%-fractile characteristic values are provided in Table 2. It should be noted that the requirements of EN1382 (CEN 1999) for the determination of $f_{ax.\alpha}$ have not been met with respect to the embedment length and the edge distances. The characteristic values are calculated according to EN14358 (CEN 2006). In comparison to the experimental results presented in the previous Section, some additional experimental results have been used in Sections 5.2 and 5.3.

Table 2. Values of the withdrawal strength parameter $f_{ax.\alpha}$

	Number of tests	$f_{ax.\alpha} = F_{max} / d \cdot l_{ef}$ (MPa)			
		Mean	C.o.V.	Median	5% - fractile
$\alpha = 0°$	25	13.81	0.152	13.79	10.19
$\alpha = 10°$	22	14.14	0.168	13.90	10.06
$\alpha = 20°$	20	15.70	0.145	16.05	11.46
$\alpha = 30°$	20	15.16	0.136	15.52	11.47
$\alpha = 60°$	16	15.17	0.124	15.75	11.50
$\alpha = 90°$	20	14.88	0.108	15.04	11.92

* Note: the requirements of EN 1382 with respect to l_{ef} and the edge distances were not met for all specimens

The variability decreases with increasing angle. The ratio $f_{ax.90.k} / f_{ax.0.k}$ is equal to 1.17 which is very close to the ratio 1.20 according to Equation (2). Moreover, the withdrawal strength for rod-to grain angles 0° and 10° is significantly smaller than the withdrawal strength for greater angles. The experimental results together with the estimations by Equations (2) and (3) are presented in Figure 5.
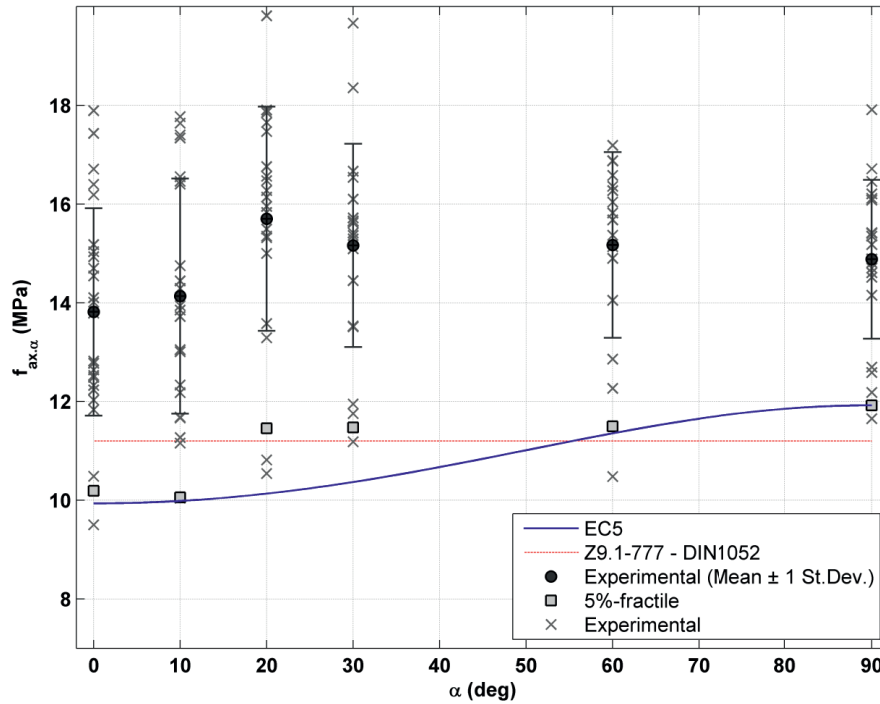
Figure 5. Withdrawal strength parameter as function of α

5.3   Withdrawal capacity

All specimens with $l_{ef} \leq 450$ mm failed due to withdrawal of the rod. In a few specimens with $l_{ef} = 450$ mm yielding of the rod was observed, however the increasing force due to steel hardening led to withdrawal failure prior to steel fracture. In the vast majority of the specimens with $l_{ef} = 600$ mm yielding of the rod was observed. All 5 specimens in S20-600 and S30-600 series and 3 out of 5 specimens in S10-600 series failed due to steel fracture (none in the S0-600 series). These values have been excluded from the calculation of $f_{ax.\alpha}$ in the previous Section. Yielding and steel fracture of the rods occurred at load levels which were significantly higher than those predicted by the nominal yield and ultimate strength properties of steel. The observed increase in strength of the steel can probably be attributed to steel hardening due to thread rolling.

The mean experimentally recorded capacities and their C.o.V. as well as the characteristic capacity for all embedment lengths and rod-to-grain angles are summarized in Table 3. The characteristic capacities have also been calculated according to EN 14358. A minimum C.o.V equal to 0.05 was used to calculate the characteristic capacities, in cases where C.o.V. was smaller.

The experimentally recorded capacities, together with the EC5 and the analytical estimations are plotted as function of the embedment length for all rod-to-grain angles in Figure 6. The withdrawal strength parameter was determined by Equation (2) and

9

by setting $f_{ax.90.k}$ = 11.92 MPa (from Table 2). Note that Equation (2) has been used also outside its valid range for α.

Table 3. Experimentally recorded withdrawal capacity for all specimens (in kN)

	l_{ef} =100 mm (10 tests)	l_{ef} =300 mm (5 tests)	l_{ef} = 450 mm (5 tests)	l_{ef} = 600 mm (5 tests)
	$F_{ax.Rm}$ / C.o.V. / $F_{ax.Rk}$	$F_{ax.Rm}$ / C.o.V. / $F_{ax.Rk}$	$F_{ax.Rm}$ / C.o.V. / $F_{ax.Rk}$	$F_{ax.Rm}$ / C.o.V. / $F_{ax.Rk}$
α = 0°	26.2 / 0.14 / 19.6	89.7 / 0.12 / 66.8	130.2 / 0.24 / 66.7	161.6 / 0.05 / 141.8
α = 10°	25.8 / 0.18 / 17.9	99.8 / 0.10 / 76.9	127.5 / 0.14 / 88.7	173.1[1a] / (-) / (-)
α = 20°	30.2 / 0.19 / 19.5	98.7 / 0.11 / 74.3	145.8 / 0.06 / 124.7	175.7/0.01/155.3[1b]
α = 30°	27.9 / 0.13 / 20.9	99.9 / 0.11 / 77.4	144.6 / 0.09 / 115.5	176.7/0.01/156.2[1b]
α = 60°	28.7 / 0.17 / 18.3 [2]	93.6 / 0.12 / 66.9	141.7 / 0.03 / 125.2	(-) [3]
α = 90°	28.0 / 0.12 / 21.7	96.5 / 0.07 / 80.8	139.2 / 0.05 / 121.9	(-) [3]

[1a] Steel and withdrawal failures were observed and thus no characteristic capacity was calculated, [1b] Steel failure, characteristic value calculated with C.o.V = 0.05, [2] 6 tests (instead of 10), have been performed for l_{ef} = 100mm and α = 60°, [3] No experiments performed for l_{ef} = 600mm and α = 60°, 90.
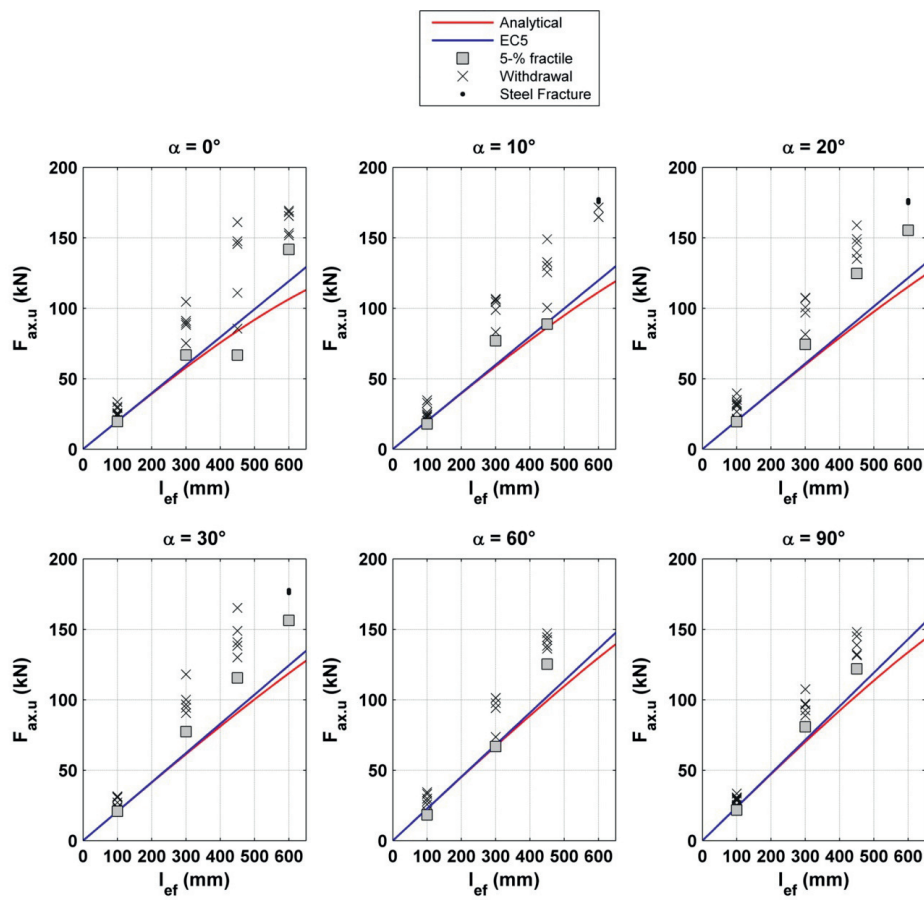
Figure 6. Withdrawal capacity as function of l_{ef}

As shown in Figure 6, Equation (5) results in a nearly linear relation between the capacity and the embedment length and thus the difference between Equations (1) and (5) is small. The estimations by Equations (1) and (5) are generally conservative, especially for $l_{ef} \geq 300$ mm and for $\alpha \geq 20°$. According to the experimental results, the withdrawal capacity of specimens with $\alpha = 20°$ was equally reliable as the capacity of specimens with greater angles. On the other hand, for $\alpha < 20°$ the capacity may be less reliable like in series S0-450 where the evaluated from experiments characteristic capacity was smaller than the analytical prediction.

Finally, it has been reported (Ringhofer and Schickhofer 2014) that the long-term behaviour of axially loaded screws inserted parallel to the grain is very poor. It follows that the long-term behaviour of threaded rods (as function of the rod-to-grain angle and the embedment length) should be further explored.

6 Conclusions

The withdrawal of axially loaded threaded rods with a diameter of 20 mm, screwed into glulam was studied using experimental and analytical methods. The following main conclusions are drawn:

- The withdrawal stiffness and capacity can be estimated by use of a simple analytical procedure, based on the principle of Volkersen model.

- The characteristic withdrawal strength, as estimated by EC5 expression, is on the safe side especially for rod-to grain angles 20° and 30°.

- The characteristic withdrawal strengths for rod-to grain angles 0° and 10° are significantly smaller than the strengths for greater angles.

- The capacity of specimens with a rod-to-grain angle equal to 20° was equally reliable as the capacity of specimens with greater angles.

- Experimental, analytical and numerical results suggest that the increase of withdrawal stiffness due to increasing embedment length becomes gradually smaller as the embedment length increases.

- According to experimental observation, initial slip did not occur when the steel coupling parts of the set-up were tightly fastened.

- Steel fracture of the rods occurred at load levels which were significantly higher than those predicted by the nominal yield and ultimate strength properties of steel.

7 Acknowledgements

8 References

CEN, European committee for standardization. 1991. EN 26891:1991 (ISO 6891:1983): Timber structures- Joints made with mechanical fasteners-General principles for the determination of strength and deformation characteristics. Brussels, Belgium.

CEN, European committee for standardization. 1999. EN 1382-1999: Timber structures- - Tests methods - Withdrawal capacity of timber fasteners. Brussels, Belgium.

CEN, European committee for standardization. 2004. EN 1995-1-1:2004: Design of timber structures. Part 1-1: General-Common rules and rules for buildings. Brussels, Belgium.

CEN, European committee for standardization. 2006. EN 14358-2006: Timber structures- Calculation of characteristic 5-percentile values and acceptance criteria of a samle. Brussels, Belgium.

CEN, European committee for standardization. 2013. EN 14080-2013: Timber structures- Glued laminated timber and glued solid timber - Requirements. Brussels, Belgium.

DIBt, Deutsches Institut für Bautechnik. 2010. SFS intec, GmbH., Gewindestangen mit Holzgewinde als Holzverbindungsmittel, Allgemeine bauaufsichtliche Zulassung Z-9.1-777.

DIN, Deutsches Institut für Normung. 1975. DIN 7998:Gewinde und Schraubenenden für Holz-schrauben. Berlin, Germany.

Frese, M. & H. J. Blaß. 2009. Models for the calculation of the withdrawal capacity of self-tapping screws. In *Proceedings of the 42nd CIB-W18 meeting* Dübendorf, Switzerland.

Jensen, J. L., A. Koizumi, T. Sasaki, Y. Tamura & Y. Iijima (2001) Axially loaded glued-in hardwood dowels. *Wood Science and Technology,* 35**,** 73-83.

Jensen, J. L., M. Nakatani, P. Quenneville & B. Walford (2011) A simple unified model for withdrawal of lag screws and glued-in rods. *European Journal of Wood and Wood Products,* 69**,** 537-544.

Jensen, J. L., M. Nakatani, P. Quenneville & B. Walford (2012) A simplified model for withdrawal of screws from end-grain of timber. *Construction and Building Materials,* 29, 557-563.

Malo, K. A. & P. Ellingsbø. 2010. On connections for timber bridges. In *Proceedings of the International Conference Timber Bridges (ICTB)*, 297-312. Lillehammer, Norway.

Mischler, A. & A. Frangi. 2001. Pull-out tests on glued-in-rods at high temperatures. In *Proceedings of the 34th CIB-W18 meeting* Venice, Italy.

Mori, T., M. Nakatani, S. Kawahara, T. Shimizu & K. Komatsu. 2008. Influence of the number of fastener on tensile strength of lagscrewbolted glulam joint. In *10th World Conference on Timber Engineering*, 1100-1107.

Nakatani, M. & K. Komatsu. 2004. Development and verification of theory on pull-out properties of Lagscrewbolted timber joints. In *Proceedings of the 8th World Conference on Timber Engineering*, 95-99. Lahti, Finland.

Pirnbacher, G., R. Brandner & G. Schickhofer. 2009. Base parameters of self-tapping screws. In *Proceedings of the 42nd CIB-W18 meeting* Dübendorf, Switzerland.

Ringhofer, A. & G. Schickhofer. 2014. Influencing parameters on the experimental determination of the withdrawal capacity of self-tapping screws. In *Proceedings of the 13th World Conference on Timber Engineering*. Quebec City, Canada.

Stamatopoulos, H. & K. A. Malo (2015a) Withdrawal capacity of threaded rods embedded in timber elements. *Construction and Building Materials,* 94, 387-397.

Stamatopoulos, H. & K. A. Malo (2015b) Withdrawal stiffness of threaded rods embedded in timber elements. *Submitted to Construction and Building Materials.*

Tomasi, R., A. Crosatti & M. Piazza (2010) Theoretical and experimental analysis of timber-to-timber joints connected with inclined screws. *Construction and Building Materials,* 24, 1560-1571.

Volkersen, O. (1938) Die nietkraftverteilung in zugbeanspruchten nietverbindungen mit konstanten laschenquerschnitten. *Luftfahrtforschung,* 15, 41-47.

Part III:

Appendices

A. Some analytical remarks

A.1. Secant withdrawal stiffness for various force levels

The withdrawal displacement can be obtained by subtracting the elongation of the rod from the total displacement:

$$\delta_w = \delta_{tot} - \frac{P}{K_0} \tag{A.1}$$

Here $K_0 = A_s \cdot E_s / l_0$ is the axial stiffness of the free part of the rod (l_0 = 25mm in the present investigation for single rods) which is not embedded in the timber element. Equation (A.1) is valid only as long as the rod behaves elastically. Due to the small value of l_0, the difference between δ_{tot} and δ_w is very small. It is noted that any initial slip has been removed from the experimental recordings of δ_{tot}.

The withdrawal stiffness, K_w, was determined by use of Equation (A.2) in accordance with EN 26891:1991 (ISO6891:1983) [114]. It is noted that Equation (A.2) was very sufficient to fit the linear-elastic part of the curves. In very few cases the fitting was manually performed.

$$K_w = \frac{0.4 \cdot P_{est}}{4/3 \cdot (\delta_{w.04} - \delta_{w.01})} \tag{A.2}$$

In Equation (A.2), P_{est} is the estimated maximum load for each test and $\delta_{w.01}$, $\delta_{w.04}$ are the withdrawal displacements for load levels equal to 10% and 40% of P_{est} respectively. The 40% of the load is assumed to correspond to the serviceability limit state.

Moreover, three secant withdrawal stiffness values ($K_{w.06}$, $K_{w.08}$, $K_{w.u}$) for load levels equal to 60%, 80% and 100% of P_u were obtained from the test results for all specimens, by dividing each force level with the corresponding withdrawal displacement, as shown in Equations (A.3)-(A.5). These results are presented in detail for all specimens in Appendix B.

$$K_{w.06} = \frac{0.6 \cdot P_u}{\delta_{w.06}} \tag{A.3}$$

$$K_{w.08} = \frac{0.8 \cdot P_u}{\delta_{w.08}} \tag{A.4}$$

$$K_{w.u} = \frac{P_u}{\delta_{w.u}} \tag{A.5}$$

The secant withdrawal stiffness for load levels 60% and 80% of the maximum force are assumed by some researchers, e.g. [58, 59], to correspond to the ultimate limit state and the near collapse limit state respectively.

By use of regression analysis on the experimental results, the secant withdrawal stiffness for various load levels was determined as a function of the withdrawal stiffness under service load, K_w, and the rod-to-grain angle:

- 60% of maximum force:

$$\frac{K_{w.06}}{K_w} = \frac{0.93}{1.10 \cdot sin^2\alpha + cos^2\alpha} \tag{A.6}$$

- 80% of maximum force:

$$\frac{K_{w.08}}{K_w} = \frac{0.85}{1.35 \cdot sin^2\alpha + cos^2\alpha} \tag{A.7}$$

- 100% of maximum force:

$$\frac{K_{w.u}}{K_w} = \frac{0.60}{1.5 \cdot sin^{1.5}\alpha + cos^{1.5}\alpha} \tag{A.8}$$

For the derivation of Equation (A.8), results for specimens in which either yielding of the rod or excessive axial inelastic deformation of wood below the supports (S90-450 series) occurred were excluded from the database.

A.2. Effective length

Equations (4.8)-(4.10) which provide the parameters $\Gamma_{e.\alpha}$, $f_{w.\alpha}$, m_α have been derived assuming $l = l_{ef}$, i.e. assuming that the shear stress at failure is uniformly distributed over the entire embedment length of the rod. However, the shear stress at the entrance point is zero and therefore a certain length is required for the shear stress to build up. Therefore the determination of the withdrawal strength by use of the experimental results from specimens with $l = 100$ mm, may result in low values for $f_{w.\alpha}$. This is probably one of the reasons for the conservatism of the analytical model for increasing embedment lengths.

As it can be seen from the numerically estimated shear stress distributions in **Appendix C**, the shear stress is lower for a length between the entrance point and a coordinate approximately equal to 1-2 pitch distances, depending on α. Moreover, it is reasonable to assume that some damage is accumulated at the entrance point during the process of screwing-in. To take these effects into account, an effective length, l_{ef}, according to Equation (A.9) is assumed:

$$l_{ef} = l - 0.5 \cdot d \tag{A.9}$$

By use of l_{ef} instead of l the corresponding parameters ($\Gamma_{e.\alpha}$, $f_{w.\alpha}$, m_α) are re-calculated and by use of regression analysis Equations (A.10)-(A.12) are obtained. The results from all specimens have been used for the determination of $\Gamma_{e.\alpha}$. The withdrawal strength f_w and the parameter m were derived from the experimental results for all specimens with the smallest embedment length, i.e. $l = 100$ mm ($l_{ef} = 90$ mm), for which the shear stress distribution at and after failure is assumed to be uniformly distributed over l_{ef}. It is noted that some additional experimental results (which were also used in Paper iv [116]), have been used for the determination of $f_{w.\alpha}$.

$$\Gamma_{e.\alpha}^* = \frac{9.65}{1.5 \cdot \sin^{2.2}\alpha + \cos^{2.2}\alpha} \tag{A.10}$$

$$f_{w.\alpha}^* = \frac{4.70}{0.95 \cdot \sin^{2.2}\alpha + \cos^{2.2}\alpha} \tag{A.11}$$

$$m_\alpha^* = \frac{0.332}{1.73 \cdot \sin\alpha + \cos\alpha} \tag{A.12}$$

Compared to Equations (4.8)-(4.10), m_α turned out to be unaltered by the introduction of Equation (A.9).

Due to the lack of additional data in S60-100 series, an expression for the characteristic withdrawal strength was not developed. It is worth noting that the characteristic withdrawal strength for $\alpha = 0°$ and l_{ef} = 90 mm was found equal to $f^*_{w.0.k}$ = 3.46 MPa, which is approximately equal to the characteristic shear strength of L40c glulam ($f_{v.k}$ = 3.5 MPa).

The withdrawal capacity and stiffness are plotted as function of l for all α in Figures A.1 and A.2, respectively. The red lines correspond to the analytical estimations by use of Equations (4.8)-(4.10) and the red dashed lines correspond to the analytical estimations by use of Equations (A.9)-(A.12)). As shown in these Figures, the use of an effective length and the corresponding parameters leads to less conservative estimations for the withdrawal capacity. There is essentially no difference between the stiffness estimations.
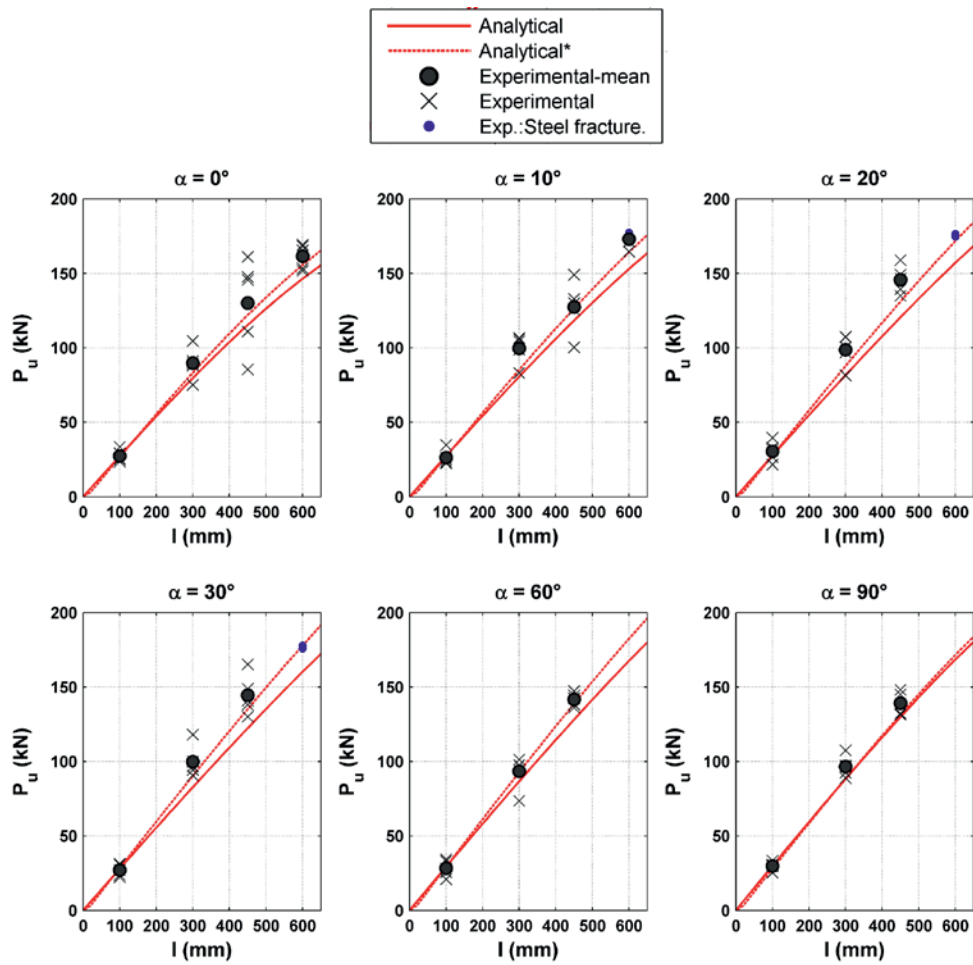
Figure A.1: Withdrawal capacity as function of the embedment length
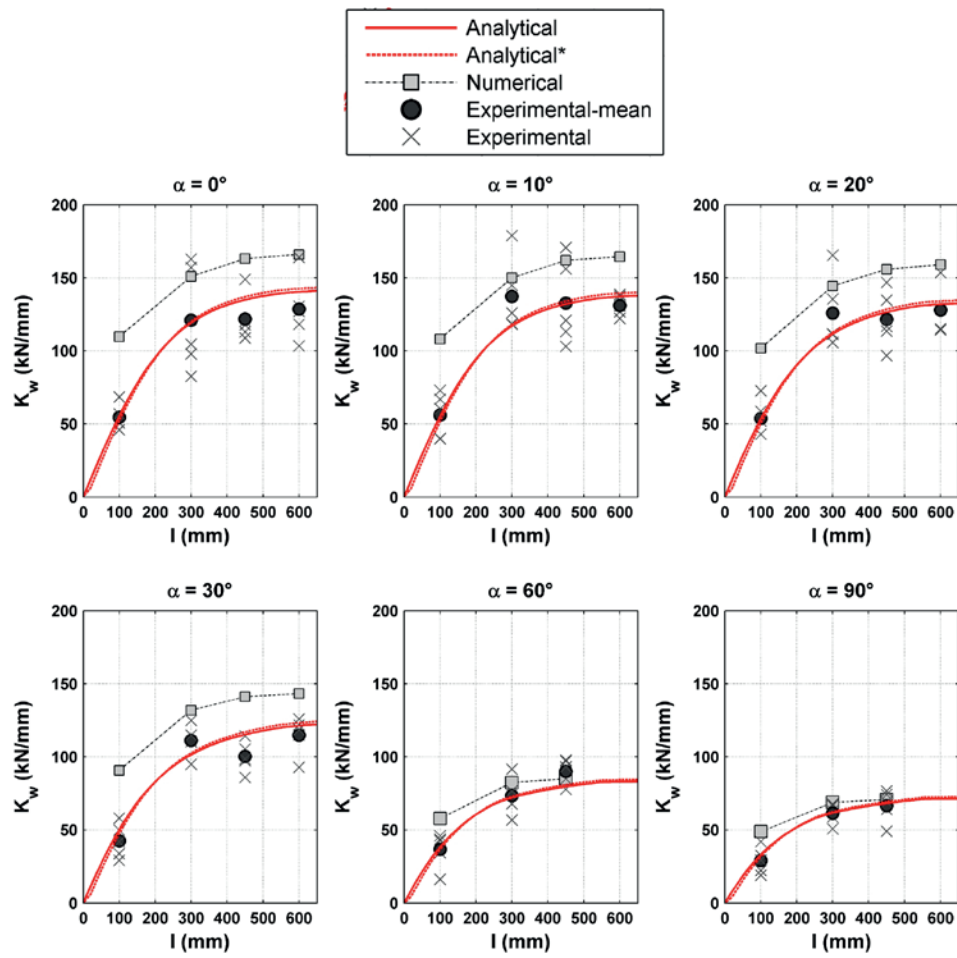
Figure A.2: Withdrawal stiffness as function of the embedment length

In Figure A.3 the analytical model (by use of the modified embedment length and the corresponding parameters according to Equations (A.9)-(A.12)) is compared to models which are valid for different diameters for screws embedded perpendicular to the grain; in particular with the models by Frese and Blaß [55] and Pirnbacher et al [24, 28]. The material properties of L40c have been used as input.

The withdrawal strength is increasing with decreasing diameter due to the size-effect. The model by Frese and Blaß [55] for d= 14 mm, results in similar strength as the obtained strength in the present investigation. However it would result in a much lower strength if it was used for d= 20 mm which is outside the range of this model. It may be assumed that the size effect takes place up to a certain diameter.

Moreover the analytical estimation for the elastic capacity is provided. The elastic capacity would correspond to the actual capacity if a linear constitutive τ-δ relationship (i.e. maximum stress criterion) was assumed. It is clear that the use of maximum stress criterion leads to inaccurate estimations for long threaded rods.
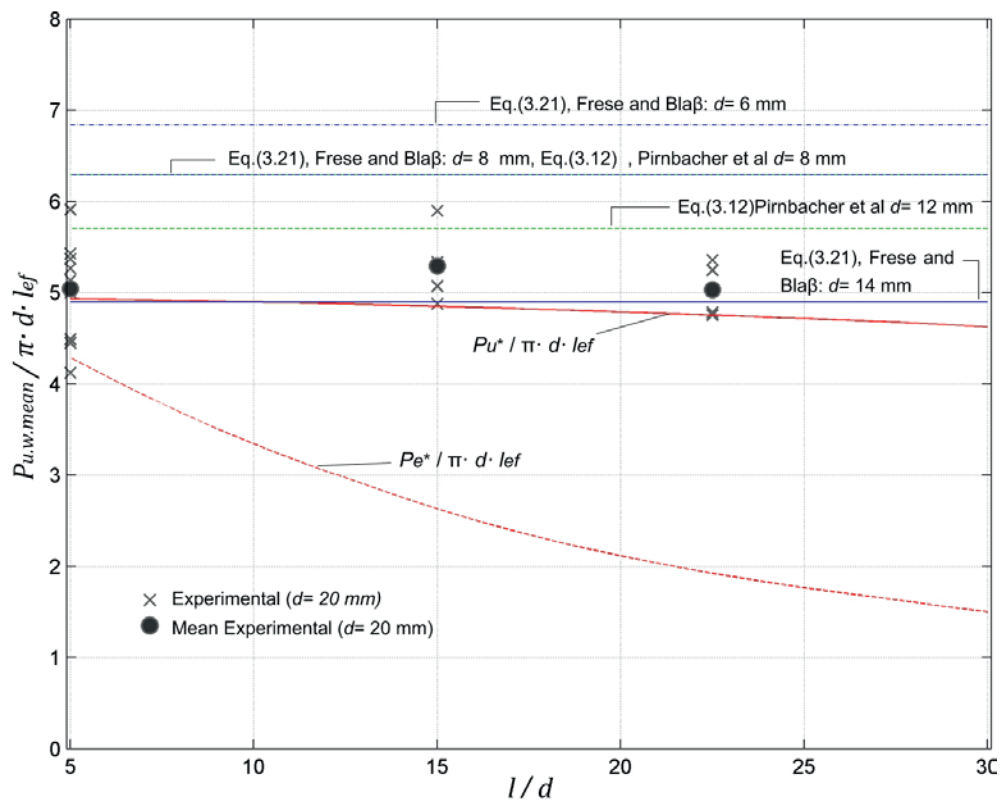
Figure A.3: Analytical model and experimental results vs other models (α= 90º)

A.3. Withdrawal stiffness for pull-shear loading conditions

According to the analytical model the withdrawal stiffness for an axially loaded threaded rod is given by:

$$K_w = \pi \cdot d \cdot l \cdot \Gamma_e \cdot \frac{\tanh\omega}{\omega} \qquad (A.13)$$

The limits of Equation (A.13) as l approaches zero (short embedment lengths) or infinity (long embedment lengths) are given by Equations (A.14) and (A.15). According to Equation (A.14) the withdrawal stiffness is linearly dependent on l for small values of l. On the other hand, for long embedment lengths the withdrawal stiffness is independent of l and its value converges to a constant which is given by Equation (A.15).

$$\lim_{l \to 0} K_w = \pi \cdot d \cdot l \cdot \Gamma_e \qquad (A.14)$$

$$\lim_{l \to \infty} K_w = \frac{\pi \cdot d \cdot l \cdot \Gamma_e}{\omega} = \sqrt{\frac{\pi \cdot d \cdot \Gamma_e}{\beta}} \qquad (A.15)$$

Assuming pull-shear loading condition (which is quite common in practice), $A_w = \infty$ and therefore $\beta = 1/A_s E_s$. By substituting β in Equation (A.15) and by use of the limits given by Equations (A.14) and (A.15), an approximating closed-form expression for the withdrawal stiffness is obtained:

$$K_w \approx \begin{cases} \pi \cdot d \cdot l \cdot \Gamma_e, & l < 0.85 \cdot \sqrt{\dfrac{A_s \cdot E_s}{\pi \cdot d \cdot \Gamma_e}} \\[4mm] 0.85 \cdot \sqrt{\pi \cdot d \cdot \Gamma_e \cdot A_s \cdot E_s}, & l \geq 0.85 \cdot \sqrt{\dfrac{A_s \cdot E_s}{\pi \cdot d \cdot \Gamma_e}} \end{cases} \qquad (A.16)$$

In Equation (A.16), the factor 0.85 has been used to avoid overestimation due to the fact that Equation (A.15) always provides an upper limit value. This factor was a result of optimization by use of the least squares method for Equations (A.13) and (A.16), for screws with varying diameters and angles to the grain. The value of Γ_e can be obtained either by Equation (4.8) or Equation (A.10) depending whether l or l_{ef} is considered. Equations (A.13)-(A.16) are plotted as function of embedment length in Figures A.4 and A.5, for d= 10, 20 mm and α= 0°, 30°, 60°, 90°. The predictions of Equations (2.7) and (2.8) which are proposed in technical

approvals are also given in these Figures. As it can be seen the Equations (2.7) and (2.8) can lead to very different estimations. Equation (2.8) is generally in good agreement with the present approach but only for small values of the embedment length.
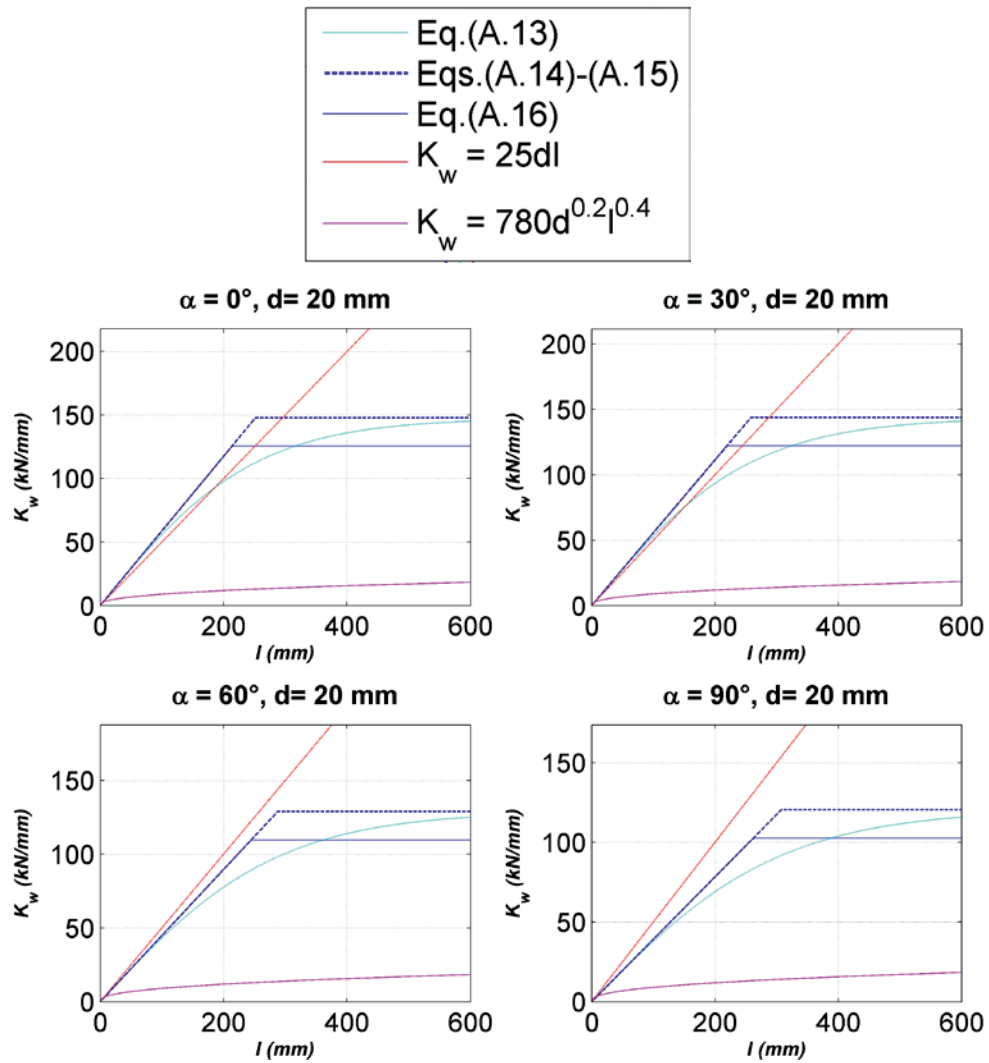
Figure A.4: Withdrawal stiffness as function of l for the pull-shear loading condition (d= 20mm)
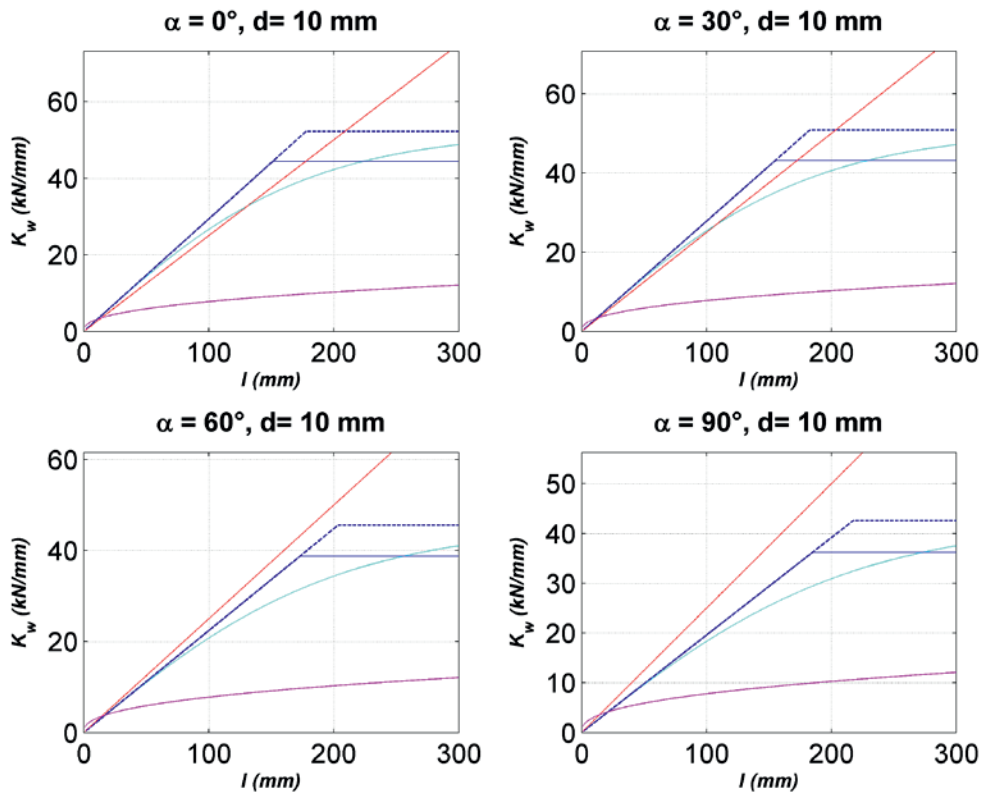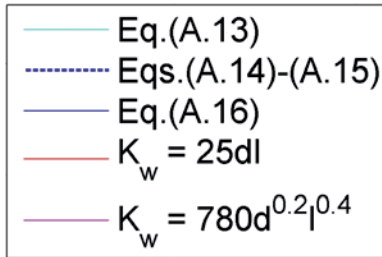
Figure A.5: Withdrawal stiffness as function of *l* for the pull-shear loading condition (*d*= 10mm)

B. Detailed experimental results

The experimental results for single rods are provided in detail in this Appendix. The experimentally recorded P-δ_{tot} curves are plotted together with the analytical estimation (red line) for all experimental series. The estimation by use of Equations (A.9)-(A.12) is also given (red dashed line). It should be noted that any initial slip, which is only due to the fixing details in the experimental setup, has been removed from the experimental recordings of δ_{tot}. The experimental results are summarized in a table containing the following experimentally recorded parameters:

- Failure load (P_u).
- The displacements which correspond to P_u ($\delta_{tot.u}$ and $\delta_{w.u}$).
- The withdrawal stiffness (K_w).
- The secant withdrawal stiffness values ($K_{w.06}$, $K_{w.08}$, $K_{w.u}$) for load levels equal to 60%, 80% and 100% of P_u and their ratios over K_w.
- The mean withdrawal strength ($f_w = P_u / \pi dl$).
- The equivalent shear stiffness parameters Γ_e and Γ_f and the brittleness parameter m where quantified as discussed in Papers I and II [60, 115]. Γ_f was determined by fitting a line in the descending part of the τ_{mean}- δ_w diagram. For long rods, the shear stress distribution along the rod after failure may not be uniform and therefore Γ_f represent a mean value.

S0-100 series
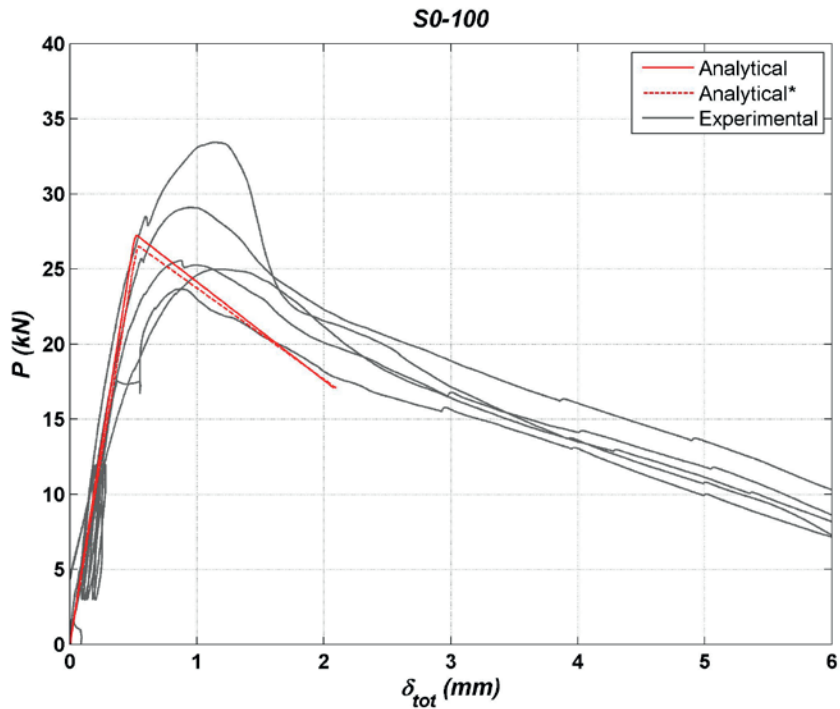
Figure B.1: Force-displacement curves for S0-100 series

Table B.1: Experimental results for S0-100 series

	$S_{0-100-1}$	$S_{0-100-2}$	$S_{0-100-3}$	$S_{0-100-4}$	$S_{0-100-5}$	**Mean**	**CoV**
P_u (kN)	25.55	23.67	24.98	33.42	29.09	27.34	0.14
$\delta_{tot.u}$ (mm)	0.87	0.87	1.18	1.13	0.93	1.00	0.15
$\delta_{w.u}$ (mm)	0.85	0.86	1.16	1.11	0.91	0.98	0.15
K_w (kN/mm)	50.81	50.73	45.99	68.52	56.81	54.57	0.16
K_{w06} (kN/mm)	49.95	50.66	41.98	62.17	54.81	51.91	0.14
K_{w06}/K_w	0.98	1.00	0.91	0.91	0.96	0.95	0.04
K_{w08} (kN/mm)	47.19	34.99	34.25	52.56	50.60	43.92	0.20
K_{w08}/K_w	0.93	0.69	0.74	0.77	0.89	0.80	0.13
K_{wu} (kN/mm)	29.95	27.67	21.46	30.19	31.99	28.25	0.15
K_{wu}/K_w	0.59	0.55	0.47	0.44	0.56	0.52	0.12
f_w (MPa)	4.07	3.77	3.98	5.32	4.63	4.35	0.14
Γ_e (MPa/mm)	8.54	8.52	7.69	11.74	9.61	9.22	0.17
Γ_f (MPa/mm)	0.70	0.69	0.77	2.56	0.88	1.12	0.72
m	0.29	0.29	0.32	0.47	0.30	0.33	0.23

S0-300 series
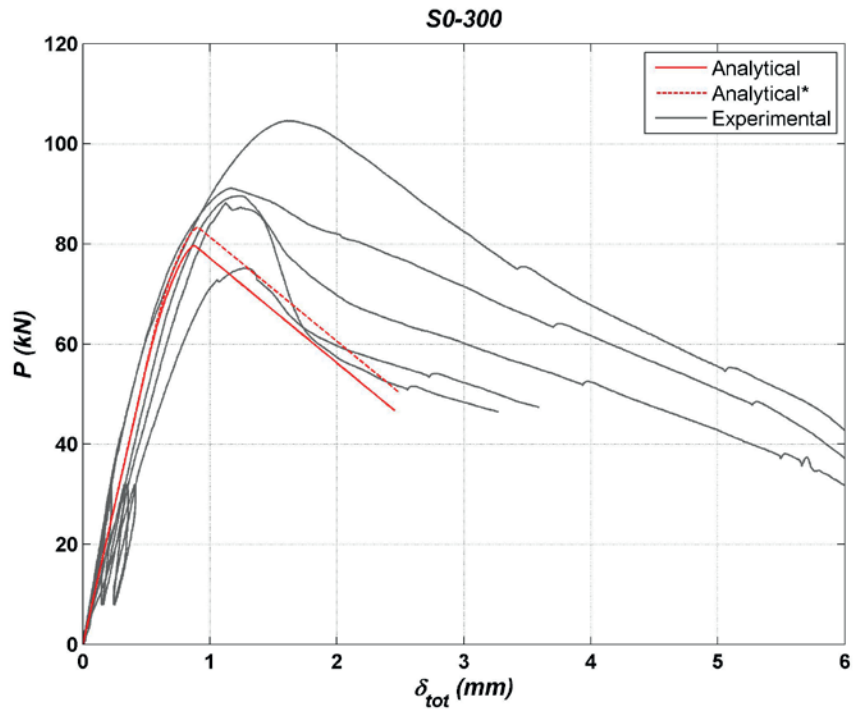
Figure B.2: Force-displacement curves for S0-300 series

Table B.2: Experimental results for S0-300 series

	$S_{0\text{-}300\text{-}1}$	$S_{0\text{-}300\text{-}2}$	$S_{0\text{-}300\text{-}3}$	$S_{0\text{-}300\text{-}4}$	$S_{0\text{-}300\text{-}5}$	Mean	CoV
P_u (kN)	75.16	104.60	88.20	89.60	91.08	89.73	0.12
$\delta_{tot.u}$ (mm)	1.26	1.61	1.12	1.22	1.15	1.28	0.15
$\delta_{w.u}$ (mm)	1.21	1.54	1.07	1.16	1.09	1.21	0.16
K_w (kN/mm)	82.62	157.08	97.96	104.58	162.80	121.01	0.30
K_{w06} (kN/mm)	82.72	130.44	96.78	107.13	138.88	111.19	0.21
K_{w06}/K_w	1.00 [a]	0.83	0.99	1.00 [a]	0.85	0.93	0.09
K_{w08} (kN/mm)	80.27	102.03	94.60	104.42	121.76	100.62	0.15
K_{w08}/K_w	0.97	0.65	0.97	1.00	0.75	0.87	0.18
K_{wu} (kN/mm)	61.90	67.97	82.79	77.01	83.36	74.61	0.13
K_{wu}/K_w	0.75	0.43	0.85	0.74	0.51	0.66	0.27
f_w (MPa)	3.99	5.55	4.68	4.75	4.83	4.76	0.12
Γ_e (MPa/mm)	5.71	14.10	7.14	7.80	14.91	9.93	0.43
Γ_f (MPa/mm)	0.98	0.82	1.85	1.40	0.55	1.12	0.46
m	0.42	0.24	0.51	0.42	0.19	0.36	0.38

[a] value set equal to 1.0

S0-450 series
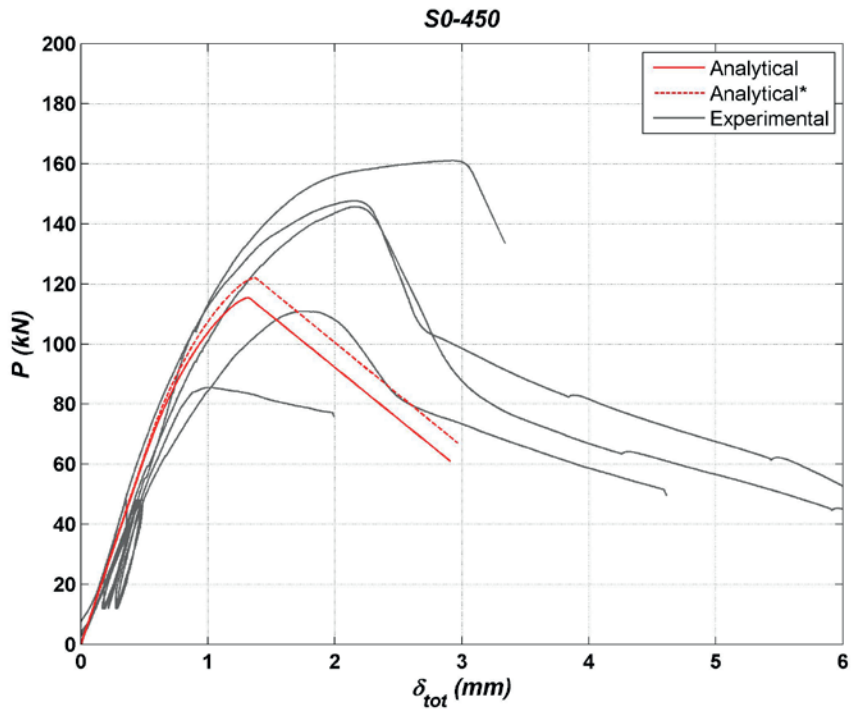
Figure B.3: Force-displacement curves for S0-450 series

Table B.3: Experimental results for S0-450 series

	$S_{0-450-1}$	$S_{0-450-2}$	$S_{0-450-3}$	$S_{0-450-4}$	$S_{0-450-5}$	**Mean**	**CoV**
P_u (kN)	145.68	110.92	161.04[a]	147.60	85.52	130.15	0.24
$\delta_{tot.u}$ (mm)	2.15	1.74	2.90	2.14	1.00	1.99	0.35
$\delta_{w.u}$ (mm)	2.06	1.66	N/A[a]	2.04	0.94	1.67	0.31
K_w (kN/mm)	120.32	108.86	117.75	148.95	113.02	121.78	0.13
K_{w06} (kN/mm)	114.82	97.94	129.46	136.42	110.62	117.85	0.13
K_{w06}/K_w	0.95	0.90	1.00[b]	0.92	0.98	0.95	0.04
K_{w08} (kN/mm)	101.25	86.92	112.97	116.34	109.02	105.30	0.11
K_{w08}/K_w	0.84	0.80	0.96	0.78	0.96	0.87	0.10
K_{wu} (kN/mm)	70.84	66.68	N/A[a]	72.39	91.03	75.23	0.17
K_{wu}/K_w	0.59	0.61	N/A[a]	0.49	0.81	0.62	0.14
f_w (MPa)	5.15	3.92	5.70	5.22	3.02	4.60	0.21
Γ_e (MPa/mm)	7.72	6.58	7.45	11.08	6.98	7.96	0.23
Γ_f (MPa/mm)	2.30	1.13	0.41	2.33	0.30	1.29	0.76
m	0.55	0.41	0.23	0.46	0.21	0.37	0.39

[a] Steel yielding-withdrawal failure, [b] value set equal to 1.0

S0-600 series
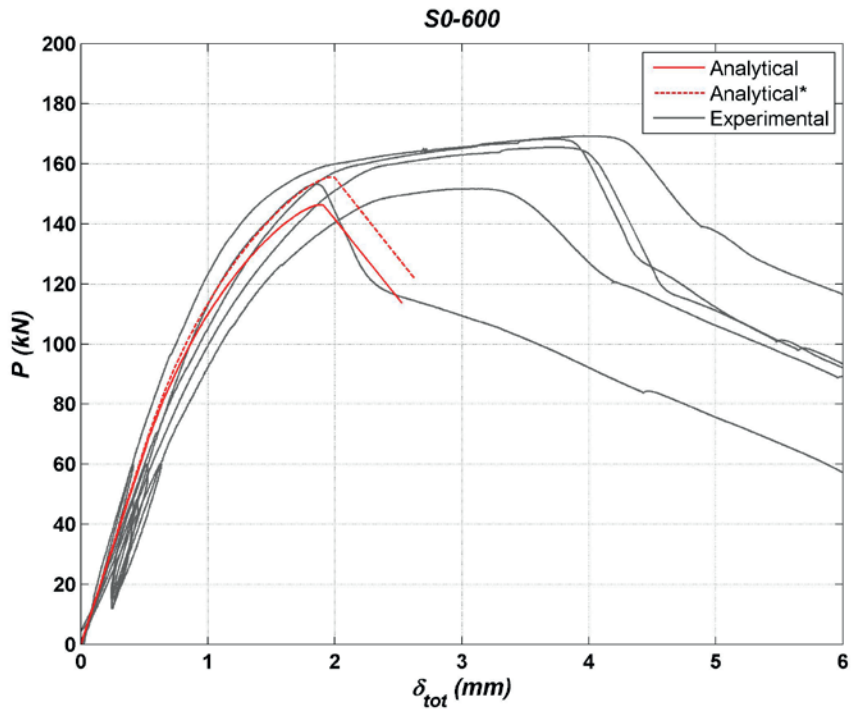
Figure B.4: Force-displacement curves for S0-600 series

Table B.4: Experimental results for S0-600 series

	$S_{0-600-1}$	$S_{0-600-2}$	$S_{0-600-3}$	$S_{0-600-4}$	$S_{0-600-5}$	**Mean**	**CoV**
P_u (kN)	151.68	169.24[a]	165.48[a]	153.28	168.16[a]	161.57	0.05
$\delta_{tot.u}$ (mm)	3.14	3.96	3.67	1.84	3.67	3.26	0.26
$\delta_{w.u}$ (mm)	N/A[a]	N/A[a]	N/A[a]	1.74	N/A[a]	N/A[a]	N/A[a]
K_w (kN/mm)	103.35	130.58	118.19	127.09	164.01	128.64	0.17
K_{w06} (kN/mm)	98.37	114.76	106.51	126.22	145.93	118.36	0.16
K_{w06}/K_w	0.95	0.88	0.90	0.99	0.89	0.92	0.05
K_{w08} (kN/mm)	87.63	100.32	91.06	116.94	125.87	104.36	0.16
K_{w08}/K_w	0.85	0.77	0.77	0.92	0.77	0.81	0.08
K_{wu} (kN/mm)	N/A[a]	N/A[a]	N/A[a]	88.06	N/A[a]	N/A[a]	N/A[a]
K_{wu}/K_w	N/A[a]	N/A[a]	N/A[a]	0.69	N/A[a]	N/A[a]	N/A[a]
f_w (MPa)	4.02	4.49	4.39	4.07	4.46	4.29	0.05
Γ_e (MPa/mm)	5.41	8.18	6.83	7.78	12.57	8.15	0.33
Γ_f (MPa/mm)	0.60	0.61	0.79	1.83	0.98	0.97	0.53
m	0.33	0.27	0.34	0.49	0.28	0.34	0.25

[a] Steel yielding-withdrawal failure

S10-100 series
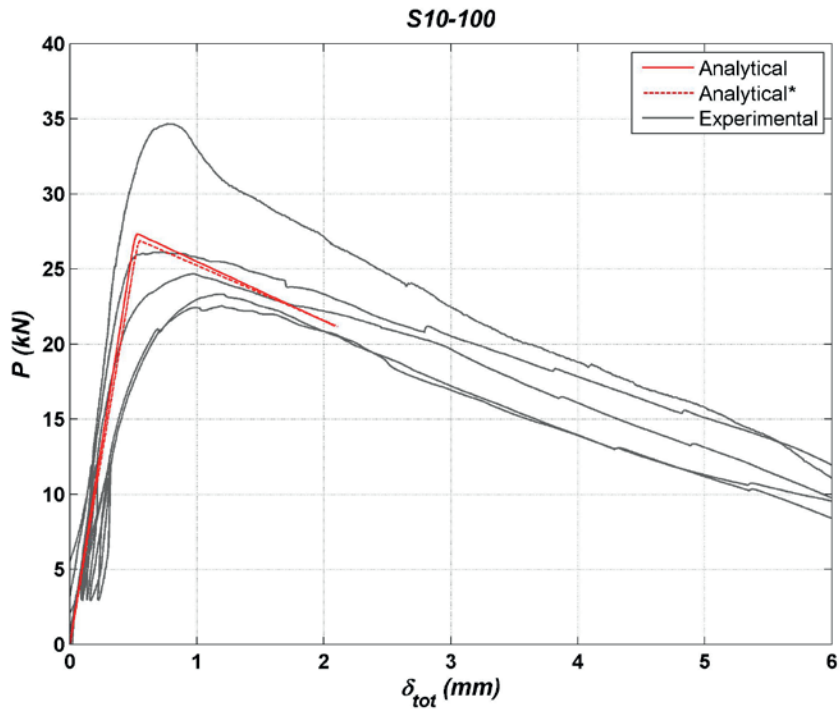
Figure B.5: Force-displacement curves for S10-100 series

Table B.5: Experimental results for S10-100 series

	$S_{10\text{-}100\text{-}1}$	$S_{10\text{-}100\text{-}2}$	$S_{10\text{-}100\text{-}3}$	$S_{10\text{-}100\text{-}4}$	$S_{10\text{-}100\text{-}5}$	**Mean**	**CoV**
P_u (kN)	26.10	22.54	34.68	23.33	24.67	26.26	0.19
$\delta_{tot.u}$ (mm)	0.66	1.19	0.77	1.18	0.97	0.95	0.25
$\delta_{w.u}$ (mm)	0.64	1.18	0.75	1.17	0.95	0.94	0.26
K_w (kN/mm)	66.92	39.80	72.92	40.11	60.39	56.03	0.27
K_{w06} (kN/mm)	66.74	38.44	72.68	40.61	59.36	55.57	0.28
K_{w06}/K_w	1.00	0.97	1.00	1.00 [a]	0.98	0.99	0.01
K_{w08} (kN/mm)	63.36	34.74	70.98	35.49	52.31	51.38	0.32
K_{w08}/K_w	0.95	0.87	0.97	0.88	0.87	0.91	0.05
K_{wu} (kN/mm)	40.68	19.12	46.50	19.97	25.91	30.44	0.41
K_{wu}/K_w	0.61	0.48	0.64	0.50	0.43	0.53	0.17
f_w (MPa)	4.15	3.59	5.52	3.71	3.93	4.18	0.19
Γ_e (MPa/mm)	11.51	6.63	12.64	6.69	10.31	9.56	0.29
Γ_f (MPa/mm)	0.36	0.45	0.94	0.52	0.38	0.53	0.45
m	0.18	0.26	0.27	0.28	0.19	0.24	0.20

[a] value set equal to 1.0

S10-300 series
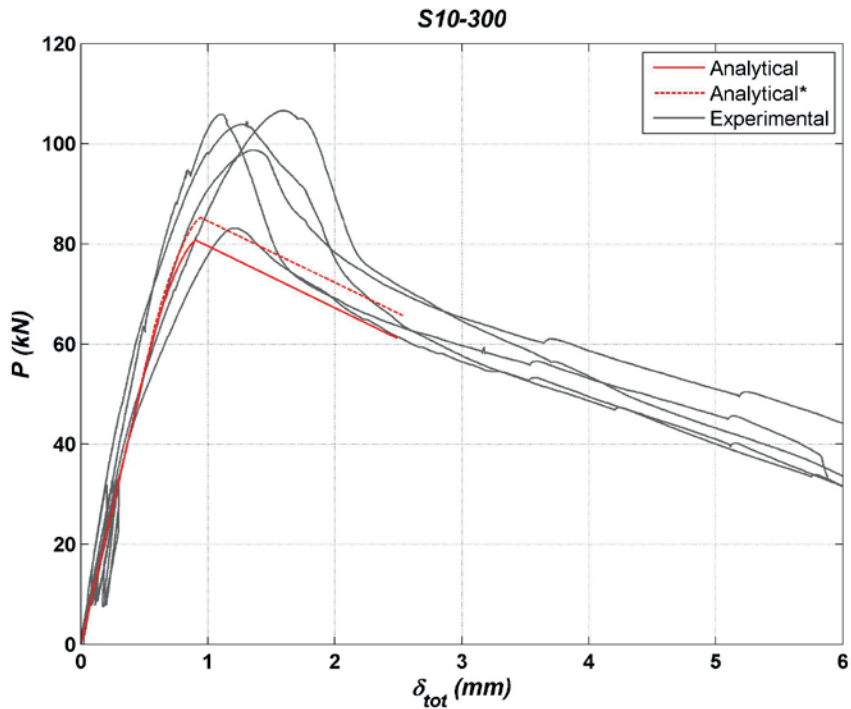
Figure B.6: Force-displacement curves for S10-300 series

Table B.6: Experimental results for S10-300 series

	S$_{10\text{-}300\text{-}1}$	S$_{10\text{-}300\text{-}2}$	S$_{10\text{-}300\text{-}3}$	S$_{10\text{-}300\text{-}4}$	S$_{10\text{-}300\text{-}5}$	Mean	CoV
P_u (kN)	83.12	104.40	105.84	106.64	98.76	99.75	0.10
$\delta_{tot.u}$ (mm)	1.20	1.31	1.09	1.59	1.36	1.31	0.14
$\delta_{w.u}$ (mm)	1.14	1.24	1.02	1.52	1.29	1.24	0.15
K_w (kN/mm)	118.14	178.83	144.96	125.91	118.65	137.30	0.19
K_{w06} (kN/mm)	107.41	150.16	141.49	107.63	115.12	124.36	0.16
K_{w06}/K_w	0.91	0.84	0.98	0.85	0.97	0.91	0.07
K_{w08} (kN/mm)	91.33	123.18	130.84	92.67	107.83	109.17	0.16
K_{w08}/K_w	0.77	0.69	0.90	0.74	0.91	0.80	0.12
K_{wu} (kN/mm)	72.88	84.37	103.91	70.35	76.29	81.56	0.17
K_{wu}/K_w	0.62	0.47	0.72	0.56	0.64	0.60	0.15
f_w (MPa)	4.41	5.54	5.61	5.66	5.24	5.29	0.10
Γ_e (MPa/mm)	9.49	18.08	12.89	10.41	9.55	12.08	0.30
Γ_f (MPa/mm)	0.92	1.87	2.62	2.18	1.40	1.80	0.37
m	0.31	0.32	0.45	0.46	0.38	0.38	0.18

S10-450 series
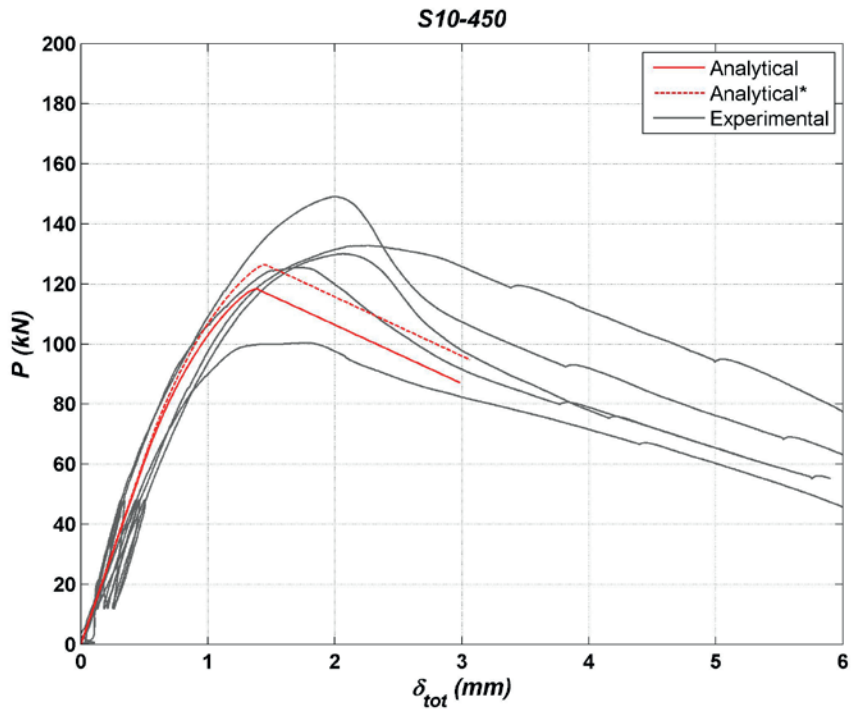
Figure B.7: Force-displacement curves for S10-450 series

Table B.7: Experimental results for S10-450 series

	$S_{10\text{-}450\text{-}1}$	$S_{10\text{-}450\text{-}2}$	$S_{10\text{-}450\text{-}3}$	$S_{10\text{-}450\text{-}4}$	$S_{10\text{-}450\text{-}5}$	**Mean**	**CoV**
P_u (kN)	130.00	100.40	149.00	132.76	125.48	127.53	0.14
$\delta_{tot.u}$ (mm)	2.06	1.79	1.99	2.25	1.74	1.97	0.11
$\delta_{w.u}$ (mm)	1.97	1.72	1.89	2.17	1.65	1.88	0.11
K_w (kN/mm)	103.09	120.85	170.67	113.14	156.11	132.77	0.22
K_{w06} (kN/mm)	102.92	115.54	131.88	110.17	143.47	120.80	0.14
K_{w06}/K_w	1.00	0.96	0.77	0.97	0.92	0.92	0.10
K_{w08} (kN/mm)	95.94	105.33	110.57	100.24	122.11	106.84	0.09
K_{w08}/K_w	0.93	0.87	0.65	0.89	0.78	0.82	0.14
K_{wu} (kN/mm)	66.01	58.24	78.71	61.31	75.89	68.03	0.13
K_{wu}/K_w	0.64	0.48	0.46	0.54	0.49	0.52	0.14
f_w (MPa)	4.60	3.55	5.27	4.70	4.44	4.51	0.14
Γ_e (MPa/mm)	6.23	8.06	14.81	7.23	12.57	9.78	0.38
Γ_f (MPa/mm)	1.15	0.46	1.44	0.50	0.96	0.90	0.47
m	0.43	0.24	0.31	0.26	0.28	0.30	0.25

S10-600 series
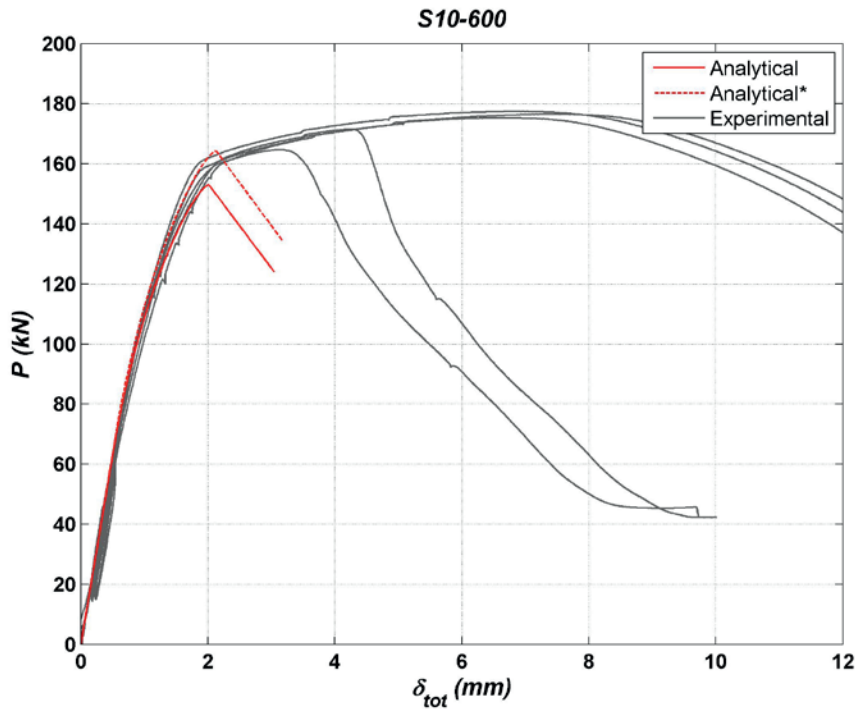
Figure B.8: Force-displacement curves for S10-600 series

Table B.8: Experimental results for S10-600 series

	$S_{10-600-1}$	$S_{10-600-2}$	$S_{10-600-3}$	$S_{10-600-4}$	$S_{10-600-5}$	**Mean**	**CoV**
P_u (kN)	176.52[a]	171.52[b]	175.32[a]	177.44[a]	164.68[b]	173.10	0.03
$\delta_{tot.u}$ (mm)	7.41	4.23	6.35	6.68	3.07	5.55	0.33
$\delta_{w.u}$ (mm)	N/A[a]	N/A[b]	N/A[a]	N/A[a]	N/A[b]	N/A	N/A
K_w (kN/mm)	122.19	126.71	138.60	130.63	137.30	131.08	0.05
K_{w06} (kN/mm)	107.37	115.35	124.07	121.41	123.09	118.26	0.06
K_{w06}/K_w	0.88	0.91	0.90	0.93	0.90	0.90	0.02
K_{w08} (kN/mm)	90.36	97.53	101.36	105.78	104.16	99.84	0.06
K_{w08}/K_w	0.74	0.77	0.73	0.81	0.76	0.76	0.04
K_{wu} (kN/mm)	N/A[a]	N/A[b]	N/A[a]	N/A[a]	N/A[b]	N/A	N/A
K_{wu}/K_w	N/A[a]	N/A[b]	N/A[a]	N/A[a]	N/A[b]	N/A	N/A
f_w (MPa)	N/A[a]	4.55	N/A[a]	N/A[a]	4.37	N/A	N/A
Γ_e (MPa/mm)	7.55	8.07	9.54	8.54	9.37	8.61	0.10
Γ_f (MPa/mm)	N/A[a]	1.12	N/A[a]	N/A[a]	0.65	N/A	N/A
m	N/A[a]	0.37	N/A[a]	N/A[a]	0.26	N/A	N/A

[a] Steel yielding and fracture [b] Steel yielding-withdrawal failure

S20-100 series
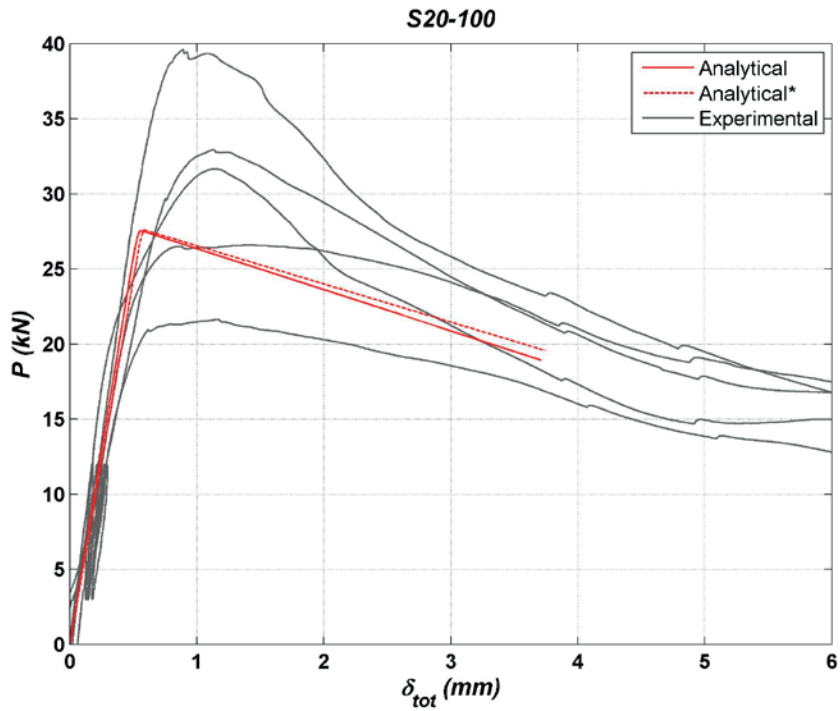
Figure B.9: Force-displacement curves for S20-100 series

Table B.9: Experimental results for S20-100 series

	$S_{20\text{-}100\text{-}1}$	$S_{20\text{-}100\text{-}2}$	$S_{20\text{-}100\text{-}3}$	$S_{20\text{-}100\text{-}4}$	$S_{20\text{-}100\text{-}5}$	**Mean**	**CoV**
P_u (kN)	21.63	26.58	31.66	32.95	39.63	30.49	0.22
$\delta_{tot.u}$ (mm)	1.16	1.38	1.12	1.13	0.89	1.14	0.15
$\delta_{w.u}$ (mm)	1.14	1.36	1.10	1.11	0.87	1.12	0.16
K_w (kN/mm)	42.98	51.92	72.68	42.96	58.60	53.83	0.23
K_{w06} (kN/mm)	43.68	50.04	68.51	42.55	59.27	52.81	0.21
K_{w06}/K_w	1.00 [a]	0.96	0.94	0.99	1.00 [a]	0.98	0.03
K_{w08} (kN/mm)	41.91	48.83	46.75	42.54	57.92	47.59	0.14
K_{w08}/K_w	0.98	0.94	0.64	0.99	0.99	0.91	0.16
K_{wu} (kN/mm)	18.90	19.55	28.74	29.80	45.79	28.56	0.38
K_{wu}/K_w	0.44	0.38	0.40	0.69	0.78	0.54	0.35
f_w (MPa)	3.44	4.23	5.04	5.24	6.31	4.85	0.22
Γ_e (MPa/mm)	7.30	8.93	12.92	7.29	10.19	9.33	0.25
Γ_f (MPa/mm)	0.26	0.28	0.96	0.69	1.06	0.65	0.57
m	0.19	0.18	0.27	0.31	0.32	0.25	0.26

[a] value set equal to 1.0

S20-300 series
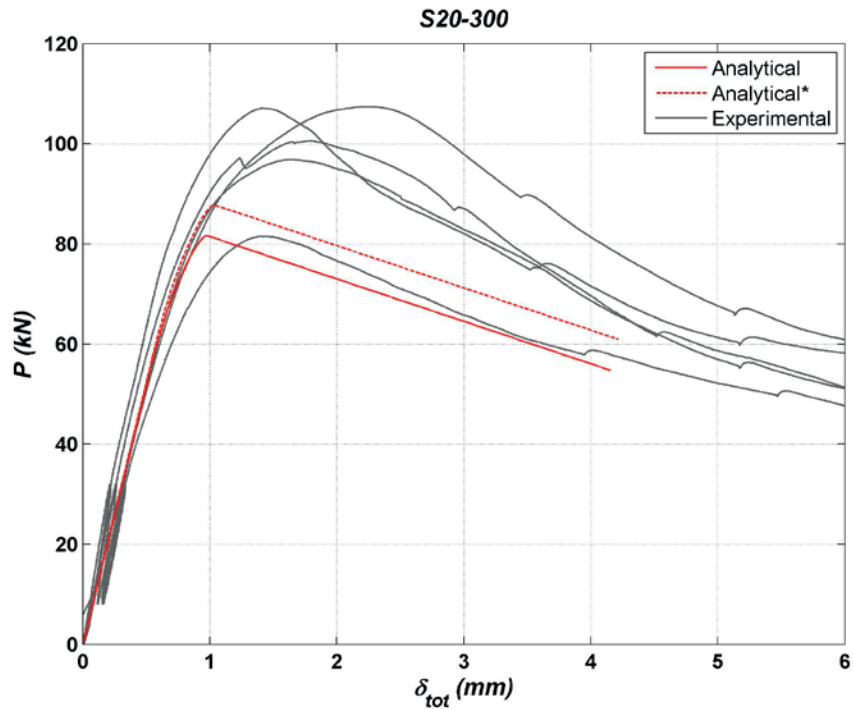
Figure B.10: Force-displacement curves for S20-300 series

Table B.10: Experimental results for S20-300 series

	S$_{20\text{-}300\text{-}1}$	S$_{20\text{-}300\text{-}2}$	S$_{20\text{-}300\text{-}3}$	S$_{20\text{-}300\text{-}4}$	S$_{20\text{-}300\text{-}5}$	Mean	CoV
P_u (kN)	81.48	107.12	96.84	107.44	100.56	98.69	0.11
$\delta_{tot.u}$ (mm)	1.42	1.40	1.64	2.24	1.79	1.70	0.20
$\delta_{w.u}$ (mm)	1.36	1.33	1.57	2.17	1.72	1.63	0.21
K_w (kN/mm)	105.73	165.33	111.73	111.31	135.49	125.92	0.20
K_{w06} (kN/mm)	96.90	137.75	109.61	104.78	123.24	114.45	0.14
K_{w06}/K_w	0.92	0.83	0.98	0.94	0.91	0.92	0.06
K_{w08} (kN/mm)	87.49	121.78	102.03	90.97	107.12	101.88	0.13
K_{w08}/K_w	0.83	0.74	0.91	0.82	0.79	0.82	0.08
K_{wu} (kN/mm)	59.74	80.45	61.65	49.61	58.41	61.97	0.18
K_{wu}/K_w	0.57	0.49	0.55	0.45	0.43	0.50	0.12
f_w (MPa)	4.32	5.68	5.14	5.70	5.33	5.24	0.11
Γ_e (MPa/mm)	8.53	17.20	9.25	9.20	12.41	11.32	0.32
Γ_f (MPa/mm)	0.51	0.82	0.56	0.75	0.68	0.66	0.20
m	0.24	0.22	0.25	0.29	0.23	0.25	0.10

S20-450 series
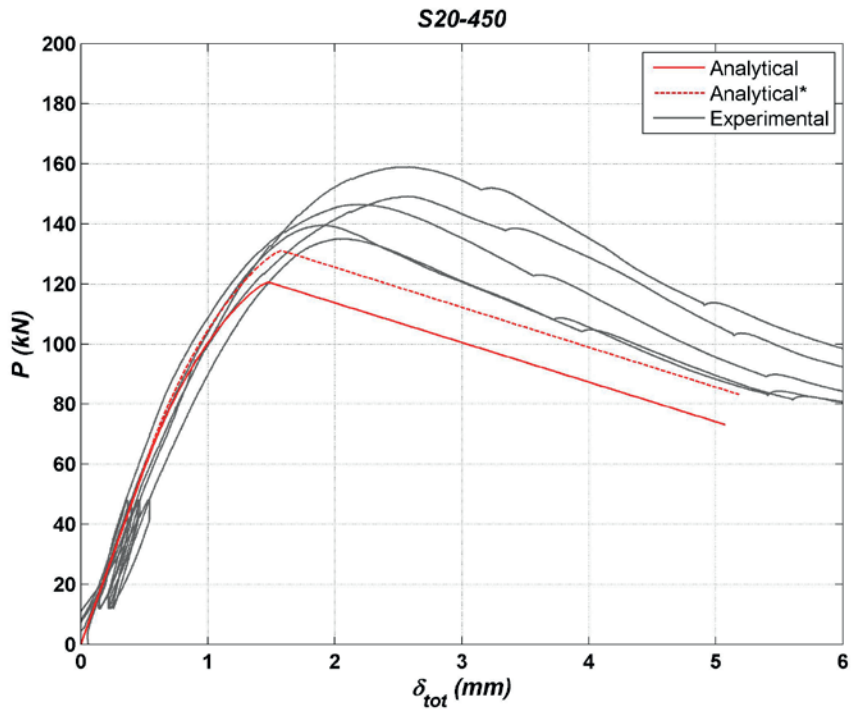
Figure B.11: Force-displacement curves for S20-450 series

Table B.11: Experimental results for S20-450 series

	$S_{20\text{-}450\text{-}1}$	$S_{20\text{-}450\text{-}2}$	$S_{20\text{-}450\text{-}3}$	$S_{20\text{-}450\text{-}4}$	$S_{20\text{-}450\text{-}5}$	**Mean**	**CoV**
P_u (kN)	146.48	135.00	139.44	149.08	158.88	145.78	0.06
$\delta_{tot.u}$ (mm)	2.19	2.03	1.90	2.57	2.53	2.24	0.13
$\delta_{w.u}$ (mm)	2.09	1.94	1.80	2.47	2.42	2.15	0.14
K_w (kN/mm)	146.80	96.79	134.68	113.55	116.68	121.70	0.16
K_{w06} (kN/mm)	133.37	96.61	120.74	112.18	108.67	114.31	0.12
K_{w06}/K_w	0.91	1.00	0.90	0.99	0.93	0.94	0.05
K_{w08} (kN/mm)	110.92	91.43	107.75	94.33	97.56	100.40	0.08
K_{w08}/K_w	0.76	0.94	0.80	0.83	0.84	0.83	0.08
K_{wu} (kN/mm)	70.13	69.50	77.36	60.29	65.59	68.57	0.09
K_{wu}/K_w	0.48	0.72	0.57	0.53	0.56	0.57	0.16
f_w (MPa)	5.18	4.77	4.93	5.27	5.62	5.16	0.06
Γ_e (MPa/mm)	12.02	5.92	10.30	7.67	8.03	8.79	0.27
Γ_f (MPa/mm)	0.56	0.53	0.58	0.57	0.61	0.57	0.05
m	0.22	0.30	0.24	0.27	0.27	0.26	0.13

S20-600 series
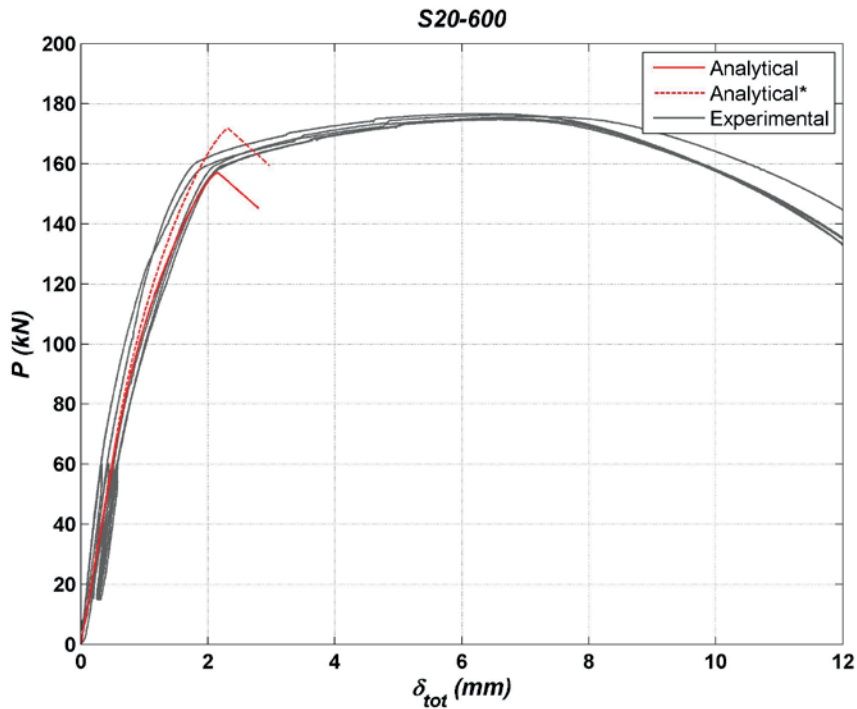
Figure B.12: Force-displacement curves for S20-600 series

Table B.12: Experimental results for S20-600 series

	$S_{20\text{-}600\text{-}1}$	$S_{20\text{-}600\text{-}2}$	$S_{20\text{-}600\text{-}3}$	$S_{20\text{-}600\text{-}4}$	$S_{20\text{-}600\text{-}5}$	Mean	CoV
P_u (kN)	175.12[a]	176.68[a]	176.16[a]	175.68[a]	174.68[a]	175.66	0.01
$\delta_{tot.u}$ (mm)	6.54	6.16	6.37	7.09	6.53	6.54	0.05
$\delta_{w.u}$ (mm)	N/A[a]	N/A[a]	N/A[a]	N/A[a]	N/A[a]	N/A	N/A
K_w (kN/mm)	216.1[b]	153.50	129.01	115.13	114.39	128.01	0.14
K_{w06} (kN/mm)	154.4[b]	135.89	110.00	101.73	104.46	113.02	0.14
K_{w06}/K_w	N/A	0.89	0.85	0.88	0.91	0.88	0.03
K_{w08} (kN/mm)	109.4[b]	116.42	92.83	87.84	90.71	96.95	0.14
K_{w08}/K_w	N/A	0.76	0.72	0.76	0.79	0.76	0.04
K_{wu} (kN/mm)	N/A[a]	N/A[a]	N/A[a]	N/A[a]	N/A[a]	N/A	N/A
K_{wu}/K_w	N/A[a]	N/A[a]	N/A[a]	N/A[a]	N/A[a]	N/A	N/A
f_w (MPa)	N/A[a]	N/A[a]	N/A[a]	N/A[a]	N/A[a]	N/A	N/A
Γ_e (MPa/mm)	24.21[b]	12.33	8.84	7.15	7.07	8.85	0.28
Γ_f (MPa/mm)	N/A[a]	N/A[a]	N/A[a]	N/A[a]	N/A[a]	N/A	N/A
m	N/A[a]	N/A[a]	N/A[a]	N/A[a]	N/A[a]	N/A	N/A

[a] Steel yielding and fracture, [b] Excluded as outlier, not used in the mean and CoV values

S30-100 series

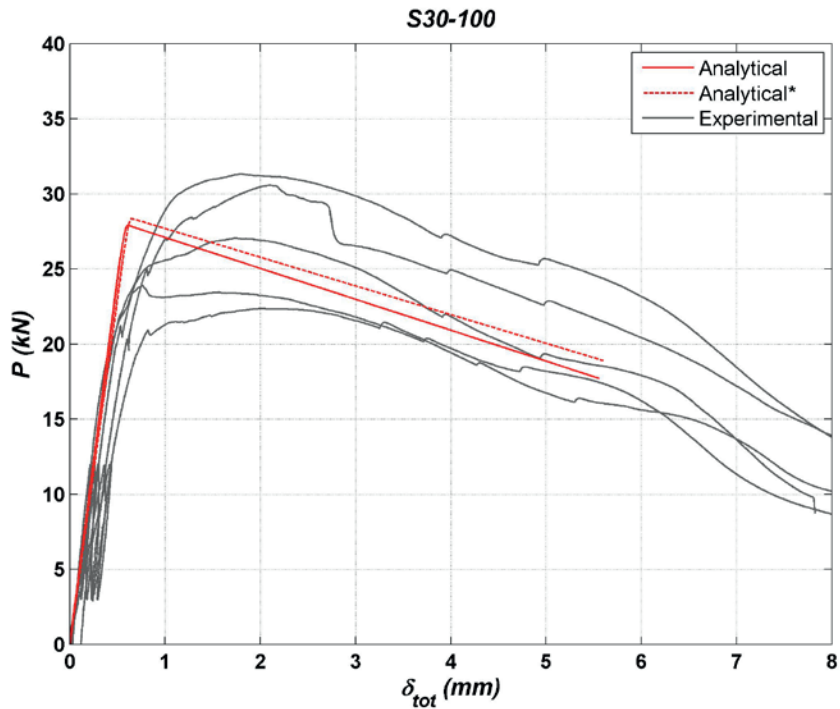**Figure B.13:** Force-displacement curves for S30-100 series

Table B.13: Experimental results for S30-100 series

	$S_{30\text{-}100\text{-}1}$	$S_{30\text{-}100\text{-}2}$	$S_{30\text{-}100\text{-}3}$	$S_{30\text{-}100\text{-}4}$	$S_{30\text{-}100\text{-}5}$	**Mean**	**CoV**
P_u (kN)	22.37	23.90	30.59	27.03	31.32	27.04	0.15
$\delta_{tot.u}$ (mm)	2.02	0.76	2.10	1.72	1.78	1.68	0.32
$\delta_{w.u}$ (mm)	2.01	0.74	2.08	1.70	1.76	1.66	0.32
K_w (kN/mm)	29.22	58.02	33.85	49.95	41.92	42.59	0.27
K_{w06} (kN/mm)	28.96	55.58	34.67	48.13	42.66	42.00	0.25
K_{w06}/K_w	0.99	0.96	1.00 [a]	0.96	1.00 [a]	0.98	0.02
K_{w08} (kN/mm)	28.88	50.14	32.15	43.61	34.69	37.89	0.23
K_{w08}/K_w	0.99	0.86	0.95	0.87	0.83	0.90	0.07
K_{wu} (kN/mm)	11.15	32.20	14.69	15.90	17.76	18.34	0.44
K_{wu}/K_w	0.38	0.56	0.43	0.32	0.42	0.42	0.21
f_w (MPa)	3.56	3.80	4.87	4.30	4.98	4.30	0.15
Γ_e (MPa/mm)	4.93	10.40	5.77	8.80	7.26	7.43	0.30
Γ_f (MPa/mm)	0.16	0.16	0.56	0.31	0.25	0.29	0.56
m	0.18	0.12	0.31	0.19	0.19	0.20	0.34

[a] value set equal to 1.0

S30-300 series
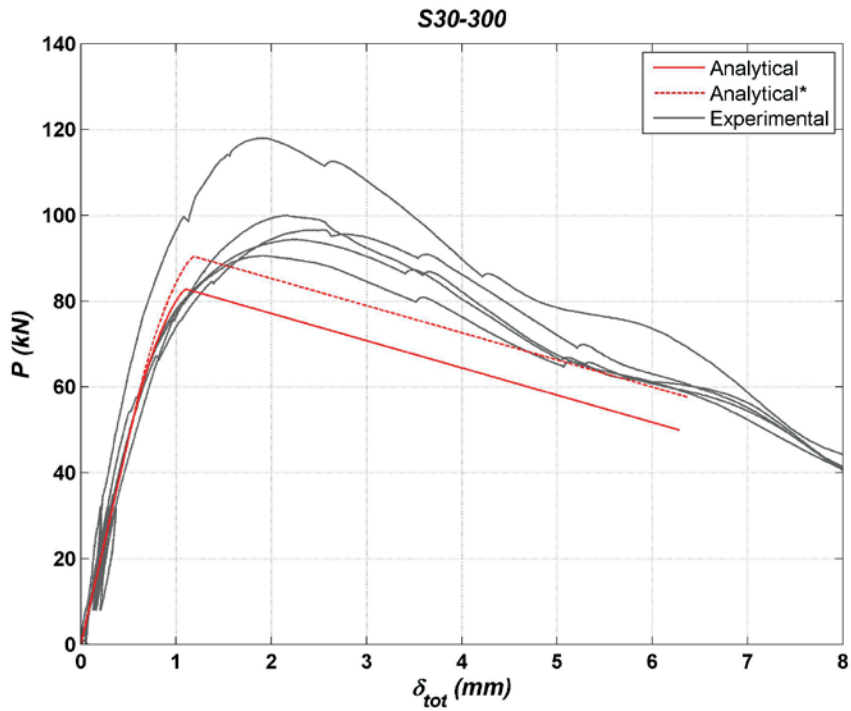
Figure B.14: Force-displacement curves for S30-300 series

Table B.14: Experimental results for S30-300 series

	$S_{30\text{-}300\text{-}1}$	$S_{30\text{-}300\text{-}2}$	$S_{30\text{-}300\text{-}3}$	$S_{30\text{-}300\text{-}4}$	$S_{30\text{-}300\text{-}5}$	**Mean**	**CoV**
P_u (kN)	100.00	96.60	118.00	90.56	94.32	99.90	0.11
$\delta_{tot.u}$ (mm)	2.16	2.54	1.91	1.89	2.21	2.14	0.12
$\delta_{w.u}$ (mm)	2.10	2.47	1.83	1.83	2.15	2.08	0.13
K_w (kN/mm)	95.02	110.28	171.84[a]	124.87	114.79	111.24	0.11
K_{w06} (kN/mm)	88.80	98.94	131.03[a]	110.35	101.01	99.77	0.09
K_{w06}/K_w	0.93	0.90	N/A	0.88	0.88	0.90	0.03
K_{w08} (kN/mm)	76.78	73.30	106.07[a]	88.07	86.34	81.12	0.09
K_{w08}/K_w	0.81	0.66	N/A	0.71	0.75	0.73	0,08
K_{wu} (kN/mm)	47.72	39.05	64.36[a]	49.39	43.93	45.02	0.10
K_{wu}/K_w	0.50	0.35	N/A	0.40	0.38	0.41	0.16
f_w (MPa)	5.31	5.12	6.26	4.80	5.00	5.06	0.04
Γ_e (MPa/mm)	8.02	10.08	21.49[a]	12.31	10.74	10.29	0,17
Γ_f (MPa/mm)	0.48	0.47	0.63	0.38	0.46	0.48	0.19
m	0.24	0.22	0.17	0.18	0.20	0.20	0.15

[a] Excluded as outlier, not used in the mean and CoV values

S30-450 series
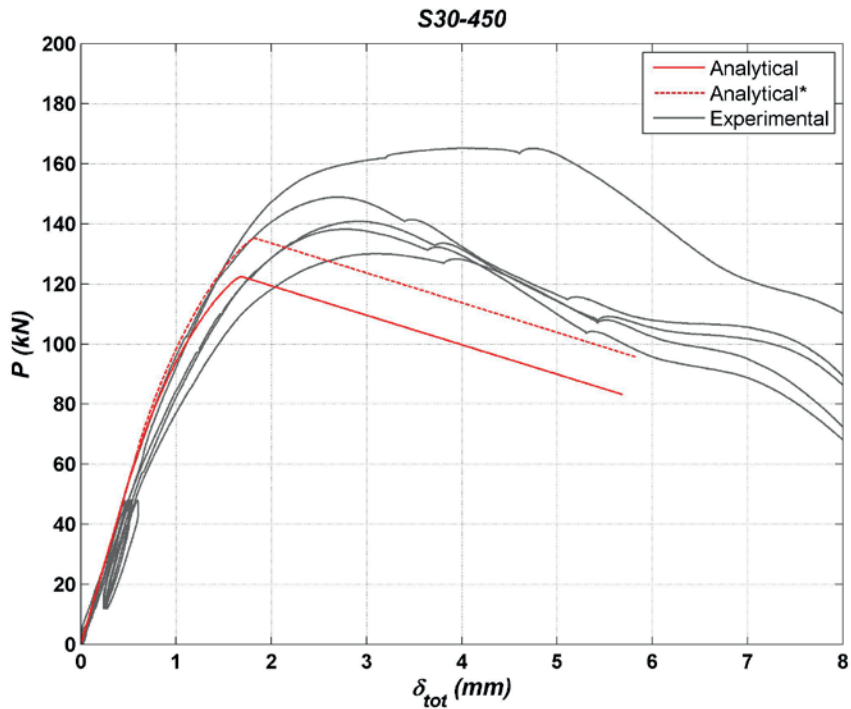
Figure B.15: Force-displacement curves for S30-450 series

Table B.15: Experimental results for S30-450 series

	$S_{30\text{-}450\text{-}1}$	$S_{30\text{-}450\text{-}2}$	$S_{30\text{-}450\text{-}3}$	$S_{30\text{-}450\text{-}4}$	$S_{30\text{-}450\text{-}5}$	Mean	CoV
P_u (kN)	140.84	148.88	138.28	130.04	165.20[a]	144.65	0.09
$\delta_{tot.u}$ (mm)	2.88	2.65	2.74	3.06	4.03	3.07	0.18
$\delta_{w.u}$ (mm)	2.79	2.55	2.65	2.97	N/A[a]	2.74	0.07
K_w (kN/mm)	105.37	114.37	97.43	85.98	98.58	100.35	0.10
K_{w06} (kN/mm)	89.46	105.62	86.86	80.84	96.34	91.83	0.10
K_{w06}/K_w	0.85	0.92	0.89	0.94	0.98	0.92	0.05
K_{w08} (kN/mm)	77.58	90.80	77.68	70.86	85.88	80.56	0.10
K_{w08}/K_w	0.74	0.79	0.80	0.82	0.87	0.80	0.06
K_{wu} (kN/mm)	50.48	58.37	52.23	43.74	N/A[a]	51.2	0.12
K_{wu}/K_w	0.48	0.51	0.54	0.51	N/A[a]	0.51	0.05
f_w (MPa)	4.98	5.27	4.89	4.60	5.84	5.12	0.09
Γ_e (MPa/mm)	7.57	8.74	6.62	5.39	6.75	7.01	0.18
Γ_f (MPa/mm)	0.41	0.45	0.42	0.39	0.51	0.43	0.11
m	0.23	0.23	0.25	0.27	0.27	0.25	0.08

[a] Steel yielding

S30-600 series
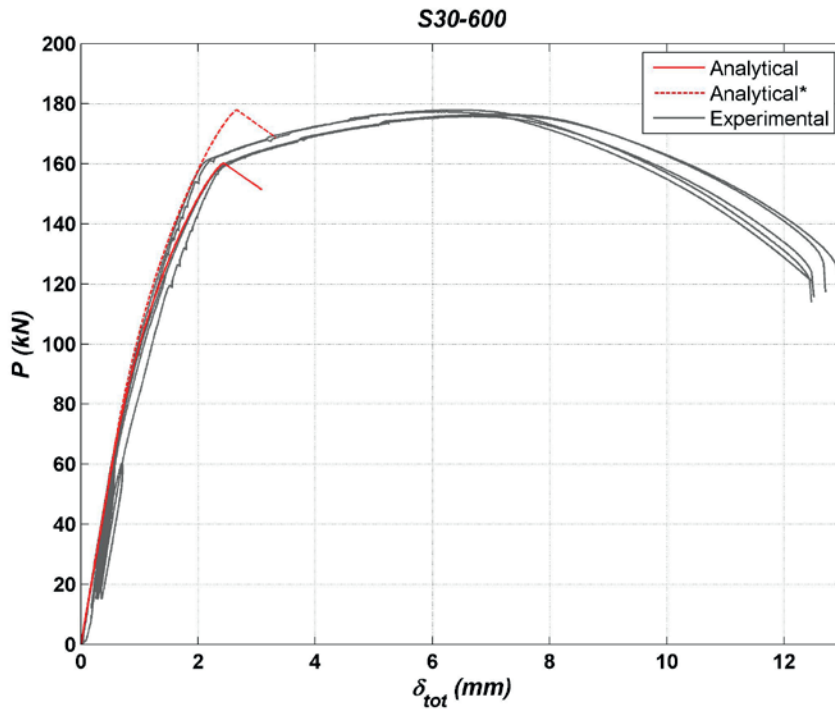
Figure B.16: Force-displacement curves for S30-600 series

Table B.16: Experimental results for S30-600 series

	$S_{30\text{-}600\text{-}1}$	$S_{30\text{-}600\text{-}2}$	$S_{30\text{-}600\text{-}3}$	$S_{30\text{-}600\text{-}4}$	$S_{30\text{-}600\text{-}5}$	Mean	CoV
P_u (kN)	177.32[a]	175.76[a]	176.52[a]	176.12[a]	177.92[a]	176.73	0.01
$\delta_{tot.u}$ (mm)	6.24	6.68	6.96	7.04	6.37	6.66	0.05
$\delta_{w.u}$ (mm)	N/A[a]	N/A[a]	N/A[a]	N/A[a]	N/A[a]	N/A	N/A
K_w (kN/mm)	125.93	92.88	121.75	114.97	118.64	114.83	0.11
K_{w06} (kN/mm)	107.31	86.25	100.10	96.38	100.95	98.20	0.08
K_{w06}/K_w	0.85	0.93	0.82	0.84	0.85	0.86	0.05
K_{w08} (kN/mm)	90.58	76.25	81.37	81.62	87.92	83.55	0.07
K_{w08}/K_w	0.72	0.82	0.67	0.71	0.74	0.73	0.08
K_{wu} (kN/mm)	N/A[a]	N/A[a]	N/A[a]	N/A[a]	N/A[a]	N/A	N/A
K_{wu}/K_w	N/A[a]	N/A[a]	N/A[a]	N/A[a]	N/A[a]	N/A	N/A
f_w (MPa)	N/A[a]	N/A[a]	N/A[a]	N/A[a]	N/A[a]	N/A	N/A
Γ_e (MPa/mm)	9.52	5.40	8.92	8.00	8.49	8.07	0.20
Γ_f (MPa/mm)	N/A[a]	N/A[a]	N/A[a]	N/A[a]	N/A[a]	N/A	N/A
m	N/A[a]	N/A[a]	N/A[a]	N/A[a]	N/A[a]	N/A	N/A

[a] Steel yielding and fracture

S60-100 series
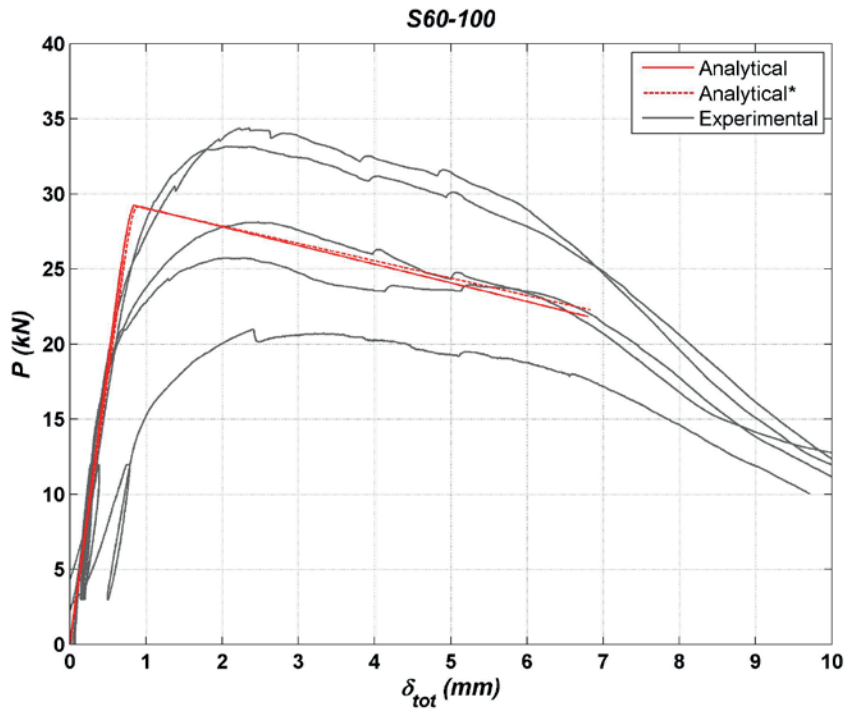
Figure B.17: Force-displacement curves for S60-100 series

Table B.17: Experimental results for S60-100 series

	$S_{60\text{-}100\text{-}1}$	$S_{60\text{-}100\text{-}2}$	$S_{60\text{-}100\text{-}3}$	$S_{60\text{-}100\text{-}4}$	$S_{60\text{-}100\text{-}5}$	**Mean**	**CoV**
P_u (kN)	33.16	28.10	25.72	34.38	20.96	28.46	0.19
$\delta_{tot.u}$ (mm)	2.06	2.46	2.10	2.23	2.39	2.25	0.08
$\delta_{w.u}$ (mm)	2.04	2.44	2.08	2.21	2.37	2.23	0.08
K_w (kN/mm)	34.47	45.96	42.71	43.70	16.28	36.62	0.33
K_{w06} (kN/mm)	33.92	40.15	40.64	37.97	15.59	33.65	0.31
K_{w06}/K_w	0.98	0.87	0.95	0.87	0.96	0.93	0.06
K_{w08} (kN/mm)	30.62	27.34	31.22	27.26	13.84	26.06	0.27
K_{w08}/K_w	0.89	0.59	0.73	0.62	0.85	0.74	0.18
K_{wu} (kN/mm)	16.26	11.53	12.35	15.57	8.84	12.91	0.24
K_{wu}/K_w	0.47	0.25	0.29	0.36	0.54	0.38	0.32
f_w (MPa)	5.28	4.47	4.09	5.47	3.34	4.53	0.19
Γ_e (MPa/mm)	6.31	8.83	8.10	8.32	2.76	6.86	0.36
Γ_f (MPa/mm)	0.17	0.22	0.15	0.18	0.08	0.16	0.31
m	0.16	0.16	0.14	0.15	0.17	0.16	0.09

S60-300 series
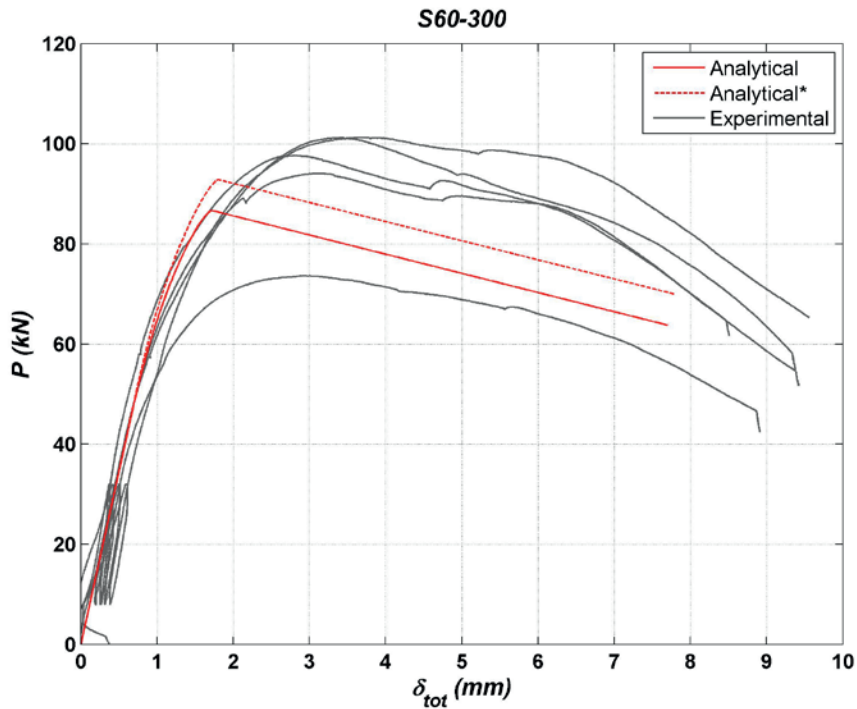
Figure B.18: Force-displacement curves for S60-300 series

Table B.18: Experimental results for S60-300 series

	$S_{60\text{-}300\text{-}1}$	$S_{60\text{-}300\text{-}2}$	$S_{60\text{-}300\text{-}3}$	$S_{60\text{-}300\text{-}4}$	$S_{60\text{-}300\text{-}5}$	**Mean**	**CoV**
P_u (kN)	97.64	101.28	73.60	101.24	94.08	93.57	0.12
$\delta_{tot.u}$ (mm)	2.79	3.60	2.88	3.43	3.05	3.15	0.11
$\delta_{w.u}$ (mm)	2.73	3.53	2.83	3.36	2.98	3.09	0.11
K_w (kN/mm)	91.58	56.80	67.86	74.58	76.59	73.48	0.17
K_{w06} (kN/mm)	78.41	56.35	62.75	65.09	68.92	66.30	0.12
K_{w06}/K_w	0.86	0.99	0.92	0.87	0.90	0.91	0.06
K_{w08} (kN/mm)	62.51	50.27	51.98	49.73	56.80	54.26	0.10
K_{w08}/K_w	0.68	0.89	0.77	0.67	0.74	0.75	0.12
K_{wu} (kN/mm)	35.83	28.66	26.03	30.14	31.54	30.44	0.12
K_{wu}/K_w	0.39	0.50	0.38	0.40	0.41	0.42	0.12
f_w (MPa)	5.18	5.37	3.90	5.37	4.99	4.96	0.12
Γ_e (MPa/mm)	10.80	4.90	6.47	7.56	7.91	7.53	0.29
Γ_f (MPa/mm)	0.18	0.09	0.11	0.23	0.17	0.16	0.36
m	0.13	0.14	0.13	0.18	0.15	0.14	0.13

S60-450 series
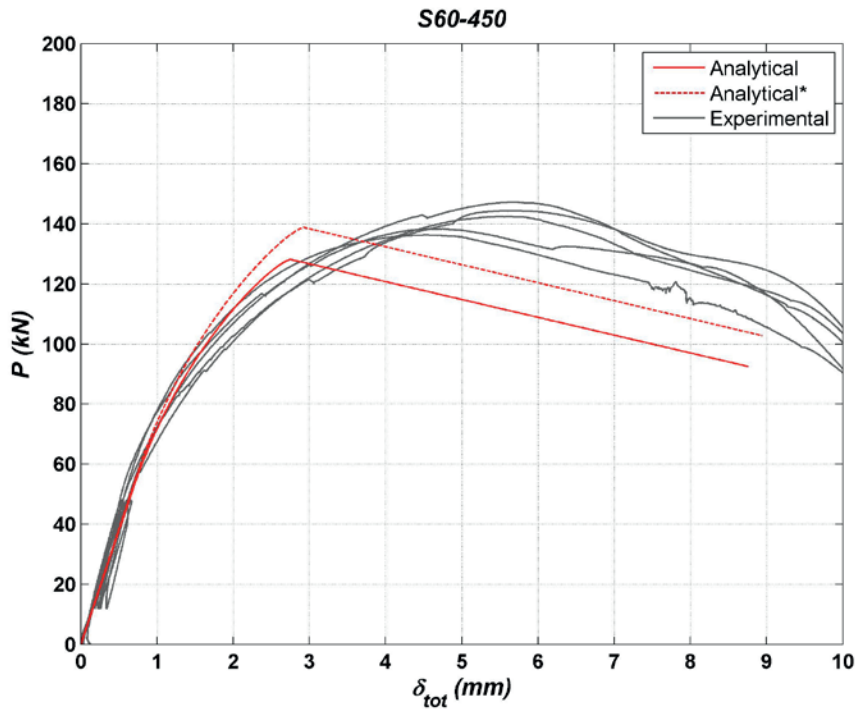
Figure B.19: Force-displacement curves for S60-450 series

Table B.19: Experimental results for S60-450 series

	$S_{60\text{-}450\text{-}1}$	$S_{60\text{-}450\text{-}2}$	$S_{60\text{-}450\text{-}3}$	$S_{60\text{-}450\text{-}4}$	$S_{60\text{-}450\text{-}5}$	**Mean**	**CoV**
P_u (kN)	144.36	138.32	142.40	147.24	136.24	141.71	0.03
$\delta_{tot.u}$ (mm)	5.59	4.56	5.44	5.67	4.44	5.14	0.11
$\delta_{w.u}$ (mm)	5.49[a]	4.46[a]	5.34[a]	5.57[a]	4.35[a]	5.04	0.12
K_w (kN/mm)	97.01	85.03	77.86	97.75	93.06	90.14	0.09
K_{w06} (kN/mm)	63.21	70.21	61.58	72.71	79.44	69.43	0.10
K_{w06}/K_w	0.65	0.83	0.79	0.74	0.85	0.77	0.10
K_{w08} (kN/mm)	45.53	53.15	46.07	48.58	59.88	50.64	0.12
K_{w08}/K_w	0.47	0.63	0.59	0.50	0.64	0.57	0.14
K_{wu} (kN/mm)	26.28[a]	30.99[a]	26.67[a]	26.43[a]	31.31[a]	28.34	0.09
K_{wu}/K_w	0.27[a]	0.36[a]	0.34[a]	0.27[a]	0.34[a]	0.32	0.14
f_w (MPa)	5.11	4.89	5.04	5.21	4.82	5.01	0.03
Γ_e (MPa/mm)	10.41	8.08	6.85	10.57	9.61	9.10	0.18
Γ_f (MPa/mm)	0.19	0.11	0.24	0.32	0.22	0.22	0.35
m	0.13	0.12	0.19	0.17	0.15	0.15	0.19

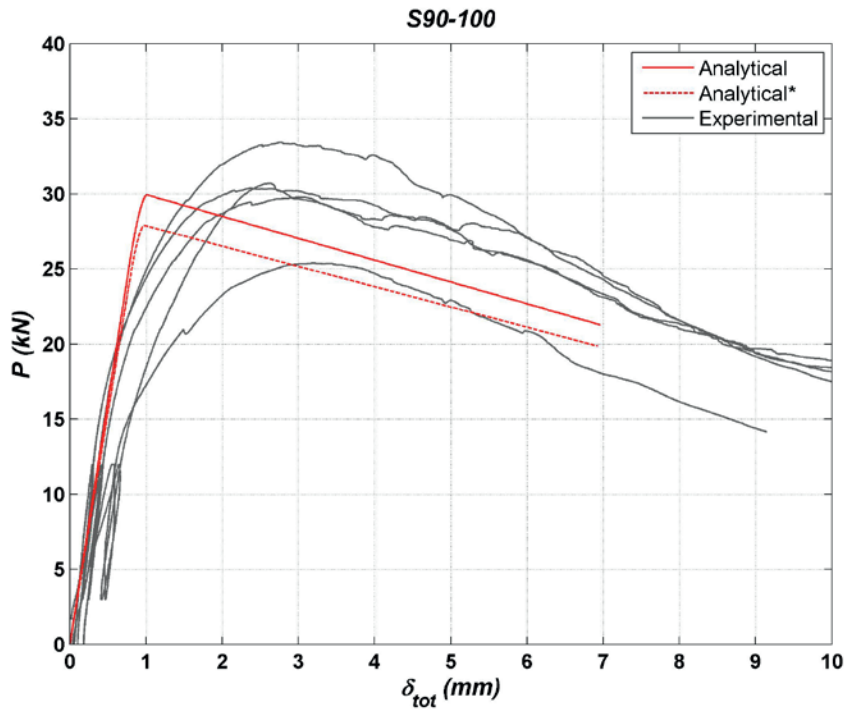[a] Values may be influenced by inelastic behaviour of wood below the supports

S90-100 series

Figure B.20: Force-displacement curves for S90-100 series

Table B.20: Experimental results for S90-100 series

	S$_{90\text{-}100\text{-}1}$	S$_{90\text{-}100\text{-}2}$	S$_{90\text{-}100\text{-}3}$	S$_{90\text{-}100\text{-}4}$	S$_{90\text{-}100\text{-}5}$	**Mean**	**CoV**
P_u (kN)	30.70	33.43	30.36	25.39	29.78	29.93	0.10
$\delta_{tot.u}$ (mm)	2.61	2.77	2.35	3.18	3.03	2.79	0.12
$\delta_{w.u}$ (mm)	2.59	2.75	2.33	3.16	3.01	2.77	0.12
K_w (kN/mm)	19.00	32.54	42.00	22.28	29.42	29.05	0.31
K_{w06} (kN/mm)	18.65	31.46	35.67	19.67	27.57	26.60	0.28
K_{w06}/K_w	0.98	0.97	0.85	0.88	0.94	0.92	0.06
K_{w08} (kN/mm)	16.28	23.12	24.94	14.74	20.99	20.02	0.22
K_{w08}/K_w	0.86	0.71	0.59	0.66	0.71	0.71	0.14
K_{wu} (kN/mm)	11.87	12.17	13.03	8.04	9.90	11.00	0.18
K_{wu}/K_w	0.62	0.37	0.31	0.36	0.34	0.40	0.32
f_w (MPa)	4.89	5.32	4.83	4.04	4.74	4.76	0.10
Γ_e (MPa/mm)	3.32	6.11	8.30	3.96	5.43	5.43	0.36
Γ_f (MPa/mm)	0.19	0.13	0.15	0.20	0.25	0.18	0.25
m	0.24	0.15	0.14	0.23	0.21	0.19	0.25

S90-300 series
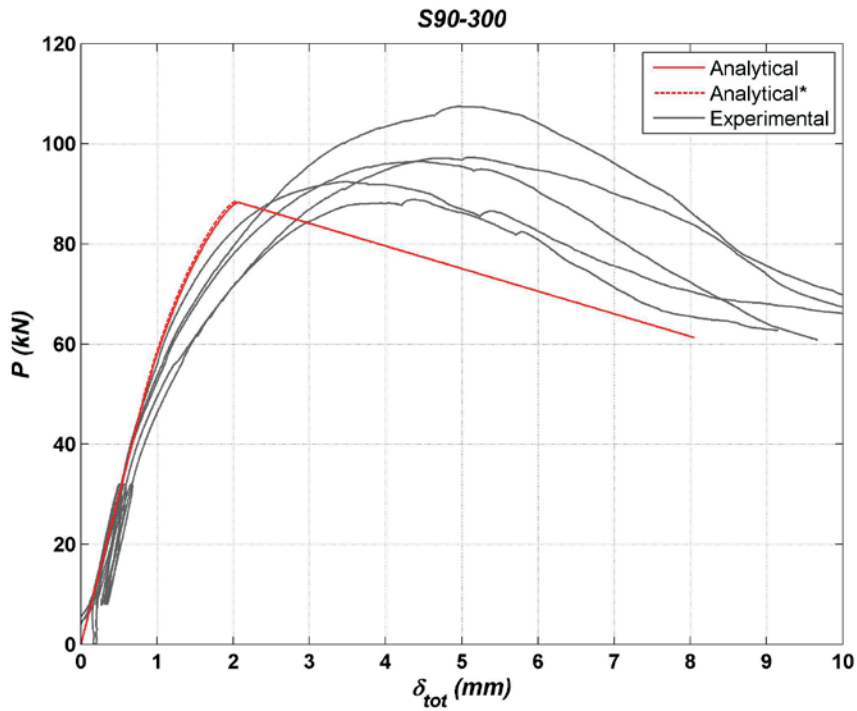
Figure B.21: Force-displacement curves for S90-300 series

Table B.21: Experimental results for S90-300 series

	$S_{90\text{-}300\text{-}1}$	$S_{90\text{-}300\text{-}2}$	$S_{90\text{-}300\text{-}3}$	$S_{90\text{-}300\text{-}4}$	$S_{90\text{-}300\text{-}5}$	**Mean**	**CoV**
P_u (kN)	88.88	92.44	96.48	107.48	97.24	96.50	0.07
$\delta_{tot.u}$ (mm)	4.38	3.47	4.41	4.95	5.07	4.46	0.14
$\delta_{w.u}$ (mm)	4.32	3.41	4.34	4.88	5.00	4.39	0.14
K_w (kN/mm)	58.76	66.67	67.68	63.00	50.86	61.39	0.11
K_{w06} (kN/mm)	48.85	58.22	52.41	49.96	43.28	50.54	0.11
K_{w06}/K_w	0.83	0.87	0.77	0.79	0.85	0.82	0.05
K_{w08} (kN/mm)	36.85	49.36	40.53	37.49	33.74	39.59	0.15
K_{w08}/K_w	0.63	0.74	0.60	0.60	0.66	0.64	0.09
K_{wu} (kN/mm)	20.56	27.14	22.22	22.02	19.43	22.28	0.13
K_{wu}/K_w	0.35	0.41	0.33	0.35	0.38	0.36	0.09
f_w (MPa)	4.72	4.90	5.12	5.70	5.16	5.12	0.07
Γ_e (MPa/mm)	5.76	7.13	7.32	6.47	4.57	6.25	0.18
Γ_f (MPa/mm)	0.33	0.24	0.33	0.36	0.24	0.30	0.19
m	0.24	0.18	0.21	0.23	0.23	0.22	0.11

S90-450 series
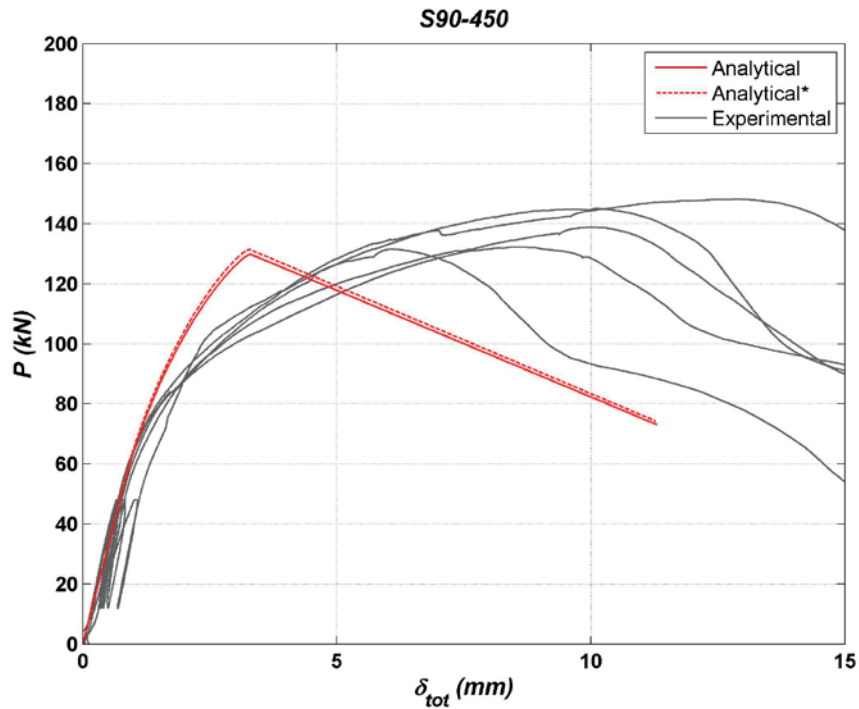
Figure B.22: Force-displacement curves for S90-450 series

Table B.22: Experimental results for S90-450 series

	$S_{90\text{-}450\text{-}1}$	$S_{90\text{-}450\text{-}2}$	$S_{90\text{-}450\text{-}3}$	$S_{90\text{-}450\text{-}4}$	$S_{90\text{-}450\text{-}5}$	Mean	CoV
P_u (kN)	131.48	138.80	145.04	148.12	132.32	139.15	0.05
$\delta_{tot.u}$ (mm)	6.05	10.03	10.13	12.77	8.49	9.49	0.26
$\delta_{w.u}$ (mm)	5.96 [a]	9.94 [a]	10.03 [a]	12.67 [a]	8.40 [a]	9.40	0.26
K_w (kN/mm)	76.61	64.12	49.15	74.30	69.03	66.64	0.16
K_{w06} (kN/mm)	55.22	48.25	45.61	48.67	54.22	50.39	0.08
K_{w06}/K_w	0.72	0.75	0.93	0.66	0.79	0.77	0.13
K_{w08} (kN/mm)	35.30	30.25	31.69	30.07	29.32	31.33	0.08
K_{w08}/K_w	0.46	0.47	0.64	0.40	0.42	0.48	0.20
K_{wu} (kN/mm)	22.07 [a]	13.97 [a]	14.46 [a]	11.69 [a]	15.75 [a]	15.59 [a]	0.25
K_{wu}/K_w	0.29 [a]	0.22 [a]	0.29 [a]	0.16 [a]	0.23 [a]	0.24 [a]	0.24
f_w (MPa)	4.65	4.91	5.13	5.24	4.68	4.92	0.05
Γ_e (MPa/mm)	7.79	5.56	3.46	7.34	6.38	6.10	0.28
Γ_f (MPa/mm)	0.29	0.33	0.38	0.12	0.23	0.27	0.37
m	0.19	0.24	0.33	0.13	0.19	0.22	0.35

[a] Values influenced by inelastic behaviour of wood below the supports

C. Detailed numerical results

The numerical results for the single rod specimens are presented in detail in this appendix. In two simulations (specimens S0-450-5 and S90-450-2), the actual annular ring pattern of the laminations of these specimens has been described and wood was modelled as orthotropic. The results of these simulations showed that the difference between modelling wood as orthotropic and transversely isotropic is small and therefore wood was modelled as transversely isotropic in the other simulations. The material properties given in Table 1 were used for the simulations. A full description of the FE model is given in Paper i [60].

Table C.1: Material properties for numerical simulations

Material	Material property	Symbol	Transversely Isotropic	Orthotropic
Wood	Young's Moduli (MPa)	E_L	13000	13000
		E_R	410	820
		E_T		410
	Shear Moduli (MPa)	$G_{LR} = G_{LT}$	760	760
		G_{RT}	30	30
	Poisson ratios	ν_{LR}	0.60	0.50
		ν_{LT}		0.70
		ν_{TR}	0.60	0.60
		ν_{RT}		
Steel	Young's Modulus (MPa)	E_S	210000	
	Poisson ratio	ν	0.30	
Wood-steel	Friction coefficient	μ	0.20	

The following numerical results for each simulation (for a unit withdrawal force $P=$ 1kN) are presented:

- **The lengthwise distributions of shear stresses:** The shear stresses are given for the centroid of the finite elements at the interface (the nodal shear stresses have also been quantified but the differences were very small). The shear stress distribution for each circumferential path (16 in total) of the interface together with the mean shear stress are provided (the maximum mean shear stress is given in a table). The analytical

estimation for the shear stress distribution along the rod length is also given.

- **The axial stress distribution in the rod:** The axial stress in the rod is normalized by the maximum stress, $\sigma_s(0) = P/A_s$ and compared to the analytical estimation which is also provided.
- **The lengthwise displacement distributions:** The displacements of the rod and the wood at the interface with respect to the supports are provided. The mean displacement distribution and the individual displacement distributions for 16 circumferential nodes of the interface are plotted. The mean relative slip distribution, $\delta_{slip}(x_e)$, obtained as the subtraction of the mean wood interfacial displacement from the displacement of the threaded rod, is also plotted. The numerical estimations for the withdrawal stiffness, the withdrawal displacement and the relative slip at the entrance are given in a table.
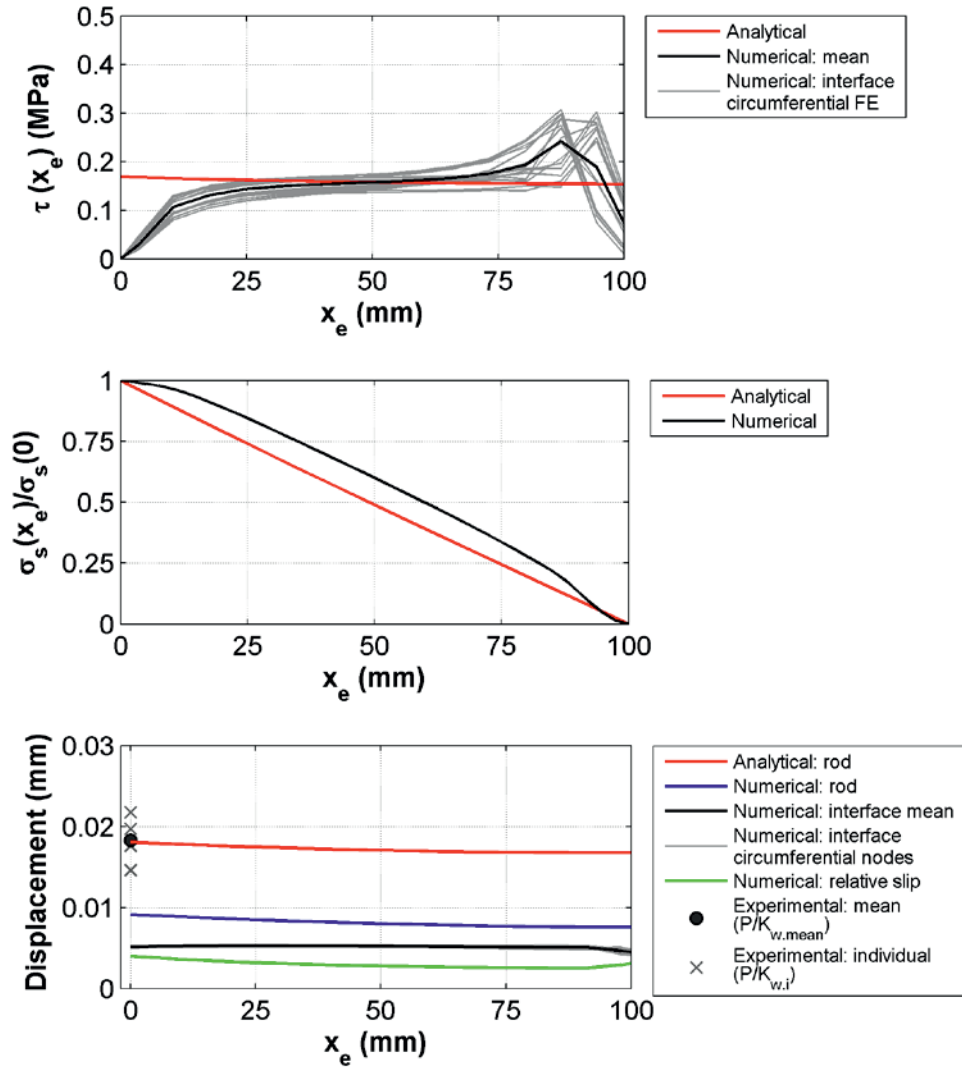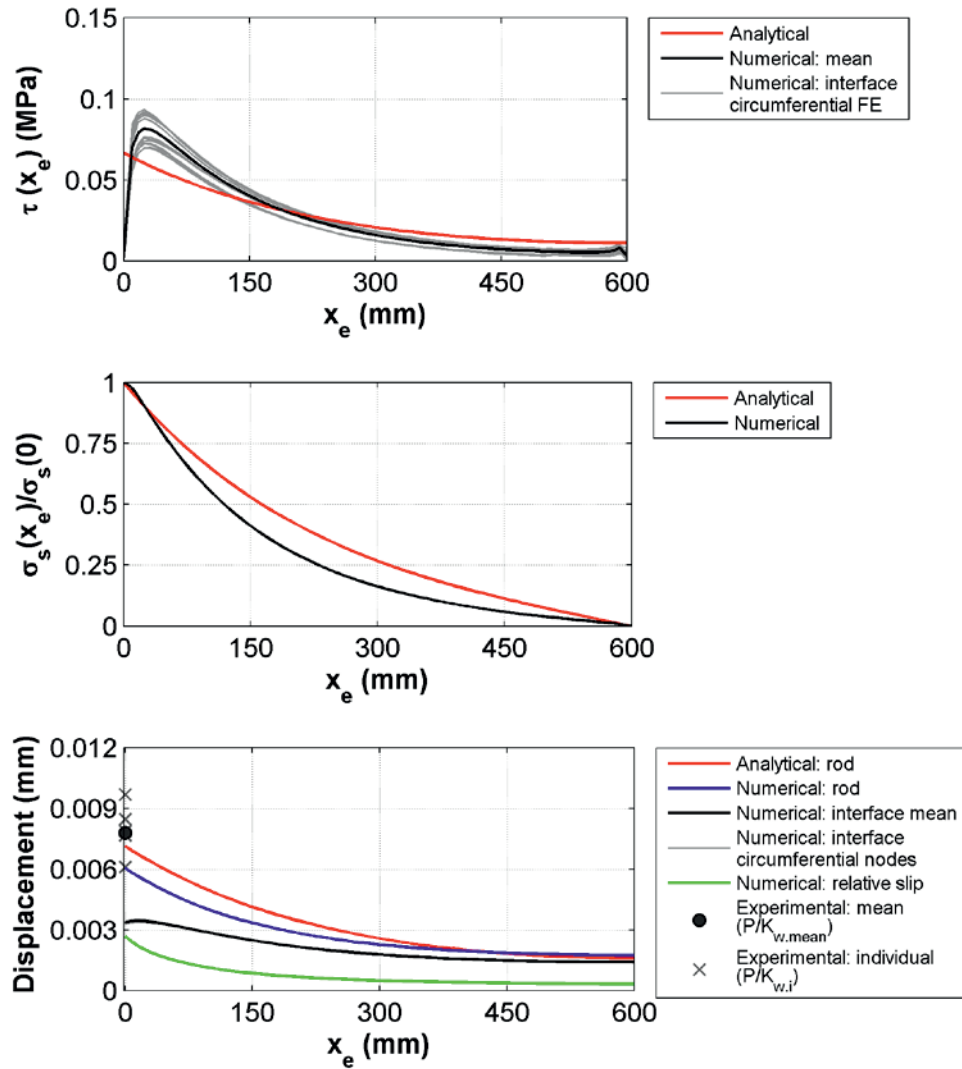
Figure C.1: Lengthwise distributions of $\tau(x_e)$, $\sigma_s(x_e)$ and displacements for S0-100 (P= 1kN)

Table C.2: Numerical results for S0-100 (P= 1kN)

K_w (kN/mm)	109.80
δ_w (mm)	0.0091
δ_{slip} (mm)	0.0040
δ_{slip} / δ_w	0.44
τ_{max} (MPa)	0.24
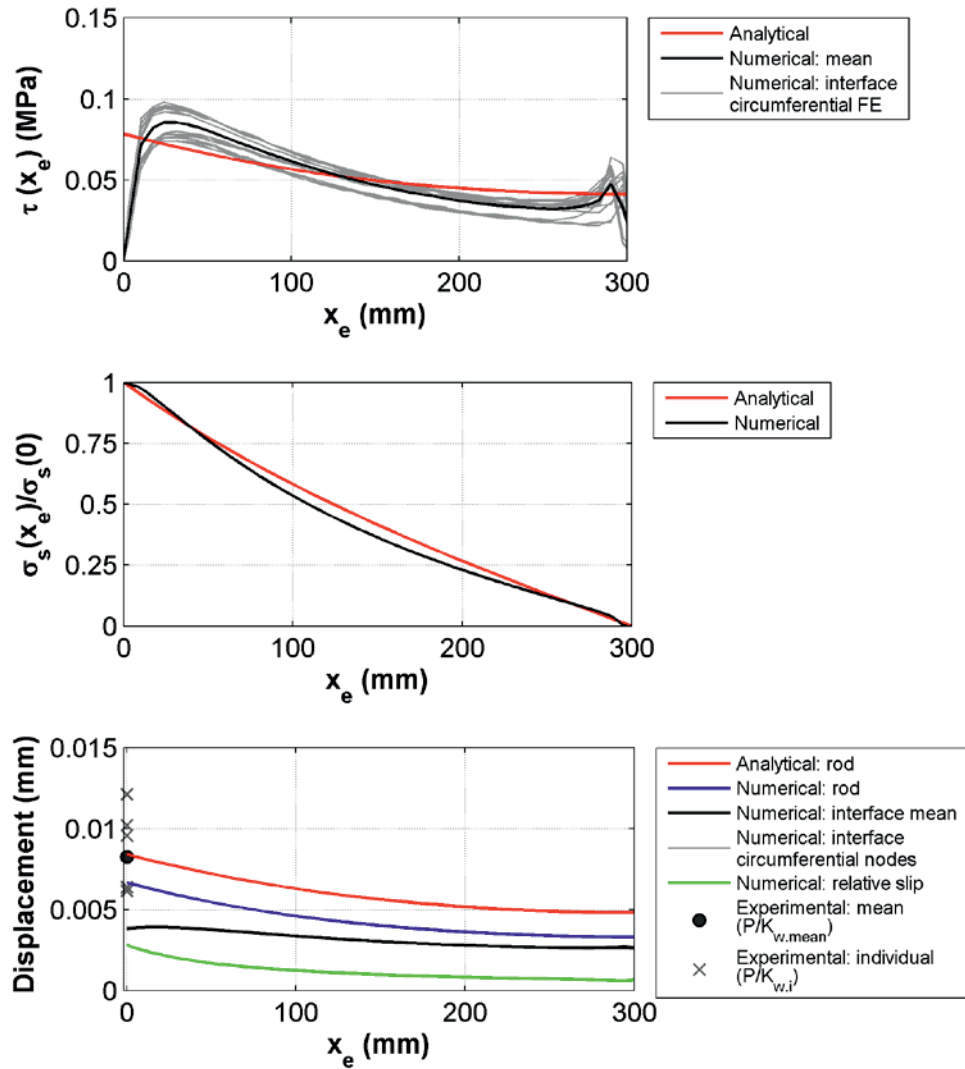
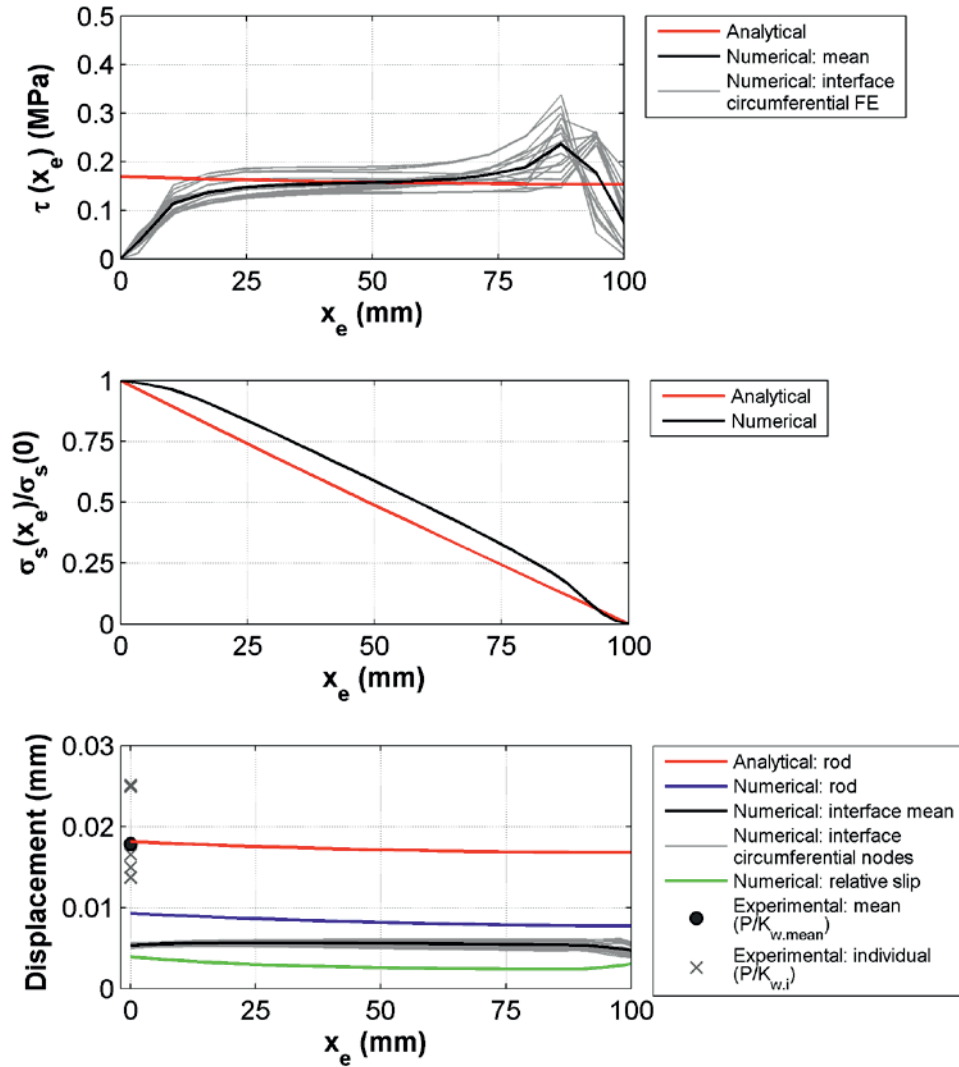**Figure C.2:** Lengthwise distributions of $\tau(x_e)$, $\sigma_s(x_e)$ and displacements for S0-300 (P= 1kN)

Table C.3: Numerical results for S0-300 (P= 1kN)

|	
K_w (kN/mm)	150.9
δ_w (mm)	0.0066
δ_{slip} (mm)	0.0028
δ_{slip} / δ_w	0.42
τ_{max} (MPa)	0.086
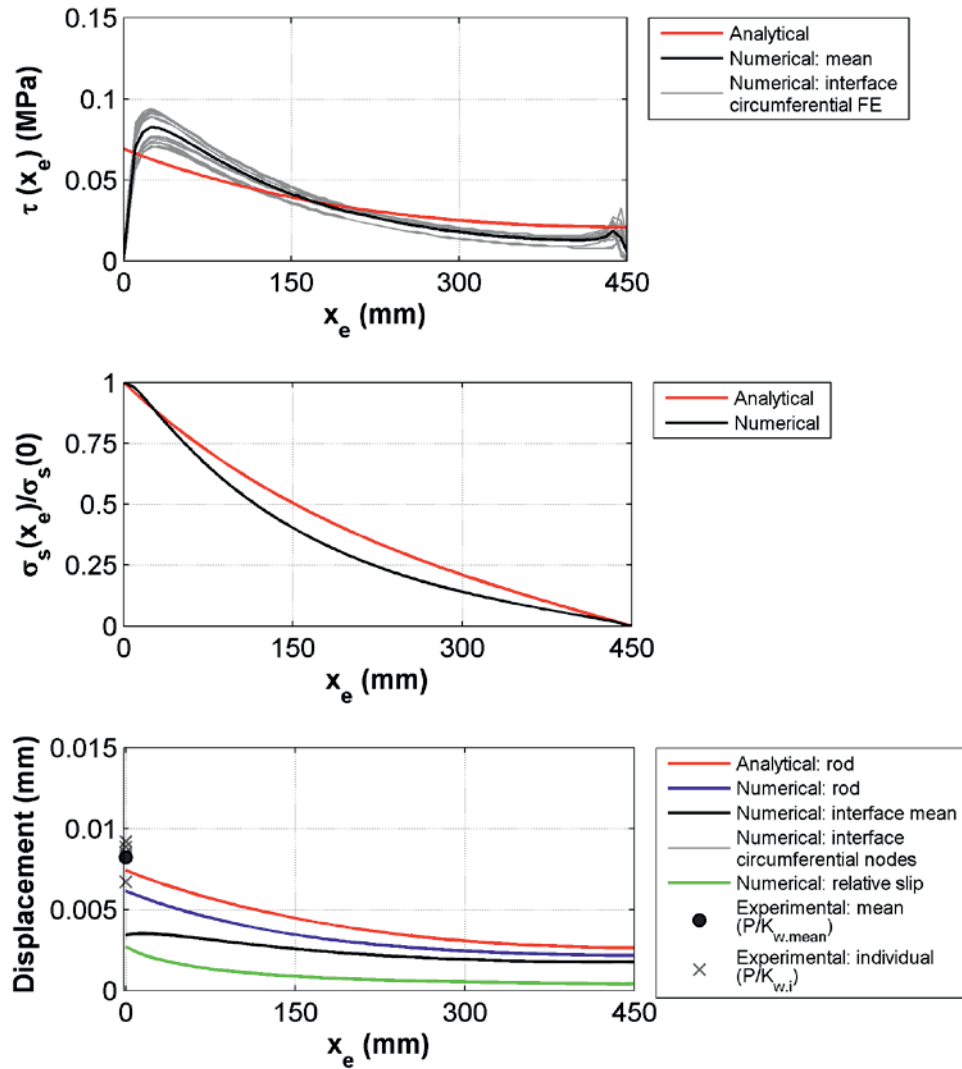
Figure C.3: Lengthwise distributions of $\tau(x_e)$, $\sigma_s(x_e)$ and displacements for S0-450 (P= 1kN)

Table C.4: Numerical results for S0-450 (P= 1kN)

K_w (kN/mm)	163.2
δ_w (mm)	0.0061
δ_{slip} (mm)	0.0027
δ_{slip} / δ_w	0.44
τ_{max} (MPa)	0.083

S0-450-5 (wood modelled as orthotropic)
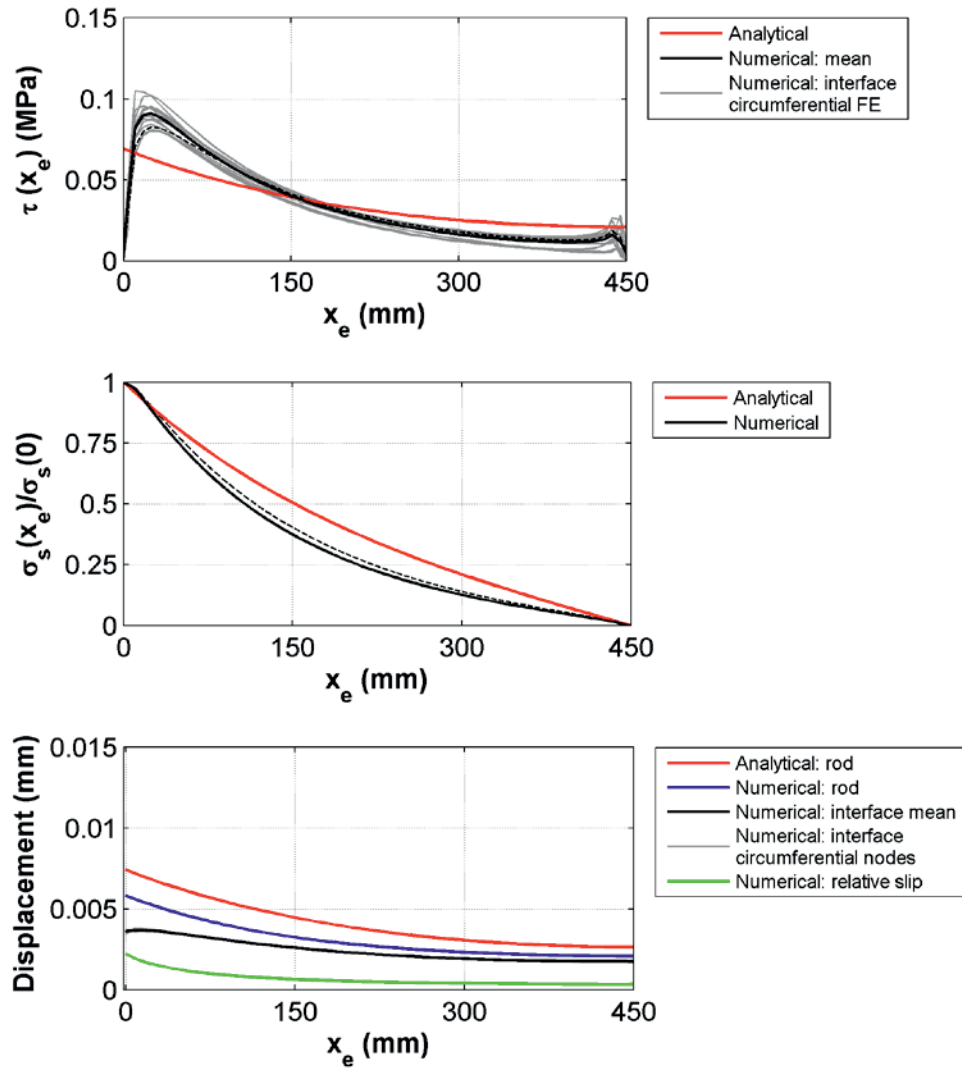
Figure C.4: Lengthwise distributions of $\tau(x_e)$, $\sigma_s(x_e)$ and displacements for S0-450-5 (P= 1kN) – dashed lines correspond to the transverse isotropy solution

Table C.5: Numerical results for S0-450-5 (P= 1kN)

|	
K_w (kN/mm)	171.6
δ_w (mm)	0.0058
δ_{slip} (mm)	0.0022
δ_{slip} / δ_w	0.38
τ_{max} (MPa)	0.091

Figure C.5: Lengthwise distributions of $\tau(x_e)$, $\sigma_s(x_e)$ and displacements for S0-600 (P= 1kN)

Table C.6: Numerical results for S0-600 (P= 1kN)

K_w (kN/mm)	165.9
δ_w (mm)	0.0060
δ_{slip} (mm)	0.0027
δ_{slip} / δ_w	0.44
τ_{max} (MPa)	0.082

S10-100 series

Figure C.6: Lengthwise distributions of $\tau(x_e)$, $\sigma_s(x_e)$ and displacements for S10-100 (P= 1kN)

Table C.7: Numerical results for S10-100 (P= 1kN)

|	
K_w (kN/mm)	108.2
δ_w (mm)	0.0092
δ_{slip} (mm)	0.0039
δ_{slip} / δ_w	0.42
τ_{max} (MPa)	0.236
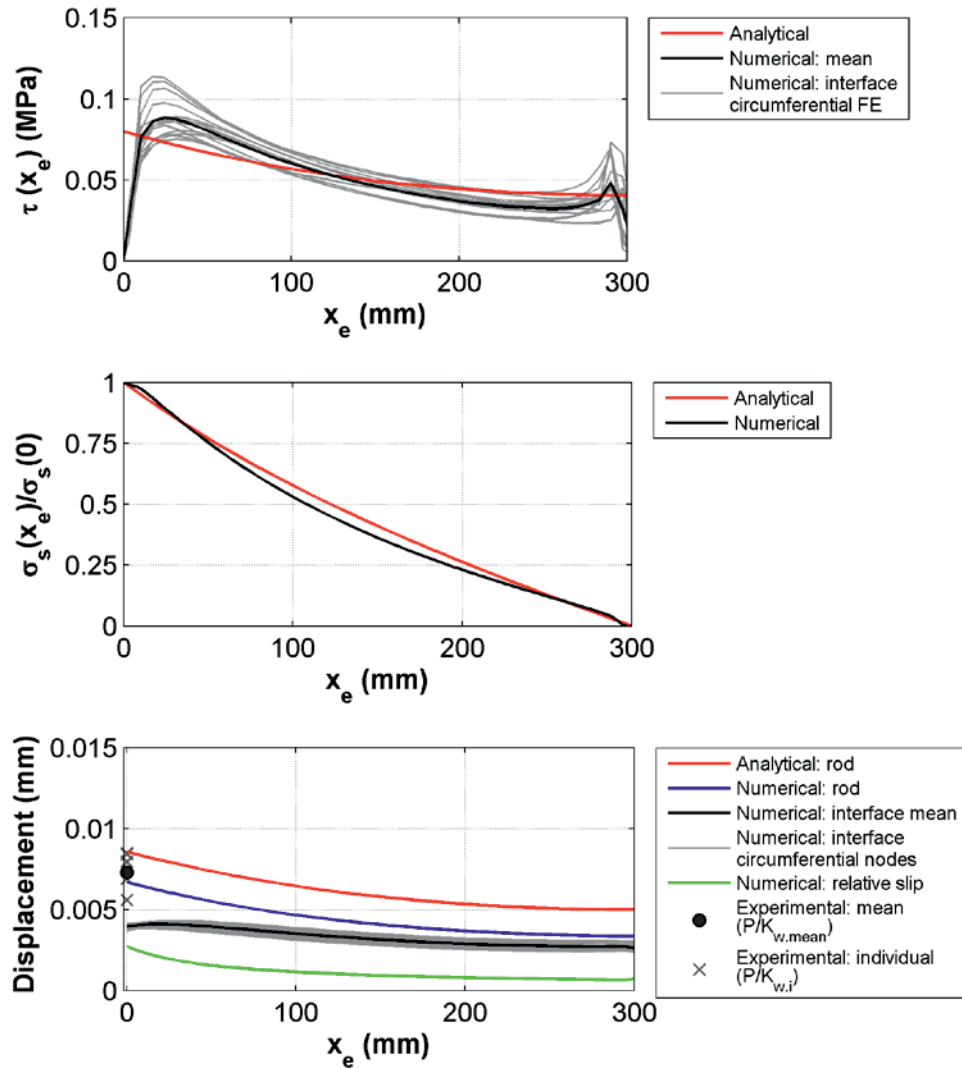
Figure C.7: Lengthwise distributions of $\tau(x_e)$, $\sigma_s(x_e)$ and displacements for S10-300 (P= 1kN)

Table C.8: Numerical results for S10-300 (P= 1kN)

|	
K_w (kN/mm)	150.0
δ_w (mm)	0.0067
δ_{slip} (mm)	0.0027
δ_{slip} / δ_w	0.41
τ_{max} (MPa)	0.089
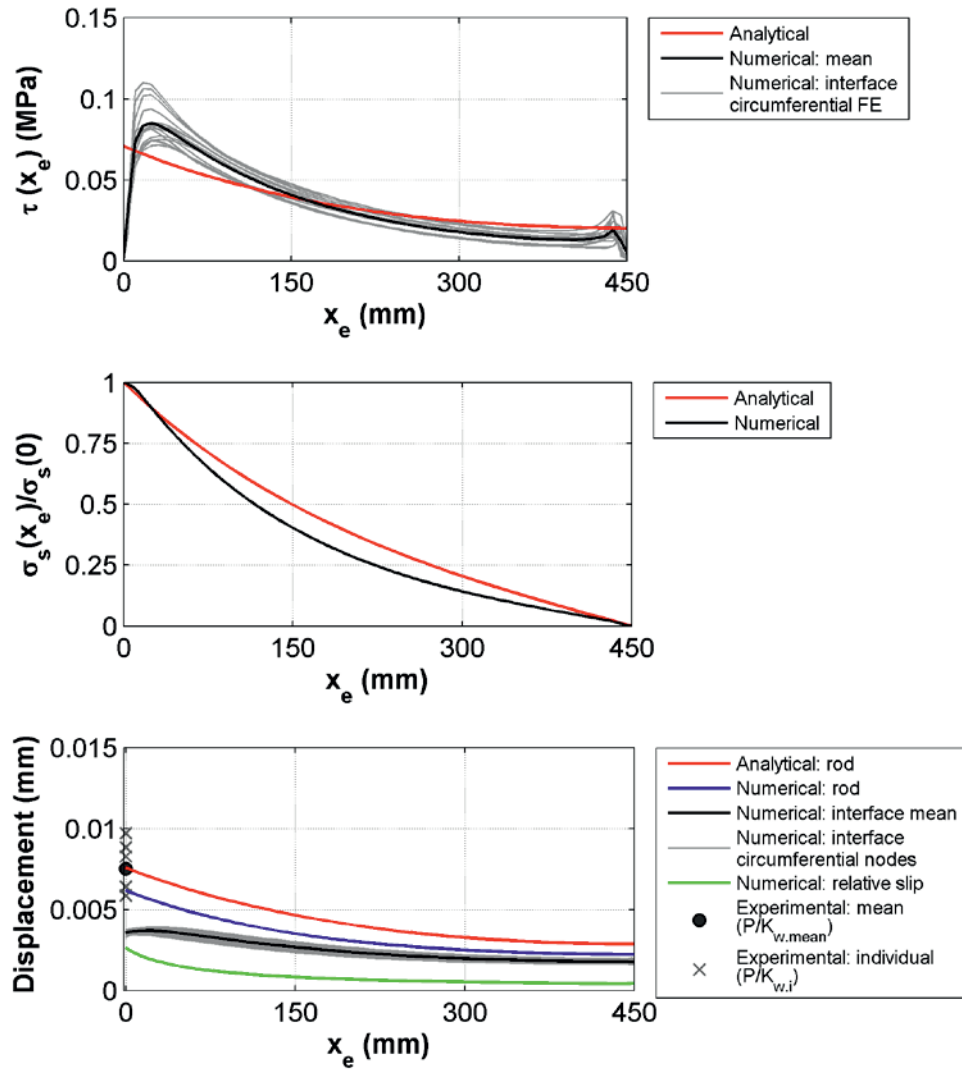
Figure C.8: Lengthwise distributions of $\tau(x_e)$, $\sigma_s(x_e)$ and displacements for S10-450
(P= 1kN)

Table C.9: Numerical results for S10-450 (P= 1kN)

|	
K_w (kN/mm)	161.9
δ_w (mm)	0.0062
δ_{slip} (mm)	0.0026
δ_{slip} / δ_w	0.42
τ_{max} (MPa)	0.085
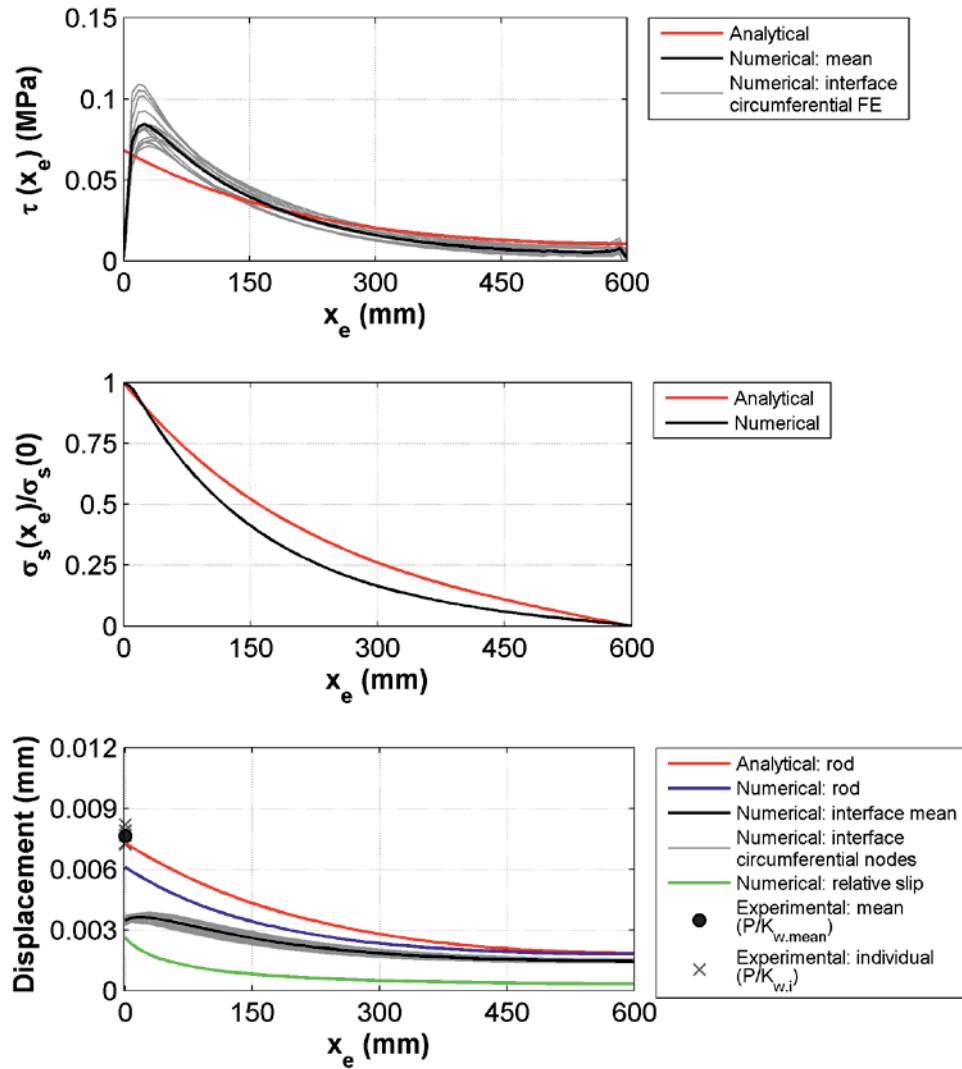
Figure C.9: Lengthwise distributions of $\tau(x_e)$, $\sigma_s(x_e)$ and displacements for S10-600 (P= 1kN)

Table C.10: Numerical results for S10-600 (P= 1kN)

| K_w (kN/mm)	164.5
δ_w (mm)	0.0061
δ_{slip} (mm)	0.0026
δ_{slip} / δ_w	0.43
τ_{max} (MPa)	0.084
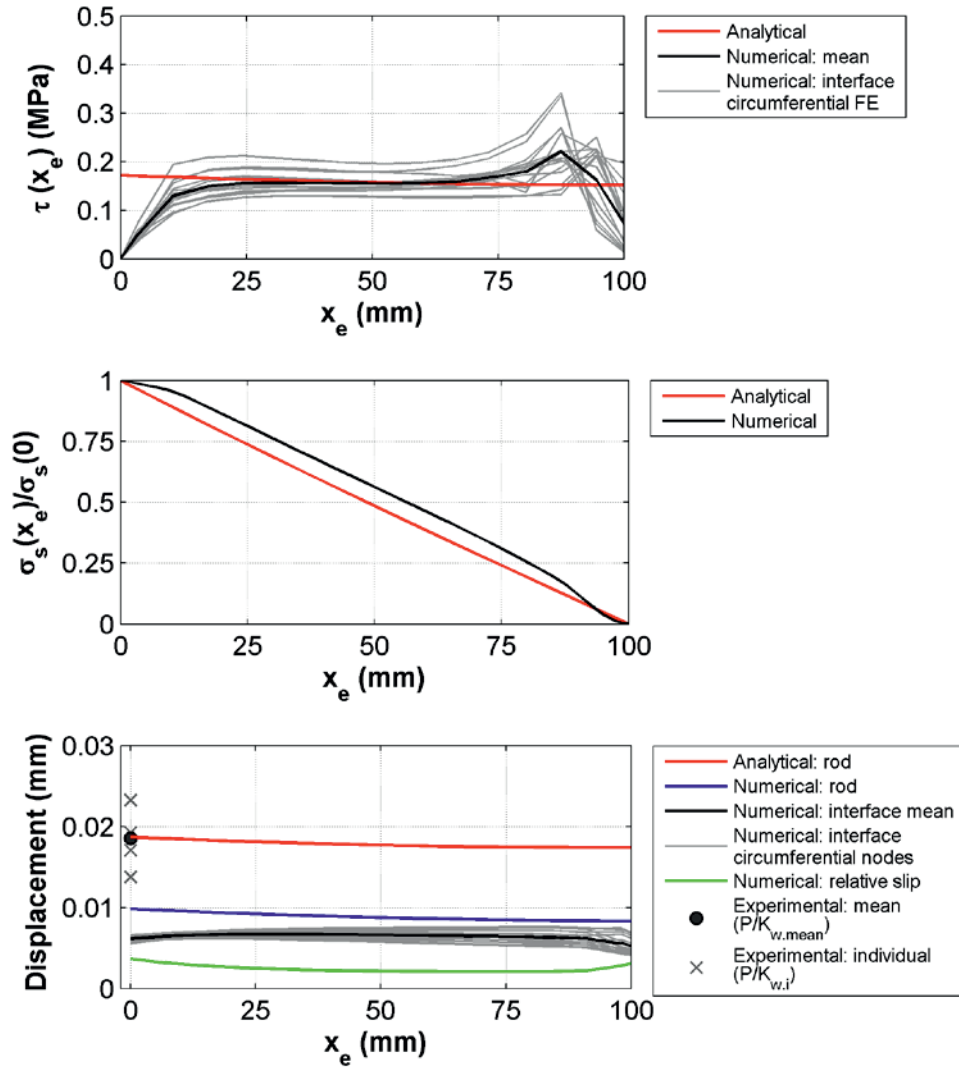
Figure C.10: Lengthwise distributions of $\tau(x_e)$, $\sigma_s(x_e)$ and displacements for S20-100 (P= 1kN)

Table C.11: Numerical results for S20-100 (P= 1kN)

K_w (kN/mm)	101.8
δ_w (mm)	0.0098
δ_{slip} (mm)	0.0037
δ_{slip} / δ_w	0.37
τ_{max} (MPa)	0.221

S20-300 series
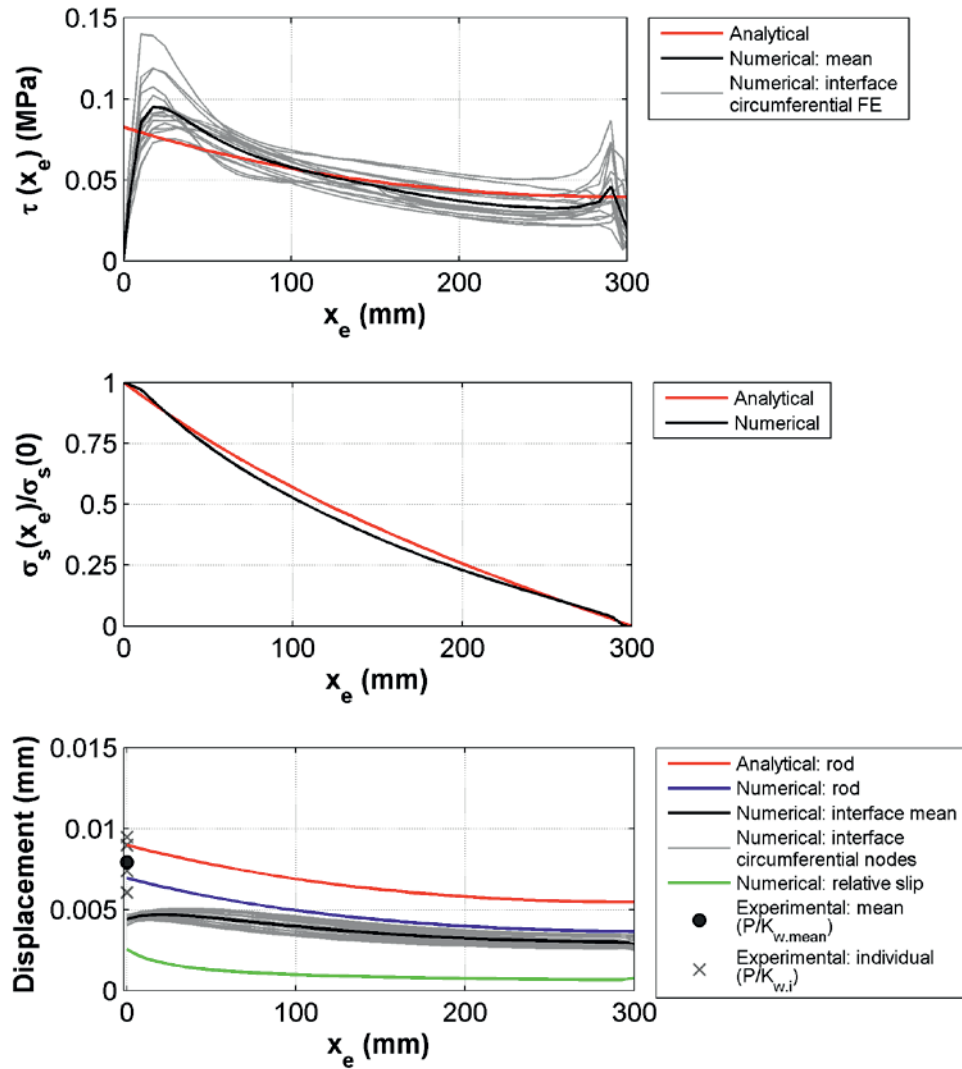
Figure C.11: Lengthwise distributions of $\tau(x_e)$, $\sigma_s(x_e)$ and displacements for S20-300 (P= 1kN)

Table C.12: Numerical results for S20-300 (P= 1kN)

|	
K_w (kN/mm)	144.4
δ_w (mm)	0.0069
δ_{slip} (mm)	0.0025
δ_{slip} / δ_w	0.37
τ_{max} (MPa)	0.095

S20-450 series
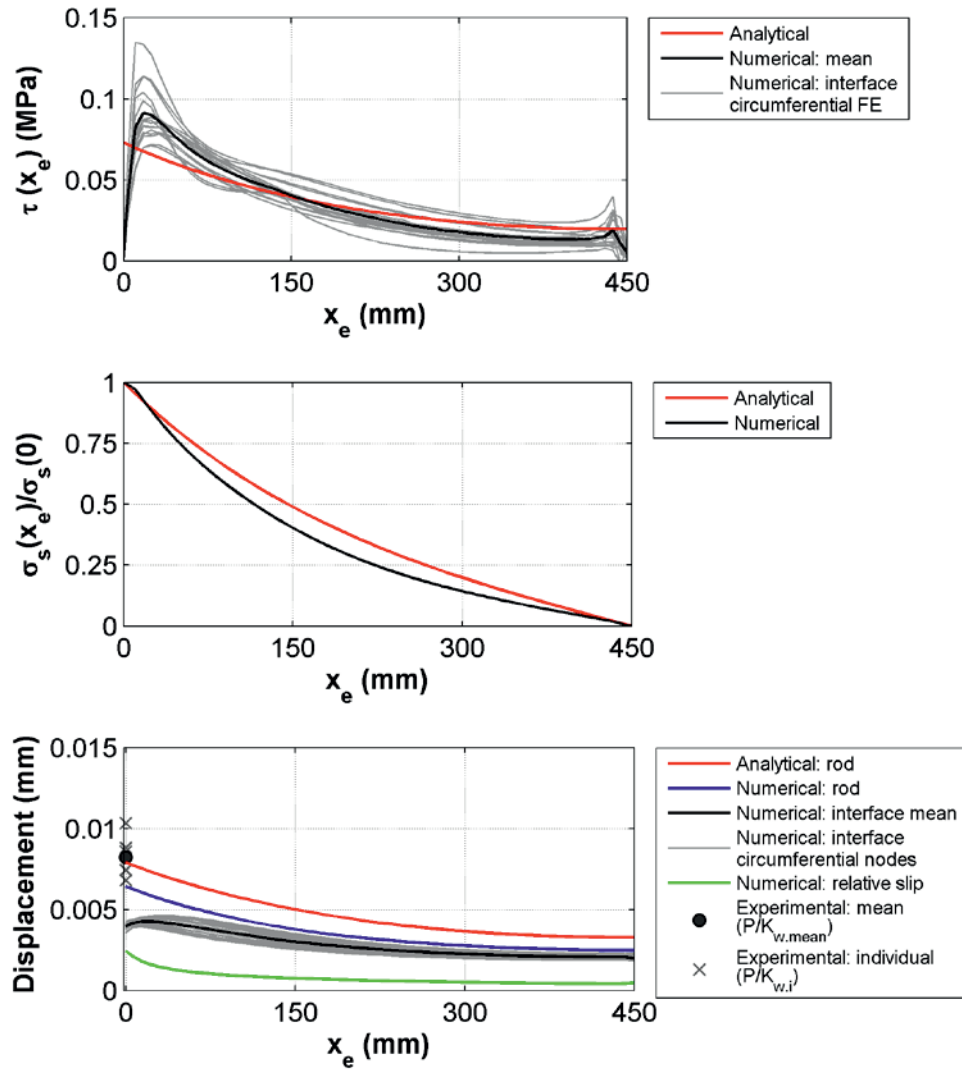
Figure C.12: Lengthwise distributions of $\tau(x_e)$, $\sigma_s(x_e)$ and displacements for S20-450 ($P=$ 1kN)

Table C.13: Numerical results for S20-450 ($P=$ 1kN)

| K_w (kN/mm)	155.9
δ_w (mm)	0.0064
δ_{slip} (mm)	0.0024
δ_{slip} / δ_w	0.38
τ_{max} (MPa)	0.091

S20-600 series
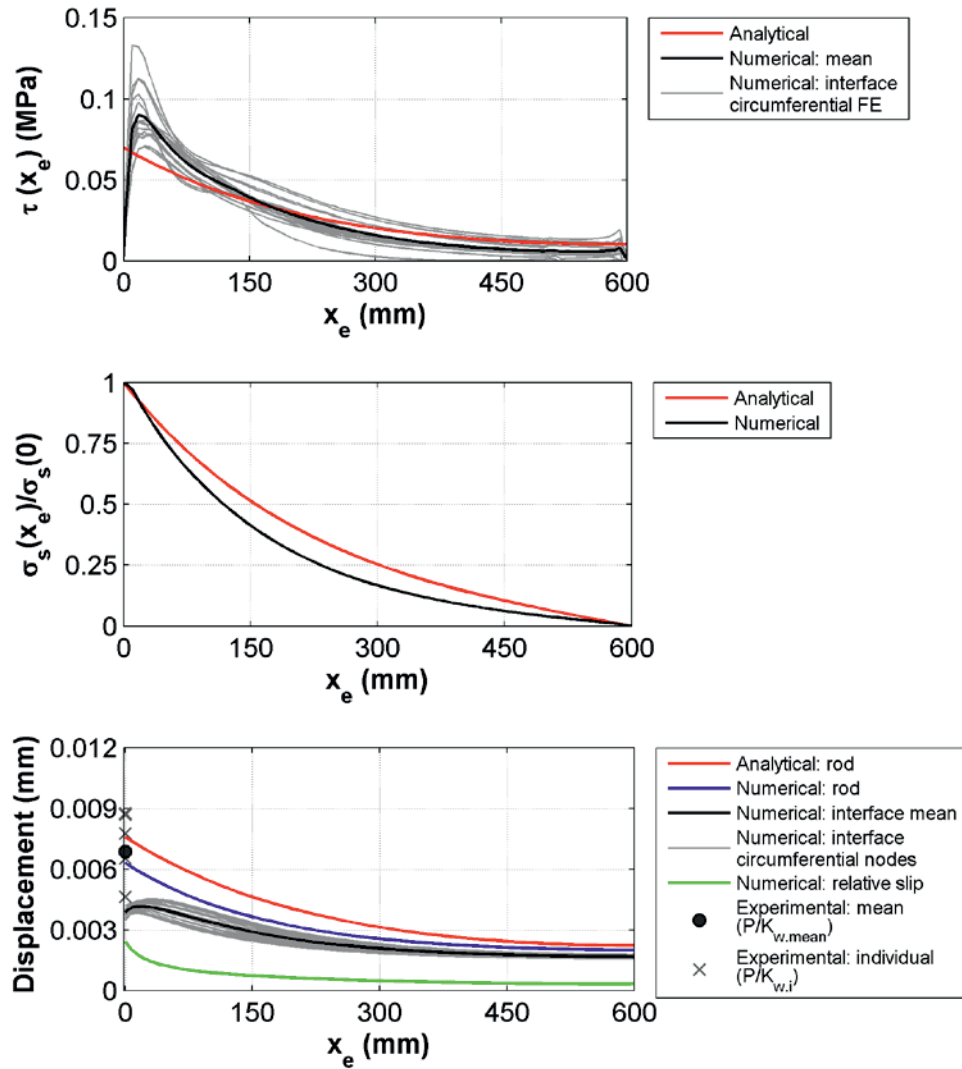
Figure C.13: Lengthwise distributions of $\tau(x_e)$, $\sigma_s(x_e)$ and displacements for S20-600 (P= 1kN)

Table C.14: Numerical results for S20-600 (P= 1kN)

|	
K_w (kN/mm)	159.0
δ_w (mm)	0.0063
δ_{slip} (mm)	0.0024
δ_{slip} / δ_w	0.38
τ_{max} (MPa)	0.090
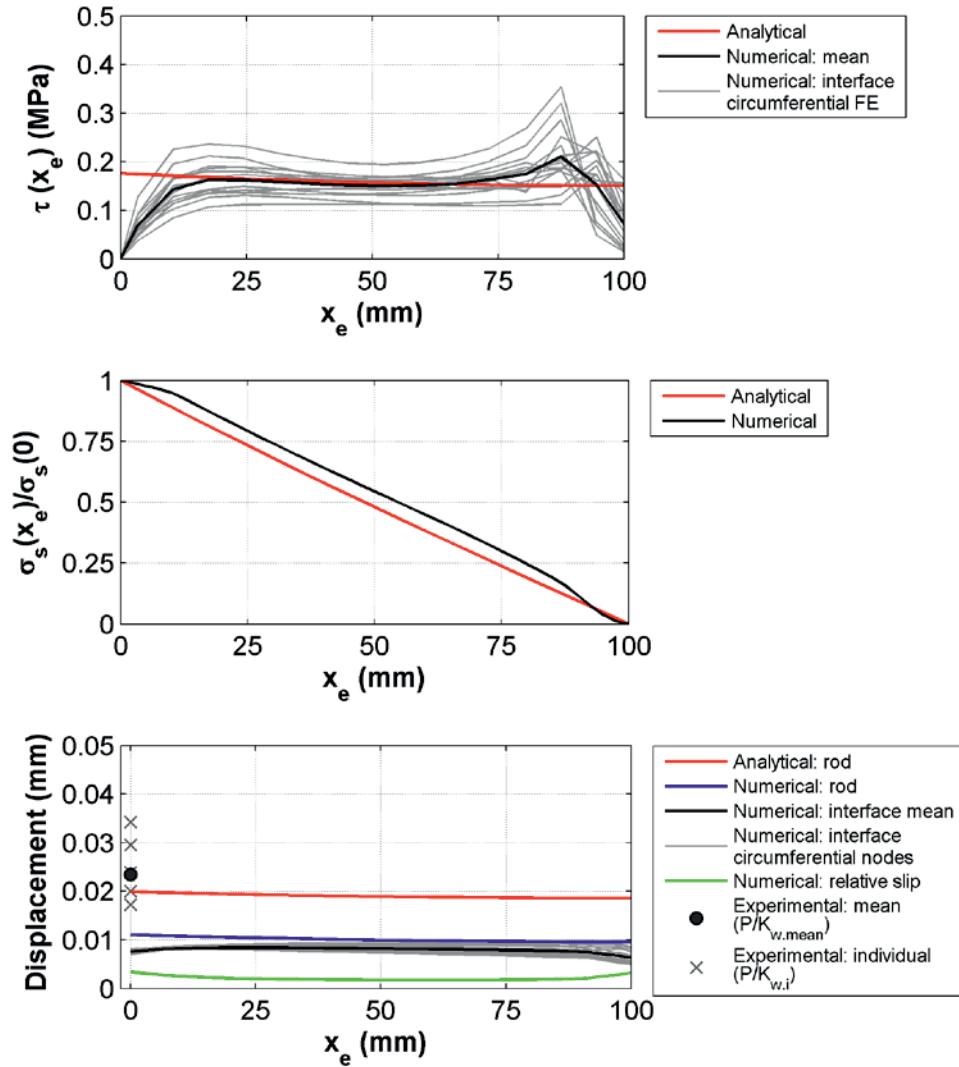
Figure C.14: Lengthwise distributions of $\tau(x_e)$, $\sigma_s(x_e)$ and displacements for S30-100 (P= 1kN)

Table C.15: Numerical results for S30-100 (P= 1kN)

|	
K_w (kN/mm)	90.8
δ_w (mm)	0.011
δ_{slip} (mm)	0.0034
δ_{slip} / δ_w	0.31
τ_{max} (MPa)	0.211
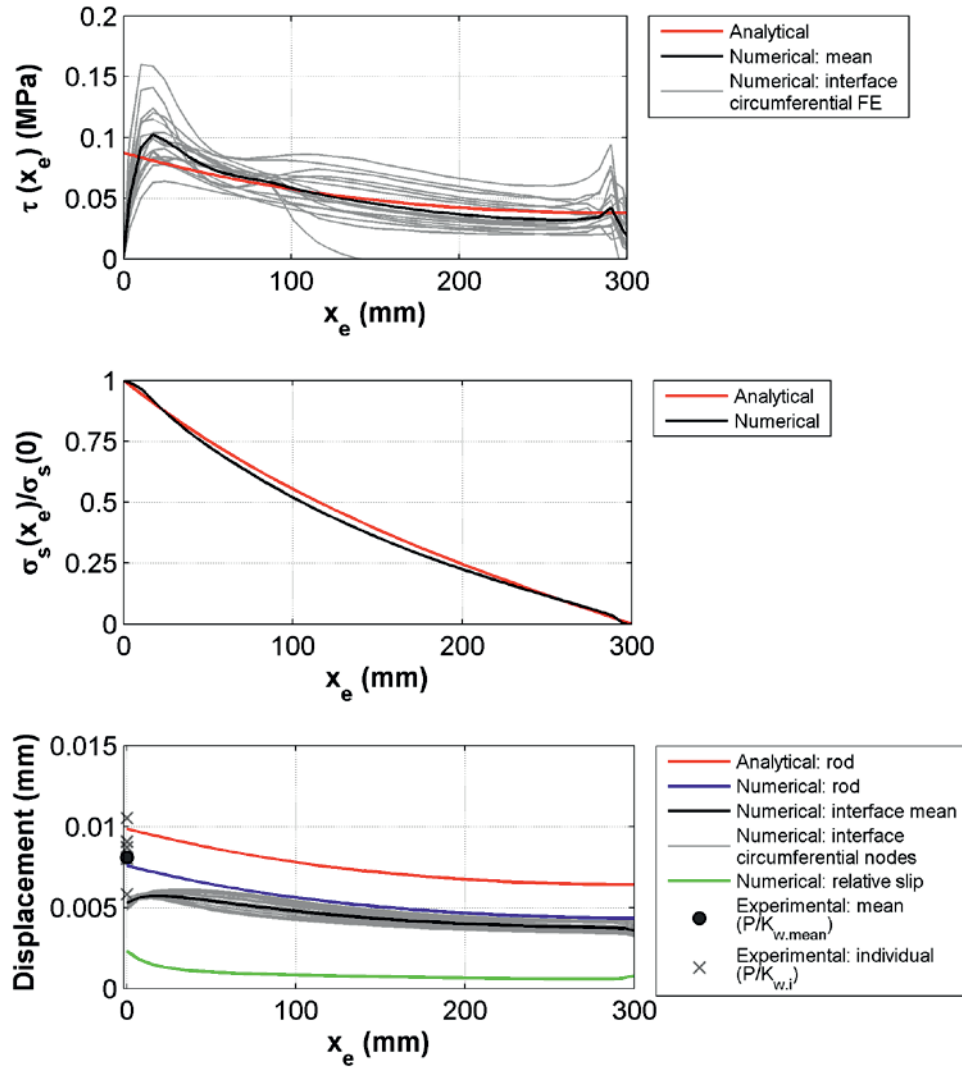
Figure C.15: Lengthwise distributions of $\tau(x_e)$, $\sigma_s(x_e)$ and displacements for S30-300 (P= 1kN)

Table C.16: Numerical results for S30-300 (P= 1kN)

K_w (kN/mm)	131.9
δ_w (mm)	0.0076
δ_{slip} (mm)	0.0023
δ_{slip} / δ_w	0.30
τ_{max} (MPa)	0.102
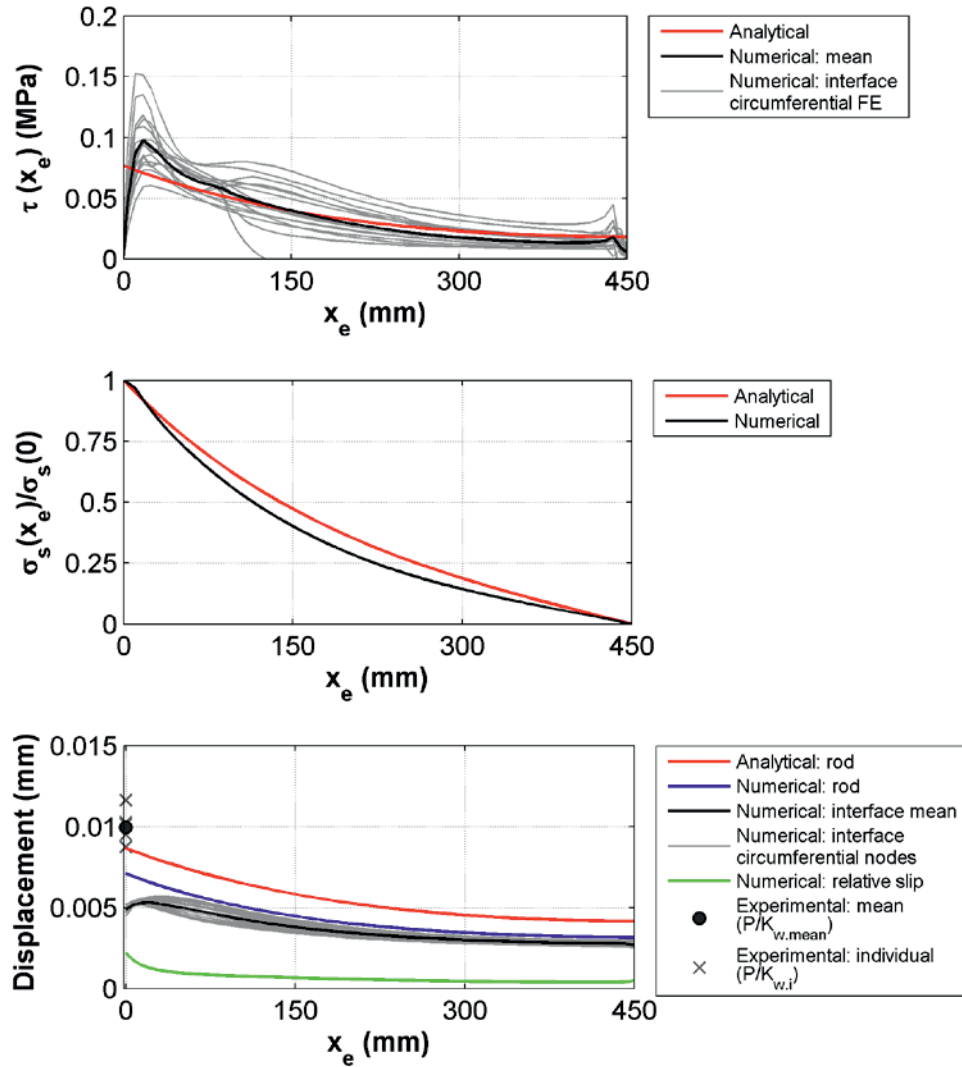
Figure C.16: Lengthwise distributions of $\tau(x_e)$, $\sigma_s(x_e)$ and displacements for S30-450 (P= 1kN)

Table C.17: Numerical results for S30-450 (P= 1kN)

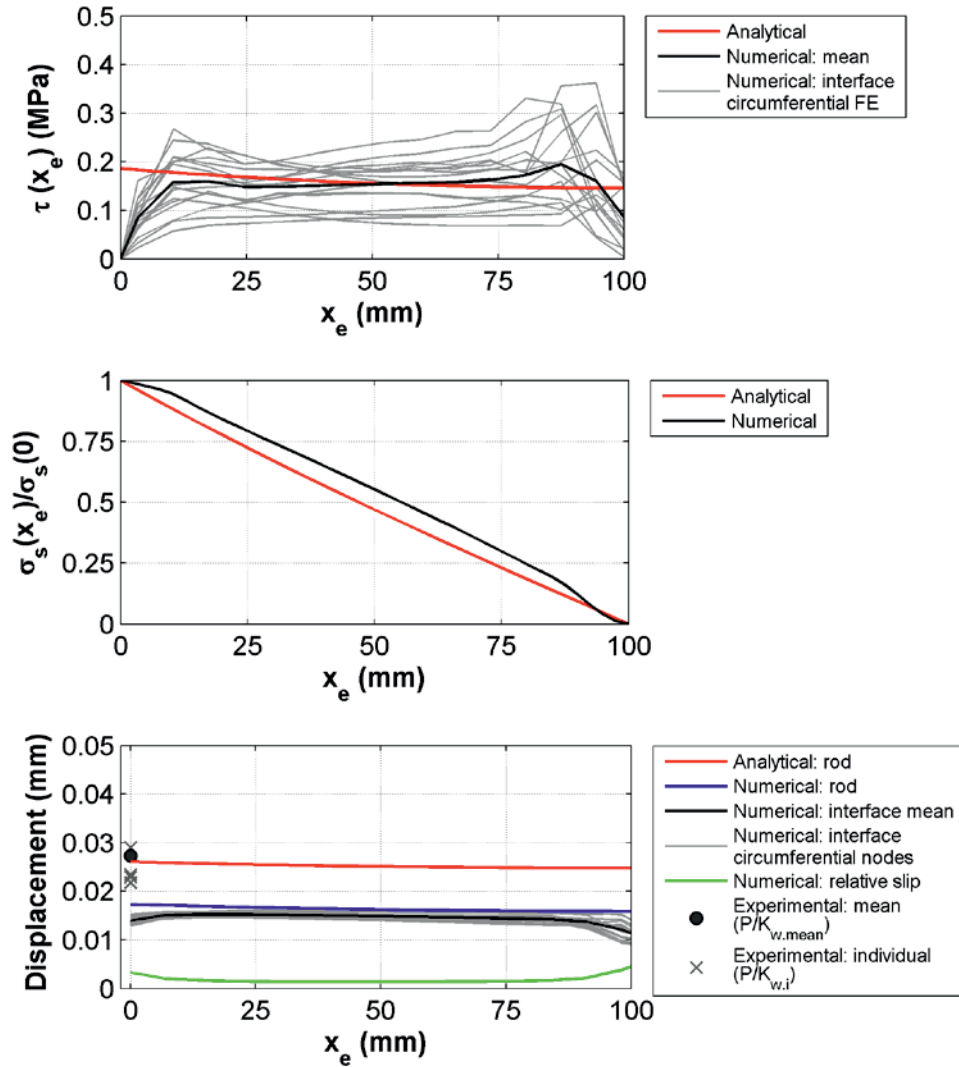|	
K_w (kN/mm)	141.1
δ_w (mm)	0.0071
δ_{slip} (mm)	0.0022
δ_{slip} / δ_w	0.31
τ_{max} (MPa)	0.098

S30-600 series
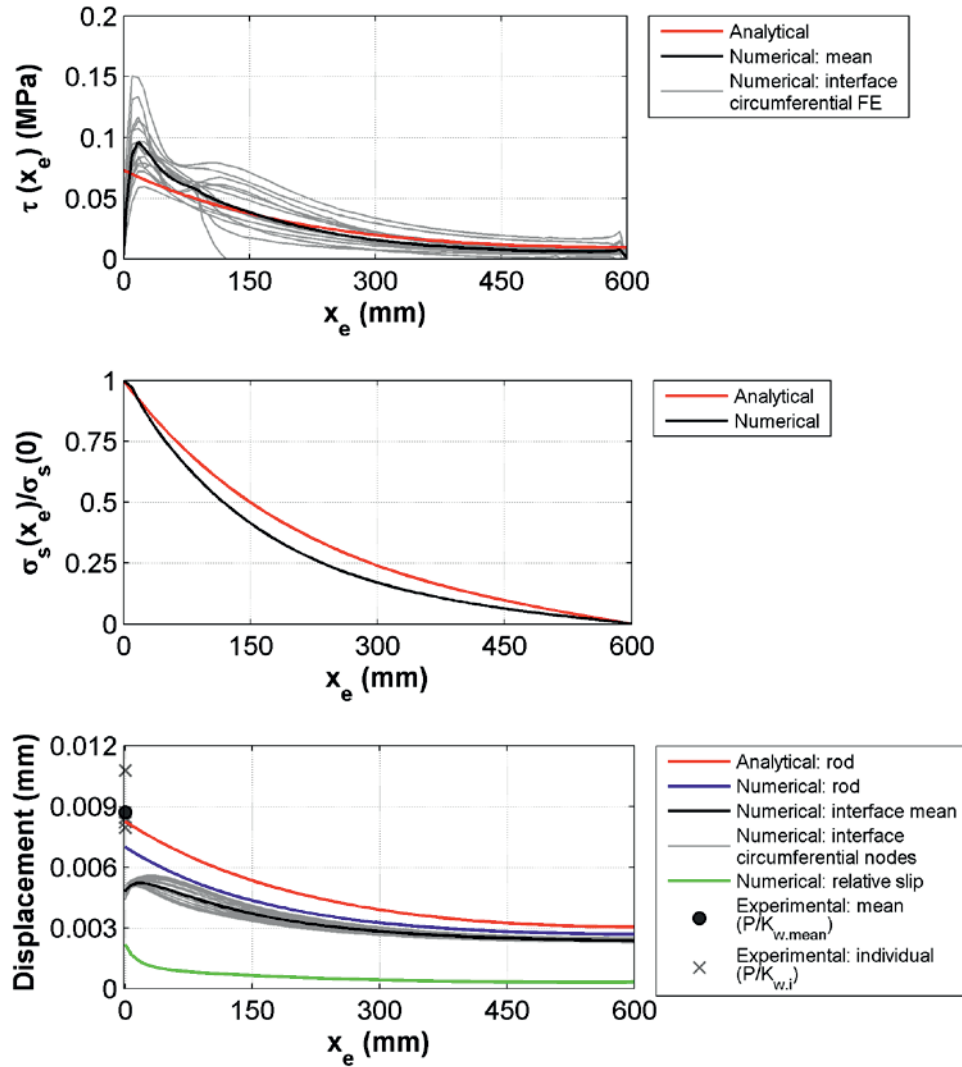
Figure C.17: Lengthwise distributions of $\tau(x_e)$, $\sigma_s(x_e)$ and displacements for S30-600 (P= 1kN)

Table C.18: Numerical results for S30-600 (P= 1kN)

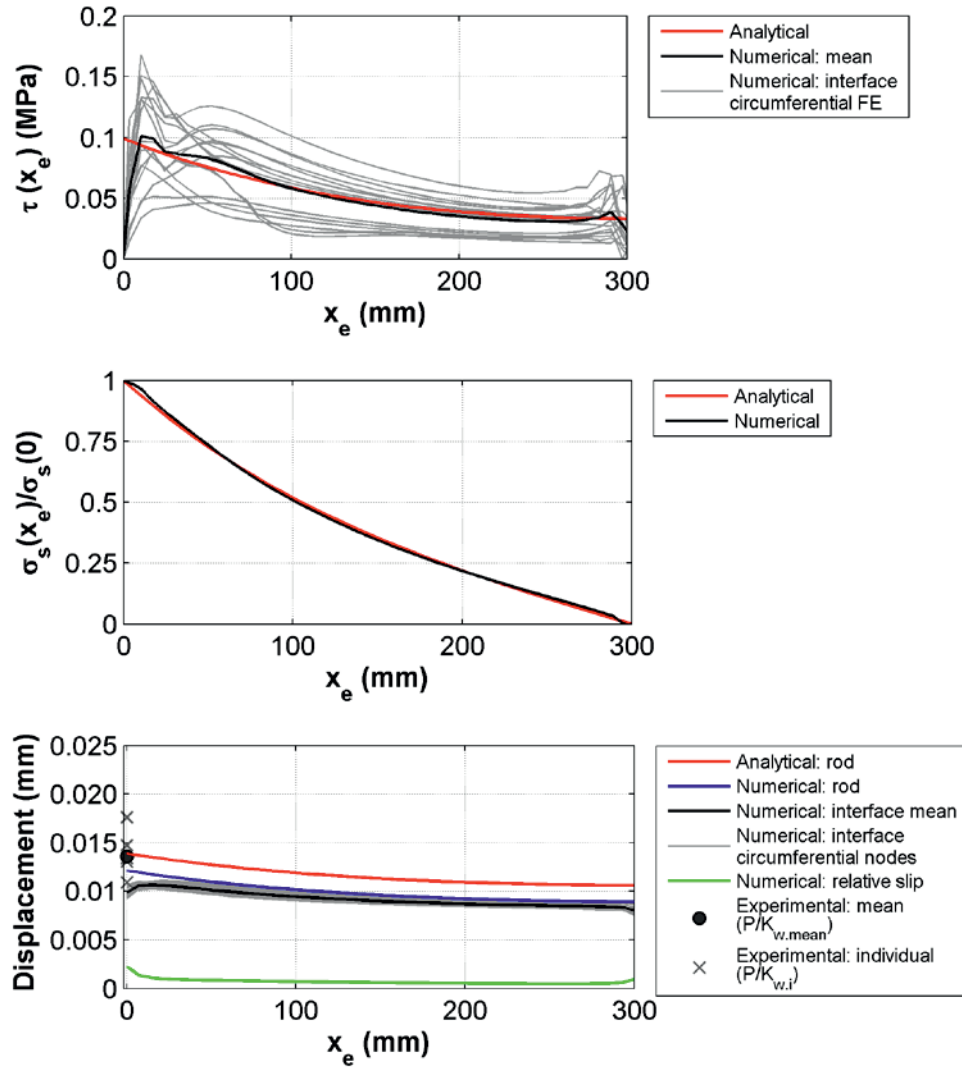|	
K_w (kN/mm)	143.3
δ_w (mm)	0.0070
δ_{slip} (mm)	0.0022
δ_{slip} / δ_w	0.31
τ_{max} (MPa)	0.096

S60-100 series

Figure C.18: Lengthwise distributions of $\tau(x_e)$, $\sigma_s(x_e)$ and displacements for S60-100 (P= 1kN)

Table C.19: Numerical results for S60-100 (P= 1kN)

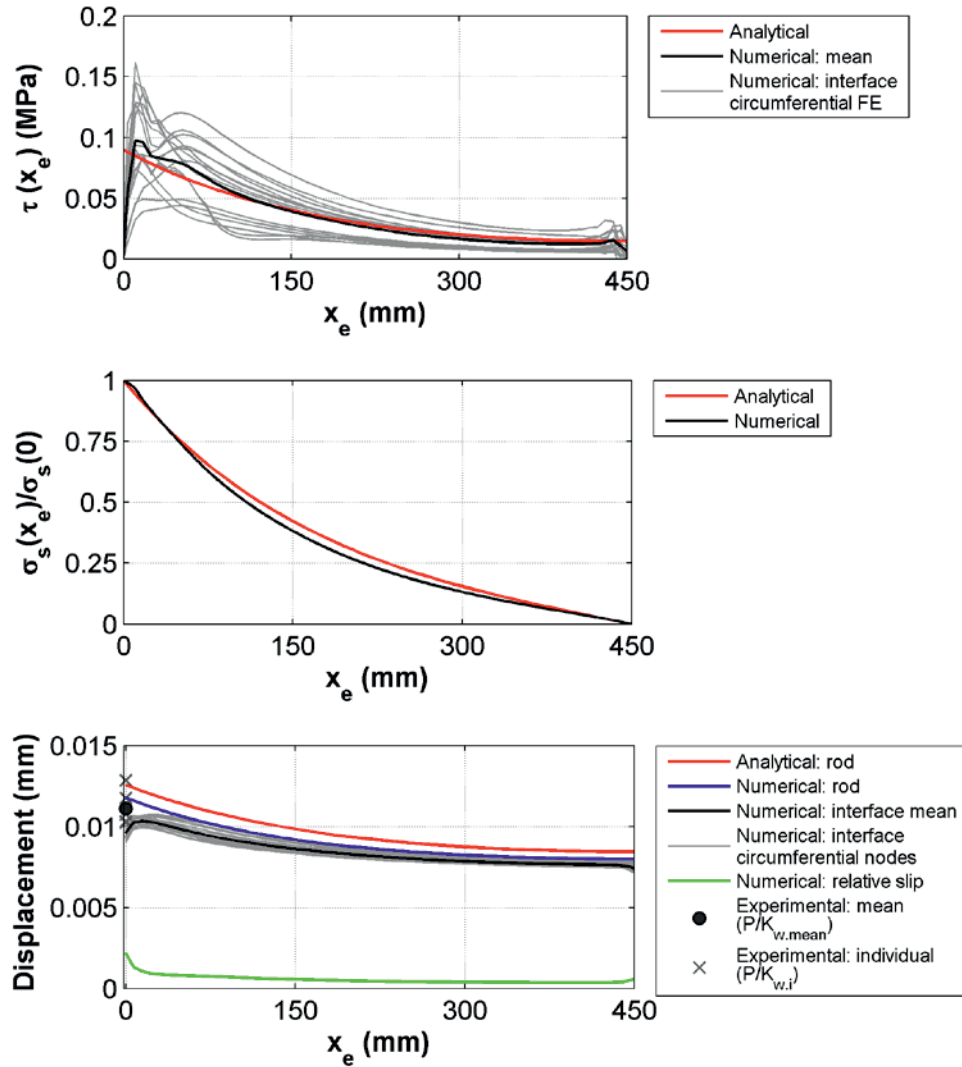|	
K_w (kN/mm)	57.8
δ_w (mm)	0.0173
δ_{slip} (mm)	0.0033
δ_{slip} / δ_w	0.19
τ_{max} (MPa)	0.195

Figure C.19: Lengthwise distributions of $\tau(x_e)$, $\sigma_s(x_e)$ and displacements for S60-300 (P= 1kN)

Table C.20: Numerical results for S60-300 (P= 1kN)

K_w (kN/mm)	82.5
δ_w (mm)	0.0121
δ_{slip} (mm)	0.0022
δ_{slip} / δ_w	0.18
τ_{max} (MPa)	0.101

Figure C.20: Lengthwise distributions of $\tau(x_e)$, $\sigma_s(x_e)$ and displacements for S60-450 (P= 1kN)

Table C.21: Numerical results for S60-450 (P= 1kN)

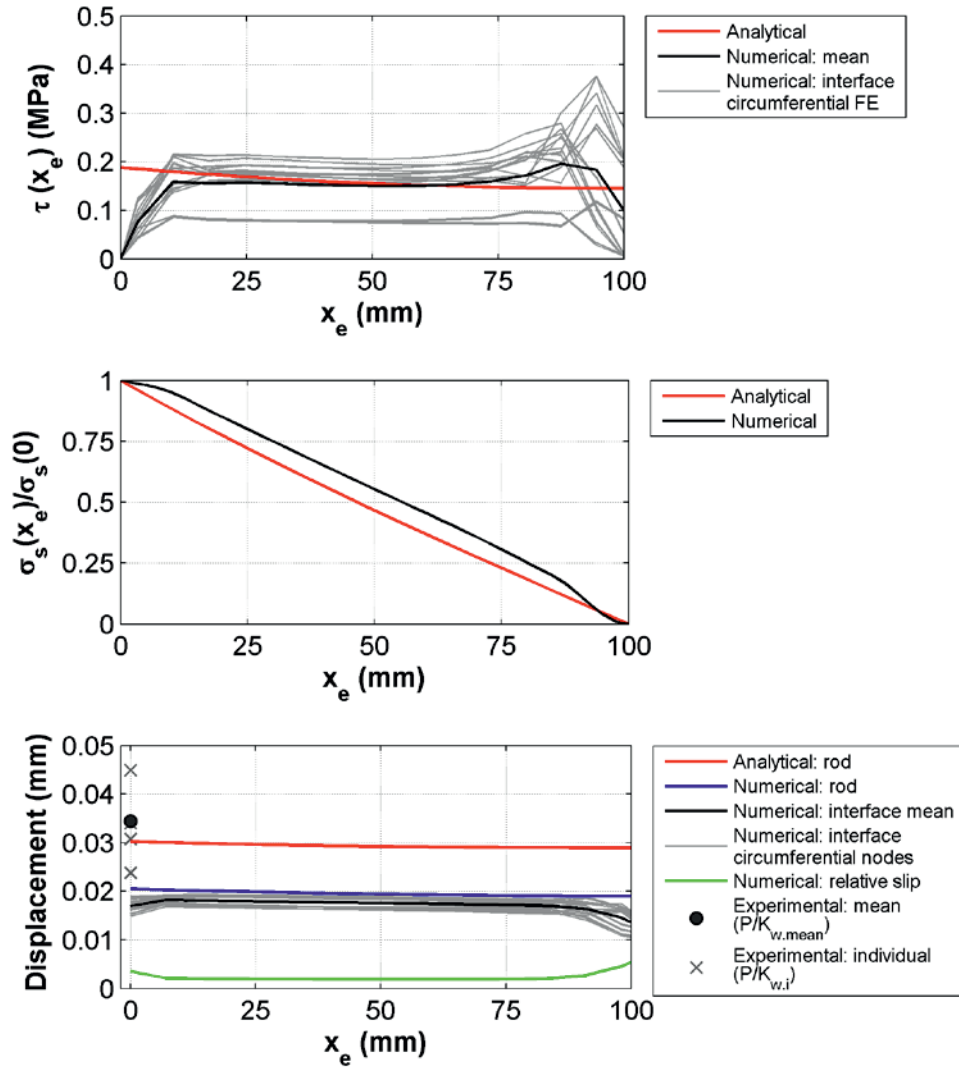|	
K_w (kN/mm)	85.0
δ_w (mm)	0.012
δ_{slip} (mm)	0.0022
δ_{slip} / δ_w	0.18
τ_{max} (MPa)	0.097

Figure C.21: Lengthwise distributions of $\tau(x_e)$, $\sigma_s(x_e)$ and displacements for S90-100 (P= 1kN)

Table C.22: Numerical results for S90-100 (P= 1kN)

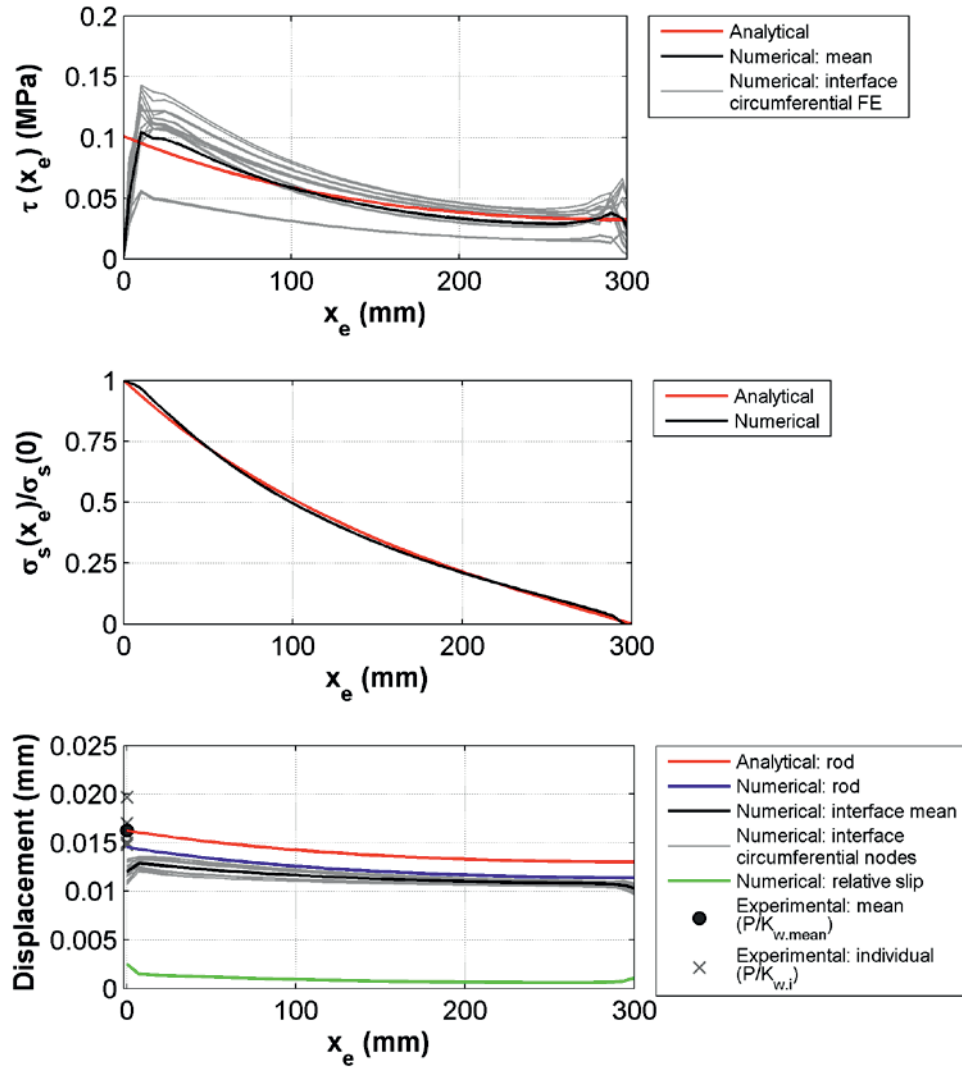|	
K_w (kN/mm)	48.8
δ_w (mm)	0.0205
δ_{slip} (mm)	0.0035
δ_{slip} / δ_w	0.17
τ_{max} (MPa)	0.196

Figure C.22: Lengthwise distributions of $\tau(x_e)$, $\sigma_s(x_e)$ and displacements for S90-300 (P= 1kN)

Table C.23: Numerical results for S90-300 (P= 1kN)

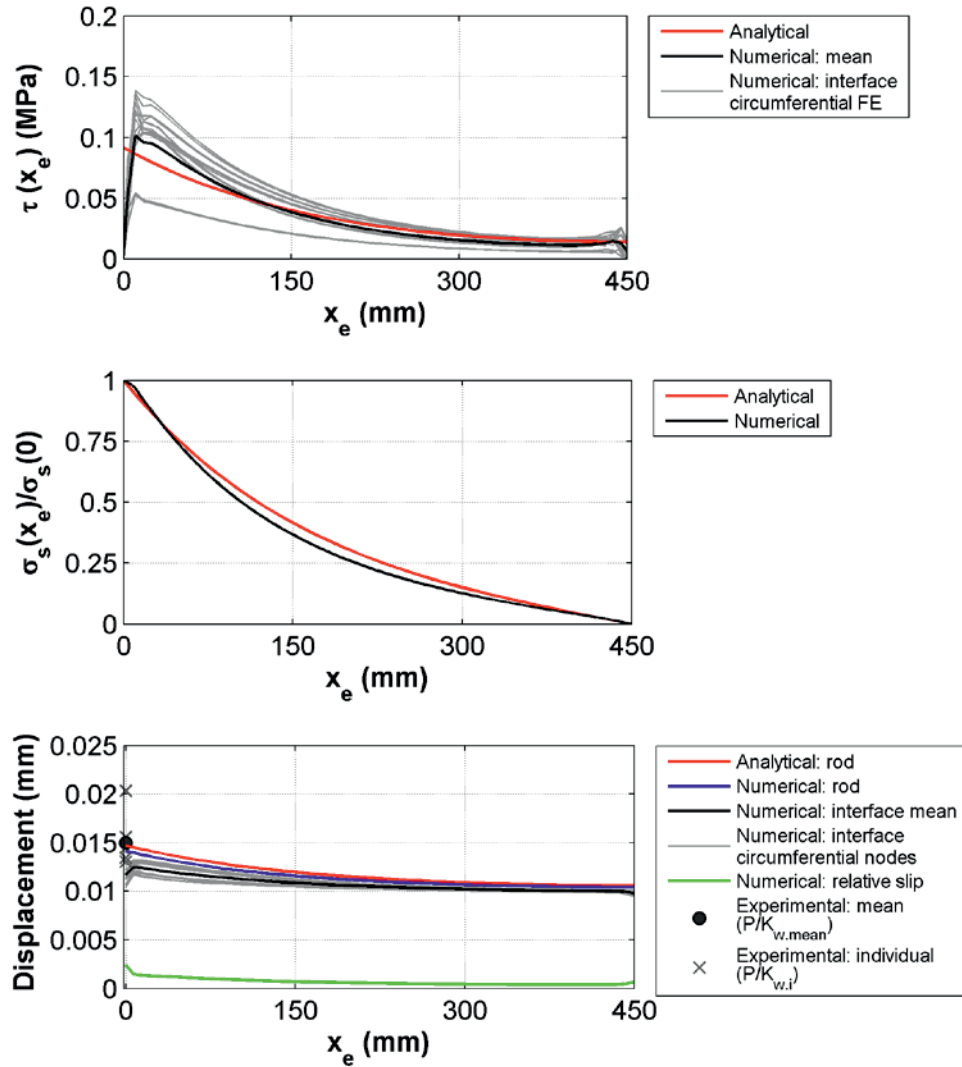|	
K_w (kN/mm)	68.9
δ_w (mm)	0.0145
δ_{slip} (mm)	0.0025
δ_{slip} / δ_w	0.17
τ_{max} (MPa)	0.105

S90-450 series

Figure C.23: Lengthwise distributions of $\tau(x_e)$, $\sigma_s(x_e)$ and displacements for S90-450 (P= 1kN)

Table C.24: Numerical results for S90-450 (P= 1kN)

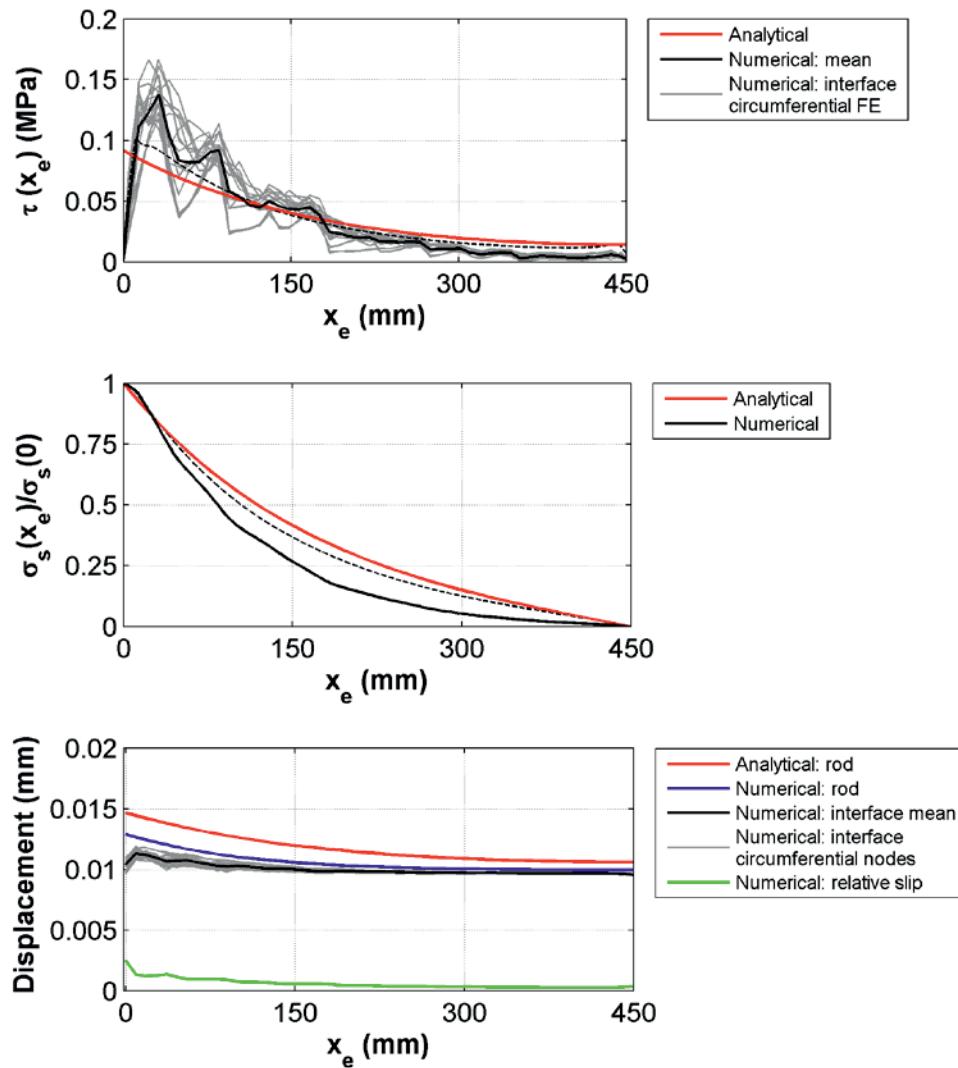| K_w (kN/mm)	70.8
δ_w (mm)	0.0141
δ_{slip} (mm)	0.0024
δ_{slip} / δ_w	0.17
τ_{max} (MPa)	0.101

S90-450-2 (wood modelled as orthotropic)

Figure C.24: Lengthwise distributions of $\tau(x_e)$, $\sigma_s(x_e)$ and displacements for S90-450-2 (P= 1kN) – dashed lines correspond to the transverse isotropy solution

Table C.25: Numerical results for S90-450-2 (P= 1kN)

K_w (kN/mm)	77.6
δ_w (mm)	0.0129
δ_{slip} (mm)	0.0025
δ_{slip} / δ_w	0.19
τ_{max} (MPa)	0.138

"Reliability Analysis of Structural Systems using Nonlinear Finite Element Methods",
C. A. Holm, 1990:23, ISBN 82-7119-178-0.

"Uniform Stratified Flow Interaction with a Submerged Horizontal Cylinder",
Ø. Arntsen, 1990:32, ISBN 82-7119-188-8.

"Large Displacement Analysis of Flexible and Rigid Systems Considering Displacement-Dependent Loads and Nonlinear Constraints",
K. M. Mathisen, 1990:33, ISBN 82-7119-189-6.

"Solid Mechanics and Material Models including Large Deformations",
E. Levold, 1990:56, ISBN 82-7119-214-0, ISSN 0802-3271.

"Inelastic Deformation Capacity of Flexurally-Loaded Aluminium Alloy Structures",
T. Welo, 1990:62, ISBN 82-7119-220-5, ISSN 0802-3271.

"Visualization of Results from Mechanical Engineering Analysis",
K. Aamnes, 1990:63, ISBN 82-7119-221-3, ISSN 0802-3271.

"Object-Oriented Product Modeling for Structural Design",
S. I. Dale, 1991:6, ISBN 82-7119-258-2, ISSN 0802-3271.

"Parallel Techniques for Solving Finite Element Problems on Transputer Networks",
T. H. Hansen, 1991:19, ISBN 82-7119-273-6, ISSN 0802-3271.

"Statistical Description and Estimation of Ocean Drift Ice Environments",
R. Korsnes, 1991:24, ISBN 82-7119-278-7, ISSN 0802-3271.

"Properties of concrete related to fatigue damage: with emphasis on high strength concrete",
G. Petkovic, 1991:35, ISBN 82-7119-290-6, ISSN 0802-3271.

"Turbidity Current Modelling",
B. Brørs, 1991:38, ISBN 82-7119-293-0, ISSN 0802-3271.

"Zero-Slump Concrete: Rheology, Degree of Compaction and Strength. Effects of Fillers as Part Cement-Replacement",
C. Sørensen, 1992:8, ISBN 82-7119-357-0, ISSN 0802-3271.

"Nonlinear Analysis of Reinforced Concrete Structures Exposed to Transient Loading",
K. V. Høiseth, 1992:15, ISBN 82-7119-364-3, ISSN 0802-3271.

"Finite Element Formulations and Solution Algorithms for Buckling and Collapse Analysis of Thin Shells",
R. O. Bjærum, 1992:30, ISBN 82-7119-380-5, ISSN 0802-3271.

"Response Statistics of Nonlinear Dynamic Systems",
J. M. Johnsen, 1992:42, ISBN 82-7119-393-7, ISSN 0802-3271.

"Digital Models in Engineering. A Study on why and how engineers build and operate digital models for decisison support",
J. Høyte, 1992:75, ISBN 82-7119-429-1, ISSN 0802-3271.

"Sparse Solution of Finite Element Equations",
A. C. Damhaug, 1992:76, ISBN 82-7119-430-5, ISSN 0802-3271.

"Some Aspects of Floating Ice Related to Sea Surface Operations in the Barents Sea",
S. Løset, 1992:95, ISBN 82-7119-452-6, ISSN 0802-3271.

"Modelling of Cyclic Plasticity with Application to Steel and Aluminium Structures",
O. S. Hopperstad, 1993:7, ISBN 82-7119-461-5, ISSN 0802-3271.

"The Free Formulation: Linear Theory and Extensions with Applications to Tetrahedral Elements
with Rotational Freedoms",
G. Skeie, 1993:17, ISBN 82-7119-472-0, ISSN 0802-3271.

"Høyfast betongs motstand mot piggdekkslitasje. Analyse av resultater fra prøving i Veisliter'n",
T. Tveter, 1993:62, ISBN 82-7119-522-0, ISSN 0802-3271.

"A Nonlinear Finite Element Based on Free Formulation Theory for Analysis of Sandwich Structures",
O. Aamlid, 1993:72, ISBN 82-7119-534-4, ISSN 0802-3271.

"The Effect of Curing Temperature and Silica Fume on Chloride Migration and Pore Structure of High Strength Concrete",
C. J. Hauck, 1993:90, ISBN 82-7119-553-0, ISSN 0802-3271.

"Failure of Concrete under Compressive Strain Gradients",
G. Markeset, 1993:110, ISBN 82-7119-575-1, ISSN 0802-3271.

"An experimental study of internal tidal amphidromes in Vestfjorden",
J. H. Nilsen, 1994:39, ISBN 82-7119-640-5, ISSN 0802-3271.

"Structural analysis of oil wells with emphasis on conductor design",
H. Larsen, 1994:46, ISBN 82-7119-648-0, ISSN 0802-3271.

"Adaptive methods for non-linear finite element analysis of shell structures",
K. M. Okstad, 1994:66, ISBN 82-7119-670-7, ISSN 0802-3271.

"On constitutive modelling in nonlinear analysis of concrete structures",
O. Fyrileiv, 1994:115, ISBN 82-7119-725-8, ISSN 0802-3271.

"Fluctuating wind load and response of a line-like engineering structure with
emphasis on motion-induced wind forces",
J. Bogunovic Jakobsen, 1995:62, ISBN 82-7119-809-2, ISSN 0802-3271.

"An experimental study of beam-columns subjected to combined torsion, bending
and axial actions",
A. Aalberg, 1995:66, ISBN 82-7119-813-0, ISSN 0802-3271.

"Scaling and cracking in unsealed freeze/thaw testing of Portland cement and silica
fume concretes",
S. Jacobsen, 1995:101, ISBN 82-7119-851-3, ISSN 0802-3271.

"Damping of water waves by submerged vegetation. A case study of laminaria
hyperborea",
A. M. Dubi, 1995:108, ISBN 82-7119-859-9, ISSN 0802-3271.

"The dynamics of a slope current in the Barents Sea",
Sheng Li, 1995:109, ISBN 82-7119-860-2, ISSN 0802-3271.

"Modellering av delmaterialenes betydning for betongens konsistens",
Ernst Mørtsell, 1996:12, ISBN 82-7119-894-7, ISSN 0802-3271.

"Bending of thin-walled aluminium extrusions",
Birgit Søvik Opheim, 1996:60, ISBN 82-7119-947-1, ISSN 0802-3271.

"Material modelling of aluminium for crashworthiness analysis",
Torodd Berstad, 1996:89, ISBN 82-7119-980-3, ISSN 0802-3271.

"Estimation of structural parameters from response measurements on submerged
floating tunnels",

Rolf Magne Larssen, 1996:119, ISBN 82-471-0014-2, ISSN 0802-3271.

"Numerical modelling of plain and reinforced concrete by damage mechanics",
Mario A. Polanco-Loria, 1997:20, ISBN 82-471-0049-5, ISSN 0802-3271.

"Nonlinear random vibrations - numerical analysis by path integration methods",
Vibeke Moe, 1997:26, ISBN 82-471-0056-8, ISSN 0802-3271.
 "Numerical prediction of vortex-induced vibration by the finite element method",
Joar Martin Dalheim, 1997:63, ISBN 82-471-0096-7, ISSN 0802-3271.

"Time domain calculations of buffeting response for wind sensitive structures",
Ketil Aas-Jakobsen, 1997:148, ISBN 82-471-0189-0, ISSN 0802-3271.

"A numerical study of flow about fixed and flexibly mounted circular cylinders",
Trond Stokka Meling, 1998:48, ISBN 82-471-0244-7, ISSN 0802-3271.

"Estimation of chloride penetration into concrete bridges in coastal areas",
Per Egil Steen, 1998:89, ISBN 82-471-0290-0, ISSN 0802-3271.

"Stress-resultant material models for reinforced concrete plates and shells",
Jan Arve Øverli, 1998:95, ISBN 82-471-0297-8, ISSN 0802-3271.

"Chloride binding in concrete. Effect of surrounding environment and concrete
composition",
Claus Kenneth Larsen, 1998:101, ISBN 82-471-0337-0, ISSN 0802-3271.

"Rotational capacity of aluminium alloy beams",
Lars A. Moen, 1999:1, ISBN 82-471-0365-6, ISSN 0802-3271.

"Stretch Bending of Aluminium Extrusions",
Arild H. Clausen, 1999:29, ISBN 82-471-0396-6, ISSN 0802-3271.

"Aluminium and Steel Beams under Concentrated Loading",
Tore Tryland, 1999:30, ISBN 82-471-0397-4, ISSN 0802-3271.

"Engineering Models of Elastoplasticity and Fracture for Aluminium Alloys",
Odd-Geir Lademo, 1999:39, ISBN 82-471-0406-7, ISSN 0802-3271.

"Kapasitet og duktilitet av dybelforbindelser i trekonstruksjoner",
Jan Siem, 1999:46, ISBN 82-471-0414-8, ISSN 0802-3271.

"Etablering av distribuert ingeniørarbeid; Teknologiske og organisatoriske
erfaringer fra en norsk ingeniørbedrift",
Lars Line, 1999:52, ISBN 82-471-0420-2, ISSN 0802-3271.

"Estimation of Earthquake-Induced Response",
Símon Ólafsson, 1999:73, ISBN 82-471-0443-1, ISSN 0802-3271.

"Coastal Concrete Bridges: Moisture State, Chloride Permeability and Aging Effects"
Ragnhild Holen Relling, 1999:74, ISBN 82-471-0445-8, ISSN 0802-3271.

"Capacity Assessment of Titanium Pipes Subjected to Bending and External Pressure",
Arve Bjørset, 1999:100, ISBN 82-471-0473-3, ISSN 0802-3271.

"Validation of Numerical Collapse Behaviour of Thin-Walled Corrugated Panels",
Håvar Ilstad, 1999:101, ISBN 82-471-0474-1, ISSN 0802-3271.

"Strength and Ductility of Welded Structures in Aluminium Alloys",
Miroslaw Matusiak, 1999:113, ISBN 82-471-0487-3, ISSN 0802-3271.

"Thermal Dilation and Autogenous Deformation as Driving Forces to Self-Induced Stresses in High Performance Concrete",
Øyvind Bjøntegaard, 1999:121, ISBN 82-7984-002-8, ISSN 0802-3271.

"Some Aspects of Ski Base Sliding Friction and Ski Base Structure",
Dag Anders Moldestad, 1999:137, ISBN 82-7984-019-2, ISSN 0802-3271.

"Electrode reactions and corrosion resistance for steel in mortar and concrete",
Roy Antonsen, 2000:10, ISBN 82-7984-030-3, ISSN 0802-3271.

"Hydro-Physical Conditions in Kelp Forests and the Effect on Wave Damping and Dune Erosion. A case study on Laminaria Hyperborea",
Stig Magnar Løvås, 2000:28, ISBN 82-7984-050-8, ISSN 0802-3271.

"Random Vibration and the Path Integral Method",
Christian Skaug, 2000:39, ISBN 82-7984-061-3, ISSN 0802-3271.

"Buckling and geometrical nonlinear beam-type analyses of timber structures",
Trond Even Eggen, 2000:56, ISBN 82-7984-081-8, ISSN 0802-3271.

"Structural Crashworthiness of Aluminium Foam-Based Components",
Arve Grønsund Hanssen, 2000:76, ISBN 82-7984-102-4, ISSN 0809-103X.

"Measurements and simulations of the consolidation in first-year sea ice ridges, and some aspects of mechanical behaviour",
Knut V. Høyland, 2000:94, ISBN 82-7984-121-0, ISSN 0809-103X.

"Kinematics in Regular and Irregular Waves based on a Lagrangian Formulation",
Svein Helge Gjøsund, 2000-86, ISBN 82-7984-112-1, ISSN 0809-103X.

"Self-Induced Cracking Problems in Hardening Concrete Structures",
Daniela Bosnjak, 2000-121, ISBN 82-7984-151-2, ISSN 0809-103X.

"Ballistic Penetration and Perforation of Steel Plates",
Tore Børvik, 2000:124, ISBN 82-7984-154-7, ISSN 0809-103X.

"Freeze-Thaw resistance of Concrete. Effect of: Curing Conditions, Moisture Exchange and Materials",
Terje Finnerup Rønning, 2001:14, ISBN 82-7984-165-2, ISSN 0809-103X

"Structural behaviour of post tensioned concrete structures. Flat slab. Slabs on ground",
Steinar Trygstad, 2001:52, ISBN 82-471-5314-9, ISSN 0809-103X.

"Slipforming of Vertical Concrete Structures. Friction between concrete and slipform panel",
Kjell Tore Fosså, 2001:61, ISBN 82-471-5325-4, ISSN 0809-103X.

"Some numerical methods for the simulation of laminar and turbulent incompressible flows",
Jens Holmen, 2002:6, ISBN 82-471-5396-3, ISSN 0809-103X.

"Improved Fatigue Performance of Threaded Drillstring Connections by Cold Rolling",
Steinar Kristoffersen, 2002:11, ISBN: 82-421-5402-1, ISSN 0809-103X.

"Deformations in Concrete Cantilever Bridges: Observations and Theoretical Modelling",
Peter F. Takâcs, 2002:23, ISBN 82-471-5415-3, ISSN 0809-103X.

"Stiffened aluminium plates subjected to impact loading",
Hilde Giæver Hildrum, 2002:69, ISBN 82-471-5467-6, ISSN 0809-103X.

"Full- and model scale study of wind effects on a medium-rise building in a built up area",
Jónas Thór Snæbjørnsson, 2002:95, ISBN82-471-5495-1, ISSN 0809-103X.

"Evaluation of Concepts for Loading of Hydrocarbons in Ice-infested water",
Arnor Jensen, 2002:114, ISBN 82-417-5506-0, ISSN 0809-103X.

"Numerical and Physical Modelling of Oil Spreading in Broken Ice",
Janne K. Økland Gjøsteen, 2002:130, ISBN 82-471-5523-0, ISSN 0809-103X.

"Diagnosis and protection of corroding steel in concrete",
Franz Pruckner, 20002:140, ISBN 82-471-5555-4, ISSN 0809-103X.

"Tensile and Compressive Creep of Young Concrete: Testing and Modelling",
Dawood Atrushi, 2003:17, ISBN 82-471-5565-6, ISSN 0809-103X.

"Rheology of Particle Suspensions. Fresh Concrete, Mortar and Cement Paste with Various Types of Lignosulfonates",
Jon Elvar Wallevik, 2003:18, ISBN 82-471-5566-4, ISSN 0809-103X.

"Oblique Loading of Aluminium Crash Components",
Aase Reyes, 2003:15, ISBN 82-471-5562-1, ISSN 0809-103X.

"Utilization of Ethiopian Natural Pozzolans",
Surafel Ketema Desta, 2003:26, ISSN 82-471-5574-5, ISSN:0809-103X.

"Behaviour and strength prediction of reinforced concrete structures with discontinuity regions", Helge Brå, 2004:11, ISBN 82-471-6222-9, ISSN 1503-8181.

"High-strength steel plates subjected to projectile impact. An experimental and numerical study", Sumita Dey, 2004:38, ISBN 82-471-6282-2 (printed version), ISBN 82-471-6281-4 (electronic version), ISSN 1503-8181.

"Alkali-reactive and inert fillers in concrete. Rheology of fresh mixtures and expansive reactions."
Bård M. Pedersen, 2004:92, ISBN 82-471-6401-9 (printed version), ISBN 82-471-6400-0 (electronic version), ISSN 1503-8181.

"On the Shear Capacity of Steel Girders with Large Web Openings".
Nils Christian Hagen, 2005:9 ISBN 82-471-6878-2 (printed version), ISBN 82-471-6877-4 (electronic version), ISSN 1503-8181.

"Behaviour of aluminium extrusions subjected to axial loading".
Østen Jensen, 2005:7, ISBN 82-471-6873-1 (printed version), ISBN 82-471-6872-3 (electronic version), ISSN 1503-8181.

"Thermal Aspects of corrosion of Steel in Concrete".
Jan-Magnus Østvik, 2005:5, ISBN 82-471-6869-3 (printed version), ISBN 82-471-6868 (electronic version), ISSN 1503-8181.

"Mechanical and adaptive behaviour of bone in relation to hip replacement." A study of bone remodelling and bone grafting.
Sébastien Muller, 2005:34, ISBN 82-471-6933-9 (printed version), ISBN 82-471-6932-0 (electronic version), ISSN 1503-8181.

"Analysis of geometrical nonlinearities with applications to timber structures".
Lars Wollebæk, 2005:74, ISBN 82-471-7050-5 (printed version), ISBN 82-471-7019-1 (electronic version), ISSN 1503-8181.

"Pedestrian induced lateral vibrations of slender footbridges",

Anders Rönnquist, 2005:102, ISBN 82-471-7082-5 (printed version), ISBN 82-471-7081-7 (electronic version), ISSN 1503-8181.

"Initial Strength Development of Fly Ash and Limestone Blended Cements at Various Temperatures Predicted by Ultrasonic Pulse Velocity",
Tom Ivar Fredvik, 2005:112, ISBN 82-471-7105-8 (printed version), ISBN 82-471-7103-1 (electronic version), ISSN 1503-8181.

"Behaviour and modelling of thin-walled cast components",
Cato Dørum, 2005:128, ISBN 82-471-7140-6 (printed version), ISBN 82-471-7139-2 (electronic version), ISSN 1503-8181.

"Behaviour and modelling of selfpiercing riveted connections",
Raffaele Porcaro, 2005:165, ISBN 82-471-7219-4 (printed version), ISBN 82-471-7218-6 (electronic version), ISSN 1503-8181.

"Behaviour and Modelling og Aluminium Plates subjected to Compressive Load",
Lars Rønning, 2005:154, ISBN 82-471-7169-1 (printed version), ISBN 82-471-7195-3 (electronic version), ISSN 1503-8181.

"Bumper beam-longitudinal system subjected to offset impact loading",
Satyanarayana Kokkula, 2005:193, ISBN 82-471-7280-1 (printed version), ISBN 82-471-7279-8 (electronic version), ISSN 1503-8181.

"Control of Chloride Penetration into Concrete Structures at Early Age",
Guofei Liu, 2006:46, ISBN 82-471-7838-9 (printed version), ISBN 82-471-7837-0 (electronic version), ISSN 1503-8181.

"Modelling of Welded Thin-Walled Aluminium Structures",
Ting Wang, 2006:78, ISBN 82-471-7907-5 (printed version), ISBN 82-471-7906-7 (electronic version), ISSN 1503-8181.

"Time-variant reliability of dynamic systems by importance sampling and probabilistic analysis of ice loads",
Anna Ivanova Olsen, 2006:139, ISBN 82-471-8041-3 (printed version), ISBN 82-471-8040-5 (electronic version), ISSN 1503-8181.

"Fatigue life prediction of an aluminium alloy automotive component using finite element analysis of surface topography".
Sigmund Kyrre Ås, 2006:25, ISBN 82-471-7791-9 (printed version), ISBN 82-471-7791-9 (electronic version), ISSN 1503-8181.

"Constitutive models of elastoplasticity and fracture for aluminium alloys under strain path change",
Dasharatha Achani, 2006:76, ISBN 82-471-7903-2 (printed version), ISBN 82-471-7902-4 (electronic version), ISSN 1503-8181.

"Simulations of 2D dynamic brittle fracture by the Element-free Galerkin method and linear fracture mechanics",
Tommy Karlsson, 2006:125, ISBN 82-471-8011-1 (printed version), ISBN 82-471-8010-3 (electronic version), ISSN 1503-8181.

"Penetration and Perforation of Granite Targets by Hard Projectiles",
Chong Chiang Seah, 2006:188, ISBN 82-471-8150-9 (printed version), ISBN 82-471-8149-5 (electronic version), ISSN 1503-8181.

"Deformations, strain capacity and cracking of concrete in plastic and early hardening phases",
Tor Arne Hammer, 2007:234, ISBN 978-82-471-5191-4 (printed version), ISBN 978-82-471-5207-2 (electronic version), ISSN 1503-8181.

"Crashworthiness of dual-phase high-strength steel: Material and Component behaviour", Venkatapathi Tarigopula, 2007:230, ISBN 82-471-5076-4 (printed version), ISBN 82-471-5093-1 (electronic version), ISSN 1503-8181.

"Fibre reinforcement in load carrying concrete structures",
Åse Lyslo Døssland, 2008:50, ISBN 978-82-471-6910-0 (printed version), ISBN 978-82-471-6924-7 (electronic version), ISSN 1503-8181.

"Low-velocity penetration of aluminium plates",
Frode Grytten, 2008:46, ISBN 978-82-471-6826-4 (printed version), ISBN 978-82-471-6843-1 (electronic version), ISSN 1503-8181.

"Robustness studies of structures subjected to large deformations",
Ørjan Fyllingen, 2008:24, ISBN 978-82-471-6339-9 (printed version), ISBN 978-82-471-6342-9 (electronic version), ISSN 1503-8181.

"Constitutive modelling of morsellised bone",
Knut Birger Lunde, 2008:92, ISBN 978-82-471-7829-4 (printed version), ISBN 978-82-471-7832-4 (electronic version), ISSN 1503-8181.

"Experimental Investigations of Wind Loading on a Suspension Bridge Girder",
Bjørn Isaksen, 2008:131, ISBN 978-82-471-8656-5 (printed version), ISBN 978-82-471-8673-2 (electronic version), ISSN 1503-8181.

"Cracking Risk of Concrete Structures in The Hardening Phase",
Guomin Ji, 2008:198, ISBN 978-82-471-1079-9 (printed version), ISBN 978-82-471-1080-5 (electronic version), ISSN 1503-8181.

"Modelling and numerical analysis of the porcine and human mitral apparatus",

Victorien Emile Prot, 2008:249, ISBN 978-82-471-1192-5 (printed version), ISBN 978-82-471-1193-2 (electronic version), ISSN 1503-8181.

"Strength analysis of net structures",
Heidi Moe, 2009:48, ISBN 978-82-471-1468-1 (printed version), ISBN 978-82-471-1469-8 (electronic version), ISSN1503-8181.

"Numerical analysis of ductile fracture in surface cracked shells",
Espen Berg, 2009:80, ISBN 978-82-471-1537-4 (printed version), ISBN 978-82-471-1538-1 (electronic version), ISSN 1503-8181.

"Subject specific finite element analysis of bone – for evaluation of the healing of a leg lengthening and evaluation of femoral stem design",
Sune Hansborg Pettersen, 2009:99, ISBN 978-82-471-1579-4 (printed version), ISBN 978-82-471-1580-0 (electronic version), ISSN 1503-8181.

"Evaluation of fracture parameters for notched multi-layered structures",
Lingyun Shang, 2009:137, ISBN 978-82-471-1662-3 (printed version), ISBN 978-82-471-1663-0 (electronic version), ISSN 1503-8181.

"Modelling of Dynamic Material Behaviour and Fracture of Aluminium Alloys for Structural Applications"
Yan Chen, 2009:69, ISBN 978-82-471-1515-2 (printed version), ISBN 978-82 471-1516-9 (electronic version), ISSN 1503-8181.

"Nanomechanics of polymer and composite particles"
Jianying He 2009:213, ISBN 978-82-471-1828-3 (printed version), ISBN 978-82-471-1829-0 (electronic version), ISSN 1503-8181.

"Mechanical properties of clear wood from Norway spruce"
Kristian Berbom Dahl 2009:250, ISBN 978-82-471-1911-2 (printed version) ISBN 978-82-471-1912-9 (electronic version), ISSN 1503-8181.

"Modeling of the degradation of TiB_2 mechanical properties by residual stresses and liquid Al penetration along grain boundaries"
Micol Pezzotta 2009:254, ISBN 978-82-471-1923-5 (printed version) ISBN 978-82-471-1924-2 (electronic version) ISSN 1503-8181.

"Effect of welding residual stress on fracture"
Xiabo Ren 2010:77, ISBN 978-82-471-2115-3 (printed version) ISBN 978-82-471-2116-0 (electronic version), ISSN 1503-8181.

"Pan-based carbon fiber as anode material in cathodic protection system for concrete structures"
Mahdi Chini 2010:122, ISBN 978-82-471-2210-5 (printed version) ISBN 978-82-471-2213-6 (electronic version), ISSN 1503-8181.

"Structural Behaviour of deteriorated and retrofitted concrete structures"
Irina Vasililjeva Sæther 2010:171, ISBN 978-82-471-2315-7 (printed version)
ISBN 978-82-471-2316-4 (electronic version) ISSN 1503-8181.

"Prediction of local snow loads on roofs"
Vivian Meløysund 2010:247, ISBN 978-82-471-2490-1 (printed version) ISBN
978-82-471-2491-8 (electronic version) ISSN 1503-8181.

"Behaviour and modelling of polymers for crash applications"
Virgile Delhaye 2010:251, ISBN 978-82-471-2501-4 (printed version) ISBN 978-
82-471-2502-1 (electronic version) ISSN 1503-8181.
"Blended cement with reduced CO_2 emission – Utilizing the Fly Ash-Limestone
Synergy",
Klaartje De Weerdt 2011:32, ISBN 978-82-471-2584-7 (printed version) ISBN
978-82-471-2584-4 (electronic version) ISSN 1503-8181.

"Chloride induced reinforcement corrosion in concrete" Concept of critical
chloride content – methods and mechanisms.
Ueli Angst 2011:113, ISBN 978-82-471-2769-9 (printed version) ISBN 978-82-
471-2763-6 (electronic version) ISSN 1503-8181.

"A thermo-electric-Mechanical study of the carbon anode and contact interface for
Energy savings in the production of aluminium".
Dag Herman Andersen 2011:157, ISBN 978-82-471-2859-6 (printed version)
ISBN 978-82-471-2860-2 (electronic version) ISSN 1503-8181.

"Structural Capacity of Anchorage Ties in Masonry Veneer Walls Subjected to
Earthquake". The implications of Eurocode 8 and Eurocode 6 on a typical
Norwegain veneer wall.
Ahmed Mohamed Yousry Hamed 2011:181, ISBN 978-82-471-2911-1 (printed
version) ISBN 978-82-471-2912-8 (electronic ver.) ISSN 1503-8181.

"Work-hardening behaviour in age-hardenable Al-Zn-Mg(-Cu) alloys".
Ida Westermann , 2011:247, ISBN 978-82-471-3056-8 (printed ver.) ISBN 978-82-
471-3057-5 (electronic ver.) ISSN 1503-8181.

"Behaviour and modelling of selfpiercing riveted connections using aluminium
rivets". Nguyen-Hieu Hoang, 2011:266, ISBN 978-82-471-3097-1 (printed ver.)
ISBN 978-82-471-3099-5 (electronic ver.) ISSN 1503-8181.

"Fibre reinforced concrete".
Sindre Sandbakk, 2011:297, ISBN 978-82-471-3167-1 (printed ver.) ISBN 978-82-
471-3168-8 (electronic ver) ISSN 1503:8181.

"Dynamic behaviour of cablesupported bridges subjected to strong natural wind".

Ole Andre Øiseth, 2011:315, ISBN 978-82-471-3209-8 (printed ver.) ISBN 978-82-471-3210-4 (electronic ver.) ISSN 1503-8181.

"Constitutive modeling of solargrade silicon materials"
Julien Cochard, 2011:307, ISBN 978-82-471-3189-3 (printed ver). ISBN 978-82-471-3190-9 (electronic ver.) ISSN 1503-8181.

"Constitutive behavior and fracture of shape memory alloys"
Jim Stian Olsen, 2012:57, ISBN 978-82-471-3382-8 (printed ver.) ISBN 978-82-471-3383-5 (electronic ver.) ISSN 1503-8181.

"Field measurements in mechanical testing using close-range photogrammetry and digital image analysis"
Egil Fagerholt, 2012:95, ISBN 978-82-471-3466-5 (printed ver.) ISBN 978-82-471-3467-2 (electronic ver.) ISSN 1503-8181.

"Towards a better under standing of the ultimate behaviour of lightweight aggregate concrete in compression and bending",
Håvard Nedrelid, 2012:123, ISBN 978-82-471-3527-3 (printed ver.) ISBN 978-82-471-3528-0 (electronic ver.) ISSN 1503-8181.

"Numerical simulations of blood flow in the left side of the heart"
Sigrid Kaarstad Dahl, 2012:135, ISBN 978-82-471-3553-2 (printed ver.) ISBN 978-82-471-3555-6 (electronic ver.) ISSN 1503-8181.

"Moisture induced stresses in glulam"
Vanessa Angst-Nicollier, 2012:139, ISBN 978-82-471-3562-4 (printed ver.) ISBN 978-82-471-3563-1 (electronic ver.) ISSN 1503-8181.

"Biomechanical aspects of distraction osteogensis"
Valentina La Russa, 2012:250, ISBN 978-82-471-3807-6 (printed ver.) ISBN 978-82-471-3808-3 (electronic ver.) ISSN 1503-8181.

"Ductile fracture in dual-phase steel. Theoretical, experimental and numerical study"
Gaute Gruben, 2012:257, ISBN 978-82-471-3822-9 (printed ver.) ISBN 978-82-471-3823-6 (electronic ver.) ISSN 1503-8181.

"Damping in Timber Structures"
Nathalie Labonnote, 2012:263, ISBN 978-82-471-3836-6 (printed ver.) ISBN 978-82-471-3837-3 (electronic ver.) ISSN 1503-8181.

"Biomechanical modeling of fetal veins: The umbilical vein and ductus venosus bifurcation"
Paul Roger Leinan, 2012:299, ISBN 978-82-471-3915-8 (printed ver.) ISBN 978-82-471-3916-5 (electronic ver.) ISSN 1503-8181.

"Large-Deformation behaviour of thermoplastics at various stress states"
Anne Serine Ognedal, 2012:298, ISBN 978-82-471-3913-4 (printed ver.) ISBN 978-82-471-3914-1 (electronic ver.) ISSN 1503-8181.

"Hardening accelerator for fly ash blended cement"
Kien Dinh Hoang, 2012:366, ISBN 978-82-471-4063-5 (printed ver.) ISBN 978-82-471-4064-2 (electronic ver.) ISSN 1503-8181.

"From molecular structure to mechanical properties"
Jianyang Wu, 2013:186, ISBN 978-82-471-4485-5 (printed ver.) ISBN 978-82-471-4486-2 (electronic ver.) ISSN 1503-8181.

"Experimental and numerical study of hybrid concrete structures"
Linn Grepstad Nes, 2013:259, ISBN 978-82-471-4644-6 (printed ver.) ISBN 978-82-471-4645-3 (electronic ver.) ISSN 1503-8181.

"Mechanics of ultra-thin multi crystalline silicon wafers"
Saber Saffar, 2013:199, ISBN 978-82-471-4511-1 (printed ver.) ISBN 978-82-471-4513-5 (electronic ver). ISSN 1503-8181.

"Through process modelling of welded aluminium structures"
Anizahyati Alisibramulisi, 2013:325, ISBN 978-82-471-4788-7 (printed ver.) ISBN 978-82-471-4789-4 (electronic ver.) ISSN 1503-8181.

"Combined blast and fragment loading on steel plates"
Knut Gaarder Rakvåg, 2013:361, ISBN978-82-471-4872-3 (printed ver.) ISBN 978-82-4873-0 (electronic ver.). ISSN 1503-8181.

"Characterization and modelling of the anisotropic behaviour of high-strength aluminium alloy"
Marion Fourmeau, 2014:37, ISBN 978-82-326-0008-3 (printed ver.) ISBN 978-82-326-0009-0 (electronic ver.) ISSN 1503-8181.

"Behaviour of threated steel fasteners at elevated deformation rates"
Henning Fransplass, 2014:65, ISBN 978-82-326-0054-0 (printed ver.) ISBN 978-82-326-0055-7 (electronic ver.) ISSN 1503-8181.

"Sedimentation and Bleeding"
Ya Peng, 2014:89, ISBN 978-82-326-0102-8 (printed ver.) ISBN 978-82-326-0103-5 (electric ver.) ISSN 1503-8181.

"Impact against X65 offshore pipelines"
Martin Kristoffersen, 2014:362, ISBN 978-82-326-0636-8 (printed ver.) ISBN 978-82-326-0637-5 (electronic ver.) ISSN 1503-8181.

"Formability of aluminium alloy subjected to prestrain by rolling"

Dmitry Vysochinskiy, 2014:363,, ISBN 978-82-326-0638-2 (printed ver.) ISBN 978-82-326-0639-9 (electronic ver.) ISSN 1503-8181.

"Experimental and numerical study of Yielding, Work-Hardening and anisotropy in textured AA6xxx alloys using crystal plasticity models"
Mikhail Khadyko, 2015:28, ISBN 978-82-326-0724-2 (printed ver.) ISBN 978-82-326-0725-9 (electronic ver.) ISSN 1503-8181.

"Behaviour and Modelling of AA6xxx Aluminium Alloys Under a Wide Range of Temperatures and Strain Rates"
Vincent Vilamosa, 2015:63, ISBN 978-82-326-0786-0 (printed ver.) ISBN 978-82-326-0787-7 (electronic ver.) ISSN 1503-8181.

"A Probabilistic Approach in Failure Modelling of Aluminium High Pressure Die-Castings"
Octavian Knoll, 2015:137, ISBN 978-82-326-0930-7 (printed ver.) ISBN 978-82-326-0931-4 (electronic ver.) ISSN 1503-8181.

"Ice Abrasion on Marine Concrete Structures"
Egil Møen, 2015:189, ISBN 978-82-326-1034-1 (printed ver.) ISBN 978-82-326-1035-8 (electronic ver.) ISSN 1503-8181.

"Fibre Orientation in Steel-Fibre-Reinforced Concrete"
Giedrius Zirgulis, 2015:229, ISBN 978-82-326-1114-0 (printed ver.) ISBN 978-82-326-1115-7 (electronic ver.) ISSN 1503-8181.

"Effect of spatial variation and possible interference of localised corrosion on the residual capacity of a reinforced concrete beam"
Mohammad Mahdi Kioumarsi, 2015:282, ISBN 978-82-326-1220-8 (printed ver.) ISBN 978-82-1221-5 (electronic ver.) ISSN 1503-8181.

"The role of concrete resistivity in chloride-induced macro-cell corrosion" Karla Horbostel, 2015:324, ISBN 978-82-326-1304-5 (printed ver.) ISBN 978-82-326-1305-2 (electonic ver.) ISSN 1503-8181.

"Flowable fibre-reinforced concrete for structural applications" Elena Vidal Sarmiento, 2015-335, ISBN 978-82-326-1324-3 (printed ver.) ISBN 978-82-326-1325-0 (electronic ver.) ISSN 1503-8181.

"Development of chushed sand for concrete production with microproportioning"
Rolands Cepuritis, 2016:19, ISBN 978-82-326-1382-3 (printed ver.) ISBN 978-82-326-1383-0 (electronic ver.) ISSN 1503-8181.